

DTIC FILE COPY

2

ARCCB-SP-90015

PROCEEDINGS OF THE

SIXTH U.S. ARMY SYMPOSIUM ON GUN DYNAMICS

VOLUME II OF II

TAMIMENT, PENNSYLVANIA

AD-A224 993

15-17 MAY 1990

DTIC
ELECTE
AUG 01 1990
S Q E D

SPONSORED BY



US ARMY ARMAMENT RESEARCH,
DEVELOPMENT AND ENGINEERING CENTER
CLOSE COMBAT ARMAMENTS CENTER
BENÉT LABORATORIES
WATERVLIET, N.Y. 12189-4050



APPROVED FOR PUBLIC RELEASE; DISTRIBUTION UNLIMITED

90 07 31 014

DISCLAIMER

The findings in this report are not to be construed as an official Department of the Army position unless so designated by other authorized documents.

The use of trade name(s) and/or manufacturer(s) does not constitute an official indorsement or approval.

DESTRUCTION NOTICE

For classified documents, follow the procedures in DoD 5200.22-M, Industrial Security Manual, Section II-19 or DoD 5200.1-R, Information Security Program Regulation, Chapter IX.

For unclassified, limited documents, destroy by any method that will prevent disclosure of contents or reconstruction of the document.

For unclassified, unlimited documents, destroy when the report is no longer needed. Do not return it to the originator.

REPORT DOCUMENTATION PAGE		READ INSTRUCTIONS BEFORE COMPLETING FORM
1. REPORT NUMBER ARCCB-SP-90015	2. GOVT ACCESSION NO.	3. RECIPIENT'S CATALOG NUMBER
4. TITLE (and Subtitle) PROCEEDINGS OF THE SIXTH U.S. ARMY SYMPOSIUM ON GUN DYNAMICS VOLUME II OF II		5. TYPE OF REPORT & PERIOD COVERED Final
		6. PERFORMING ORG. REPORT NUMBER
7. AUTHOR(s) Editor: Dr. Thomas E. Simkins		8. CONTRACT OR GRANT NUMBER(s)
9. PERFORMING ORGANIZATION NAME AND ADDRESS U.S. Army ARDEC Benet Laboratories, SMCAR-CCB-TL Watervliet, NY 12189-4050		10. PROGRAM ELEMENT, PROJECT, TASK AREA & WORK UNIT NUMBERS N/A
11. CONTROLLING OFFICE NAME AND ADDRESS U.S. Army ARDEC Close Combat Armaments Center Picatinny Arsenal, NJ 07806-5000		12. REPORT DATE May 1990
		13. NUMBER OF PAGES 245
14. MONITORING AGENCY NAME & ADDRESS (if different from Controlling Office)		15. SECURITY CLASS. (of this report) UNCLASSIFIED
		15a. DECLASSIFICATION/DOWNGRADING SCHEDULE
16. DISTRIBUTION STATEMENT (of this Report) Approved for public release; distribution unlimited.		
17. DISTRIBUTION STATEMENT (of the abstract entered in Block 20, if different from Report)		
18. SUPPLEMENTARY NOTES Presented at the Sixth U.S. Army Symposium on Gun Dynamics, Tamiment, Pennsylvania 15-17 May 1990		
19. KEY WORDS (Continue on reverse side if necessary and identify by block number) Ballistics, Precision, (42715) Barrel Vibration, Stabilization Dynamics, Symposium, Target Acquisition. (CP) 4.		
20. ABSTRACT (Continue on reverse side if necessary and identify by block number) This represents a compilation of technical papers concerning analyses, design, measurement, and automation of gun dynamics. The authors represent a cross- section of the scientific and technical community, including universities, industrial, and Government research laboratories. <i>REVISED</i>		

FOREWORD

The theme of the 1990 Symposium was Gun Dynamics. The Symposium was divided into six sessions: (I) Fluid Dynamics, (II) Experimental Work, (III) The Motion of Gun Tubes - Theory, (IV) The Motion of Gun Tubes - Measurement, (V) Modelling and Finite Element Simulation, and (VI) Projectiles and Projectile/Tube Interface.

During recent years, one has witnessed great strides in various branches of continuum mechanics, kinematic designs, and numerical and computer techniques for solving problems of great complexity as well as in the areas of experimental mechanics and instrumentation. Now more than ever it appears feasible to gain understanding and to improve the design of gun systems for greater accuracy by exploiting new technological advances. The Sixth Symposium represents the continuing interest of the United States Army in this direction.

The Proceedings of the Sixth U.S. Army Symposium on Gun Dynamics contains the technical papers presented at the Symposium held in Tamiment, Pennsylvania, 15-17 May 1990. The papers represent the current research efforts on gun dynamics and the effect on precision and design by industrial, university, and Department of the Army, Department of the Navy, and Department of Energy laboratories throughout the United States and the United Kingdom. In addition, papers not received in time for publication in the Proceedings of the Fifth Symposium are included herein.

I am grateful to everyone who submitted a paper for inclusion in the Proceedings. As in previous years, I am delighted by the number of scientific and technical people who have gathered to share their knowledge and experience.

Thomas E. Simkins, Chairman
Sixth U.S. Army Symposium on Gun Dynamics

Accession For	
NTIS GRA&I	<input checked="" type="checkbox"/>
DTIC TAB	<input type="checkbox"/>
Unannounced	<input type="checkbox"/>
Justification	
By _____	
Distribution/ _____	
Availability Codes	
Dist	Avail and/or Special
A-1	



CONTENTS

	<u>Page</u>
SESSION I: FLUID DYNAMICS	
A COMPARISON OF EXPERIMENTAL AND NUMERICAL BLAST DATA FOR PERFORATED MUZZLE BRAKES	1
G.C. Carofano —	
GENERIC GUN BORE EVACUATORS, I. EXPERIMENTAL AND AERODYNAMIC INVESTIGATIONS	18
H.T. Nagamatsu, R.E. Duffy, C.A. Andrade —	
GENERIC GUN BORE EVACUATORS, II. IDEAL AND REAL PROPELLANT GAS TRANSIENTS	41
C.A. Andrade, J.W. Haas —	
BORE EVACUATOR HOLE FLOWS	61
H.J. Sneck, P. Witting —	
STATISTICAL ANALYSIS OF 16-INCH GUN BLAST	76
J.J. Yagla, M.M. Kordich —	
A VARIABLE DISCHARGE COEFFICIENT FUNCTION FOR HEAVY ARTILLERY GUN MOUNT ANALYSIS AND DESIGN	98
W.T. Zepp —	

SESSION II: EXPERIMENTAL WORK

Page

AN ACCELEROMETER TECHNIQUE FOR THE MEASUREMENT OF GUN
MUZZLE MOTION 100

G. Barker, D.N. Bulman, A.E. Chambers

AN EXPERIMENTAL TECHNIQUE FOR MEASUREMENT OF SHOT
PARAMETERS USED IN GUN DYNAMICS MODELLING 114

G. Barker, A.E. Chambers

THE USE OF A 30MM RESEARCH GUN TO TEST THE VALIDITY
OF THE RAMA GUN DYNAMICS COMPUTER SIMULATION 115

A. Exell

THE DEVELOPMENT OF AN EXPERIMENTAL FACILITY FOR
STUDYING THE EFFECTS OF CRADLE DESIGN ON BARREL
MOTION 116

J.B. Hoyle

AUTONOMOUS ACCURACY ENHANCEMENT SYSTEM 136

T.L. Brosseau, M.D. Kregel, A.F. Baran

THERMAL DISTORTION IN CONVENTIONAL RECOIL MOUNTS 149

M.L. Bundy

SESSION III: THE MOTION OF GUN TUBES - THEORY

Page

MODE COUPLING OF GUN TUBES CAUSED BY SPACE CURVATURE
AND INITIAL TWIST 159

H.B. Kingsbury, H.-S. Tsay
—

A VARIATIONAL ANALYSIS OF RESONANCE IN GUN TUBES WITH
ECCENTRIC BORES 175

D.V. Shick, H.F. Tiersten
—

TRANSIENT VIBRATIONS AND INSTABILITY IN FLEXIBLE GUNS 199

I.G. Tadjbakhsh, Y.-A. Su
—

THE EFFECT OF BORE CURVATURE ON SHOT ACCURACY IN TANK
CANNON 230

R.G. Gast
—

POINT MASS PROJECTILE FORCES AND MOMENTS ON MOVING GUN
TUBES WITH CURVATURE AND TORSION 249

D.F. Finlayson
—

SESSION IV: THE MOTION OF GUN TUBES - MEASUREMENTS

Page

A COMPARISON OF THEORETICAL AND EXPERIMENTAL RESULTS
WITH REGARD TO THE EFFECTS OF GUN CRADLE DESIGN ON
BARREL AND SHOT MOTION 251

J.B. Hoyle, D.N. Bulman

DYNAMIC STRAINS IN A 60-MM GUN TUBE - AN EXPERIMENTAL
STUDY 252

T.E. Simkins, G.A. Pflagl, E.G. Stilson

MODELING GUN DYNAMICS WITH THREE-DIMENSIONAL BEAM
ELEMENTS 272

D.A. Hopkins

DYNAMIC STRAIN WAVES - A DEVELOPMENT PERSPECTIVE 285

R. Hasenbein, A. Gabriele, D. Finlayson
B. Artus, G. Cunningham, R. Gast

SESSION V: MODELLING AND FINITE ELEMENT SIMULATION

Page

DYNAMIC ANALYSIS OF A HAND-HELD WEAPON 298

P.D. Benzkofer

FLEXIBLE PROJECTILE MODELING USING THE LITTLE
RASCAL GUN DYNAMICS PROGRAM 317

T.F. Erline, M.D. Kregel

FINITE ELEMENT MODELS TO PREDICT THE STRUCTURAL
RESPONSE OF 120-MM SABOT/RODS DURING LAUNCH 334

D.A. Rabern, K.A. Bannister

SESSION VI: PROJECTILES AND PROJECTILE/TUBE INTERFACE

Page

A THEORETICAL STUDY INTO THE EFFECT OF SABOT
STIFFNESS ON PROJECTILE IN-BORE MOTION AND
LAUNCH ACCURACY 355

N.D. Manners
——

DEVELOPMENT OF A DESIGN METHODOLOGY FOR SLIPBAND
OBTURATORS 376

R.P. Kaste, L. Burton
——

A METHODOLOGY FOR DESIGNING PROJECTILE INTERFACES
TO SURVIVE WORN GUN TUBE LAUNCHING 394

R.C. Benson, W.R. Benson, T. Sorenson
——

COMPARISON OF COMPUTED AND MEASURED JUMP OF 120MM
CANNON 412

E.M. Schmidt, D.S. Savick, D.H. Lyon, P. Plostins
——

THE FIFTH U.S. ARMY SYMPOSIUM ON GUN DYNAMICS

Page

THE THEORETICAL MODELLING OF THE DYNAMICS OF
INITIALLY NON-STRAIGHT BARRELS USING FINITE
DIFFERENCE TECHNIQUES 432

S.E. Powell, P.H.G. Penny

THE ADAPTATION OF NASTRAN FOR THREE-DIMENSIONAL
GUN DYNAMICS PROBLEMS 451

M.A. Polcyn, P.A. Cox

AN ACCOUNT OF SOME EXPERIMENTS UNDERTAKEN TO
CORRELATE MEASURED GUN BARREL FEATURES WITH
THE MOVEMENT OF SERIAL MEAN POINTS OF IMPACT 472

P.H.G. Penny, J.A. Perry

AUTHOR INDEX

VOLUME I I-1
VOLUME II II-1

SESSION IV:

THE MOTION OF GUN TUBES - MEASUREMENTS

HOYLE, BULMAN

TITLE: A COMPARISON OF THEORETICAL AND EXPERIMENTAL RESULTS WITH REGARD TO THE EFFECTS OF GUN CRADLE DESIGN ON BARREL AND SHOT MOTION

J.B. HOYLE AND D.N. BULMAN
THE ROYAL MILITARY COLLEGE OF SCIENCE
SCHOOL OF MECHANICAL, MATERIALS AND CIVIL ENGINEERING
LAND SYSTEMS GROUP
SHRIVENHAM, SWINDON, SN6 8LA, ENGLAND

ABSTRACT

An experimental firing program has been carried out using the RMCS 30 mm Air Powered Gun into the effects of gun cradle design on barrel and shot motion. The program made use of a special gun cradle specifically designed to simulate any existing and foreseeable cradle configuration, whilst at the same time allowing many of the parameters of a real gun cradle to be varied. During the program, various parameters were systematically altered and the effects of these alterations on barrel motion were recorded. Different cradle configurations were also investigated.

Suitable data presentation techniques were developed to analyse the large amount of data that was recorded during the firing program. These techniques clearly establish the effects of changes in each cradle variable parameter and also compare different cradle configurations.

One of the main advantages of test firing small scale experimental guns as opposed to full sized guns is that it is possible to obtain exact data concerning the gun system for use in mathematical simulation packages. The firing program was therefore carried out, both in its own right for the simulation of real gun cradles, and as a means of gaining large amounts of low cost experimental data for the validation of, and comparison with, mathematical simulation packages.

The gun dynamics package SIMBAD was employed to use this data and simulate different cradle configurations together with changes in cradle parameters. The theoretical results were then analysed and compared with the experimental results, with the ultimate aim of gaining a greater understanding of the critical factors in gun cradle design.

This paper attempts to describe in a concise form the very large amount of experimental and theoretical data obtained during the project.

This paper was not available for printing in this publication.

SIMKINS, PFLEGL, STILSON

TITLE: DYNAMIC STRAINS IN A 60-MM GUN TUBE - AN EXPERIMENTAL STUDY
T.E. SIMKINS, G.A. PFLEGL, AND E.G. STILSON
U.S. ARMY ARMAMENT RESEARCH, DEVELOPMENT, AND ENGINEERING CENTER
BENET LABORATORIES
WATERVLIET, NY 12189-4050

ABSTRACT:

An exceptionally thin-walled gun tube was constructed to assess the applicability of steady-state deformations predicted by critical velocity theory. Strains created by internal pressures moving at subcritical, critical, and supercritical velocities were measured. Excellent agreement with steady-state predictions was observed throughout the entire subcritical regime. When the velocity of the moving pressure was only slightly greater than the critical value, a transitional state was noted. At higher velocities, the development of a trailing wave was observed and was found to be consistent with the theory. The existence of the predicted head wave was never actually observed. However, its presence was indicated in a frequency analysis of the data.

BIOGRAPHY:

PRESENT ASSIGNMENT: Research Mechanical Engineer, Applied Mathematics and Mechanics Branch, Research Division, Benet Laboratories.

DEGREES HELD: Ph.D. - Mechanics, Rensselaer Polytechnic Institute, Troy, NY; B.S. - Mechanical Engineering, Northeastern University, Boston, MA.

DYNAMIC STRAINS IN A 60-MM GUN TUBE - AN EXPERIMENTAL STUDY

T.E. Simkins, G.A. Pflugl, and E.G. Stilson
U.S. Army Armament Research, Development, and Engineering Center
Close Combat Armaments Center
Benet Laboratories
Watervliet, NY 12189-4050

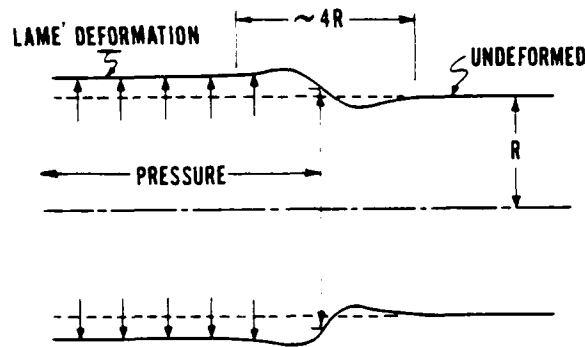
INTRODUCTION

The work reported herein was motivated by the need to further study the predictions of critical velocity theory as reported in July 1987 [1]. Whereas the circumferential strains reported in Reference 1 were in excellent agreement with those predicted by steady-state theory, questions remained as to the general applicability of the theory over a wider range of velocities. There was also great interest in the effects produced by small nonuniformities in wall thickness likely to be present in any production gun tube. With these goals in mind, funding was provided for a special set of experiments to be conducted in the Gun Dynamics Lab at Benet Laboratories.

BACKGROUND

A detailed account of the theory necessary to understand how wall strains amplify with projectile velocity is given in Reference 1. Reference 2 shows how bore eccentricity results in the excitation of nonaxisymmetric as well as axisymmetric tube strains, and Reference 3 discusses the manner in which transient vibrations produce even greater strain amplification. These references represent the state of our knowledge to date pertaining to critical velocity effects in gun tubes.

For the convenience of readers who are not acquainted with critical velocity theory and for the essential purposes of this paper, a brief summary is appropriate. Figure 1 represents the general situation. The ballistic pressure, terminating at the obturation ring near the rear face of a projectile, travels along the bore surface of a gun tube. At low velocities, the deformation of the tube wall within the pressurized region of the tube is closely approximated by the Lamé [4] formula in regions sufficiently to the rear of the plane of obturation. The Lamé solution assumes a uniform tube of infinite length subjected to a uniform and statically applied internal pressure throughout. In most gun tubes, a distance of twice the bore radius to the rear of the plane of obturation is sufficient for the Lamé formula to apply, provided the projectile velocity is not too high. Similarly, at distances greater than twice the bore radius ahead of the obturation ring, the tube deformation is



DEFORMATION OF BORE SURFACE (STATIC)

Figure 1

almost zero. Closer to the obturation ring, however, the deformation is more accurately given by the solution of Laning and Bowie [5]. Like the Lamé solution, this solution also assumes a uniform tube of infinite length but under static internal pressurization which is applied over half of the tube only. The pressure is zero throughout the remaining half. This solution shows that the static deformation of the tube wall in the neighborhood of the obturation ring has the form of a decaying harmonic. At sufficiently low projectile velocities, this deformation exceeds the Lamé deformation by only a few percent and until now was disregarded in gun tubes. However, with the advent of higher projectile velocities for armor penetration and reductions in wall thickness to reduce weight, tube dynamics has assumed a dominant role and neither of these static solutions apply. Specifically, higher projectile velocities increase the amplitude of the harmonic portion of the deformation and decrease its wavelength until, at a specific 'critical' velocity, the amplitude theoretically grows without bound. The cause of this form of resonance is the equality of group and phase velocities at this particular wavelength. This only occurs at the stationary values of the phase velocity when expressed as a function of the wave number as described in Reference 1. The magnitude of this critical velocity decreases with the wall thickness of the tube (cf. Figure 13, Reference 1). The 'theory' referred to here assumes a uniform and infinitely long tube subjected to a moving 'step' of pressure travelling at constant velocity as depicted in Figure 1. The deformation is predicted from steady-state solutions.

Admittedly, these solutions give no information about the transient development of this steady state. Figure 2 typifies the radial deformation at a fixed location along the tube for a projectile velocity close to critical, i.e., $V = 0.99 V_{cr}^*$ ($t = 0$ represents projectile passage). As can be seen, tube displacements (and hence strains and stresses) are approximately 3.7 times those calculated by the Lamé formula. Thus, the Lamé deformation, which errs only by a few percent when the velocity is, say 80 percent of its critical value, errs by 370 percent when the velocity is 99 percent critical. As $V \rightarrow V_{cr}$, this error theoretically becomes infinitely large.

*All plots of displacements are normalized with respect to those calculated by the Lamé equation.

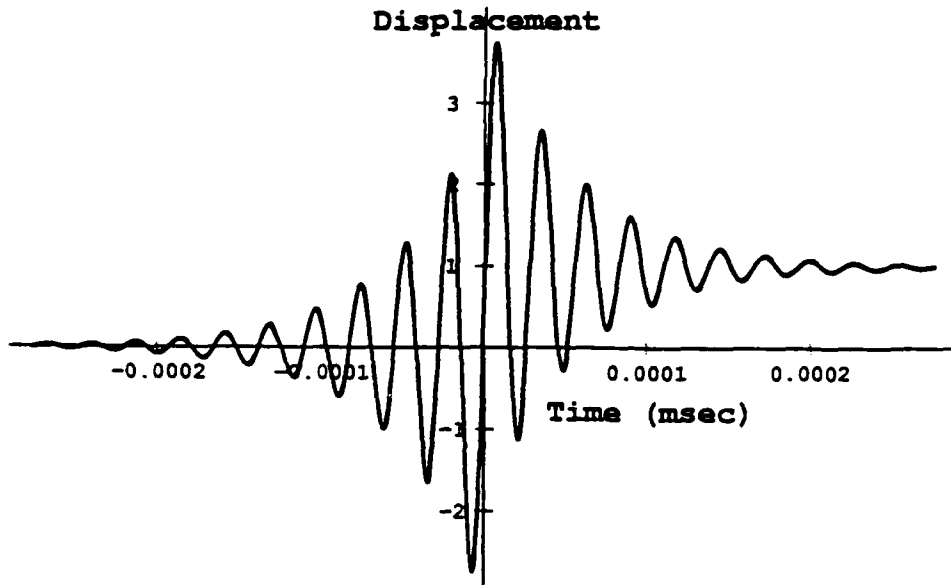


Figure 2. Theoretical steady-state radial displacement of tube wall, $V = 0.99 V_{CR}$ (pressure front passes at $t = 0$).

Referring again to Figure 2, we see that the deformation is antisymmetric about the point $(0, 1/2)$ and has an exponential rise and fall. For velocities greater than critical however, the steady-state solutions have a completely different character. As shown in Figure 3 ($V = 1.22 V_{CR}$), the steady-state deformation in the latter case consists of a trailing wave behind the obturation

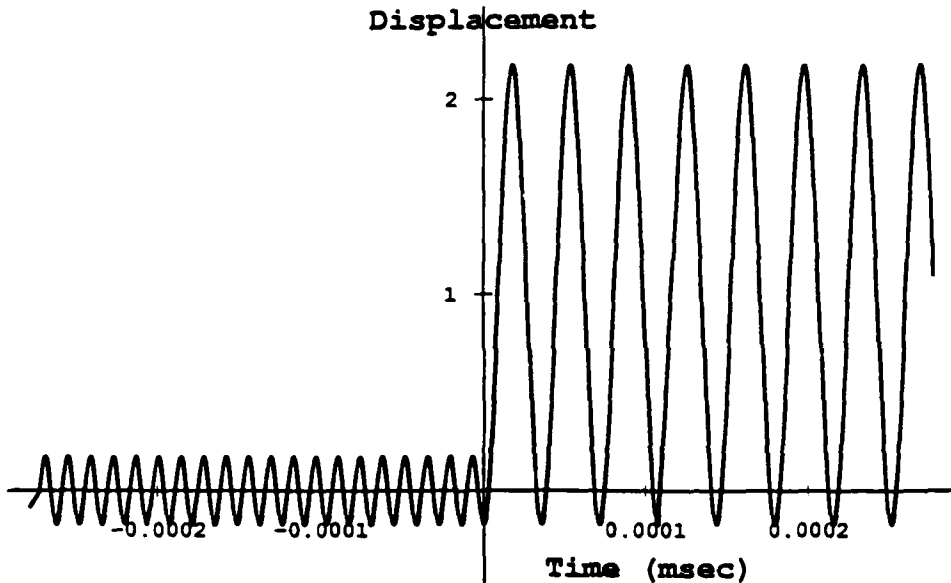


Figure 3. Theoretical steady-state radial displacement of tube wall, $V = 1.22 V_{CR}$.

plane and a head wave in front. Both waves are predicted to have constant amplitudes and the amplitude and wavelength of the trailing wave are always greater than those of the head wave. Theoretically, as the velocity of the moving pressure becomes infinite, the amplitude of the trailing wave approaches twice the displacement predicted by the Lamé formula and that of the head wave vanishes.

As previously stated, the existing critical velocity theory yields only steady-state solutions for the tube deformation. In particular, it is not known how long it will take for a steady deformation to develop. While the strain data from the 120-mm XM25 [1] showed excellent agreement with the steady-state prediction, thus verifying the usefulness of the theory at subcritical projectile velocities, no strains were measured during these firings which test the usefulness of the steady-state solutions for supercritical velocities. Thus, one goal of the research reported herein was to compare measured values of strains obtained at supercritical velocities with those predicted by steady-state critical velocity theory.

NONAXISYMMETRIC DEFORMATION

In many practical situations involving mechanical vibrations, some coupling is often present which causes excitation of more than one mode of vibration. In particular, we are concerned about the possibility of exciting nonaxisymmetric (beamlike) waves in which the bore center line assumes a travelling sinusoidal shape. Motion of the bore center line at shot ejection suggests a time variant point of aim. As it turns out, there is good reason to believe that such a mode will appear in actual test firings because a beamlike mode exists which has a critical velocity extremely close to that of the axisymmetric mode. This is most easily seen by comparing the phase velocities of each mode as a function of wavelength (Figure 4). As described in Reference 1, phase and group velocities will be equal whenever these phase velocities are stationary. In particular, the axisymmetric mode and the nonaxisymmetric beamlike mode have minimum phase velocities which are practically identical. Hence the slightest coupling can be expected to transfer energy from the axisymmetric mode to the nonaxisymmetric mode whenever the projectile velocity nears this critical value. Nonuniform tube mass has been found to provide coupling by which this can occur [2]. A more comprehensive study of this effect and the effect of nonuniform wall thickness has been made at Rensselaer Polytechnic Institute [6]. Thus, a second goal of this research was to search for possible evidence of more than one mode of vibration, in particular, modes which represent a beamlike motion of the tube.

EXPERIMENTAL SETUP

Figure 5 depicts the 60-mm gun tube manufactured for these experiments. As the figure shows, the wall thickness of the tube is quite thick except over the last four feet approaching the muzzle - the test section within which all strain measurements are made. Within this region, the wall thickness is nominally a constant 0.120 inch. This thickness was as thin as manufacturing considerations

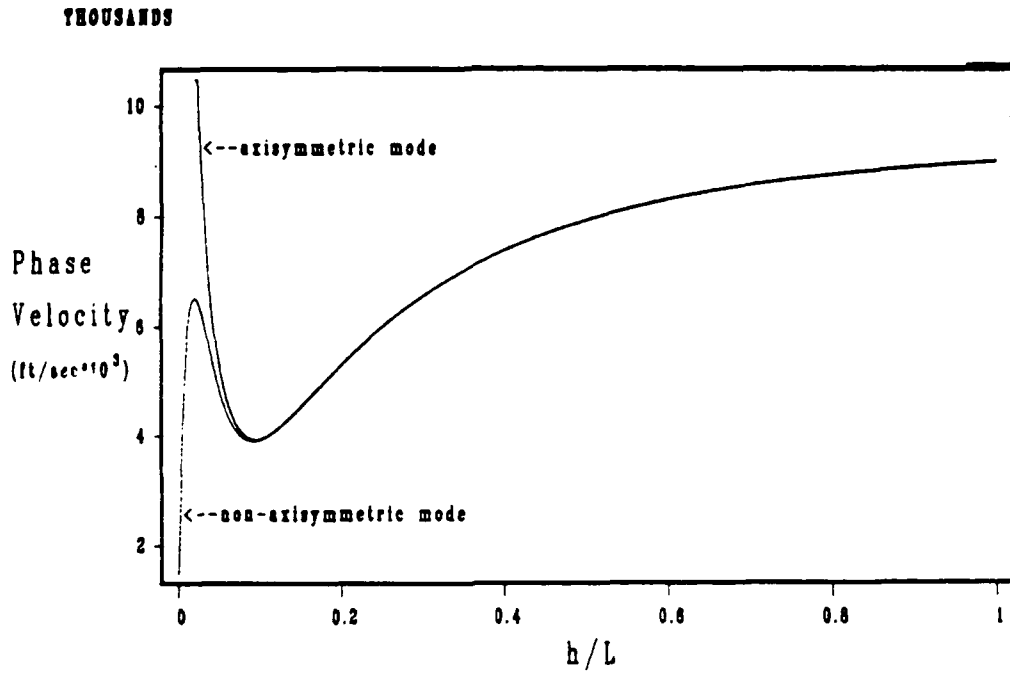


Figure 4. Dispersion curves for axisymmetric and nonaxisymmetric (beamlike) waves, h = tube wall thickness, L = wavelength.

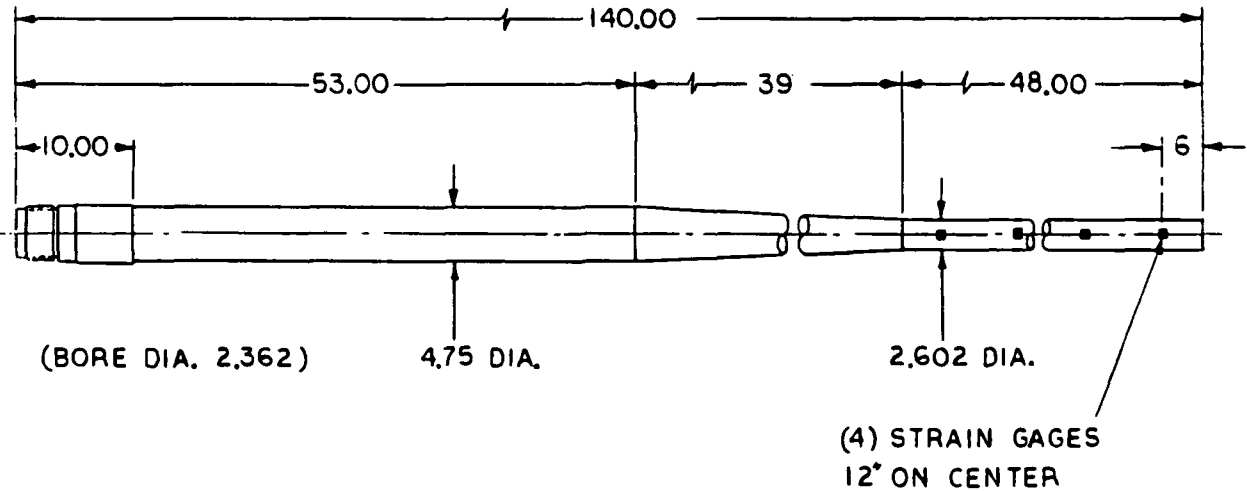


Figure 5. Schematic of 60-mm gun tube.

SIMKINS, PFLEGL, STILSON

and structural integrity would permit to lower the critical velocity of the tube as much as possible. Using the thick-wall shell theory of Mirsky and Herrmann [7], the critical velocity for generating axisymmetric waves within this test section is 3924 ft/sec and that required to generate beamlike waves is 3917 ft/sec. The thin-wall theory (cf. Reismann [8]) gives a higher figure of 4089 ft/sec for the generation of axisymmetric waves. This theory does not include nonaxisymmetric deformation.

The gun tube is suspended by two pairs of steel cables, each approximately 0.25 inch in diameter. When fired, the tube recoils as a bar-pendulum--striking a buffer system only after shot ejection. This arrangement virtually eliminates vibrations from support reactions prior to the exit of the projectile. The buffer system consists of three hydraulic shock absorbers which make contact with a plate mounted concentrically on the rear surface of the breech cap. Figure 6 is a photograph of the entire setup.

In order to attain projectile velocities in the neighborhood of 4000 ft/sec, propellants normally used in sporting ammunition were used following the advice of Mr. J. Siewert of General Electric Company, Burlington, VT. The two propellants utilized were manufactured by E.I. duPont de Nemours & Company and are known as IMR 4350 and IMR 4227. The main difference in these two propellants is their rate of burn, the latter burning faster than the former. Both propellants have burn characteristics which are very sensitive to shot start pressure. If the chamber volume increases too early as a result of projectile movement, insufficient burning results. To ensure sufficient shot start pressure, the projectile was manufactured with a shoulder which constrains the projectile motion until it fractures and allows the body of the projectile to move forward. The thickness of the fracture surface was varied until satisfactory projectile velocities were attained. In all other respects, the projectile is simply a solid right circular cylinder of aluminum alloy (6061 T6). A photograph of the projectile appears in Figure 6.

Although the projectile is 60 mm in diameter, it is fired by a 30-mm cartridge preloaded with varying amounts of propellant, depending on the projectile velocity desired. The use of a 30-mm cartridge was simply one of convenience. Electrically actuated primers, flash tubes, and 30-mm Gau-8 cartridge cases were readily available and had already been approved by safety officials for use in previous experiments involving a 30-mm tube.

INSTRUMENTATION

Breech pressure, circumferential and axial strains along the outer surface of the test section, and projectile velocity were measured over the brief interval of time between ignition and shot ejection. Breech pressure was measured using a piezoelectric pressure transducer (Kistler Instruments, Inc., Amherst, NY). Strain gages were type EA-06-187BB-120 and were purchased from Measurements Group, Inc., Raleigh, NC. Projectile velocity was measured using a radar interferometer model TROOK372A manufactured by RDL, Inc., Conshohocken, PA.

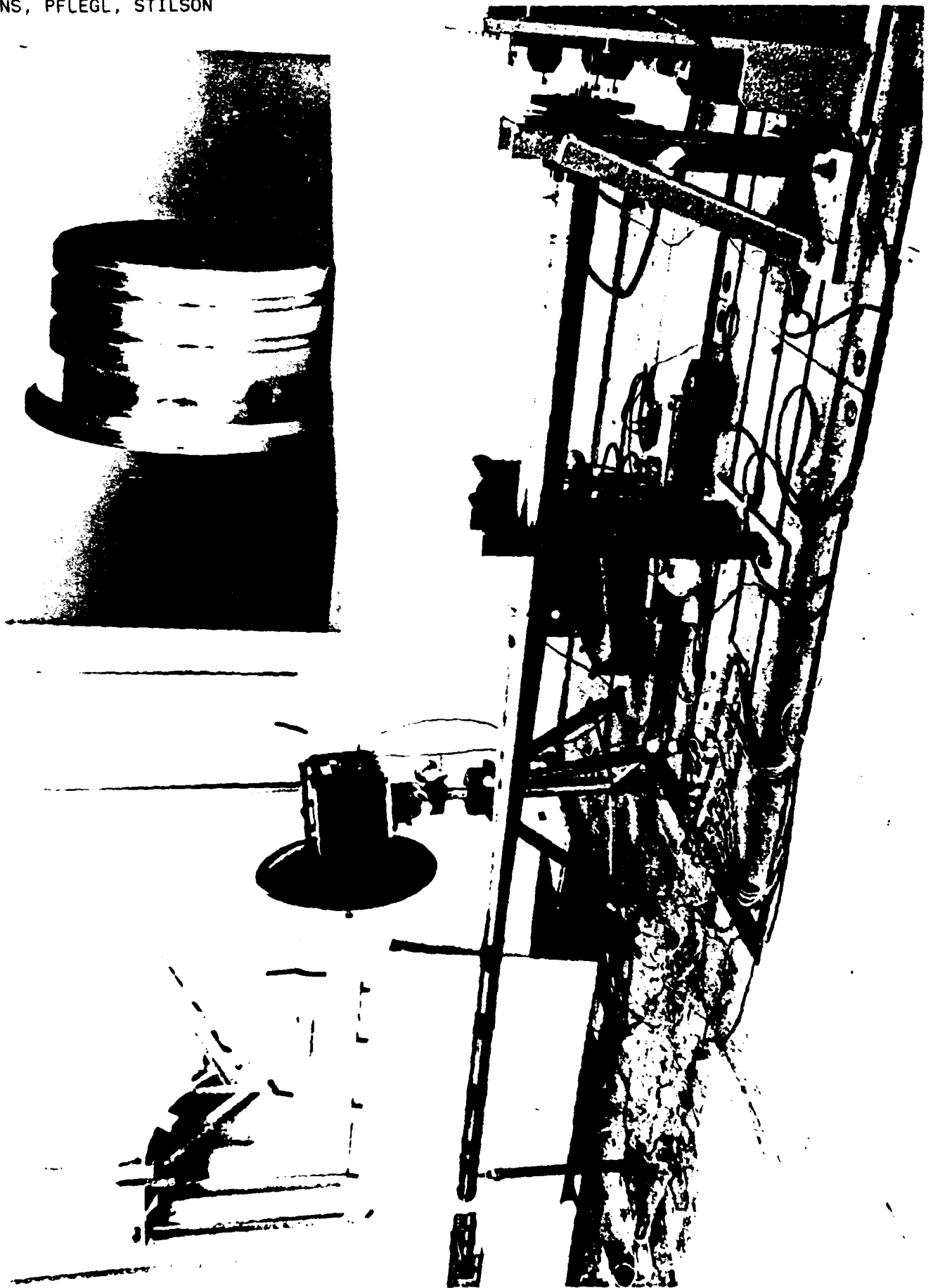


Figure 6. The laboratory gun tube and projectile.

The signals from the strain gages were received by model 8256 signal conditioning amplifiers (Pacific Instruments, Concord, CA). Output from these amplifiers and from the remainder of the transducers was received by model 9820 transient data recorders (Pacific Instruments) and also by three model 4094 Nicolet digital storage oscilloscopes. Some redundancy is provided between the Nicolet and Pacific systems. Digitized data from the Pacific system is stored on a hard disk with a tape backup and on floppy disks within the Nicolet oscilloscopes.

RESULTS

A typical set of measurements from one firing appears in Figures 7 through 10 (round ID 38). The plots were created using a computer program named VU-POINT: A Digital Data Processing System for IBM PC/XT/AT and Compatible Personal Computers, Version 1.21, March 1988. This software was purchased from S-CUBED, a division of Maxwell Laboratories, Inc., La Jolla, CA.

Figure 7 is a portion of a record of the Doppler radar output from which the projectile velocity can be calculated for any time. The radar signal has a frequency of 15 GHz which implies a wavelength of 1 cm. Thus, the time period of the oscillations is the time for the projectile to travel 1 cm.

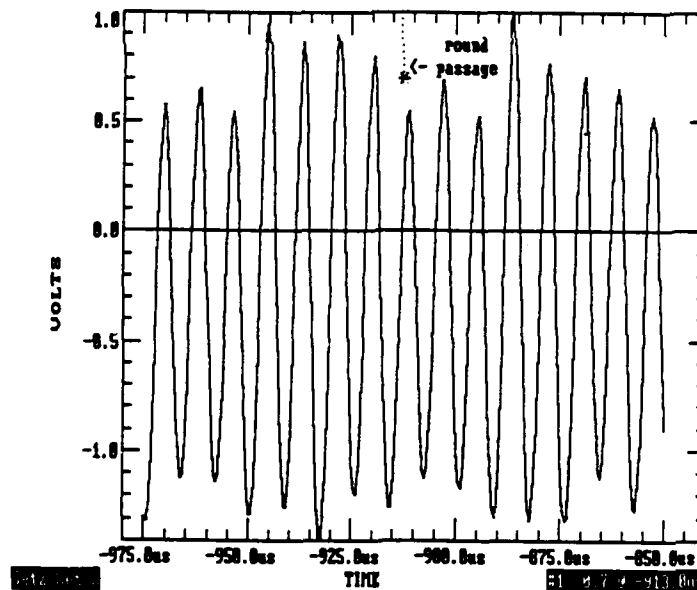


Figure 7. Doppler signal (round ID 38).

Figure 8 shows the pressure rise and fall at the initial location of the projectile in the breech end of the tube. The pressure acting on the rear face of the projectile as it traverses the bore is substantially less. In practice, the utility of the pressure measurement is marginal, serving mostly as a reference to compare burning characteristics from round to round.

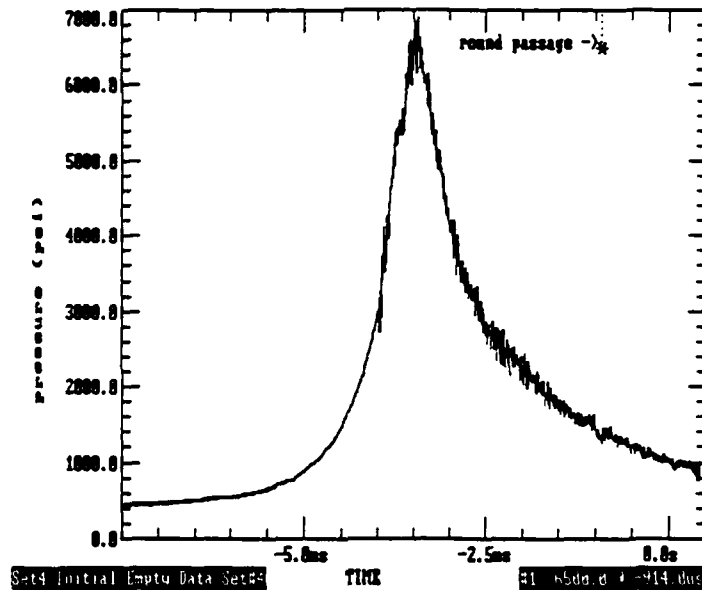


Figure 8. Breech pressure as a function of time (round ID 38).

Figure 9 shows the circumferential strain on the top surface of the gun tube located 30 inches from the muzzle. From the record, the time at which the projectile passes the gage is estimated to be $t = -914 \mu\text{s}$. (Times are measured from the time an electrical circuit is interrupted by the projectile at a location 12 inches from the muzzle.) Approximately $250 \mu\text{s}$ later ($t = -663 \mu\text{s}$), the projectile passes a similarly oriented gage located 18 inches from the muzzle. The record from this gage is shown in Figure 10. The time that the projectile passes each of these gages is shown in Figures 7 through 10.

A DETAILED ANALYSIS OF THE STRAIN RECORD OF FIGURE 9

The first signal to arrive is an axial strain created by the sudden recoil of the tube. This strain is mostly confined to the first axial mode of the tube and travels at the longitudinal wave speed of the tube material--roughly 17,000 ft/sec. The strain gage, mounted in the circumferential direction, senses the Poisson contribution from this strain, i.e., 30 percent of the axial strain appears as circumferential strain. The axial strain wave is practically constant in amplitude throughout the period of interest and can be subtracted from the record if desired. In any case, the axial strain is not of real interest in these studies.

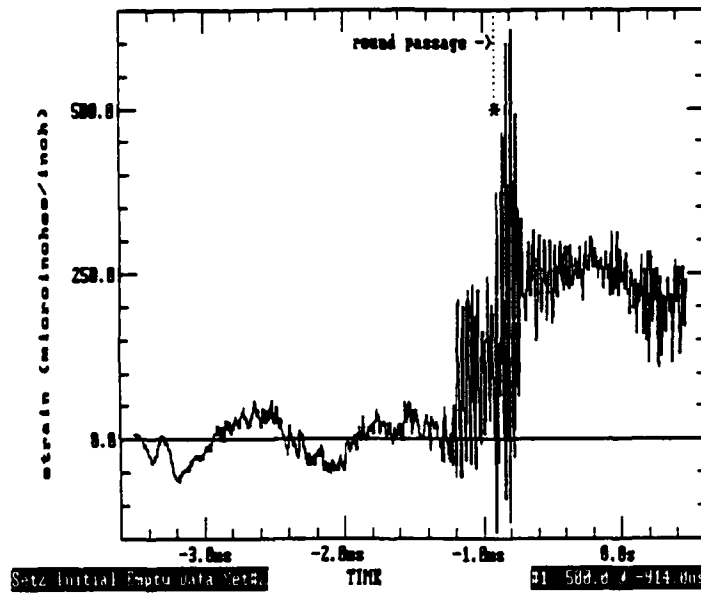


Figure 9. Circumferential strain 30 inches from muzzle.
projectile velocity = 3905 ft/sec (round ID 38).

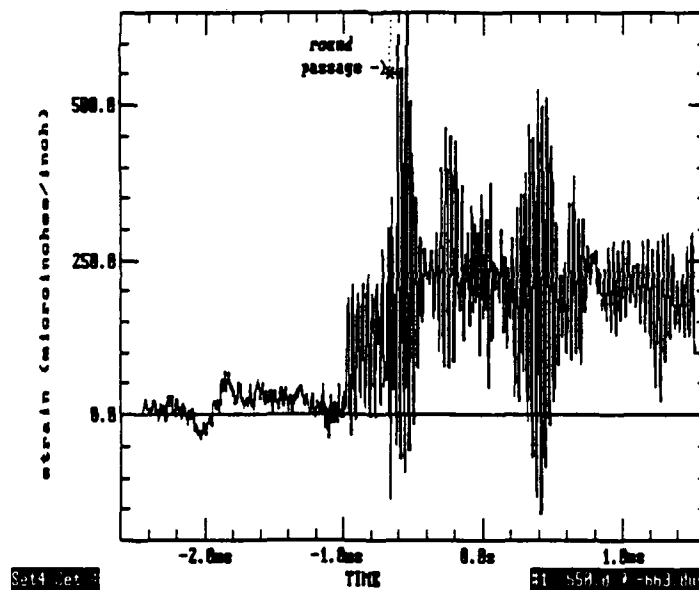


Figure 10. Circumferential strain 18 inches from muzzle
(round ID 38).

Figure 11 is a time expansion of Figure 9 in the neighborhood of the time of shot passage ($t = -914 \mu\text{s}$). From the Doppler record, the projectile velocity is 3905 ft/sec ($0.99 V_{CP}$) and therefore subcritical. Consequently, one expects to see a strain similar to the theoretical one depicted in Figure 2, but clearly this is not what is observed in Figure 11. After some study, it was realized that there is a shock front in front of the projectile which precedes the arrival of the projectile at the gage location. Between the shock front and the

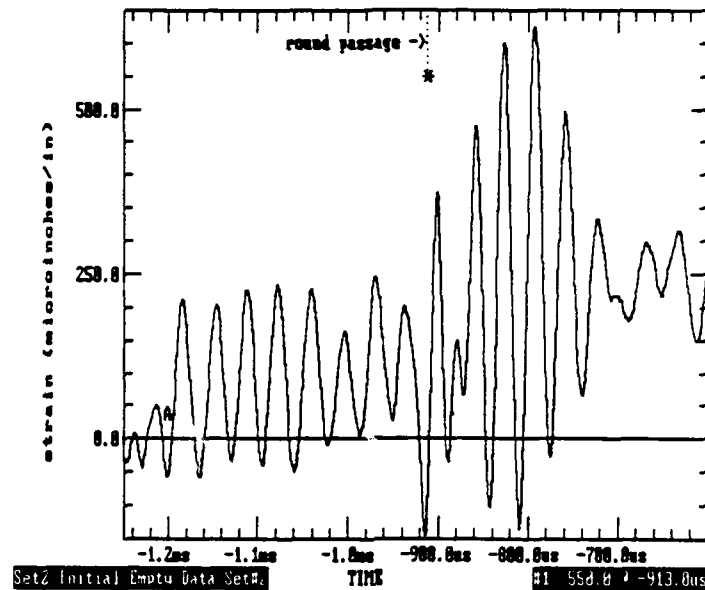


Figure 11. Figure 9 record - expanded time base.

projectile is a column of air with a pressure of about 25 atmospheres, roughly half the ballistic pressure at the rear face of the projectile. The shock front travels at a velocity which is roughly 26 percent greater than that of the projectile [9]. The situation is depicted in Figure 12. This moving column of air led by the shock front creates the same strain pattern as a (fictitious) projectile travelling at a supercritical velocity. In a field cannon this strain pattern would be negligible compared with that caused by the moving ballistic pressure since the latter is an order of magnitude greater. In the 60-mm gun tube used in this study however, the magnitudes of the two pressures are comparable and create comparable dynamic strains in the tube. If steady-state theory applies, the strain pattern created by the moving shock should have the general appearance of Figure 3, a high frequency, short head wave travelling ahead of the shock front followed by a lower frequency, longer trailing wave travelling behind the shock front. Disregarding the Poisson contribution from the axial strain, the entire head wave and a portion of the trailing wave should dominate the strain history at the gage for a time prior to the arrival of the projectile. The projectile will bring with it a strain pattern resembling that of Figure 2. Thus, at some point in time between ignition and the arrival of the projectile, one should first observe the head wave which abruptly changes to the trailing wave as the shock front passes the gage. In Figure 11, point A

clearly shows the abrupt transition and establishment of the trailing wave. Its frequency is measured at 28.0 kHz, in good agreement with the theoretical prediction of 27.6 kHz. The head wave is not clearly evident, however. One possible reason for this is that the amplitude of the head wave for a velocity which is 25 percent supercritical, is only 13 percent that of the trailing wave. In addition, the theoretical frequency of this head wave is very high--90.65 kHz! Thus, the head wave could easily be buried in the 'noise' level of the strain signal because of its low amplitude and/or be difficult to detect because of the 1-mHz sampling rate used for the digitization of the signal.

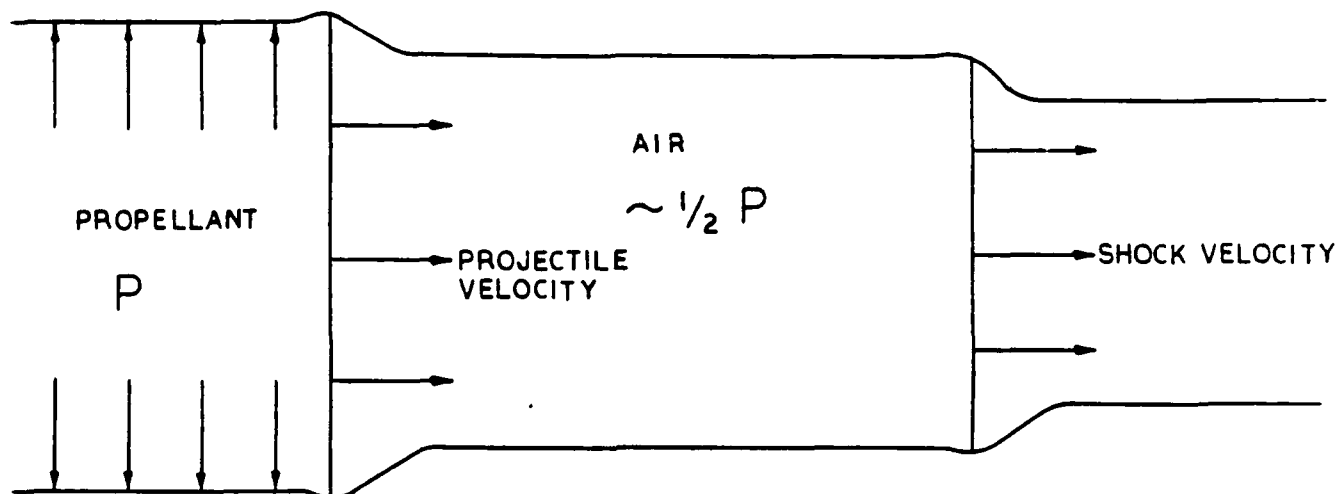


Figure 12. Schematic showing the ballistic pressure preceded by a faster moving shock.

Upon arrival of the projectile, the steady-state strain history is theoretically a linear combination of Figures 2 and 3. Figure 13 shows this superposition assuming that the pressure behind the shock front is half that behind the projectile and that the shock front arrives at the gage location 312 μ s ahead of the projectile. Both assumptions represent approximate measured values from Figure 11. It can be seen that Figures 11 and 13 are in reasonable agreement.

EVIDENCE OF NONAXISYMMETRIC WAVES

The superposition of the classical solutions of Figures 2 and 3 give a reasonably good explanation of the appearance of the measured strains of Figure 9. It is apparent, however, that the replication is at best semi-quantitative, and differences exist at several locations throughout the record. Some of these can be attributed to the presence of nonaxisymmetric motions excluded by the classical theory thus far. Nonaxisymmetric vibrations (waves) are evident in a comparison of strain records from diametrically opposed strain gages. Figure 14 is a comparison from a firing subsequent to that of Figure 9. In this round, the evidence of nonaxisymmetric (beamlike) vibrations is particularly strong.

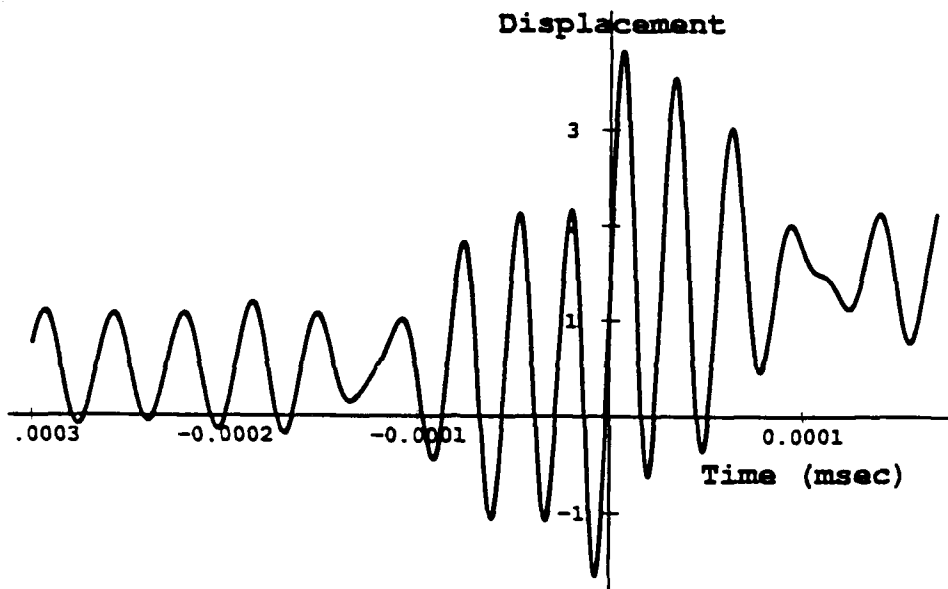


Figure 13. Theoretical superposition of steady-state displacements from Figures 2 and 3 compared with Figure 11.

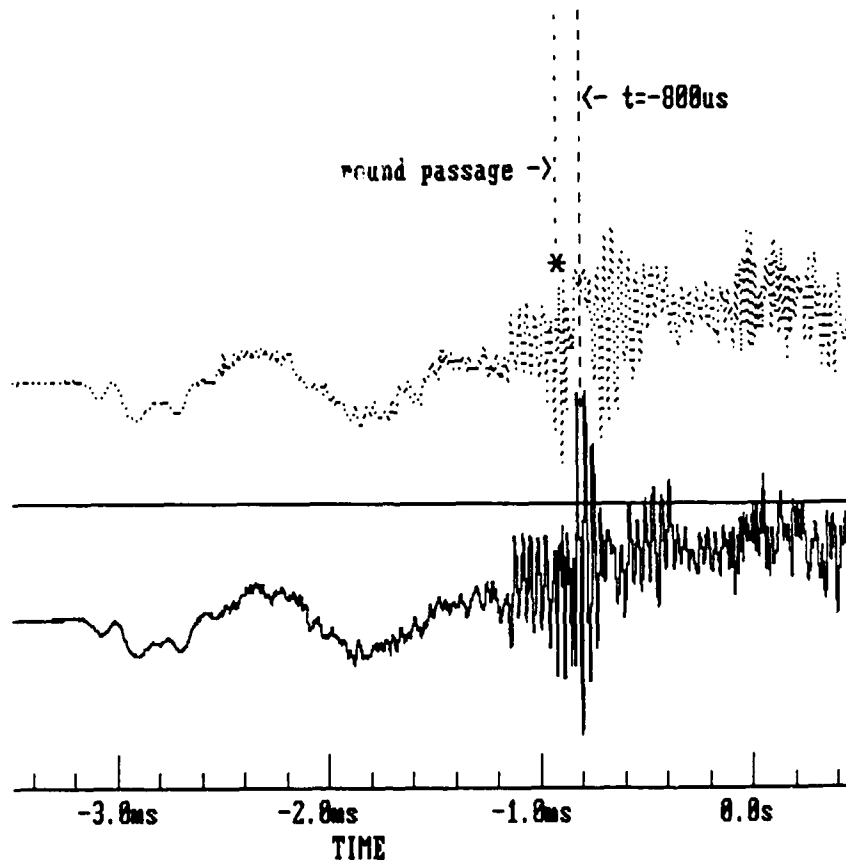


Figure 14. A comparison of diametrically opposed circumferential strain records 30 inches from muzzle, projectile velocity = 3905 ft/sec (round ID 38).

In Figure 14 we see that the strains on the diametrically opposed surfaces are in reasonable agreement. However, closer inspection reveals that there is a slight phase difference between the oscillatory motions of each side of the tube. By the time $t = -800 \mu\text{s}$, this phase difference is 180 degrees and causes a dramatic difference between the two diametrically opposed strains. Figure 15 shows these strains more clearly using an expanded time base. At $t = -800 \mu\text{s}$, the oscillations of the one surface maximize, while those of the opposite surface are practically nonexistent. It is believed that such a result can only be explained by the presence of beamlike vibrations in addition to the axisymmetric vibrations. This beamlike motion causes the tube wall beneath one gage to move radially outward, while that beneath the other moves radially inward. Quantitatively, if the magnitudes of the axisymmetric and beamlike modes are equal, there will be times when the sinusoidal components will add to twice the value on one side of the tube, while annihilating each other on the opposite side. This would explain Figure 15. In general, of course, beamlike motions and axisymmetric motions need not exist in equal amplitudes, and in other firings various amounts of each are evident. Thus, it is very probable that the strains induced by the passing projectile and shock front more generally consist of nonaxisymmetric as well as axisymmetric modes and that they interfere periodically in time. As previously mentioned, there must be some sort of coupling present to excite the nonaxisymmetric motions. No conclusions are drawn as to the nature of the coupling in this particular gun tube.

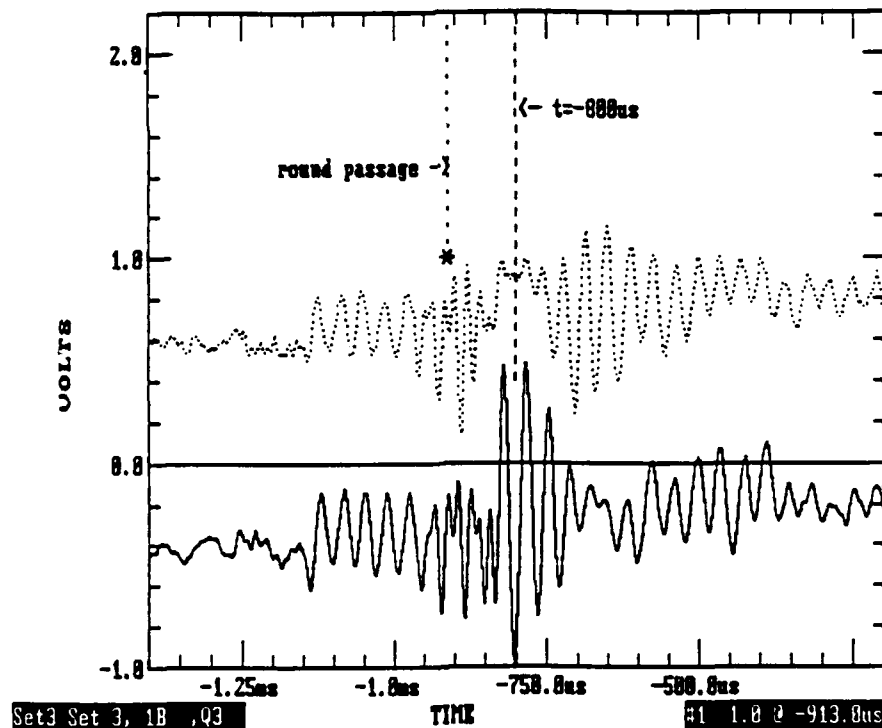


Figure 15. Figure 14 record--expanded time base.

HOW APPLICABLE ARE THE STEADY-STATE SOLUTIONS?

In all of the test firings of the 60-mm tube, the projectile enters the test section with a velocity close to critical, and the shock front enters with a velocity which is approximately 26 percent greater and therefore strongly supercritical. Under these conditions it was observed that the trailing wave associated with the shock front develops almost instantaneously and is plainly visible even at a location only six inches into the test section as shown in Figure 16. The development of the strain field associated with the motion of

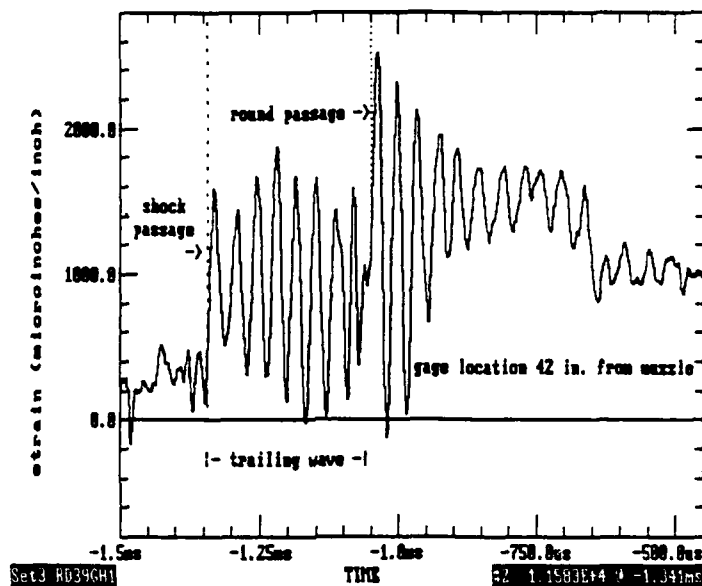


Figure 16. Circumferential strain record showing full development of wave trailing the shock front (round ID 39).

the projectile is not so easily assessed, however, owing to the interfering strains from the passage of the shock. To obtain a clearer picture, the shock front was eliminated by evacuating the tube via a vacuum pump prior to firing. This worked out very well and resulted in a sequence of strain records along the test section showing the development of the deformation caused by the moving ballistic pressure uncomplicated by the presence of the shock (Figures 17, 18, and 19). During this particular firing, the projectile has a slight acceleration through the test section so that its velocity changes from a subcritical 3860 ft/sec* to a supercritical 3984 ft/sec over a distance of two feet. (As previously mentioned, the theoretical critical velocity for axisymmetric

*Use of radar equipment to measure projectile velocity was not possible when the tube was evacuated because of the need for an expendable muzzle end cap to hold the vacuum. The velocities are average values estimated from the strain data.

deformation is 3924 ft/sec and for beamlike waves it is 3917 ft/sec.) Figure 17 shows the tube strain at a position 42 inches from the muzzle--only 6 inches into the test section where the projectile velocity is estimated to be 3860 ft/sec. The strain record closely resembles that of Figure 2--the classic steady-state deformation from critical velocity theory. As the projectile passes the next strain gage, located 30 inches from the muzzle, its velocity is estimated to be extremely close to both critical values. The strain record from this location is shown in Figure 18. A loss of symmetry is apparent, there being greater wave development following passage of the projectile than there is prior to its passage. Evidently, the trailing wave associated with supercritical velocities has started to develop. Figure 19 shows the strain at a location 18 inches from the muzzle where the velocity is estimated to be 3984 ft/sec. Further development of the trailing wave is evident. Figure 20 shows Fourier spectra of the data of Figure 19 and reveals a dominant frequency following round passage to be 35.156 kHz. The theoretical frequency of axisymmetric trailing waves corresponding to a velocity of 3983 ft/sec is 33.313 kHz. Prior to round passage, the dominant Fourier component is 42.969 kHz corresponding to a theoretical 43.485 kHz for axisymmetric head waves at this velocity. Despite the close agreement in predicted and measured frequencies, a comparison of Figure 19 with Figure 3 shows that the development of the steady-state deformation at this slightly critical velocity is far from complete.

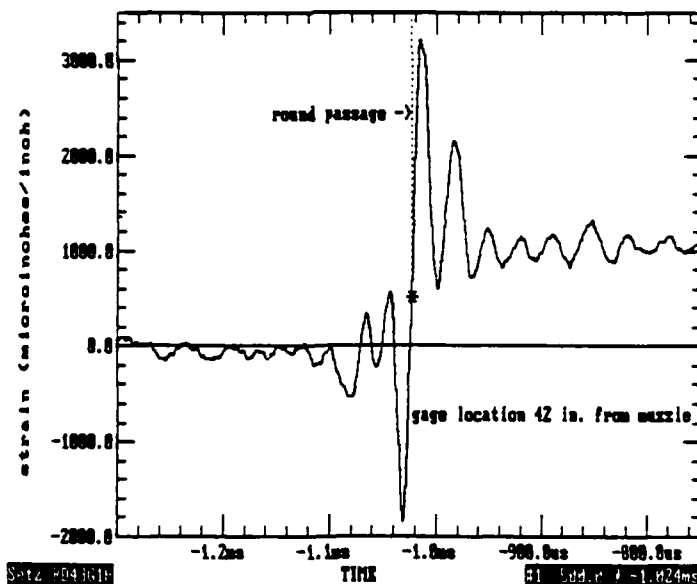


Figure 17. Circumferential strain record 42 inches from muzzle. Shock absent due to bore evacuation (round ID 43).

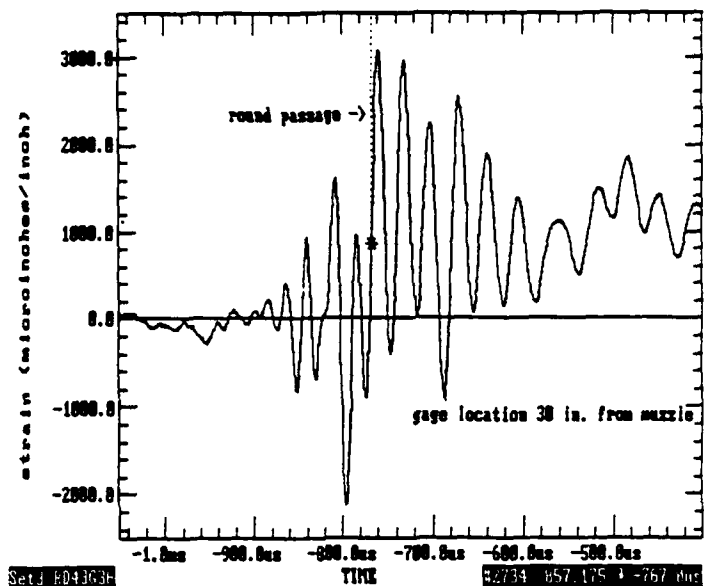


Figure 18. Circumferential strain record 30 inches from muzzle. Shock absent due to bore evacuation (round ID 43).

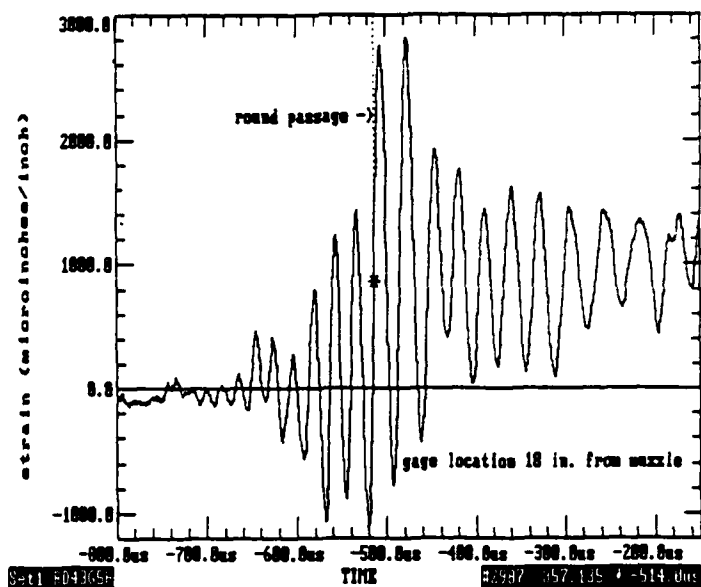


Figure 19. Circumferential strain record 18 inches from muzzle. Shock absent due to bore evacuation (round ID 43).

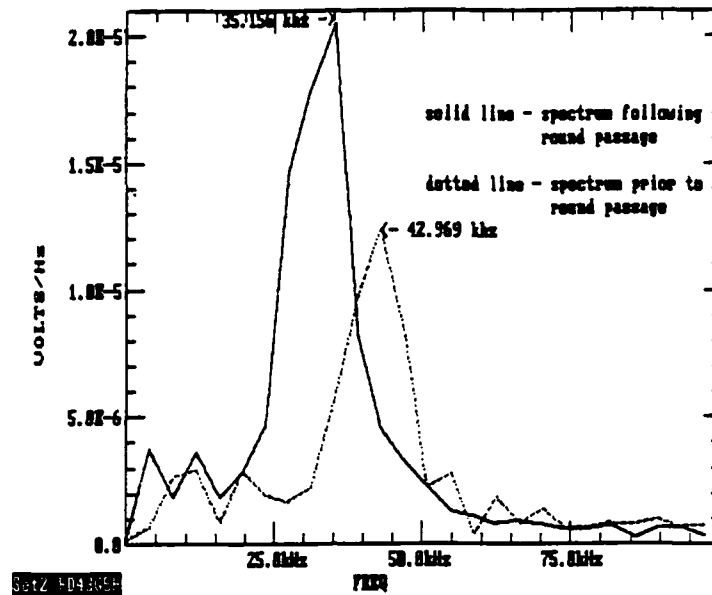


Figure 20. Fourier spectra of strain record of Figure 19 before and after round passage.

The evidence supplied by these test firings suggests that the steady-state deformation at subcritical projectile velocities (Figure 2) is established very rapidly. At velocities which are strongly supercritical (Figure 3), the development of a constant amplitude trailing wave is also very rapid. At velocities which are only slightly above critical, however, the development is much more gradual and may not even be established prior to projectile exit.

REFERENCES

1. T.E. Simkins, "Resonance of Flexural Waves in Gun Tubes," Proceedings of the Fifth U.S. Army Symposium on Gun Dynamics, ARCCB-SP-87023, 23-25 September 1987, Benet Laboratories, Watervliet, NY, pp. 64-77.
2. T.E. Simkins, "Wave Coupling and Resonance in Gun Tubes," Proceedings of the 59th Shock and Vibration Symposium, 18-20 October 1988, Albuquerque, NM; also ARCCB-TR-89008, Benet Laboratories, Watervliet, NY, March 1989.
3. T.E. Simkins, "Influence of Transient Flexural Waves on Dynamic Strains in Gun Tubes," ARCCB-TR-89020, Benet Laboratories, Watervliet, NY, August 1989.
4. S.P. Timoshenko and J.N. Goodier, Theory of Elasticity, Third Edition, McGraw-Hill, 1970, pp. 68-71.

SIMKINS, PFLEGL, STILSON

5. P.P. Radkowski, J.I. Bluhm, and O.L. Bowie (Eds.), Thick-Walled Cylinder Handbook - Stresses and Strains in Elastic, Thick-Walled Circular Cylinders Resulting From Axially Symmetric Loadings, "WAL No. 893/172, Watertown Arsenal, Watertown, NY, December 1954.
6. D.V. Shick and H.F. Tiersten, "A Variational Analysis of Resonance in Gun Tubes With Eccentric Bores," Proceedings of the Sixth U.S. Army Symposium on Gun Dynamics, ARCCB-SP-90015, 15-17 May 1990, Benet Laboratories, Watervliet, NY, pp. 175-198.
7. I. Mirsky and G. Herrmann, "Axially Symmetric Motions of Thick Cylindrical Shells," Journal of Applied Mechanics, Vol. 25, March 1958, pp. 97-102.
8. H. Reismann, "Response of a Prestressed Cylindrical Shell to Moving Pressure Load, Developments in Mechanics," in: Solid Mechanics - Proceedings of the Eighth Midwestern Mechanics Conference, Pergamon Press, Part II, Vol. 2, 1965, pp. 349-363.
9. T.E. Simkins, G.A. Pflagl, and E. Stilson, "Dynamic Strains in a 60-mm Gun Tube - An Experimental Study," ARDEC Technical Report, Benet Laboratories, Watervliet, NY, to be published.

TITLE: Modeling Gun Dynamics with Three-Dimensional Beam Elements

David A Hopkins
US Army Ballistic Research Laboratory
Aberdeen Proving Ground, Maryland 21005-5066

ABSTRACT:

The behaviour of gun systems can be determined using finite element techniques to obtain approximate solutions to the equations of continuum mechanics. However, this approach may require many hours of both human and computer time to formulate the model, and analyze the results. Models which use beam theory to describe a gun system are viable alternatives. Beam models capture the basic behavior of the gun system but require substantially less computer time to utilize. Other benefits are the ease with which geometric models can be generated, and the simplicity with which existing models can be modified to incorporate new modeling thrusts.

In this paper some basic issues in the development of a three-dimensional beam model are discussed. Application of a code implementing the method is then presented which illustrates how a tank gun system can be successfully modeled with a three-dimensional beam model. The results are compared with predictions from Dynacode-G/P, Little Rascal and with experimental data.

BIOGRAPHY:

PRESENT ASSIGNMENT: Mechanical engineer, Mechanics and Structures Branch, Internal Ballistics Division, Ballistic Research Laboratory

DEGREES HELD: M.S (Mechanical Engineering), University of Delaware, 1986;
B.S.(Aerospace Engineering), University of Florida, 1983.

Modeling Gun Dynamics with 3D Beam Elements

David A Hopkins
US Army Ballistic Research Laboratory
Aberdeen Proving Ground, Maryland 21005-5066

INTRODUCTION

The initial conditions of the free flight regime for a projectile launched from a gun tube are determined by the loads acting on the the projectile during the in-bore travel regime. Consequently, substantial research, both analytic and experimental, has been conducted in an effort to gain a basic understanding of the gun system's behaviour during the in-bore travel regime. This research has led to the development of several gun system models which are useful in predicting the launch conditions of a projectile[1,2,3]. The complexity of the gun system model appropriate in any analysis depends upon considerations of asymmetries in the gun system, detail of information desired about the gun system, the intended use of the results, and the ease of implementing the modeling technique selected. In general, the complexity of typical modeling approaches can be organized into three levels of complexity.

The simplest models conceptually are two-dimensional beam models. These models do not allow coupling between the axial, torsional, and transverse directions. Such models can provide reasonable predictions for the gun tube motion provided the coupling in the gun system between in-plane and out-of-plane motion is not significant. The Little Rascal[1] gun dynamics model is an example of this approach. The information available from this model describes the gun system's component's displacements and velocities, and the loads applied to these components. Another advantage of this model is the ease with which it is implemented. However, details concerning the stresses and strains in the components are generally not available.

The other end of the modeling spectrum is represented by complex finite element models of gun systems. The use of Dyna3d[4] in analyzing gun tube and projectile motion during the in-bore cycle illustrates the application of this approach in modeling a gun system. Models generated using this approach require substantial commitments of time and resources in both pre- and post-processing of the data and in the solution phase of the analysis. Also, while the resultant model provides desired detailed information about the local behaviour of the components, extracting information of a more general nature, such as the overall muzzle motion of a gun tube, can be difficult.

Three-dimensional beam models provide a bridge between these two approaches. A standard characteristic of these models is the allowance of six degrees of freedom (DOF) in the motion of the

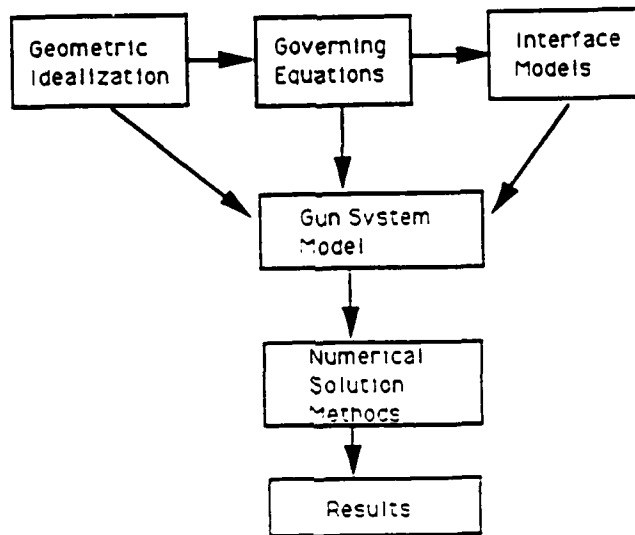


Figure 1: Modeling Process

gun system: three translational and three rotational. Like two-dimensional beam models, three-dimensional beam models are simple to develop and employ. However, they are also capable of modeling coupling between the displacements and rotations of the components of the gun system that is not allowed in the two-dimensional models. This is done in two ways. First, the *equations of motion* may be coupled by the selection of a particular beam theory. Second, the interface models which describe the interactions between gun system components may result in in-plane displacements causing out-of-plane loads. Such coupling can be important in determining how interactions between gun system components affect overall gun system performance. This paper describes the development process of a three-dimensional beam model.

MODELING PROCESS

A broad overview of the modeling process is shown in figure 1. The first phase involves modeling the gun system's geometry. This requires deciding upon an appropriate idealization of the actual geometry which allows the determination of physical quantities that are of interest in the analysis. In the second phase, the form of the governing equations for the model which either uses or specifies these quantities are developed. The third phase concerns the development of the loading models. These loading models describe the interaction between the components of the gun system. Such loading models are typically very specific to a given gun system. Consequently, while the geometric model and the governing equations may apply to a wide range of systems, the loading models will restrict the application of the resultant gun system model to a particular system. The geometric representation of the gun system, the governing equations, and the loading models, are combined to generate a mathematical model of the gun system in the fourth phase. Solution of the equations of the mathematical model is done in the fifth phase. Finally, the analysis of the results from the solution of the mathematical model constitutes the sixth phase. In this hierarchy, each phase determines the options available in the next phase. For instance, the decision on how the

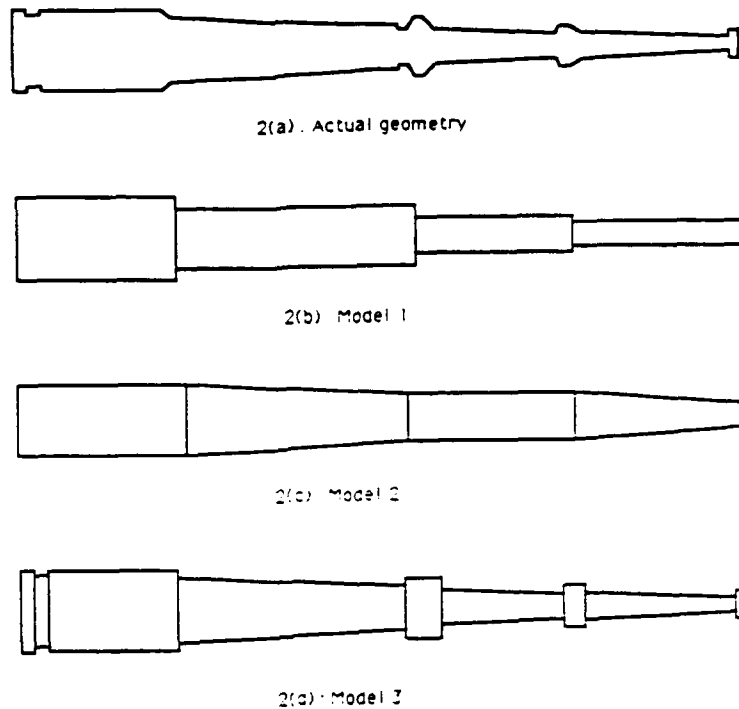


Figure 2: Gun Tube Representations

gun system geometry will be modeled influences the form of the governing equations which can be used. In the following sections, each of these phases is discussed in more detail. The goal of this process is the development of a modeling approach applicable in a three-dimensional beam model.

GEOMETRY

The first step in the modeling process is the selection of an appropriate geometric idealization for each component of the gun system. Consider a fictitious gun tube represented by figure 2(a). The actual geometry of the tube can be idealized in several ways, which are shown in figures 2(b), 2(c), and 2(d). These figures will be referred to as models 1, 2, and 3, respectively. In this paper, the type of elements allowable in modeling the gun tube is restricted to the use of beam-type elements. The decision means the geometric variables which may needed to describe the system are

- A: Cross-sectional area
- L: Length of the beam segment
- x_i : a set of parameters describing the shape of the cross-section
- I_{xx}, I_{yy}, I_{zz} : the planar moments of inertia of the cross-section
- P_{xy}, P_{xz}, P_{yz} : the planar products of inertia of the cross-section

HOPKINS

All of these properties can be used as input. However, since the area and the planar moments of inertia can be determined from the parameters L and x_i , they are not required as input data.

In model 1, the tube is represented as four interconnected beam segments. Each segment is assumed to have constant cross-sectional properties. The use of constant cross-sectional properties, such as the area, means that these properties will generally be discontinuous between adjacent beam segments. Consequently, another representation of the gun tube is shown in model 2. Again the tube is modeled by four beam segments, but now a linearly tapered beam segment is used. The use of tapered beam segments allows a more accurate representation of the gun tube. Finally, in model 3, short beam segments have been used to model the gun tube. This modeling approach may require many more segments than models 1 or 2, but will provide a better estimate of the properties of the tube. Any of these idealized geometries can be implemented in a gun system model. However, the geometry selected determines the appropriate form of the governing differential equations of motion which are used to describe the gun system.

GOVERNING EQUATIONS

In this phase, the governing differential equations for the model are determined. In the beam model to be developed, six degrees of freedom (DOF), three translational and three rotational, are desired. The form of the governing equations is further restricted by the geometric model selected in phase 1. Each of the idealized models presented results in a different set of governing equations.

For model 1, Bernoulli-Euler (B-E) beam theory with constant coefficients is sufficient. This theory is the simplest available which allows six DOF. This theory can also be used for model 2 simply by allowing variable coefficients in the governing equations. For both models, the equations of motion can be written

$$\frac{\partial}{\partial x}(EA \frac{\partial u}{\partial x}) = \rho A \frac{\partial^2 u}{\partial t^2} \quad (1)$$

$$\frac{\partial}{\partial x}(GJ_p \frac{\partial \theta}{\partial x}) = \rho J_p \frac{\partial^2 \theta}{\partial t^2} \quad (2)$$

$$\frac{\partial^2}{\partial x^2}(EI_{yy} \frac{\partial^2 w}{\partial x^2}) + (EI_{yz} \frac{\partial^2 v}{\partial x^2}) = -\rho A \frac{\partial^2 w}{\partial t^2} + p_w(x, t) \quad (3)$$

$$\frac{\partial^2}{\partial x^2}(EI_{zz} \frac{\partial^2 v}{\partial x^2}) + (EI_{yz} \frac{\partial^2 w}{\partial x^2}) = -\rho A \frac{\partial^2 v}{\partial t^2} + p_v(x, t) \quad (4)$$

where the coefficients may be functions of the axial coordinate x .

Model 3, though, uses short beam segments. Consequently, a beam theory which includes transverse shear effects is more appropriate than B - E theory. Simple Timoshenko beam theory is an example of a beam theory that may be used to describe the transverse equations of motion[5]. This would include the effects of the transverse shear without overly complicating the governing equations. The axial and torsional equations of motion would not change. Experience and experiments indicate that for a gun tube, B - E theory provides an adequate representation of the tube. Because of this, model 3 will not be considered further. Instead, discussion is limited to the use of B - E theory in modeling a gun system.

HOPKINS

Examining equations 1 - 4, it is seen that the axial and torsional equations of motion are uncoupled both from each other and from the transverse equations of motion. Furthermore, if the coordinate system is selected such that the axes are principle axes, then the equations of motion in the transverse directions are also uncoupled. Since gun tubes typically have circular cross-sections, the transverse equations will normally not be coupled through the left - hand sides. These equations therefore reduce to four uncoupled linear differential equations which describe the motion of a beam segment. If needed, a variant of B - E theory has been formulated in which the divergence of the bore centerline from a straight line is considered[6]. The equations of motion resulting from this approach are fully coupled even when the axes are principle axes. This beam theory can be used for either model 1 or 2. Use of this theory requires the description of the actual tube centerline in the model description. For the eccentricities of typical gun tube centerlines, the increase in predictive capability does not at present justify the use of these more complex governing equations in a gun dynamics model.

Finally, note that the equations of motion to be used are in a sense not necessarily three-dimensional. Although they allow six DOF, the equations presented reduce to two one-dimensional equations of motion in the axial and torsional displacements, and two two-dimensional equations of motion in the transverse displacements. What then justifies calling this model a true three-dimensional model? This question is answered by considering the form of the interface models which describe how the gun system components interact.

INTERFACE MODELS

The purpose of an interface model is to describe how either the separate components of a gun system, such as the gun tube and projectile, interact, or how external loads are applied to a particular gun system component. These loading routines determine the right-hand sides of equations 1 - 4, the loading functions. For either model 1 or model 2, these interface models are thus the only possible source of three - dimensional coupling since these equations are otherwise uncoupled.

It is beyond the scope of this paper to fully derive a detailed interface model. However, a simplistic model of gun tube/projectile interaction due to balloting is easily formulated which does illustrate the difference between two and three-dimensional interface models. Balloting occurs when the diameter of the bourellet of a kinetic energy projectile is smaller than the inside diameter of the gun tube through which it is fired. A simple model of the bourellet is to replace the bourellet by a linear spring as depicted in figure 3. Ballotting is then modeled by allowing a finite relative displacement between the gun tube and projectile before the spring, which is assumed connected to the projectile, contacts the tube. This simple model is directly applicable in the two-dimensional case. However, in the three-dimensional case a slight modification is introduced as illustrated in figure 4.

In the three-dimensional model, the single spring used in the two-dimensional case is replaced by a set of radial springs each of which represents the stiffness of the bourellet in that radial direction.

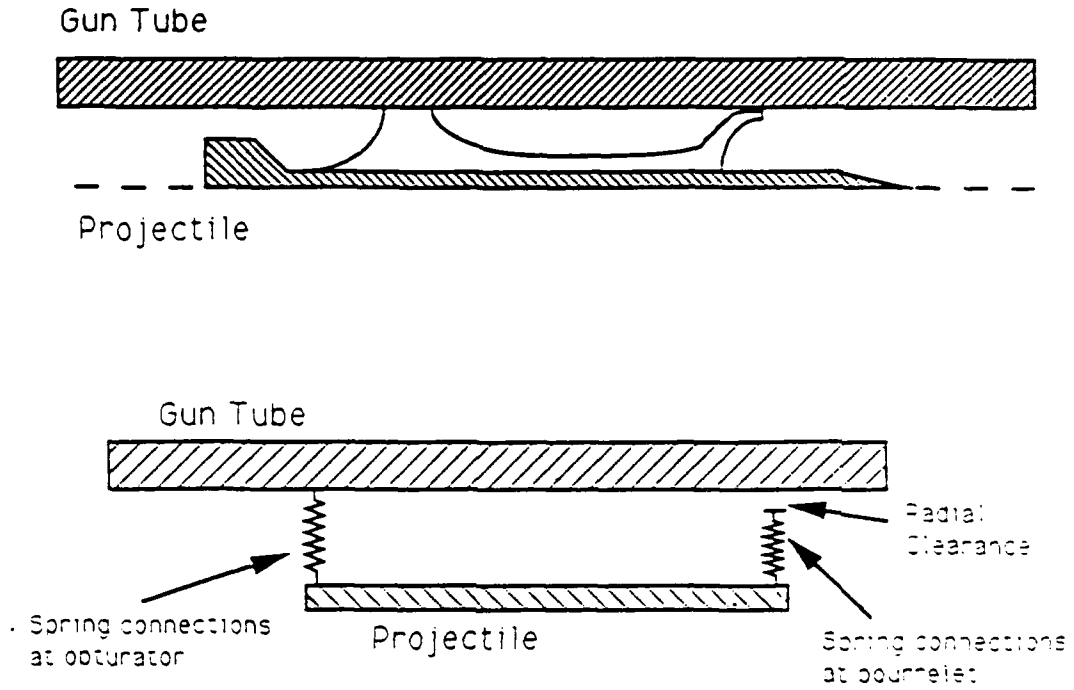


Figure 3: Simple Balloting Model for Gun Tube/Projectile Interaction

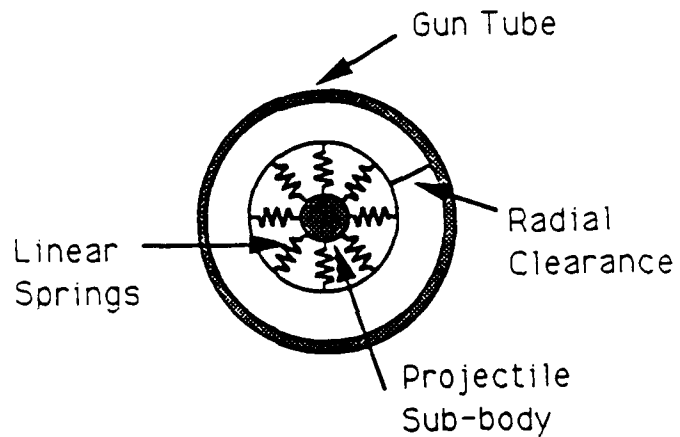


Figure 4: Three-dimensional Balloting Model

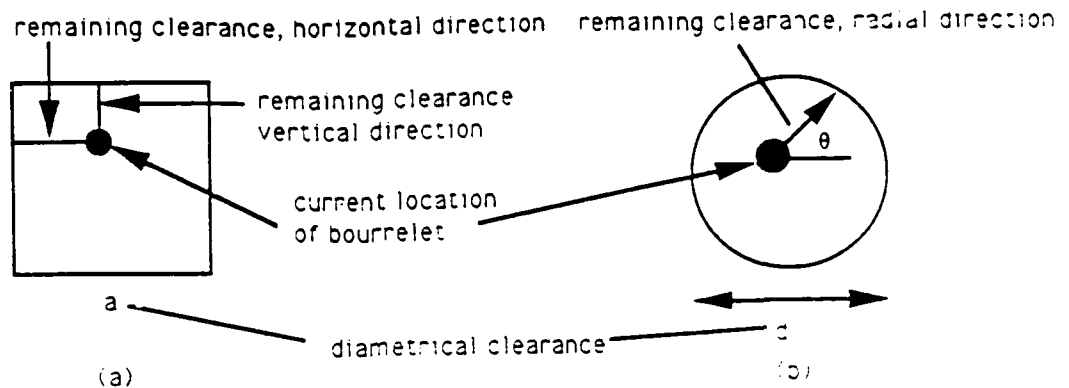


Figure 5: Geometric Representation of Impact Criterion

Impact between the bourellet and the gun tube is defined to occur when the difference between the displacements of the gun tube and the projectile is greater than the clearance remaining in the direction in which the projectile displaces. In the two-dimensional model, this impact criterion can be written

$$|w_p - w_t| > \delta_r$$

where w_t and w_p are the transverse displacements of the gun tube and projectile respectively, and δ_r is the remaining clearance in the direction in which the projectile is displaced. Since the model is two-dimensional, the projectile and tube can only displace in one plane at a time. Consequently, the criterion for detecting when balloting occurs is decoupled between the transverse planes. This means that the impact criterion can be visualized as operating on a square with the length of each side equal to the maximum diametrical clearance. This impact criterion is presented in figure 5a.

Now consider the three-dimensional model. For this model, the displacement of the projectile is given by

$$\delta_p = v_p \mathbf{j} + w_p \mathbf{k}$$

and the displacement of the gun tube is given by

$$\delta_t = v_t \mathbf{j} + w_t \mathbf{k}$$

The impact criterion for the three-dimensional model is

$$|\delta_t - \delta_p| = \sqrt{(v_t - v_p)^2 + (w_t - w_p)^2} > \delta_r$$

where δ_r is again the remaining clearance in the direction given by

$$\theta = \arctan\left(\frac{w_t - w_p}{v_t - v_p}\right)$$

However, now the equation for the impact criterion represents a circle whose maximum diameter is the diametrical clearance, figure 5b. It is seen that this simple model requires that motion in

HOPKINS

both transverse planes must be considered when determining if impact has occurred. This coupling of the transverse planes in the impact criterion is the justification for calling models 1 and 2 three-dimensional beam models.

Another interface model, which couples the axial and torsional motion with the transverse equations of motion through the loading function, is the effect of axial displacements on offset masses. Because of the equations of motion for an offset mass, axial accelerations will generate moments causing out-of-plane forces and displacements. Thus the combination of the above simple balloting model and the effect of offset masses serves to fully couple the equations of motion for the gun system through the loading functions.

GUN SYSTEM MODEL

The preceding three phases of model development are repeated for each component of the gun system which is to be included in a gun system model. Complete models for different gun systems are then obtained by combining the component models. Typically, the gun system models thus generated can be very system specific.

In the above methodology, only the development of the loading functions determines which gun system is being modeled. Therefore, if it is desired to develop a gun system model which is as generic as possible, then the loading functions should be formulated which are not interdependent. This means that use of one interface routine should not require the use of other interface routines. If care is taken to insure that such interdependencies are eliminated the resultant gun system model will be as general as possible.

SOLUTION

In most cases, it is not feasible to attempt an analytic solution of the equations of motion describing the gun system and numerical solutions must be sought. The finite element method is one of several techniques which can be used to obtain numerical solutions of the governing equations. Application of this method to the model developed leads to a set of governing differential equations which can be expressed in matrix form as

$$M\ddot{x} + Kx = F(x,t) \quad (5)$$

There are numerous numerical integration schemes available to solve this set of equations. Selection of an appropriate scheme depends upon the specific form of the coefficient matrices M and K , as well as the method by which the loads $F(x,t)$ are determined. These integration techniques are discussed in detail elsewhere[7]. The solution of these equations provides the time response of a gun system to a set of applied loads or interactions. In the next section, the proposed gun modeling approach is implemented to examine the behaviour of a large caliber tank gun system.

HOPKINS

RESULTS

The modeling approach discussed has been incorporated into a gun dynamics program called Shogun. The geometric model selected for each system component allows tapered beam elements and thus corresponds to model 2. The corresponding governing equations are therefore given by equations 1 - 4 with variable coefficients. This model can be used to examine the effects of a variety of gun system parameters including gun tube/projectile interaction, the effect of breech c.g. offset, and the effect of tube curvature. The loading routines used at this time restrict application of the model to the 120mm tank gun system. The results presented in this paper are the model's predictions for tube shape in the transverse planes at shot exit. These predictions are compared with experimental results and results obtained using Little Rascal, Dynacode - G/P. The methods for obtaining the experimental data are described by Bornstein, et al [8].

The gun dynamics codes selected for comparison use B - E theory to describe the gun system components. Little Rascal and Dynacode - G/P use constant cross-section properties while Shogun allows variable cross-section properties for each beam segment. Other differences between Shogun and Dynacode - G/P include the formulation of the mass and stiffness matrices, the type of geometric information required to describe the gun system, and the treatment of offset mass effects such as the effect of the breech center of gravity location.

In figure 6, the predictions for the tube shape at shot exit in the vertical plane for a particular tube, denoted tube A, are presented. All three codes agree well with the experimental data. It is difficult to say if any one of the codes is better or worse than the others. The close agreement between the predictions of Shogun and Dynacode - G/P is expected since they use similar governing equations and loading models. The differences are due to differences in the geometry descriptions and in the implementation of the loading models. The close agreement with Little Rascal indicates that the dynamic motion of the 120mm gun system is basically uncoupled in the transverse directions. This lends confidence to the use of simple B - E beam theory as the governing equations.

The predictions for the tube shape in the horizontal direction are shown in figure 7. Here the agreement with experimental data is not as good. It is hypothesized that the actual boundary conditions imposed on the motion of the breech in the horizontal direction have not been adequately modeled by any of the codes selected. All three codes do, however, predict the same basic shape. This further re-inforces the conclusion that the motion in the two transverse planes is uncoupled in this gun system.

Finally, in figure 8, the predicted tube shape in the vertical plane for a tube with a different centerline profile is presented. Again, all codes agree well with each other and with experimental data. However, comparison of figures 6 and 8 shows that different responses between tubes are expected due to the effect of the tube centerline profiles.

Tube A

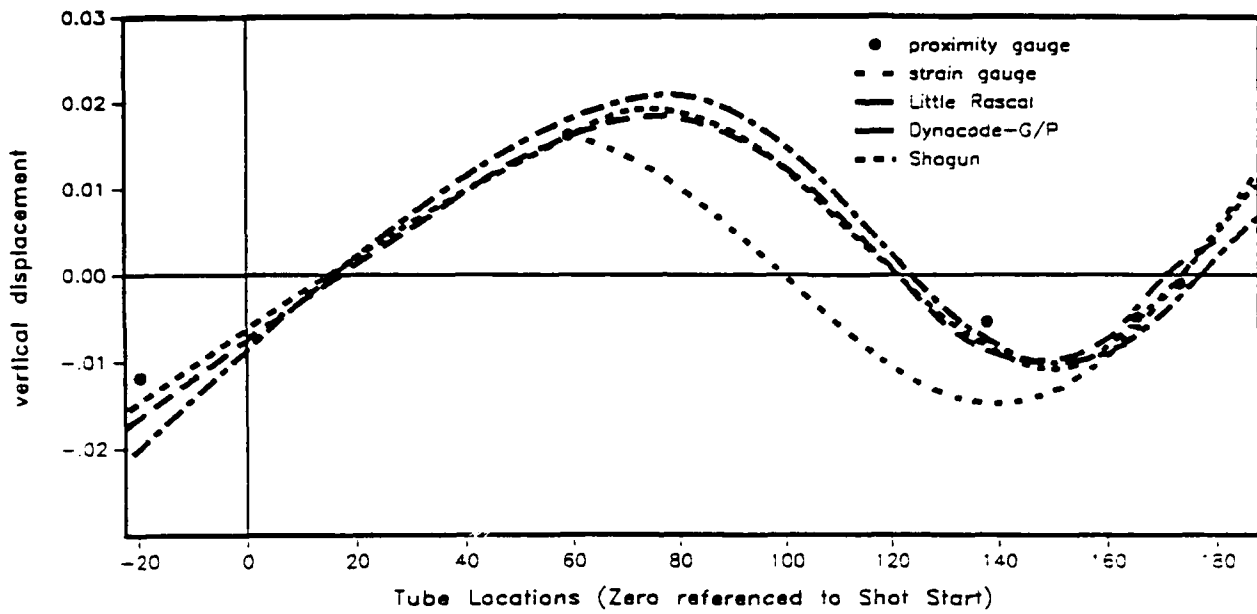


Figure 6: Tube Shape in the Vertical Plane

Tube A

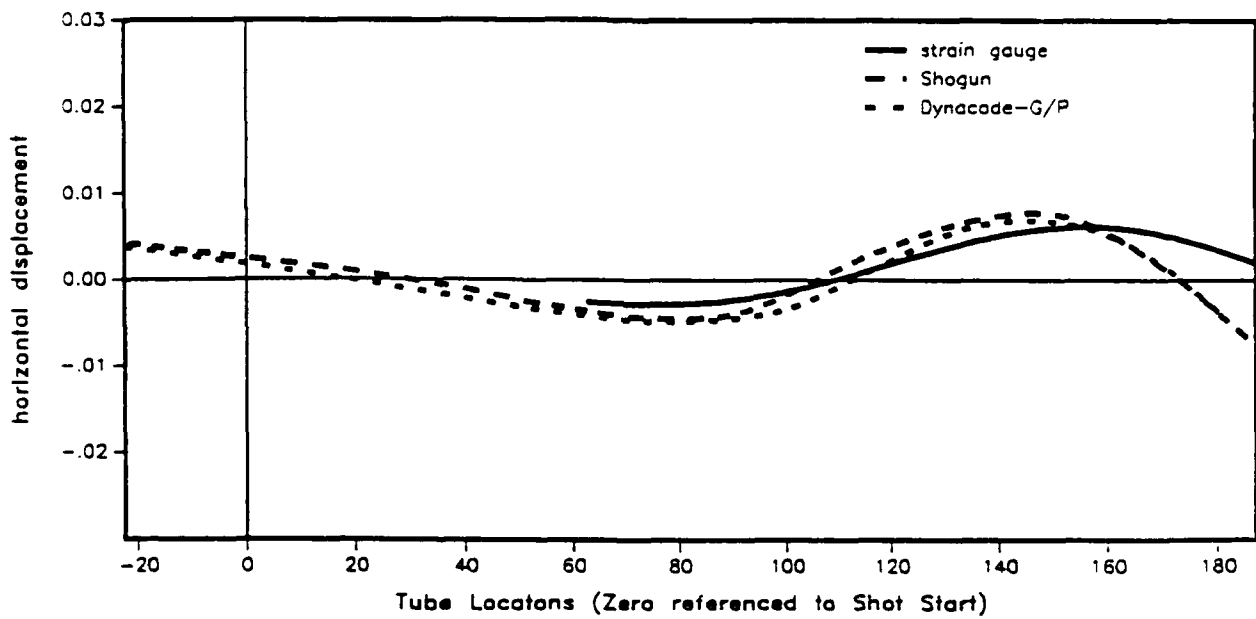


Figure 7: Tube Shape in the Horizontal Plane

Tube B

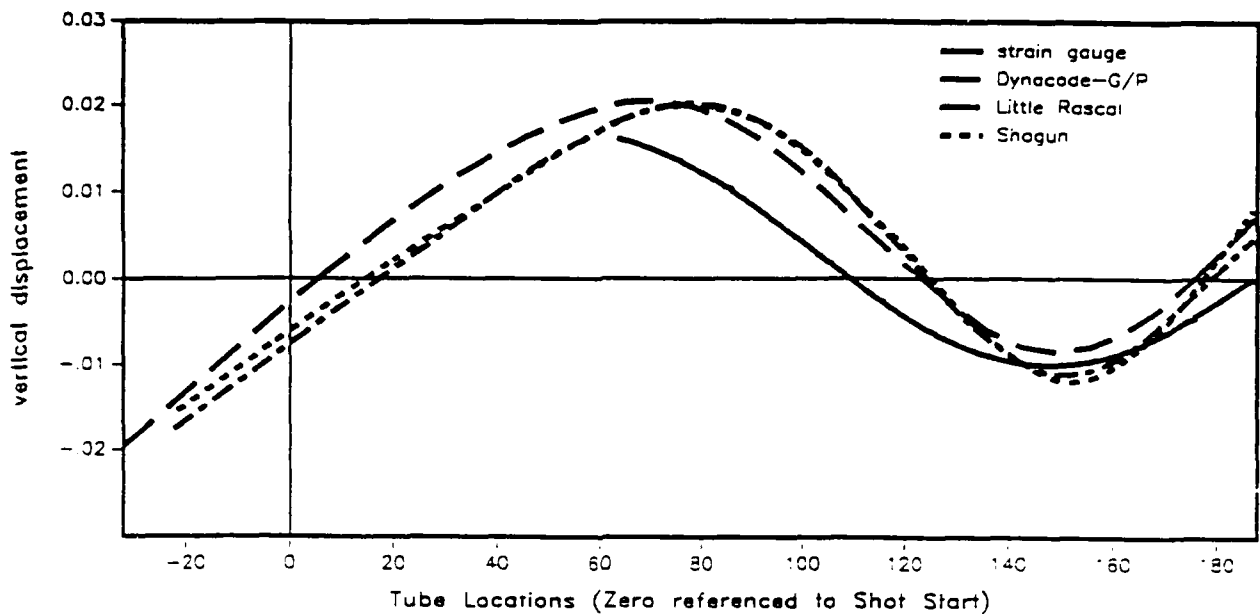


Figure 8: Tube Shape in Vertical Plane. Tube B

CONCLUSIONS

A modeling approach for developing three-dimensional beam models of gun systems has been briefly outlined. It has been shown that there are not any significant conceptual problems associated with developing these types of models. This modeling approach was incorporated into a gun dynamics program called Shogun. Comparisons of Shogun with other models indicates that this approach to modeling gun tube dynamics can provide useful qualitative predictions of the effects of various gun system parameters.

REFERENCES

1. Erline, Thomas, and Mark D. Kregel, "Modeling Gun Dynamics with Dominant Loads." BRL Memorandum Report No. 3683, U.S. Army Ballistic Research Laboratory, Aberdeen Proving Ground, Md, July 1988.
2. Soifer, Martin and Robert Becker, "Dynamic Analysis of the 120mm Tank Gun." BRL - CR - 576, U.S. Army Ballistic Research Laboratory, Aberdeen Proving Ground, Md, June 1987.
3. Rabern, Donald A. and Kenneth A. Bannister, "Full 3-D Transient Simulations of 120mm Tank Gun Firings." To be presented at the Sixth U. S. Army Symposium on Gun Dynamics, 14-17 May, 1990.

HOPKINS

4. Hallquist, John, "Theoretical Manual for DYNA3D." Lawrence Livermore National Laboratory, Livermore, Ca, March 1983.

5. Shames, Irving and Clive Dym, Energy and Finite Element Methods in Structural Mechanics, New York: McGraw-Hill Book Co., 1985.

6. Kingsbury H.B., "A Reexamination of the Equations of Motion of Curved and Twisted Rod." BRL Tech Report, U.S. Army Ballistic Research Laboratory, Aberdeen Proving Ground, Md, 1985.

7. Craig Roy Jr, Structural Dynamics. An Introduction to Computer Methods. New York: John Wiley and Sons, 1981.

8. Bornstein, Jonathan A., and Bailey T. Haug, "Gun Dynamics Measurements for Tank Gun Systems." BRL Memorandum Report No. 3688. U.S. Army Ballistic Research Laboratory. Aberdeen Proving Ground, Md. May. 1988.

HASENBEIN, GABRIELE, FINLAYSON,
ARTUS, CUNNINGHAM, GAST

TITLE: DYNAMIC STRAIN WAVES - A DEVELOPMENT PERSPECTIVE
R. HASENBEIN, A. GABRIELE, D. FINLAYSON, B. ARTUS, G. CUNNINGHAM,
AND R. GAST
U.S. ARMY ARMAMENT RESEARCH, DEVELOPMENT, AND ENGINEERING CENTER
CLOSE COMBAT ARMAMENTS CENTER
BENET LABORATORIES
WATERVLIET, NY 12189-4050

ABSTRACT:

A discussion of dynamic strain waves in large caliber cannon tubes and an extensive analytical treatment of this phenomenon was previously presented at the Fifth U.S. Army Symposium on Gun Dynamics.

This paper considers the implications these dynamic strains had on the development of a particular cannon tube, including measurement techniques which evolved during tests at the proving ground, predictive design methods which have since become standard analytical tools, and potential problems which have been identified for future study.

BIOGRAPHY:

PRESENT ASSIGNMENT: Mechanical Engineer, Systems Engineering Branch
(currently on detail to Tank Cannon Branch), Development Engineering Division,
Benet Laboratories.

DEGREES HELD: M.S. - Union College, Schenectady, NY;
B.S. - University of Rochester, Rochester, NY

HASENBEIN, GABRIELE, FINLAYSON,
ARTUS, CUNNINGHAM, GAST

DYNAMIC STRAIN WAVES - A DEVELOPMENT PERSPECTIVE

R. Hasenbein, A. Gabriele, D. Finlayson,
B. Artus, G. Cunningham, and R. Gast
U.S. Army Armament, Research, Development and Engineering Center
Close Combat Armaments Center
Benet Laboratories
Watervliet, NY 12189-4050

INTRODUCTION

A discussion of dynamic strain waves in large caliber cannon tubes and an extensive analytical treatment of this phenomenon was previously presented at the Fifth U.S. Army Symposium on Gun Dynamics [1].

This paper considers the implications these dynamic strains had on the development of a particular cannon tube, including measurement techniques which evolved during tests at the proving ground, predictive design methods which have since become standard analytical tools, and potential problems which have been identified for future study.

BACKGROUND

The 120-mm M256 cannon is the main weapon of the U.S. M1A1 Abrams Tank. This cannon was originally designed and developed by Rheinmetall in the Federal Republic of Germany, and it ranks among the most powerful tank weapons in the world. However, since its adoption by the U.S. Army into the Abrams Tank System, the armor on threat tanks has become increasingly more formidable; therefore, considerable interest existed in the mid-1980s in "upgunning" the M256 cannon simply by increasing the length of its tube (i.e., increasing its length of projectile travel in order to achieve higher muzzle velocity). The experimental tube which was envisioned to accomplish this was designated the 120-mm XM25 tube. System planners indicated a desire to make an absolute minimum of other changes to the Abrams Tank to achieve this increased firepower capability.

When the M256 cannon was integrated into the M1A1 Tank, it was a relatively easy task to balance this gun about its trunnions. This was deemed desirable since it simplified the weapon stabilization problem. However, when the tube

HASENBEIN, GABRIELE, FINLAYSON,
ARTUS, CUNNINGHAM, GAST

was extended to XM25 length using wall thicknesses similar to those in the M256 tube, designers found that a considerable imbalance resulted. For a new system design, this problem could be addressed by several methods such as the use of equilibrators, counterweights, or enhancements to the elevation/stabilization system. However, since the system guidance indicated a desire to make minimum changes to the existing M1A1 Abrams Tank, tube designers were left with the primary responsibility for minimizing the imbalance. It was quickly realized that, in the design of this conventional all-steel tube, the only method of accomplishing this was to reduce wall thicknesses towards the muzzle end to values less than the previous design practice might have deemed judicious. System planners, however, indicated that the higher risk of doing so would be acceptable for this experimental tube and urged that this approach be taken.

As expected, when the wall thicknesses towards the muzzle end of the XM25 tube were decreased, calculated stresses and strains increased since there was less material to contain the same amount of pressure. While it appeared that these values would be acceptable from a single-shot strength viewpoint, concern arose that the critical fatigue zone in the tube might shift from the chamber area to the muzzle. As a result, fracture mechanics and fatigue experts in Benet's Research Division were consulted, and they made appropriate recommendations for laboratory testing in the forward tube sections. At the same time, however, they warned that significantly reducing tube wall thicknesses near the muzzle could result in unknown end effects and loading patterns which might increase strains beyond those which might otherwise be predicted. Their considered advice that the muzzle end of the tube be studied intensively during engineering tests began the process which led to the later identification of the dynamic strain phenomenon.

PROVING GROUND TEST METHODOLOGY

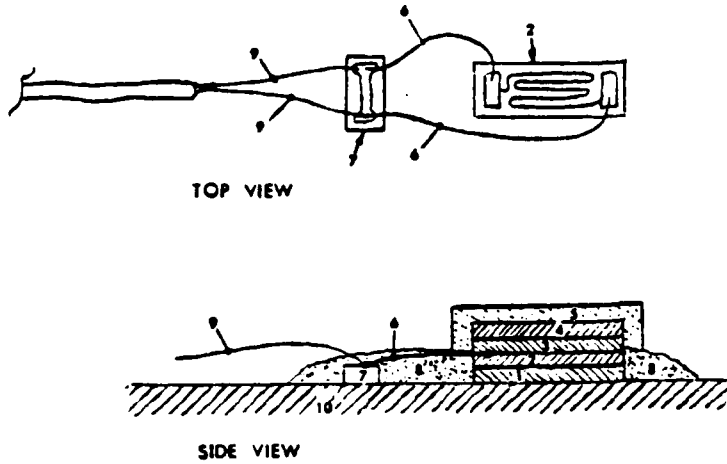
The 120-mm XM25 tube (Figure 1) was subsequently designed with wall thicknesses towards the muzzle end as low as 12.7 mm; for reference, the minimum wall thickness of the M256 tube is 17.0 mm (1/3 greater). After the tube was fabricated by the Watervliet Arsenal (NY), it was shipped to Aberdeen Proving Ground (APG) (MD) for engineering tests under the direction of the Combat Systems Test Activity (CSTA). Test plans requested that multiple strain gages (oriented both circumferentially and longitudinally) be placed at several axial locations on the tube from the bore evacuator to the muzzle and that available DM13 APFSDS-T cartridges be utilized when firing. During the initial stages of the test, considerable difficulty was encountered simply keeping the gages attached to the tube, particularly those located towards the muzzle. After a period of experimentation by CSTA, however, a satisfactory application procedure was determined (shown schematically in Figure 2). Subsequent results obtained when firing the DM13 cartridge produced "strain versus time" traces (an example is shown in Figure 3) which contained what appeared to be anomalies. For example, severe peaks were present in the strain signals well beyond those which would be predicted using equations of statics. Further, significant compressive

XM25

Figure 1. 120-mm XM25 tube.



HASENBEIN, GABRIELE, FINLAYSON,
 ARTUS, CUNNINGHAM, GAST



- | | |
|-----|--|
| 1. | M-BOND 610 |
| 2. | MICROMEASUREMENT STRAIN GAGE (EA-06-250BF-350) |
| 3. | RUBBER PAD |
| 4. | FOAM RUBBER SPONGE |
| 5. | GUM TAPE |
| 6. | SINGLE STRAND OF WIRE |
| 7. | TABSTRIP |
| 8. | M-COAT |
| 9. | WIRE FROM CABLE |
| 10. | CANNON TUBE |

Figure 2. Strain gage application to tube.

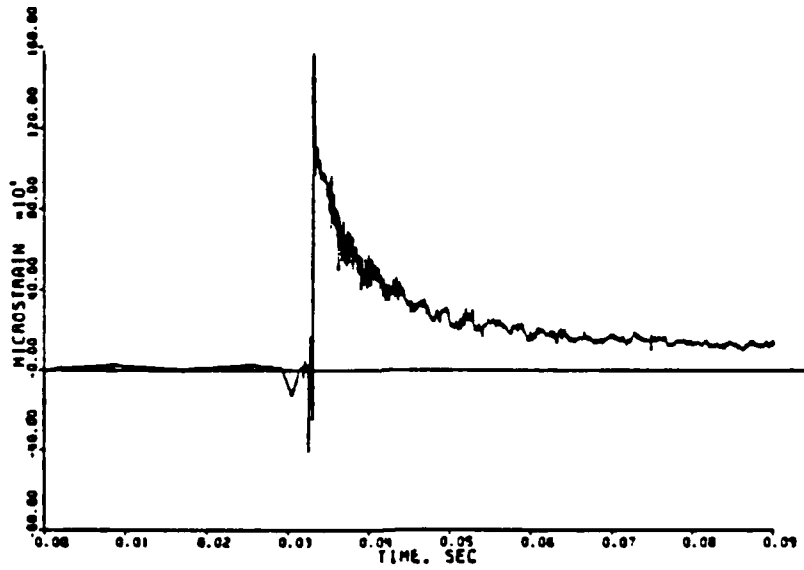


Figure 3. Initial strain versus time trace.

HASENBEIN, GABRIELE, FINLAYSON,
ARTUS, CUNNINGHAM, GAST

circumferential strains were observed as the projectile approached the strain gage locations. And finally, longitudinal strain gage results generally oscillated about "zero strain," but at amplitudes which approached those of the circumferential strain gages.

Two significant observations were made at this early juncture of the test. First, it was noted that when firing the high speed DM13 round, the lack of agreement between observed peak strains and calculated strains decreased significantly in the rearward gage locations (where projectile velocity is lower). Second, when a lower velocity M831 HEAT-TP cartridge was fired (grateful acknowledgement should be given to Mr. Clyde Musick, CSTA Test Director, for this suggestion), there was much better agreement between predicted and experimental results at all gage locations. These two observations led designers to plot "strain amplification (defined as "peak strains measured by the gages divided by calculated static strain") versus projectile velocity;" (at that gage location) for the two different cartridges. The resulting curve seemed somewhat well-behaved, the ratio being approximately 1.1 at lower velocities and increasing monotonically to approximately 4 as projectile velocity increased. This provided the first clue that the phenomenon might be somehow related to projectile velocity.

Dynamicists in Benet's Research Division were asked to consider whether the observed data were the result of an actual physical phenomenon or simply an instrumentation problem. Their subsequent closed-form analytical efforts (which were presented at the Fifth U.S. Army Symposium on Gun Dynamics [1]) revealed that the phenomenon being observed was indeed real, and they provided significant insights into its nature. Disturbingly, however, the proving ground strain traces (Figure 3) did not bear a resemblance to those predicted by the Benet researchers. After looking closely at the predicted analytical strain waves and considering the strain measuring methodology at the proving grounds, Benet researchers were able to propose two significant modifications to the latter:

- First, it was suggested that the filters being used during recording of the strain signals (10 kHz lowpass) be increased to a higher value (30 kHz lowpass), since the anticipated frequencies of the strain wave should be on the order of 15 kHz;

- Second, it was suggested that the time "window" for presentation of individual strain traces be decreased from the previous 100 milliseconds to around 5 to 10 milliseconds in order to better observe details of the wavelike nature of the strains. The time "window" should be the same for all strain gages on the entire tube for a given round:

- beginning slightly before the projectile arrives at the rearmost strain gage, and
- ending slightly after the projectile exits the tube.

HASENBEIN, GABRIELE, FINLAYSON,
ARTUS, CUNNINGHAM, GAST

The above suggestions were incorporated into the CSTA/APG firing tests, and the benefits were immediately apparent. Good correlation was noted between the analytically-predicted dynamic strain traces and those obtained from firing tests (Figure 4), including frequencies and amplitude. Moreover, specific events such as projectile passage, projectile exit from the tube, and predicted static strain could be superposed on the traces to assist with the data reduction (Figure 5).

Since that time, several additional "rules of thumb" have evolved for the conduct of dynamic strain tests at proving grounds. Best results are obtained when the test includes a wide variety of cartridge types, ranging from the slowest of those which will be fired from the tube in actual service (or training) to the fastest. In some cases it may be desirable to pre-condition the cartridge to elevated temperatures to attain the highest possible muzzle velocities. Generally, five (minimum) to ten (preferred) rounds of each type should be fired. Strain gages should be applied at several axial locations on the tube, taking care to select positions which include lower projectile velocities (e.g., slightly forward of mid-tube) as well as higher velocities towards the muzzle. Five to six axial positions are currently selected, depending on the number of available channels for recording data at the proving ground. At each of these locations, four circumferential strain gages should be attached as shown in Figure 2, taking care to locate them at precisely the same axial position. Longitudinal gages may also be used, but these are often of less general interest and are more difficult to interpret.

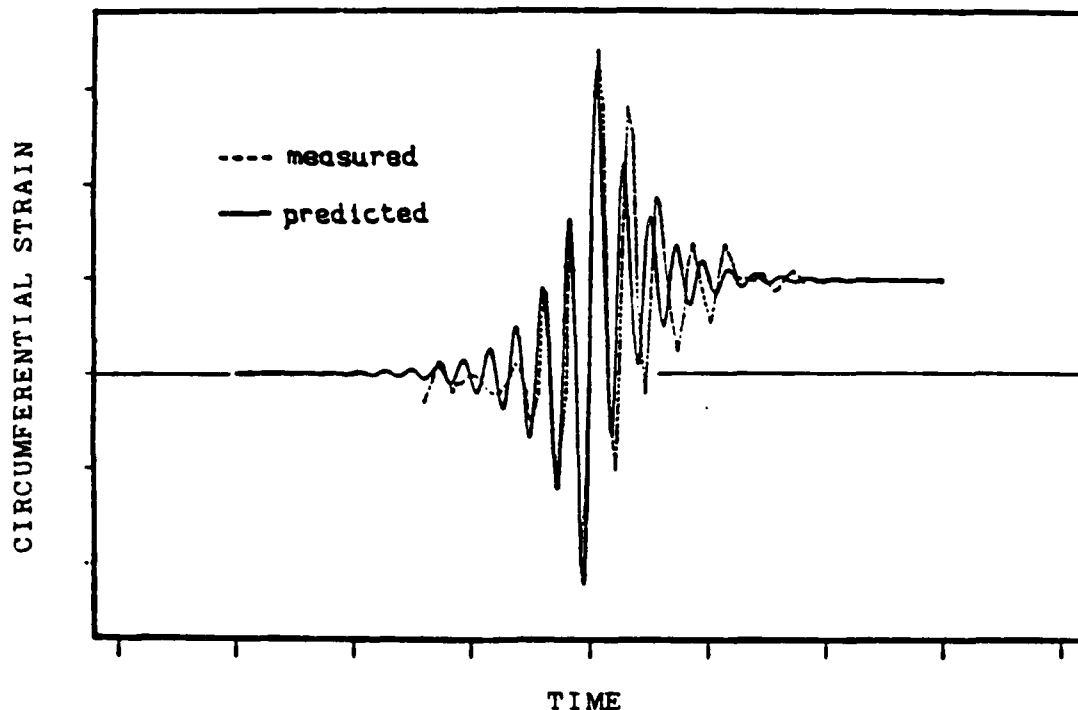


Figure 4. Correlation between strain traces
(analytical versus experimental).

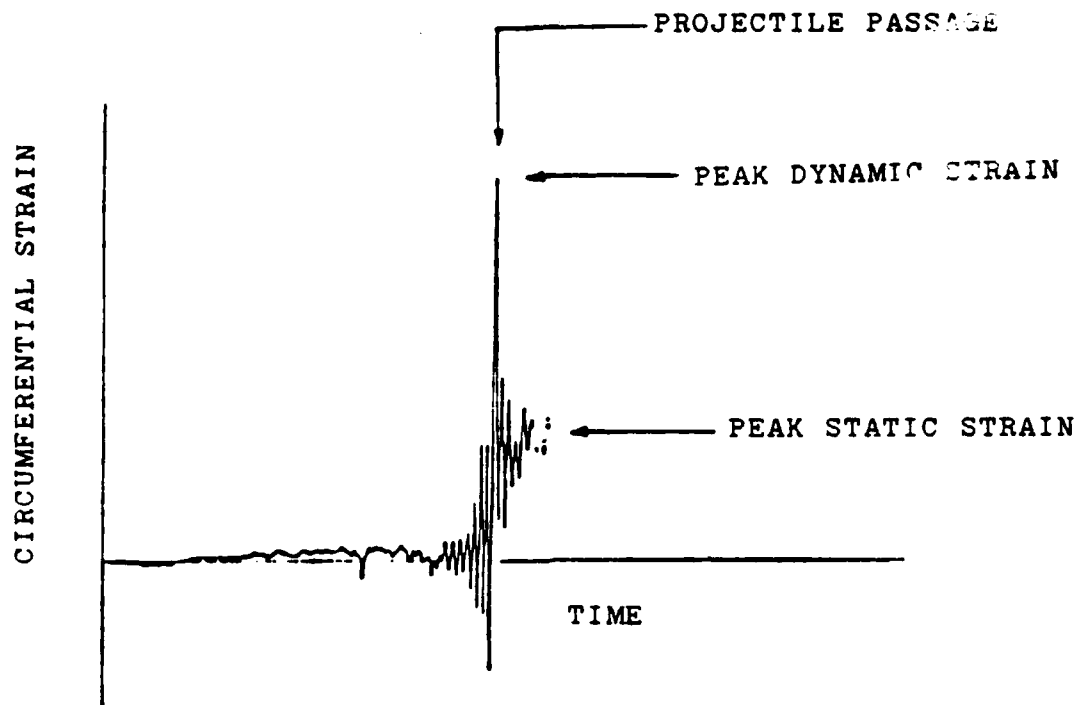


Figure 5. Dynamic strain trace with event markers.

In reducing dynamic strain data, the following procedure is now generally used:

- Determine the peak strain value at the time associated with projectile passage for each individual strain gage. In order to select the correct peak, projectile in-bore location must be known or estimated. This is done with the greatest accuracy if projectile muzzle velocity is concurrently measured during the dynamic strain test and later used to refine interior ballistic model predictions.
- In reporting the peak dynamic strain at a given axial location for any individual round fired, it is statistically best to use the average of the peak values indicated by all four strain gages. This tends to cancel out the additional strains which might be added/subtracted by bore eccentricity and axial tube flexure.
- Dynamic strain values are most simply portrayed by plotting "peak strain versus tube axial location" for each cartridge type and pre-conditioning temperature (see example in Figure 6). It is often instructive to also show the calculated static strain on the same graph. Note in Figure 6 that the results of each individual round are shown, producing a (real) array of possible results. Mean values (for later comparison with analytical predictions) and standard deviations (which increase significantly towards the muzzle) are also often calculated for the entire group of 5 to 10 rounds and displayed on a similar graph.

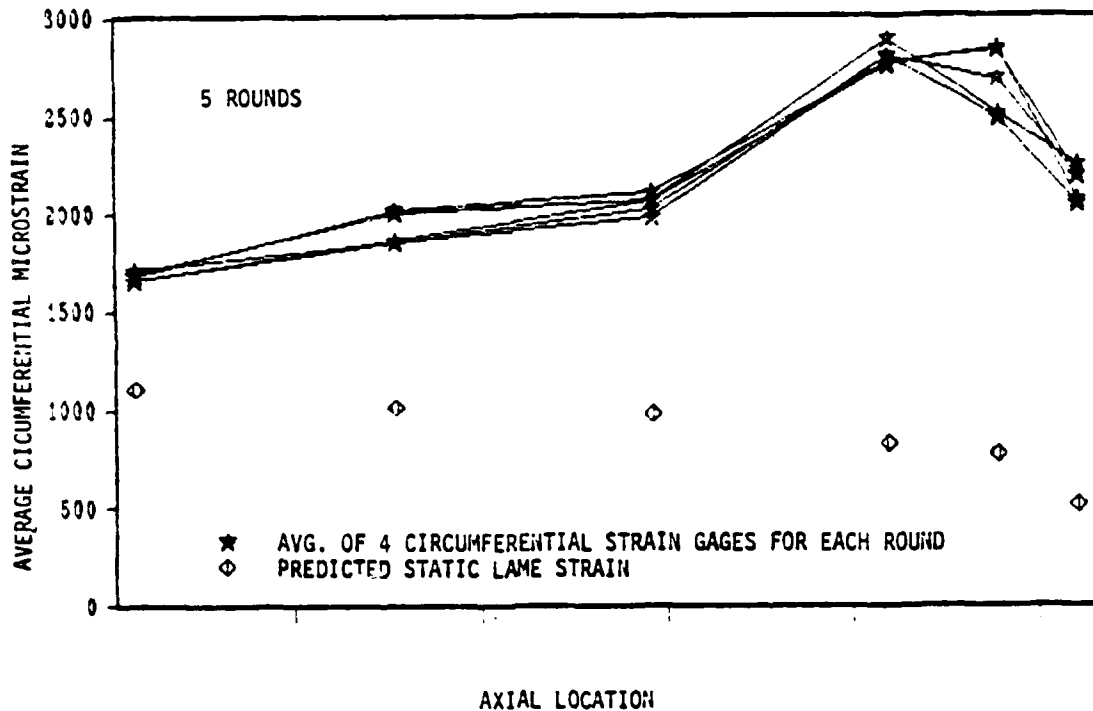


Figure 6. Typical graph of "peak dynamic strain versus tube axial position."

- Also of interest are plots of "dynamic strain amplification versus tube axial position" for each cartridge type and pre-conditioning temperature. Again, strain amplification is defined as the peak dynamic strain divided by the calculated static strain at that location and pressure. Figure 7 shows an example of this type of plot, and it is based on the mean dynamic strain value at each of the axial locations.

- A significant additional output of a dynamic strain test is a plot of "dynamic strain amplifications versus projectile velocity." One benefit of this type of curve is that the results from all cartridge types and pre-conditioning temperatures may be combined into one figure. The disadvantage, of course, is that projectile velocities are often classified, thereby limiting the opportunities for presentation of these types of results.

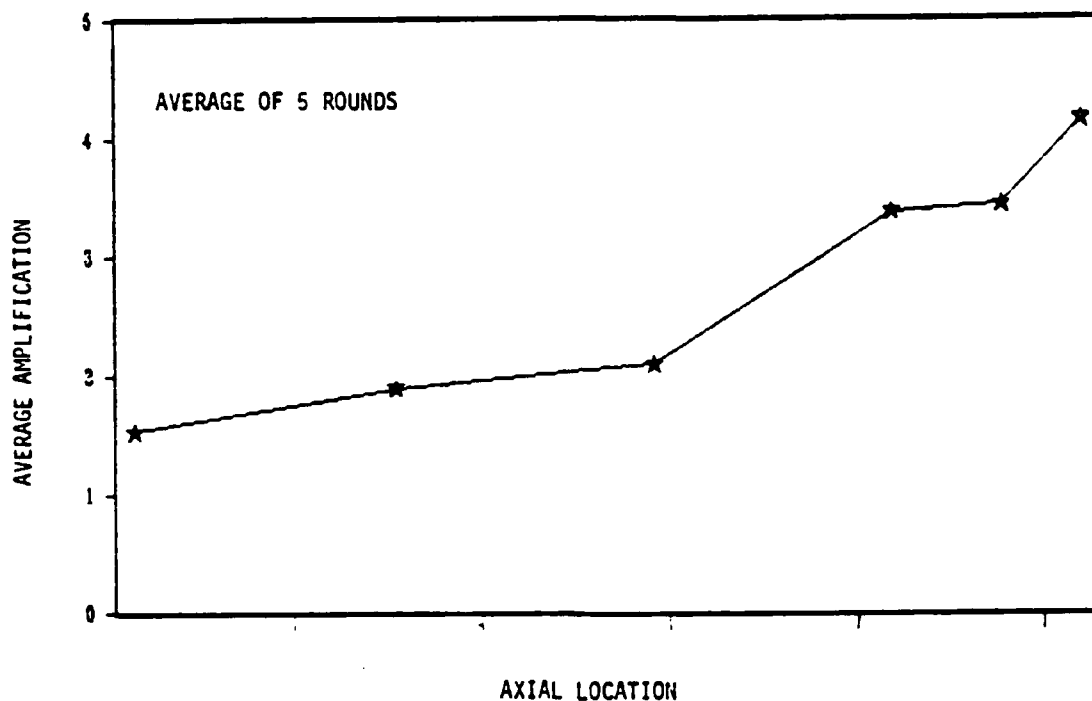


Figure 7. Typical graph of "dynamic strain amplification versus tube axial position."

FINITE ELEMENT ANALYSIS

Apart from understanding the phenomenon of dynamic strains and being able to test for them, it is important for tube designers to have at their disposal techniques for analysis of dynamic strains during the design phases prior to manufacture. The algorithms must be specifically geared towards the actual tube geometry and the array of ammunition (either existing or envisioned) to be fired through it. A satisfactory methodology for doing this has evolved which has two separate steps:

- First, the loading conditions on the tube must be determined (specifically, the applied pressure and the projectile velocity). To accomplish this step, appropriate data are supplied as inputs to an interior ballistics computer code, and output files containing the following information are created (both being functions of time):

- pressure in the bore at the base of the projectile;
- axial location of the projectile.

HASENBEIN, GABRIELE, FINLAYSON,
ARTUS, CUNNINGHAM, GAST

• Second, the data files generated in the ballistic analysis above are used as inputs into a dynamic finite element analysis (FEA). An axisymmetric gridwork which duplicates the interior and exterior diameters of the cannon tube is created for use with a non-linear finite element code capable of performing dynamic analyses (such as ABAQUS). Although this type of FEA is potentially large in scale, it can be performed in a timely manner using a supercomputer. Results produced using this technique have compared quite favorably with strain gage data from proving ground tests. A typical output graph of "circumferential strain versus time" is shown in Figure 8 and one of "peak dynamic strain versus tube axial position" is shown in Figure 9.

This analytical method can provide additional insights regarding a given tube's dynamic response in areas where actual measurements are either difficult or impossible (for example, at the extreme muzzle of the tube, at the bore, or within the walls of the tube). Outputs can also be used to create video animations which further clarify the physical nature of the dynamic strain waves.

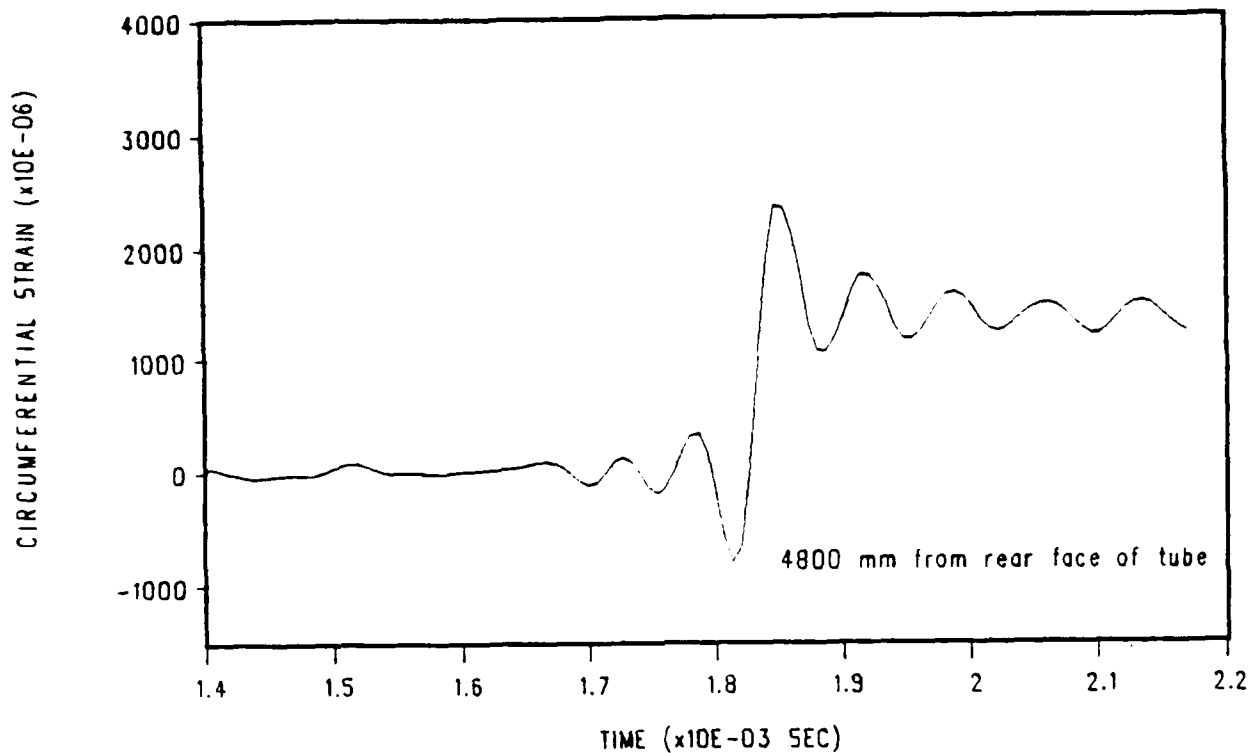


Figure 8. Typical "circumferential strain versus time" curve from dynamic finite element analysis.

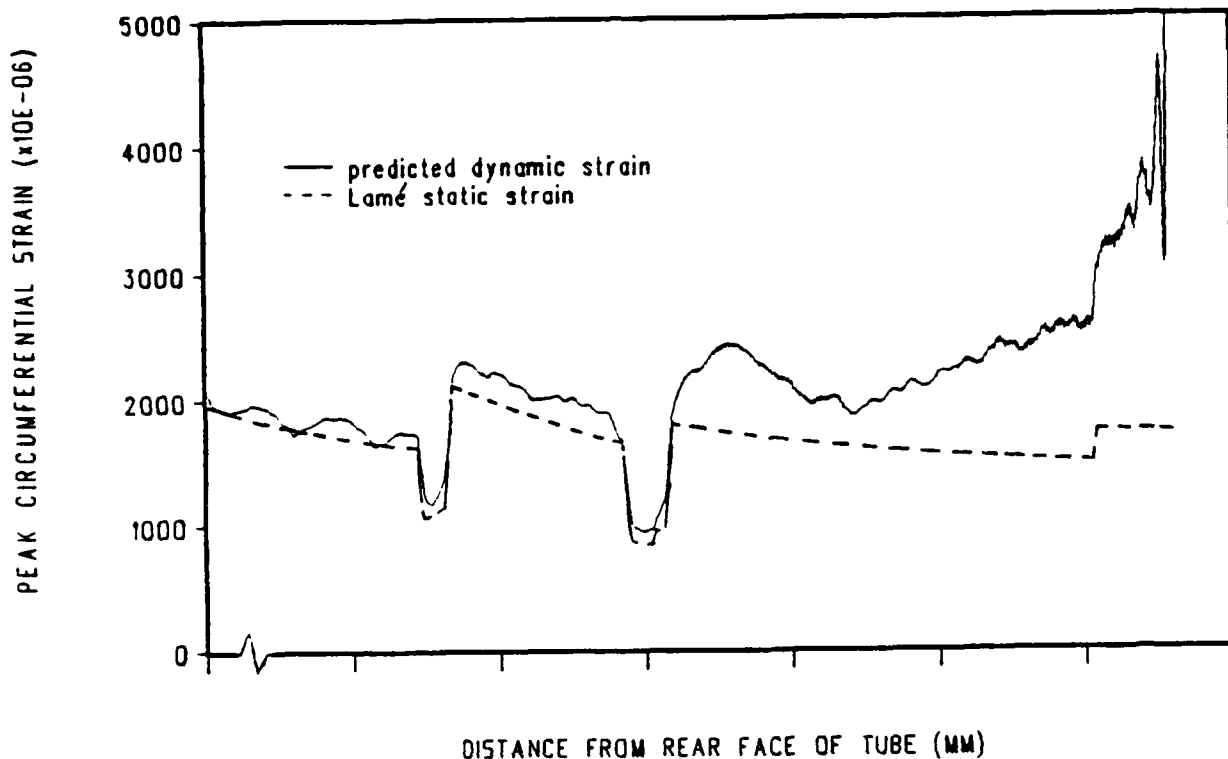


Figure 9. Typical "peak dynamic strain versus tube axial position" curve from dynamic finite element analysis.

DESIGN IMPLICATIONS OF DYNAMIC STRAINS

There are various implications of dynamic strains on developmental cannon tubes, some of which are reasonably well understood and some of which are excellent candidates for ongoing research. A partial list would include the following items:

- effect on tube strength (failure criteria);
- effect on tube fatigue life (high strain rate loading, multiple strain cycles per round fired);
- effects on projectile behavior due to local clearances or constrictions at tube-projectile interfaces (e.g., initiation of balloting, sabot tip-off, etc.);
- effect on adhesion/cohesion of bore coatings such as chromium plating;
- creation of local accelerations in the tube walls.

HASENBEIN, GABRIELE, FINLAYSON,
ARTUS, CUNNINGHAM, GAST

It is interesting that the last item on this list, which looks most innocuous, may be of the most immediate concern due to the severe environment which these accelerations create for attached components such as Muzzle Reference System Collimators. Resulting local accelerations near the muzzle can be on the order of $\pm 100,000$ g's and may result in breakage of delicate optical components.

CONCLUSIONS

Dynamic strains are a phenomenon which have only recently been identified and understood. The effort to do so has been the result of an intensive collaboration between research-oriented people (who are fundamentally interested in understanding and explaining physical phenomena) and development-oriented people (who are required to deliver functional hardware in a timely manner). From the development perspective, this problem has been (and continues to be) a prime example of the mutually beneficial relationship that can exist between the two, for truly without the researchers, the dynamic strain problem would never have been observed and understood at all.

(SPECULATIVE POSTSCRIPT: It is likely that researchers likewise feel a perverse reciprocal appreciation for developers who create exciting new problems like these in the first place by attempting to expand the limits of hardware performance.)

REFERENCES

1. T. E. Simkins, "Resonance of Flexural Waves in Gun Tubes," in: Proceedings of the Fifth U.S. Army Symposium on Gun Dynamics, ARCCB-SP-87023, Benet Laboratories, Watervliet NY, 23-25 September 1987, pp. 65-78.

SESSION V:

MODELLING AND FINITE ELEMENT SIMULATION

BENZKOFER

TITLE: DYNAMIC ANALYSIS OF A HAND-HELD WEAPON
PHILIP D. BENZKOFER

U.S. Army Armament Research, Development & Engineering Center
Close Combat Armaments Center
Light Armament Division
Simulation & Evaluation Branch
Picatinny Arsenal, NJ 07806-5000

ABSTRACT:

The motion of a small caliber, hand-held pistol resulting from an applied firing impulse is studied. The motion of each component is given by its displacement, velocity and acceleration. Relatively high levels of gas pressure due to the burning of propellant create a highly dynamic environment with multiple collisions and impacts occurring between relatively light mechanism components. In order to monitor and assess the dynamics occurring during its cyclic motion a model of the hand weapon is developed. The model defines each major mechanical component and the relative connectivity between them is defined in terms of kinematic joints. A Lagrangian methodology is utilized to formulate the rigid body dynamic equations of motion. Once the ammunition impulse is quantified and applied to the weapon, a dynamic history of the component motion is obtained. Both recoil and counterrecoil results are obtained. Discrepancy between preliminary model results and experimental has prompted a review of the critical parameters involved to include spring stiffness and damping rates for the drive spring. These differences have been assessed and accordingly comparison of recoil and counterrecoil velocities of major components for these rates has been made. Other parameters of concern include ammunition impulse and timing of locking lug motion. In addition to these parameters, another key and most relevant modeling aspect is that of the man weapon effect. In order to determine the influence of the shooter on the overall dynamic motion of the pistol, modeling of the human's control and reaction to the pistol firing is considered.

BIOGRAPHY:

PRESENT ASSIGNMENT: Armament/Weapon/Mechanisms Analysis, US Army Armament Research and Development Center, 1977 to present.

PAST EXPERIENCE: Math Analysis, GEN T. J. Rodman Laboratory, Rock Island, IL, 1966 to 1977.

DEGREES HELD: B.S., Mathematics, Iowa State University, 1965, M.S., Mechanical Engineering, University of Iowa, 1980.

BENZKOFER

DYNAMIC ANALYSIS OF A HAND-HELD WEAPON

PHILIP D. BENZKOFER

U.S. Army Armament Research, Development and Engineering Center
Close Combat Armaments Center
Picatinny Arsenal, NJ 07806-5000

INTRODUCTION

Substantial internal pressures are developed by the propellant burning during firing of the M9 pistol. These pressures exert high force loads on the components of the weapon. In particular, the loads imposed upon the locking blocks and pistol slide are extreme. These extreme loads have caused damage to componentry as evidenced by broken parts. Safety then becomes an issue. In light of these considerations a dynamic analysis of the pistol and its critical components has been deemed valuable, both in an immediate sense and also as a basis for any further analysis.

THE WEAPON SYSTEM

System Definition

In order to address the analysis of the weapon a brief description of the weapon is relevant. The M9 pistol is a semiautomatic, magazine-fed, recoil operated, double action pistol, chambered for the M9 cartridge [1]. The weapon system is shown in figure 1. The components of the weapon are shown in figure 2. A brief discussion of the major system components follows.

1. Slide Assembly. Houses the firing pin, striker, extractor, and cocks the hammer during the recoil cycle.
2. Barrel Assembly. Houses the cartridge for firing and directs the projectile. Locking blocks lock the barrel in position during firing.



Figure 1. M9 pistol

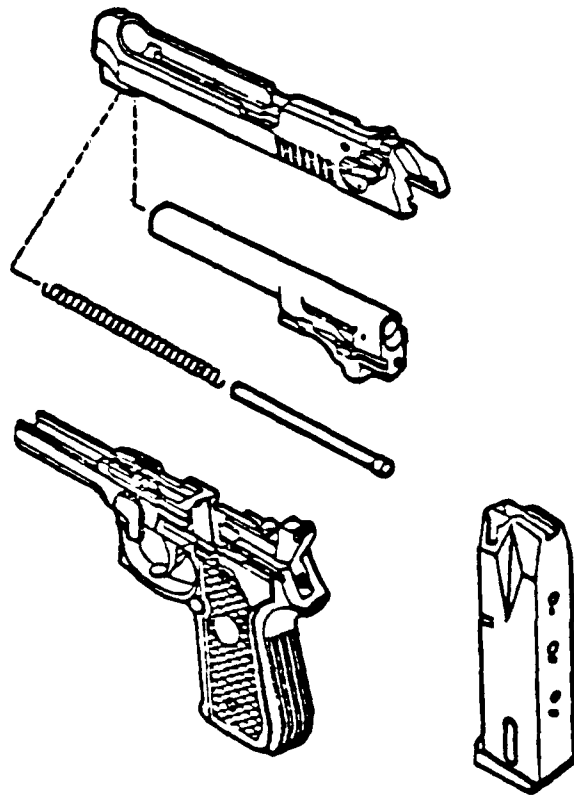


Figure 2. M9 pistol componentry

BENZKOFER

3. Recoil Springs and Recoil Spring Guide. Absorbs recoil and returns the slide assembly to its forward position.

4. Receiver. Serves as a support for all major components. Controls the action of the pistol through the four major components.

5. Magazine. Holds 15 cartridges in place for feeding and chambering.

System Operation

The M9 pistol has a short recoil system utilizing a falling locking block. Upon firing, the pressure developed by the propellant gases recoils the slide and barrel assembly rearward. After a short run, the locking block will stop the rearward motion of the barrel and release the slide which will continue in rearward motion. The slide will then extract and eject the fired cartridge case, cock the hammer and compress the recoil spring. The slide moves forward under recoil spring pressure, feeding the next round from the magazine into the chamber. The slide stop holds the slide and barrel assembly open after the last round has been fired and ejected. The pistol is disassembled as follows:

1. Clear/unload the pistol.
2. Allow slide to return fully forward.
3. Hold pistol in right hand with muzzle slightly elevated. With forefinger press disassembly lever release button and with thumb, rotate disassembly lever downward until it stops.
4. Pull the slide and barrel assembly forward and remove.
5. Slightly compress recoil spring and spring guide, while at the same time lifting and removing recoil spring and guide. Allow the recoil spring to expand slowly.
6. Separate recoil spring from spring guide.
7. Push in on locking block plunger while pushing barrel forward slightly. Lift and remove locking block and barrel assembly from slide.

Weapon system data is shown in table 1 below [1].

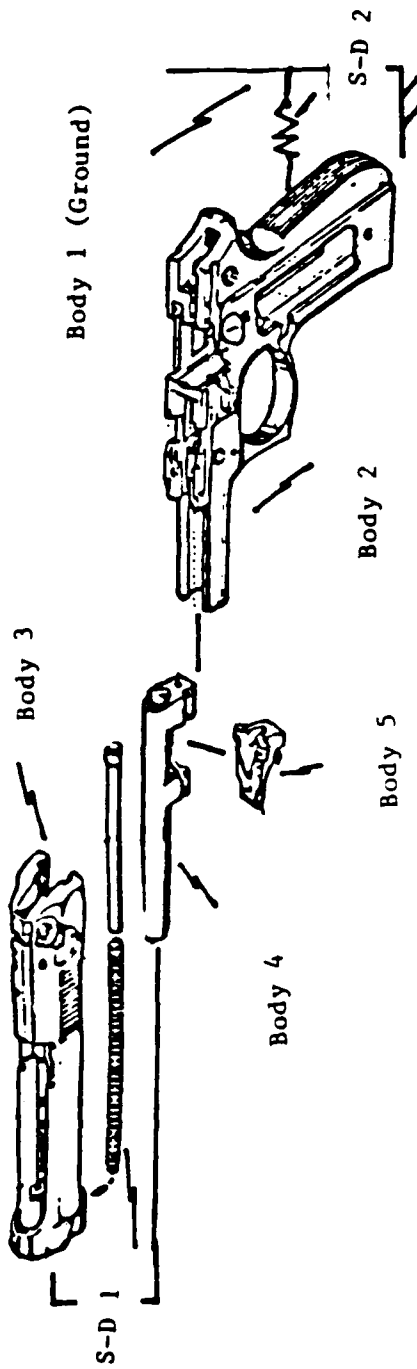
Table 1. M9 system data

Caliber.....	9 x 19mm (9mm NATO)
System of Operation.....	short recoil, semiautomatic
Locking system.....	falling locking block
Length.....	217mm (8.54 in.)
Width.....	38mm (1.50 in.)
Height.....	140mm (5.51 in.)
Weight (w/15 round magazine).....	1145 gr (40.89 oz.)
Weight (w/empty magazine.....)	960 gr (33.86 oz.)
Barrel length.....	125mm (4.92 in.)
Rifling.....	R.H., 6 groove [pitch 250mm (approx 1 turn in 10 in.)]
Muzzle velocity.....	375 meters/sec (1230.3 ft/sec)
Muzzle energy.....	569.5 newton meters (420 ft lbs)
Maximum effective range.....	50 meters (54.7 yards)
Front Sight.....	blade, integral with slide
Rear Sight.....	notched bar, dovetailed to slide
Sight radius.....	158mm (6.22 in.)
Safety features.....	- ambidextrous safety - firing pin block
Hammer (half cock).....	helps prevent accidental discharge
Magazine.....	staggered, 15 round capacity
Slide.....	held open upon firing of last round
Grips.....	plastic, checkered

BENZKOFER

A schematic model of the pistol depicting the bodies or components of the system is shown in figure 3. The ground system, or body 1, is required by the computer code as an Inertial Reference Frame (IRF) from which all other component measurements are made. This system then is an absolute one. In this particular model body 2 is defined to be the pistol stock, or the receiver. The connectivity between bodies 1 and 2 is represented by a spring-damper element, which has a spring force and spring damping effect on connecting bodies. In actual application this spring rate is very rigid and represents the soldier's resistance to the pistol moving in his or her hand, with a large damping force existing. The spring-damper force between bodies 1 and 2 can be adjusted, then, to evaluate the damping effects for various coefficients. The third body is the locking block, which rotates at the connection to the barrel, and the barrel is defined to be body 4. Body 5 is defined as the pistol slide. At initial position, the lugs of the locking block are upright and essentially locked to body 5. For the purpose of modeling, the weapon cycle is divided into phases, each phase representing a unique configuration/condition of the weapon. The equations representing a specific phase are unique to that phase. For the M9 pistol, 7 phases are identified. This is not to say that other phases could not be considered, but rather that based upon the assumptions and complexity of the model, a specific number of phases are required to adequately represent the system. Phase 1 represents the firing of the pistol, and the time for this phase is the in-bore time of the projectile. At this point phase 1 is completed and phase 2 begins. At this point the projectile has left the barrel and the barrel and slide are still locked up. When the lugs of the locking block have moved a distance of approximately one fourth inch they align with slots in the slide and are free to move downward. Phase 2 ends at this point of initial lug movement and phase 3 begins. Phase 3 represents the recoil motion of the slide to the point of impact with the receiver. This motion is approximately 2 inches. Phase 4 represents the impact of the slide and receiver. This is modeled utilizing a spring-damper element with a high spring and damping rate. Phase 5 is the beginning of counterrecoil. This phase brings the slide back to the position where the locking lugs of the locking block are free to move upward and lock up the barrel and slide. Phase 6 represents the motion of the slide back to its battery position. At the time it reaches battery position, the slide has velocity and impacts the receiver. Phase 7, then, represents the damping out of the slide motion and eventual static position of the weapon system. These 7 phases, then, represent one cycle of the pistol motion.

The dynamics are generated and solved by Lagrangian formulations. The driving force for the system is the pressure-time history for the round and the specific data is that for ammunition FNB83L-002-037, with a peak pressure of 35K psi. The results of the analyses are discussed in the following section. The data for the mathematical/computer model is shown in table 2 below, these being the weights of each body, or component, its initial position as measured from the IRF, spring data and connectivity between bodies.



- Body 1 - Ground
- Body 2 - Receiver (Pistol Stock)
- Body 3 - Slide
- Body 4 - Barrel
- Body 5 - Locking Block
- Body 6 - Projectile

Figure 3. Schematic model of the M9 pistol

Table 2. Data for M9 computer model

Component Weights:

Body 1 - Ground
Body 2 - 1.018 lbs
Body 3 - 0.045 lbs
Body 4 - 0.282 lbs
Body 5 - 0.730 lbs
Body 6 - 0.018 lbs

Spring Identification:

Recoil spring : Slide - Locking Block; $k = 3.08$ lbs/inch, $c = 0.0$

Impact springs: Ground - Receiver; man - weapon interface
 $k = 15000$ lbs/inch, $c = 10.06$ lb-sec/inch

Barrel - Receiver: stop barrel motion
 $k = 5000.$ lbs/inch, $c = 0.0$ lb-sec/inch

Slide - Receiver: end of recoil
 $k = 10000.$ lbs/inch, $c = 8.218$ lb-sec/inch

Slide - Barrel: pickup of barrel in c recoil
 $k = 5000.$ lbs/inch, $c = 0.0$ lb-sec/inch

Slide - Locking Block/Receiver: end of cycle
 $k = 5000.$ lbs/inch, $c = 0.0$ lb-sec/inch

Connectivity:

Translational joints: between bodies 2 and 3
 between bodies 2 and 4

Rotation joint : between bodies 4 and 5

WEAPON SYSTEM MODELING

In order to simulate the motion of a weapon system, such as the M9 pistol, several steps are necessary. The first step is to develop a mathematical model of the system which when computerized will reflect the actual motion of the system. The computer model details the mathematics for each defined component of the system. The motion will be quantified in terms of each component's displacement, velocity and acceleration. A dynamics computer code is utilized to generate and solve the equations of motion describing the pistol [2]. Essentially a set of rigid body dynamic equations are generated based upon the given generalized coordinates for each rigid body. In order to assemble a set of equations which account for all the defined components of the pistol, the connectivity between components is also defined. The external forces acting upon the system are defined in order to complete the model. A pressure versus time history for the M9 round of ammunition is given as this external force for the model. The equations of motion generated are of the form [3]

$$\frac{d}{dt} \left(\frac{\partial T}{\partial \dot{q}_i} \right) - \frac{\partial T}{\partial q_i} - Q_i + \frac{\partial \phi}{\partial q_i} \lambda = 0, \quad i = 1, \dots, N \quad (1)$$

where

- T is the kinetic energy (translational and rotational)
- q is the generalized coordinates to be defined
- Q is the set of external forces acting on the system
- λ is the set of Lagrange Multipliers [4] associated with the constraints imposed on the system.

The equations of constraint are of the form

$$\phi(q, t) = 0 \quad (2)$$

These equations represent the mathematical description of constraining motion, such as imposing or allowing only translation between bodies of the system. These equations of constraint are then appended to the equations of motion. This model, then, can be exercised to obtain the dynamic motion for given parameter changes such as recoil spring rate and pressure versus time history. The results of these analyses will provide the input necessary for a dynamic stress analysis to determine stress levels experienced by the pistol during a firing situation. These analyses also provide the basis for any future redesign efforts directed toward improving pistol performance and extending its useful field life. The details of the model are provided below.

DYNAMIC SIMULATION

The author has had significant experience not only in the formulation of dynamic equations of motion for rigid bodies and in particular weapon and armament systems, but has developed a systematic methodology for the automated generation of these equations for a special class of mechanisms [4]. This development has given the author an excellent background and basis for utilization of more recent general and powerful codes [2]. This code is utilized in [5] through [11]. The dynamics for the subject analysis utilizes this dynamics code.

The motion of the weapon system is initiated when the pistol is fired. The external force on the system is the propellant burning, which drives the projectile down the rifled barrel and at the same time exerting a rearward force on the barrel. Although the projectile is not denoted on figure 3 as one of the defined rigid bodies, its displacement, velocity and acceleration are shown in figures 4 through 6, with units as shown. The motion represents that for the in-bore cycle, with a time of approximately .5 millisecond. All referenced bodies from this point will be from figure 3. The motion depicted in the figures will represent that of the identified body for the entire weapon cycle from firing to return to initial position. The receiver motion, body 2, is shown in figures 7 through 12. The receiver displacement is shown in figure 7. The units of displacement are inches and time is shown in seconds. Key events are denoted on the figures. These events are specifically projectile exit, barrel and receiver impact, slide and receiver impact, end of recoil, pickup of barrel in counterrecoil, impact in counterrecoil and finally rest position. The actual recoil motion in figure 7 is slight. This is due to the fact that the spring-damper between the ground reference frame and the receiver as shown in figure 3 is relatively rigid (see Table 2). The velocity of the receiver is shown in figure 8. The units of motion for velocity are as shown, inches per second. As would be expected from viewing the displacement curve, the velocity is relatively low. Acceleration of the receiver is shown in figure 9. Units of acceleration are inches per second per second. The angular motion of the receiver is given in figures 10 through 12. Angular displacement is given in radians, angular velocity in radians per second and acceleration in radians per second per second. Impacts are denoted on the figures and in addition to the above include the pickup of the slide by the barrel during counterrecoil. The values of the spring constants for the impact springs have significant effects on the time and the angular displacement (see Table 2). This will be discussed later in the paper. The displacement, velocity and acceleration, respectively, of the slide are shown in figures 13 through 15. The units are the same as for the receiver. The motion occurring during the full cycle of the pistol is predominantly of this component. Note that the slide motion shown in figure 13 is relatively smooth but is affected somewhat when it picks up the barrel during counterrecoil. This is of course based upon the spring damper values utilized, relatively rigid, to represent this collision (see Table 2). Key events are denoted on the figures. From figure 14 it can be seen that the velocity of the slide is relatively large, in excess of 200 inches per second. The end of recoil is abrupt due to the high spring constant and damping coefficient utilized to represent the slide receiver impact. The velocity of the slide is reduced upon picking up the barrel in counterrecoil.

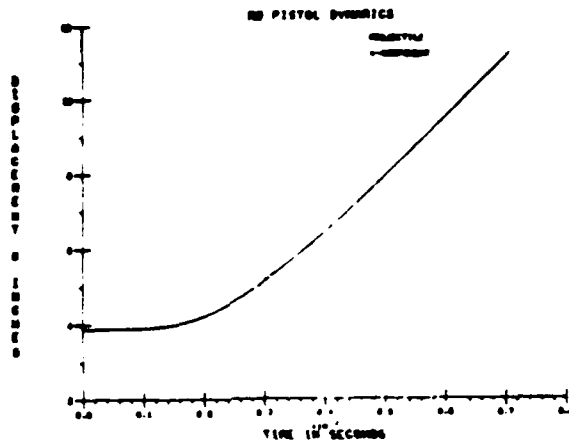


Figure 4. Projectile displacement versus time

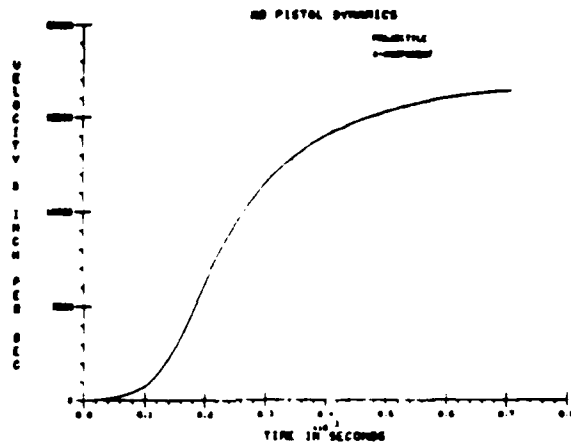


Figure 5. Projectile velocity versus time

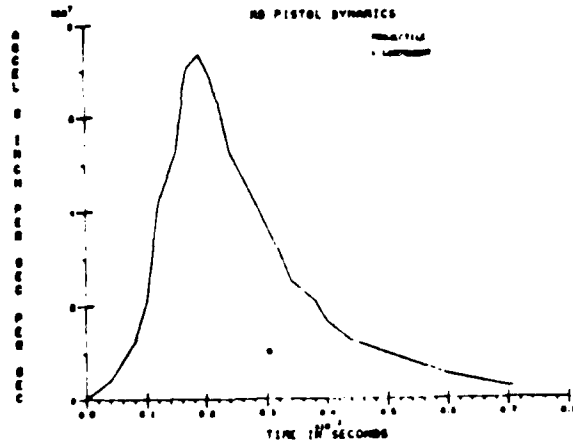


Figure 6. Projectile acceleration versus time

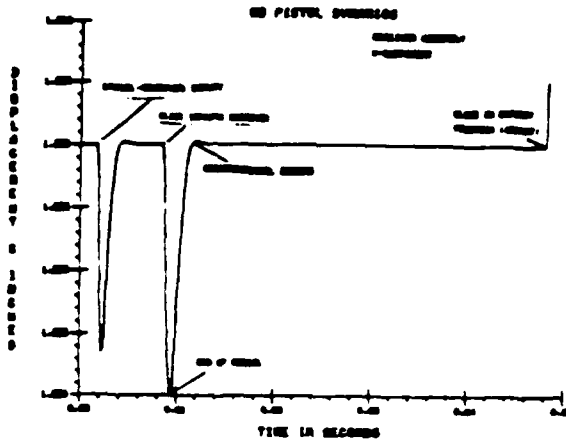


Figure 7. Receiver displacement versus time

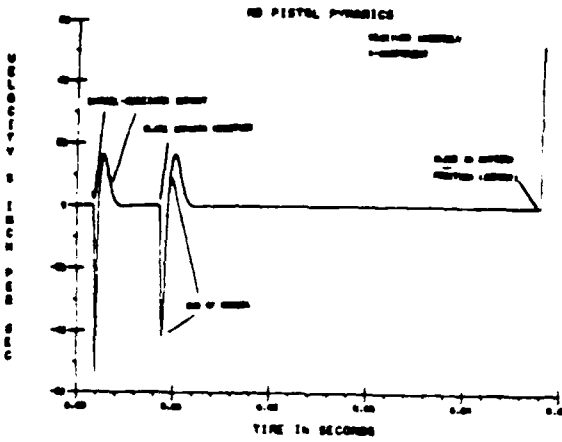


Figure 8. Receiver velocity versus time

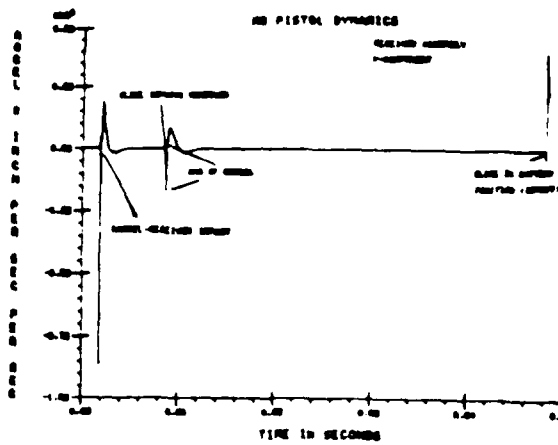


Figure 9. Receiver acceleration versus time

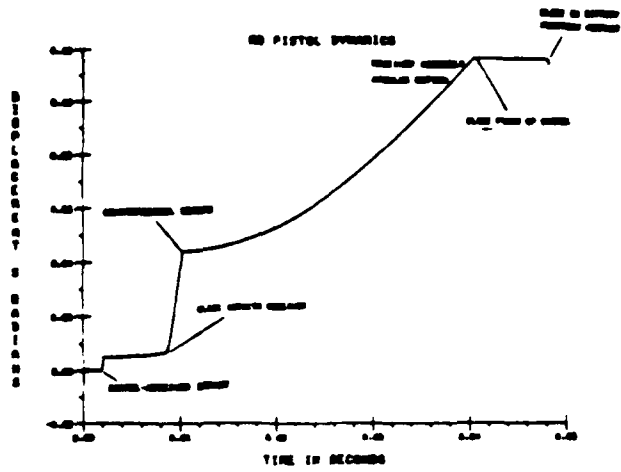


Figure 10. Receiver displacement versus time

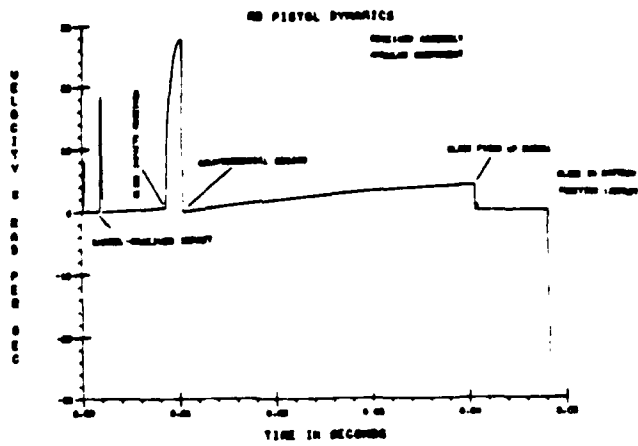


Figure 11. Receiver velocity versus time

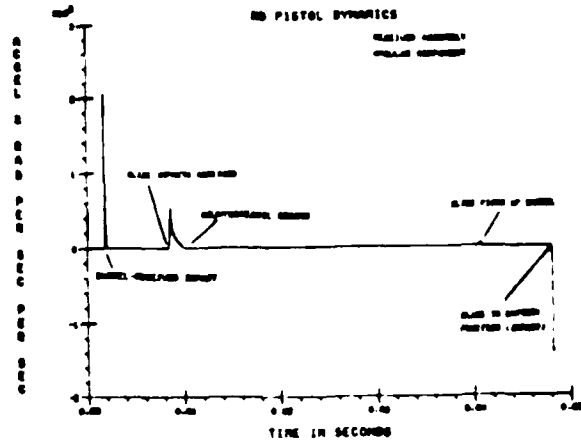


Figure 12. Receiver acceleration versus time

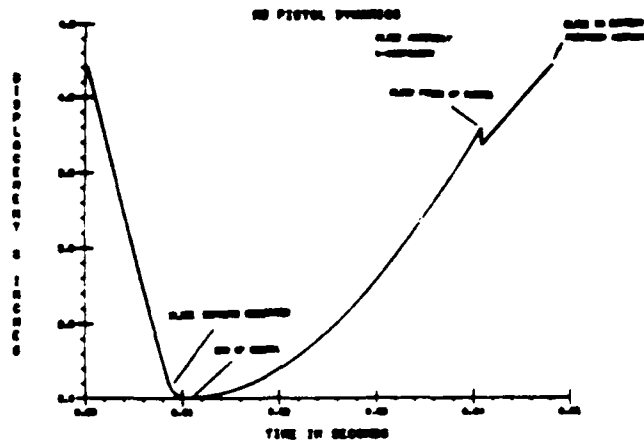


Figure 13. Slide displacement versus time

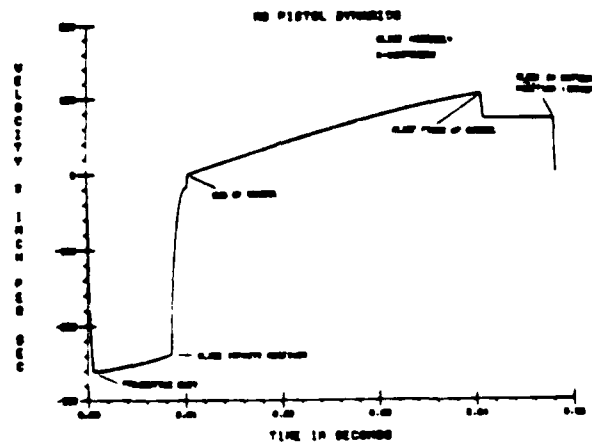


Figure 14. Slide velocity versus time

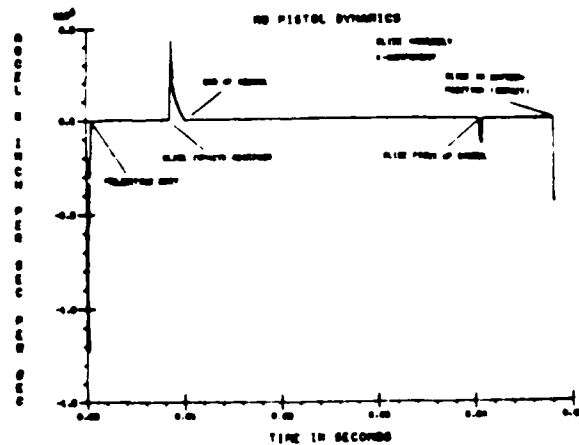


Figure 15. Slide acceleration versus time

BENZKOFER

The motion of the barrel is given in figures 16 through 18. Figure 16 gives barrel displacement in inches versus time in seconds. The significant events are denoted as the impact of the slide with the receiver and subsequently the stopping of the barrel due to impact with the receiver. During counterrecoil the slide picks up the barrel and brings it back to its battery position. Note that the displacement of the barrel is occurring only during the very early and the very late portions of the cycle, and that it is relatively small. In figure 17, the velocity in inches per second is shown. Since it is initially locked to the slide its velocity is high at this time. Note, however, that this is a very short period of time until it impacts the receiver and stops. This simulation is based upon the spring damper (see Table 2) utilized for this impact. In addition to the events noted on the displacement figure, the projectile exit is also given. As shown the time to projectile exit from the barrel is extremely small in comparison to the total cycle time. Finally the acceleration is given in figure 18.

Based upon analysis of the slide counterrecoil velocity, differences between simulated values and experimentally determined values do exist. This has promoted a review of the simulation model, and this is discussed in the following section.

PARAMETRIC ANALYSIS

As discussed above, observed differences between model and actual values do exist. Additional simulation analysis suggests that one parameter which may account for the disparities is the recoil spring stiffness. In order to further address this issue, then, the spring constant stiffness will be evaluated. Three values of the spring parameter have been arbitrarily selected and subsequently utilized in the model. These results will be discussed below.

Slide displacement for three unique values of spring stiffness, as noted in the legend, is shown in figure 19. Similarly, the velocities and accelerations for these three values are shown in figures 20 and 21. The lowest spring constant value utilized, 1.08 lbs/inch, results in the longest cycle time as shown on the figures. As expected, this value of spring constant results in the lowest value of counterrecoil velocity. As shown on the three figures, the value for the constant has little effect during the recoil cycle. This is sensible in the physical sense due to the relatively high velocity attained by the slide. However, during counterrecoil the stored energy in the compressed recoil spring is more significant and the velocities of recoil have been significantly reduced due to the damping effect of the impact with the receiver. There appears to be less variations when looking at the acceleration values in Figure 21, except to note that the spikes at or near the end of the cycle occur at different times, as would be expected. Review of actual experimental data suggests that the actual velocity of the slide is best simulated when using a different value for spring stiffness than that given on the technical drawing of the spring. One possible explanation for this difference is that due to the repeated firing of the weapon, the recoil spring is subjected to extensive loading and consequently its stiffness is diminished. The technical drawing calls for a spring constant closer to the high end of the values utilized here. The middle and lowest value of spring constant when utilized in the model most accurately simulate actual firing test data.

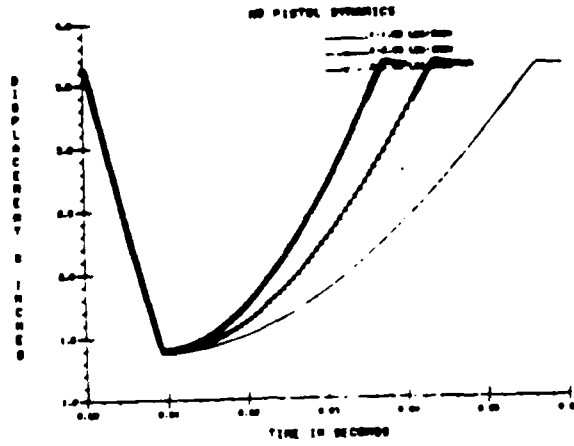


Figure 19. Slide displacement versus time

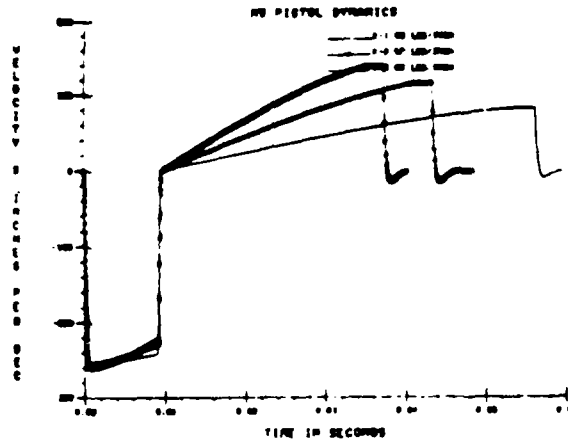


Figure 20. Slide velocity versus time

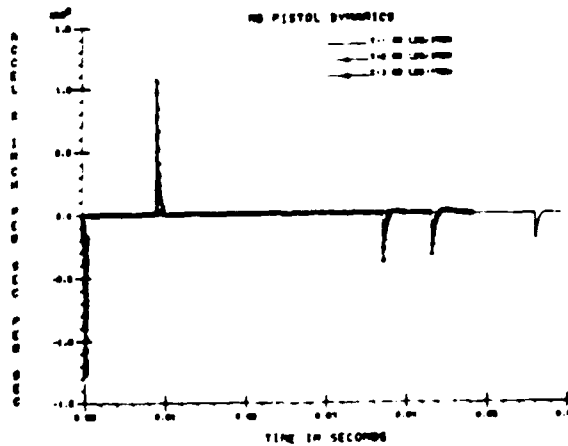


Figure 21. Slide acceleration versus time

BENZKOFER

CONCLUSIONS

Some inaccuracies in the model are apparent when observing motion results during the counterrecoil cycle, as simulation values do not fully coincide with test data. This appears to be dependent upon the recoil spring as discussed above. When the value of 2.08 lbs/inch is utilized for the recoil spring constant, reasonable values are obtained in the counter-recoil simulation. Good simulation values for recoil motion is evidenced, and total cycle time appears to be comparable with test data.

Another area of critical concern is interaction between the man and the pistol. This can best be modeled by allowing spring and damper action where the soldier grips the pistol. This technique will provide a wide range of parameter variation. The spring and damping coefficients utilized (see Table 2) in this analysis for the man-weapon interaction represent a relatively rigid system as evidenced in the recoil motion of Body 2, the receiver.

RECOMMENDATIONS

The inaccuracies and changes discussed above will be further investigated and subsequently be incorporated into the model. The simulation values obtained to date, however, are preliminary in the sense that new test data for pressure-time may preclude that which is utilized in this model.

Current efforts in modeling of a hand-held weapon include the evaluation of a full range of spring-damper variations for the impact springs as well as for the man-weapon connectivity. In essence, this model, with corrections and updates as discussed, will serve as a good reference in design and redesign efforts, as well as input to a dynamic stress analysis.

BENZKOFER

REFERENCES

1. Unit and Intermediate Direct Support Maintenance Manual, PISTOL, SEMIAUTOMATIC, 9mm, M9, Technical Manual TM 9-1005-317-23&P, U.S. Army Armament, Munitions and Chemical Command, Rock Island, IL Jan 1986.
2. DADS 2D/3D Theoretical and User Manuals, University of Iowa, Iowa City, IA, 1982.
3. T.R. Kane, Dynamics, Second Edition, Stanford University, CA, 1972.
4. Philip D. Benzkofer, Master of Science Dissertation, "An Equation-Generating Computer Code for the Dynamic Analysis of a Class of Mechanisms", University of Iowa, College of Engineering, Graduate College, Dec 1980.
5. Philip D. Benzkofer, "Dynamics of High Cyclic Rate Weapon Systems", proceedings of the Fifth U.S. Army Gun Dynamics Symposium, Sep, 1987.
6. Philip D. Benzkofer, "Automated Dynamic Analysis of Weapon Systems", proceedings of the Fourth U.S. Army Gun Dynamics Symposium, May 1985.
7. Philip D. Benzkofer, "Dynamic Analysis of the 20mm General Purpose Heavy Machine Gun", proceedings of the Third U.S. Army Gun Dynamics Symposium, May 1982.
8. Philip D. Benzkofer, "Dynamic Analysis of the Caliber .45 M1911A1 Pistol", Technical Report, U.S. Army Armament Research, Development and Engineering Center, ARDEC, Dover, NJ, Dec 1989.
9. Philip D. Benzkofer, "An Evaluation of the Dynamics Inherent in an Advanced Primer Ignition Weapon System", Technical Report, U.S. Army Armament Research, Development and Engineering Center, ARDEC, Dover, NJ, Jan 1988.
10. Philip D. Benzkofer, "Precision Aircraft Armament Control Experiment Armament System Dynamics", Technical Report, U.S. Army Armament Research, Development and Engineering Center, ARDEC, Dover, NJ, Jan 1988.
11. Philip D. Benzkofer, "Automated Dynamic Analysis in Support of a Future Air Defense Test Bed", Technical Report, U.S. Army, Armament Research and Development Center, ARDC, Dover, NJ, May 1986.

ERLINE, KREGEL

TITLE: Flexible Projectile Modeling Using The
Little Rascal Gun Dynamics Program
Thomas F. Erline, Mark D. Kregel
U.S. Army Ballistic Research Laboratory
Aberdeen Proving Grounds, Md 21005-5066

ABSTRACT:

The original version of the "Little Rascal" gun dynamics program used a two mass point rigid body projectile model. The results from gun dynamics modeling using the rigid body projectile were generally within experimental error. The results supplied approximate shot exit conditions (as far as rigid bodies can emulate real projectiles). In reality projectiles flex on their way out a gun tube, especially modern sabot type projectiles. Flexible projectile modeling was recently incorporated within the Little Rascal gun dynamics program by translating the salient features the original FORTRAN version into the TURBO-PASCAL language for personal computers. The method for forming a lumped parameter finite element model for the projectile resembles the method for modeling the flexible gun tube.

Two contact points for the flexible projectile model are defined by the user. These contacts are interfaced to the model of the gun tube's dynamic centerline by springs. It turns out these two spring constants are extremely important to the structural response of both the gun tube and the projectile model. This paper will focus on the effects various spring constant values have on gun and projectile dynamics.

When the projectile is described for input, care must be taken in defining the spring constants to be used. If the spring constants are too low, ie. soft, then the gun tube will not respond dynamically as expected. Correspondingly, soft springs do not transmit much load onto the projectile model and the projectile will emulate rigid body motion traveling down the bore of a barrel. When the spring constants are very high, ie. stiff, gun dynamics results emulate the action of rigid body projectile simulation. Large loads are transmitted to flexible projectile model and may produce excessive projectile vibration.

BIOGRAPHY:

PRESENT ASSIGNMENT: Mathematician, Mechanics and Structures Branch, Interior Ballistics Division, BRL.

PAST EXPERIENCE: Mathematician, Vulnerability Lethality Division, BRL, 1973-1982. Research Scientist, Physics Division Chemical Research and Development Center - PAD, 1982-1985.

DEGREES HELD: B. S., Towson State University, 1973.

Flexible Projectile Modeling Using The
Little Rascal Gun Dynamics Program

Thomas F. Erline, Mark D. Kregel
U.S. Army Ballistic Research Laboratory
Aberdeen Proving Grounds, Md 21005-5066

Introduction

At the Fifth U.S. Army Symposium on Gun Dynamics, 23-25 September 1987, the author presented a modified version of a paper on the gun dynamics program known as the Little Rascal (the paper was not published due to security reasons) co-authored by Dr. Mark D. Kregel of Systems Engineering & Concepts Analysis Division, Ballistic Research Laboratory. In that presentation, the Little Rascal gun dynamics predictions of barrel motion agreed quite well with experimental results over a wide range of gun system size and type. Comparisons have been made with both rifle barrels[1] and smoothbore tank weapons[2].

The original FORTRAN version of the Little Rascal code used a two mass point rigid body type of projectile model. This model preserved the center of gravity (cg), and mass moments of the projectile. The projectile model had two user definable contact points that allowed the gun dynamics code to predict projectile exit conditions, such as pitch, pitch rate and projectile cg direction.

Two recent developments enhance the Little Rascal code. The Little Rascal is new program written in the Turbo-PASCAL language for IBM AT type personal computers. The new code is now generic so that almost any gun system and projectile can be modeled. In addition, an increase in accuracy has been accomplished by the incorporating the flexible projectile model in the code.

A finite element projectile model is interfaced to the finite element model of the gun barrel by two user definable contact springs. Since accurate modeling results occur only when proper input values are used, this paper will focus on the contact spring constants used to interface these two models together. The values needed for the spring constants are the most difficult to find. All other values of projectile input are easily found from the material properties or geometry. This paper illustrates insights formed by modeling a gun and projectiles with various values for those spring constants.

ERLINE, KREGEL

The Little Rascal simulates firing a projectile down the bore of a gun tube. The dominant transverse loading conditions are applied and the resulting transverse displacements of both the gun and the projectile model in the analysis plane are tracked from ignition to a short time interval after shot exit. This study analyzes a range of spring constant values for the projectile contact points. It will be shown that a wide interval of spring constant values can produce gun dynamics predictions that are comparable to experimental results. The range of acceptable gun dynamics predictions allows a wide range of projectile responses to be predicted. Thus, it behoves the modeler to find the proper values to use for the projectile spring contacts.

Initial shot exit conditions of the projectile can be extracted from a simulation. Little Rascal has output options of nodal displacements, nodal velocities, angles of interest (ie. gun pointing, projectile pitch, etc.) and angular velocities of interest will be utilized for comparing experimental results with modeling predictions of one particular gun tube and projectile. Holding the experimental values of gun dynamics as a baseline direct comparison of Little Rascal simulations of various projectile spring constants will be presented.

BACKGROUND

In the early 1970's Dr. M. Kregel realized that relatively simple mathematical expressions can be written from first principles of Newton's laws of motion to describe the complex motion of a projectile during launch. Inclusion of all the relevant physical phenomena of first and second order can be the basis of solutions that are second order accurate. An ordinary differential equation solver capable of solving numerically stiff non-linear coupled ordinary first order differential equations (odes) in rapid and optimal manner is required. He developed a state of the art ordinary differential equation solver that was used to solve large numbers of coupled, non-linear and stiff odes that arose from work in upper atmospheric physics[3,4,5]. By using a variational technique this ode stiff equation solver can be used to solve the odes arising from a finite element description of a projectile and a barrel. A variational technique used preserves the various stability matrices used in the ode solver and allows optimal run time performance while assuring integration convergence to better than one part in ten to the tenth power per time step.

By incorporating inertial and pressure forces, as well as projectile interaction with the barrel and mounting constraints, a gun dynamics program was developed named "Little Rascal". Since that time the Little Rascal simulation has evolved considerably. In 1985, the Mr. T. Erline started using the Little Rascal after demonstrating that this small FORTRAN program could indeed emulate simple elastic vibrational experiments. Together Erline and

ERLINE. KREGEL

Kregel modified the program to mathematically model two well documented experimental gun systems, a small bore and a large bore, (through the 1987 time frame) to certify the computations and support the BRL Accuracy Program. The old expanded FORTRAN version of the Little Rascal represented the projectile model as a two mass point rigid body which preserved center of gravity and mass moments of inertia and had user definable contact points.

It was pointed out that the gun dynamics simulations from this FORTRAN version were emulated properly as far a rigid body projectile model was concerned. It was understood in the ballistics community that projectiles flex on their way out the barrel, especially the modern sabotated encased kinetic energy rounds. The flexural dynamics of the modern day projectile can cause significantly different shot exit conditions in comparison to rigid body projectile dynamics. The 1988-89 time frame was used to rewrite the gun dynamics simulation program, incorporating flexible projectile capability, and testing the new gun dynamics models to previously successful models.

The projectile designer is or should be concerned with lateral loads as well as the interior combustion pressure loads on the structural integrity of the projectile designs. The structural dynamics of a projectile may play a significant role in shot exit conditions. These projectile exit conditions serve as the initial conditions for the exterior ballisticsian who is concerned about flight performance. The Little Rascal gun dynamics simulation program finds these planar transverse loads and motions of a gun barrel and of a projectile through the in-bore firing cycle to a short time interval after shot exit. Though not as sophisticated as six degree of freedom simulations [6,7,8], the Little Rascal serves the ballistics community through its ease of modeling, quick turn around time, desk top computational capabilities, and modeling results that have been shown to be within experimental error for the gun systems modeled thus far.

Modeling is accomplished by dividing the barrel and the projectile each into a series of discrete equally spaced mass points (called nodes). This generates a corresponding number of cylindrical elements which are represented as connected masses. Each node, except the end nodes, is thus joined to two adjacent nodes. The mass associated with each node is simply the mass of the corresponding mass element which that node represents. The stiffness of the interconnecting spring elements is computed to be that of the corresponding barrel or projectile segment. The numerical description is based on the assumption of cylindrical geometry of the barrel and projectile in which uniform radii (both inner and outer), density and modulus are assumed at each of the corresponding node locations. Conversions of the barrel and projectile's geometry to equivalent node mass and spring stiffness used in the simulation are made in the program using standard engineering formulae.

ERLINE, KREGEL

The gun system, including the barrel, breech and two supports, and the projectile are two separate models. They are handled separately in the program except for the variational scheme which handles their interaction. The interaction of the projectile and the barrel occurs through contact points. The location of the projectile's contact points relative to the projectile are fixed. On the barrel the projectile's contact points are dynamic and change as the projectile travels down the bore. The two supports of the gun system are the trunnion and the elevation station, and they are considered to be contact points of the barrel relative to the earth.

Lateral motions arise for both the projectile and the barrel from either changes in the contact forces or of their location. The moving projectile causes numerous changes in both the magnitude of these forces as well as their location, due to the projectile's inertia and changing location along the bore.

An assumption is made in the Little Rascal that the contact points between the projectile and the barrel and the barrel and the earth remain fixed in location at each time step of integration. From one time step to the next the projectile's location changes and thus the projectile and its two contact points constitutes a traveling load on the barrel. The lateral displacement at each of these two contact points associated with the projectile is forced by the integrator to match the corresponding lateral displacements of the barrel.

Every barrel has a unique centerline. Even a perfectly manufactured tube will suffer a gravity droop and deflection due to thermal variations. Thus the static centerline of a barrel is a linear combination of the gravity droop and manufacturing irregularities. A barrel's centerline is normally measured statically as the barrel is mounted in a tank from the muzzle to the forcing cone of the chamber. Ideally the centerline measurements define the displacement in both the horizontal and vertical planes from a line defined by the center's of the muzzle and the forcing cone. During firing the projectile initially sees this centerline. Due to recoil effects, internal pressure effects as well as inertial forces arising at the various contacts this centerline is altered. The job of the integrator in the Little Rascal code is to: (1) Generate projectile barrel contact forces at each time step that assures that the lateral positions at the contact points of the projectile, including deformations, match the corresponding lateral positions of the barrel, including its deformations. (2) Generate barrel and barrel support contact forces that accurately track barrel flexure and barrel support flexure. Only by doing this can the integrator be assured of having the projectile track the dynamic centerline and have the barrel be properly positioned at all times in its support.

ERLINE, KREGEL

As mentioned, the barrel has contact points associated with its support structure. The Little Rascal allows for the defining of various properties of these contacts also. In addition, the simulation of the barrel allows for torques and forces arising from recoil, due principally to axial asymmetry of the breech[9]. Such forces and torques are said to arise from the "powder pressure couple". The Little Rascal demonstrates clearly that for larger caliber gun systems breech asymmetry, arising from the breech's design, is a significant term driving barrel motion in the vertical plane where most imbalance occurs. The Little Rascal emulates this couple by taking into account the cg offset of the massive breech component from the centerline of the barrel with the breech block in the closed position. The resulting torque during recoil is simply the product of the offset in the analysis plane times the breech mass times the barrel's recoil acceleration. Another factor affecting barrel motion arises from manufacturing irregularities which dominate in the horizontal plane and is about a factor of ten less than the breech imbalance effect in the vertical.

Because of the strong coupling between the projectile and the barrel and the overturning moment due to recoil, complex motions can arise during shot travel that may be counter intuitive. In fact a projectile may leave a barrel in a direction and at an angle different from the angle defined by the muzzle. This arises from the fact that the muzzle is subjected to strong accelerative forces due both to the exiting projectile and the whipping of the barrel by the breech overturning moments. Although the overturning moment due to recoil acts at the breech, the effect is amplified at the muzzle because of the barrel's reduction in stiffness near the muzzle.

The Little Rascal has demonstrated the importance of the breech overturning moments on barrel motion during projectile travel and launch for tank guns. With a flexible projectile model a simulation clearly shows the extent and nature of rod flexure for sabot rounds. The Little Rascal output allows "snapshots" to be made at any time within the simulation of barrel and projectile shapes as well as temporal histories of displacements, velocities and forces. These snapshots are important in developing fundamental insight into projectile and barrel interactions.

Future versions of the Little Rascal will contain additional effects or features. "Balloting" is an effect of allowing the projectile to have clearances within the barrel where it can "bounce" off the interior walls of the barrel on its way out. Balloting will be included in the next Little Rascal version. As other effects are found by comparisons with experimental data, the Little Rascal will be upgraded to include them.

ERLINE, KREGEL

THE SIMULATIONS

All the simulations will use one specific large caliber weapon system that has been studied previously both by experiment[10] and by mathematical modeling. The gun system modeled here is represented by: the breech mass and any offset in its cg location, the barrel and its unique centerline, and two supports - trunnion and elevation station. Figure 1. presents a physical layout of the gun system model. The vertical breech 'cg' offset symbol is noted as are the trunnion 'tr' location and the elevation 'el' station. Horizontal plane simulations use a breech cg offset of zero.

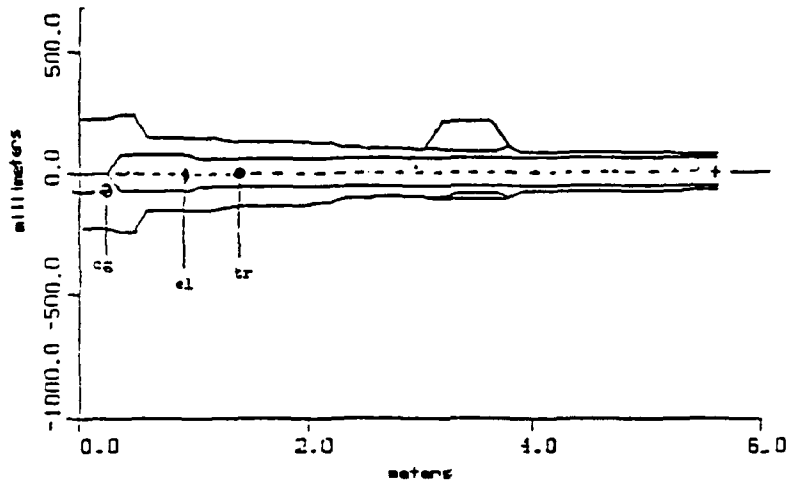


Figure 1. The Large Caliber Gun System

The barrel centerline of this gun system is seen in Figure 2.

Centerline Data

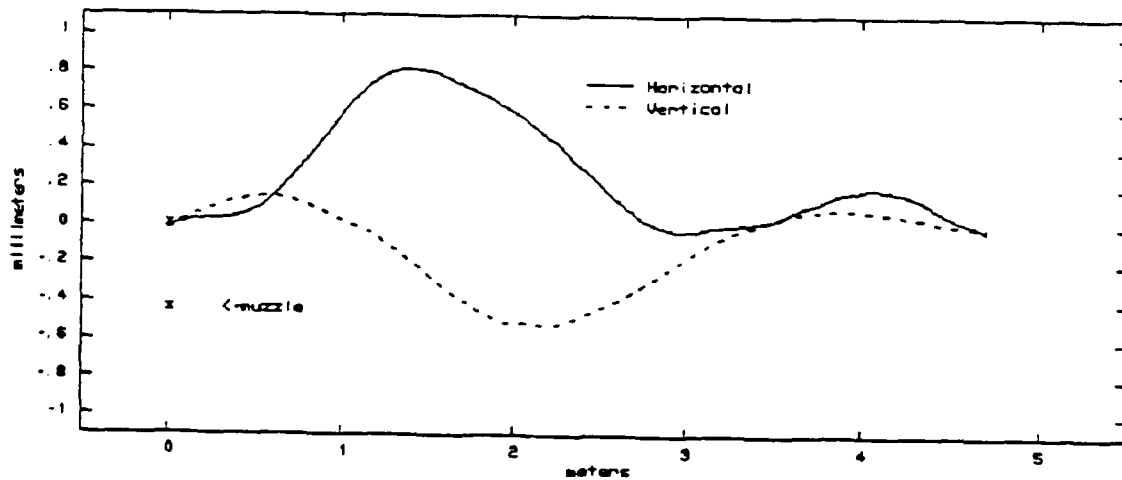


Figure 2. The Barrel Centerline

ERLINE, KREGEL

Each simulation will use the same particular sabot kinetic energy projectile. Thus, the projectile material and geometry remain constant. The positions of the contact springs on the projectile model will also remain constant. The projectile model appears similar to the one presented in Figure 3.

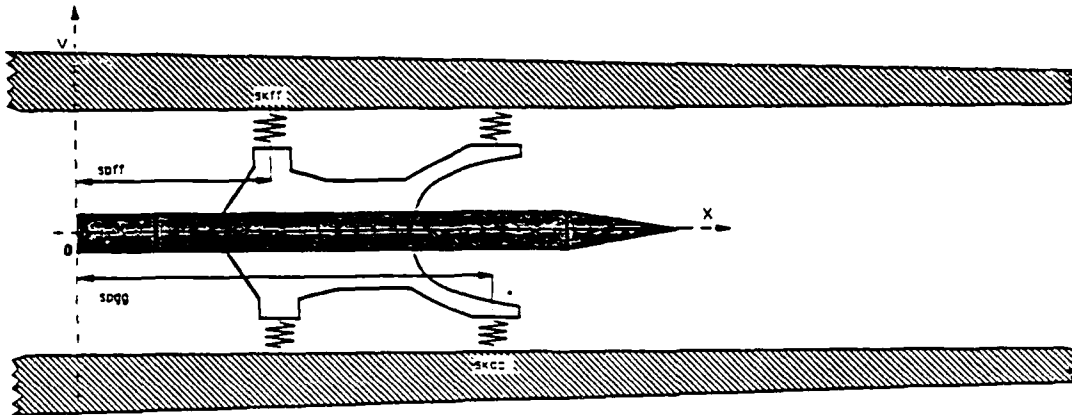


Figure 3. Projectile Model Represented In A Barrel

An assumption is made in the Little Rascal that there are no clearances between the barrel and the projectile. Thus, the representation of the projectile's spring contacts on both top and bottom of the projectile and connected continuously to the barrel until shot exit as shown in Figure 3. is a fair visualization. These contact springs known as 'skff' and 'skgg', rear and front respectively, inside the program are the linear spring constants that will be varied in this study. For comparison purposes experimental data plus gun dynamics predictions using the flexible projectile model will be presented.

DYNAMIC LOADS

The traveling load of the projectile on the barrel is the interaction of the projectile with the barrel's dynamic centerline (the static centerline plus any displacements). This traveling load produces transverse forces applied to both the projectile and the barrel. The program uses an iterative technique to model this interaction which is evident in any plane. To track the travel of the projectile an interior ballistics simulation velocity curve (seen in Figure 4.) is input into the program and integrated to provide projectile location in time. The projectile velocity curve is differentiated to provide the pressure. Breech pressure also seen in Figure 4. is calculated from the projectile and propellant mass and projectile velocity history providing impetus for the recoil forces, pivoting torques and the 'bourdon effect'.

Interior Ballistics

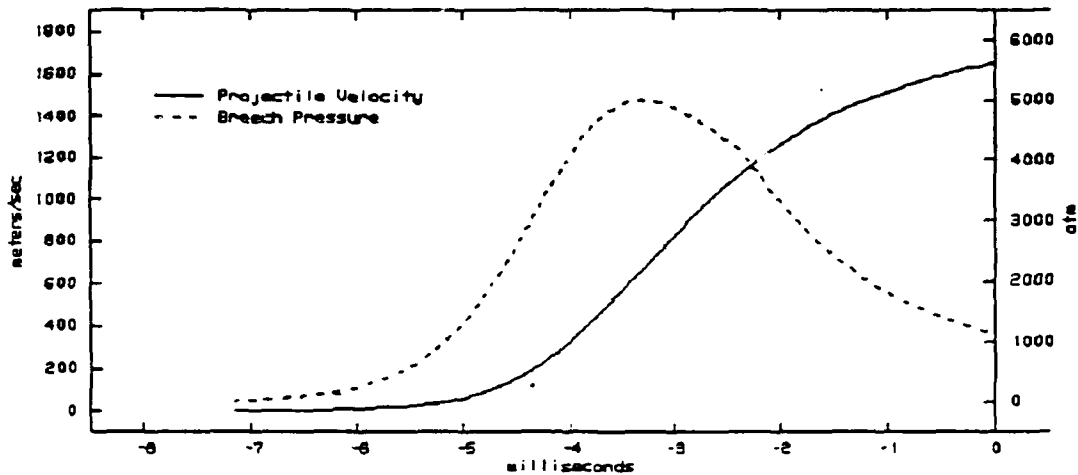


Figure 4. Interior Ballistics Curves

What are good values to use for the spring constants on the particular sabot projectile in this study? Spring constants for projectiles are not found in the literature. Therefore, detailed finite element models should be generated and subjected to application of graduated static loads to obtain displacements. Next, graph the force over displacements curve to obtain a spring constant. Next, obtain a specimen of the sabot, mount it on jig in the laboratory, then load and measure displacements. Finally, verify the finite element model by comparing results with the laboratory measurements.

Since time is of the essence and the above mentioned procedures have not been accomplished, conjecture is the route taken. Recently, Mr. J. Diebler[11] supplied us with spring constant values for the forward bell of a couple of sabot projectiles that were tested at Battelle, Pacific Northwest Laboratories. The measurements supplied were not for the projectile of this study. However, maybe a good estimate can be selected from the range of values supplied (48000 lb/in low to 105000 lb/in high). A first guess uses 1.0×10^7 N/m (approx. 57000 lb/in) for the forward bell. Based on geometry of the sabot driving band compared to the bell assume 7.5 times the value of the bell to be fair estimate for the rear spring constant. (For brevity sake call the first guess spring constants 'NORM'.) Next, select values for a hard spring and a soft spring configuration to simply be a change by a power of

ERLINE, KREGEL

ten increase or decrease, respectively. Thus, the first cut at gun dynamics observations and the effect of projectile spring constants will be from three cases in units of Newtons per meter:

	HARD	NORM	SOFT
Forward Bell	1.0e8	1.0e7	1.0e6
Driving Band	7.5e8	7.5e7	7.5e6

RESULTS AND DISCUSSION

The gun dynamics results are the first items to be compared with experimental data. The HARD spring gun dynamics case will be compared with the rigid body projectile from the FORTRAN version of the Little Rascal. One caveat to be noted about the new model comparisons with the old model is that the two models are not exactly alike. The most significant difference between the two gun models is that old model is stiffer and more massive in the breech end of the tube because the recoil piston was modeled. Whereas the new model does not include the recoil piston. There exist other minor differences.

In the first case observe the gun dynamics at shot exit due to the HARD spring configuration in Figures 5. and 6. where direct comparisons can be made to experiment and old modeling. Direct comparison of the old FORTRAN rigid body projectile model effects on its gun motion appear very similar to the effects of the HARD spring configuration of the new flexible projectile model on its gun motion, especially in the horizontal plane Figure 6.

Vertical Shape @ Shot Exit

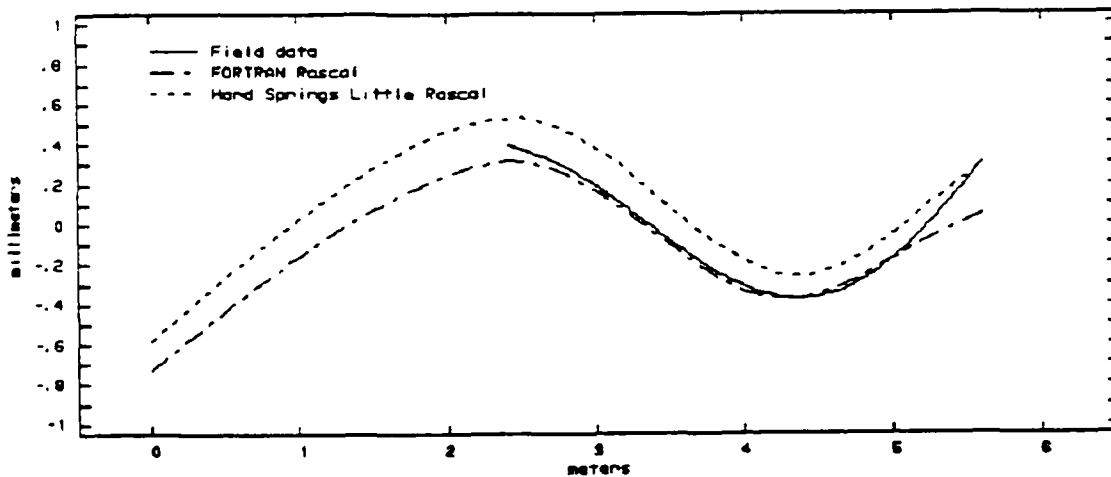


Figure 5. HARD Springs - The Vertical Gun Shape at Shot Exit.

Horizontal Shapes at Exit

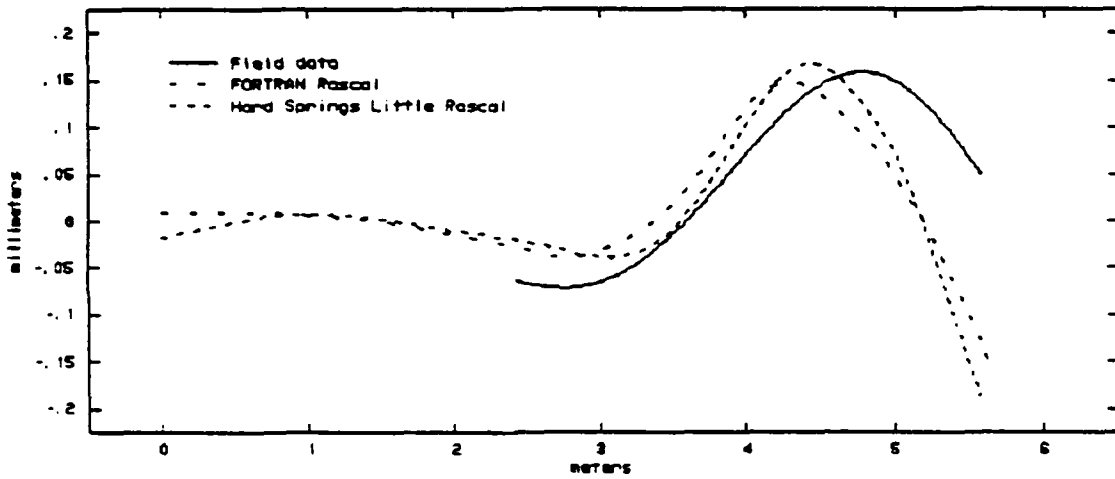


Figure 6. HARD Springs - The Horizontal Gun Shape at Shot Exit

In the second case observe the gun dynamics at shot exit due to the NORM spring configuration in Figures 7. and 8. where direct comparisons can be made to experiment. Here direct comparison of the experimental gun motion appears very similar to the effects of the NORM spring configuration of the new flexible projectile model on its gun motion, especially in the vertical plane Figure 7. The NORM case also shows a little closer match to experiment in the horizontal plane noted in Figure 8.

Vertical Shape @ Shot Exit

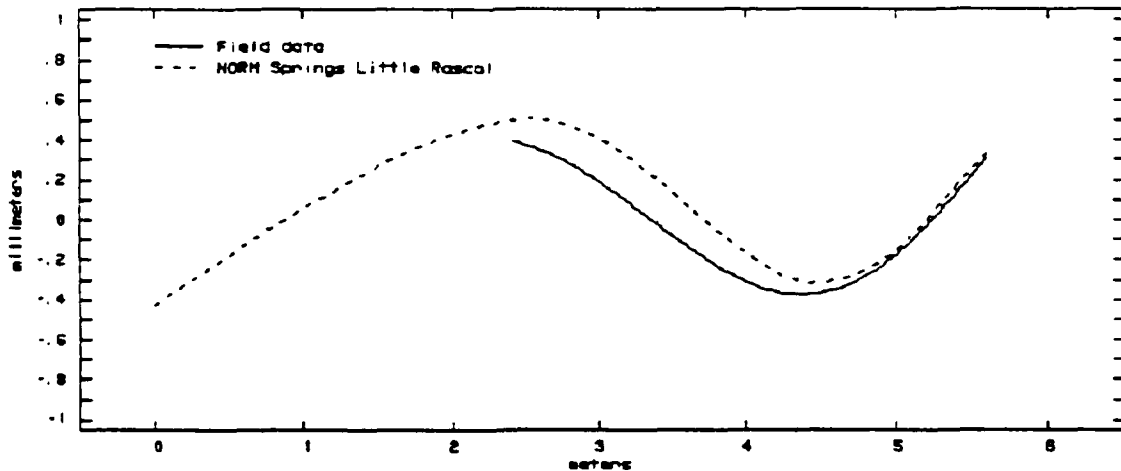


Figure 7. NORM Springs - The Vertical Gun Shape at Shot Exit.

Horizontal Shapes at Exit

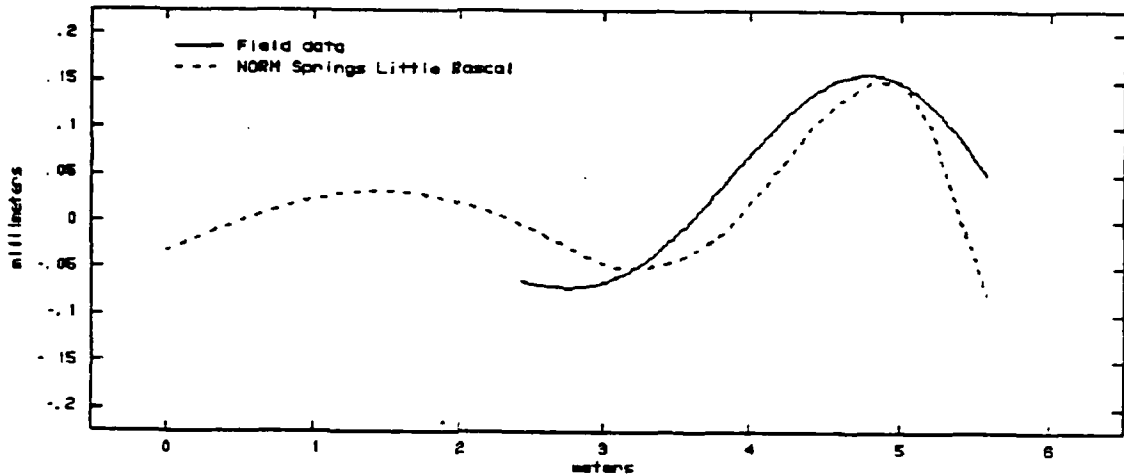


Figure 8. NORM Springs - The Horizontal Gun Shape at Shot Exit.

In the third case observe the gun dynamics at shot exit due to the SOFT spring configuration in Figures 9. and 10. where direct comparisons are made to experimental results. Only in the vertical plane do the model predictions look somewhat like experiment. In Figure 10. note that softness of the projectile spring constants imparts only a slight loading in the horizontal plane.

Vertical Shape @ Shot Exit

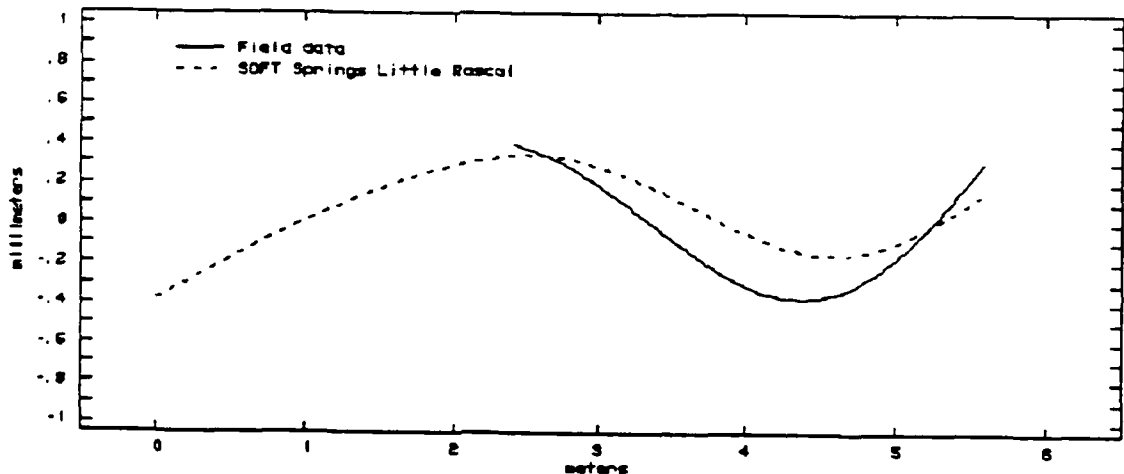


Figure 9. SOFT Springs - The Vertical Gun Shape at Shot Exit.

Horizontal Shapes at Exit

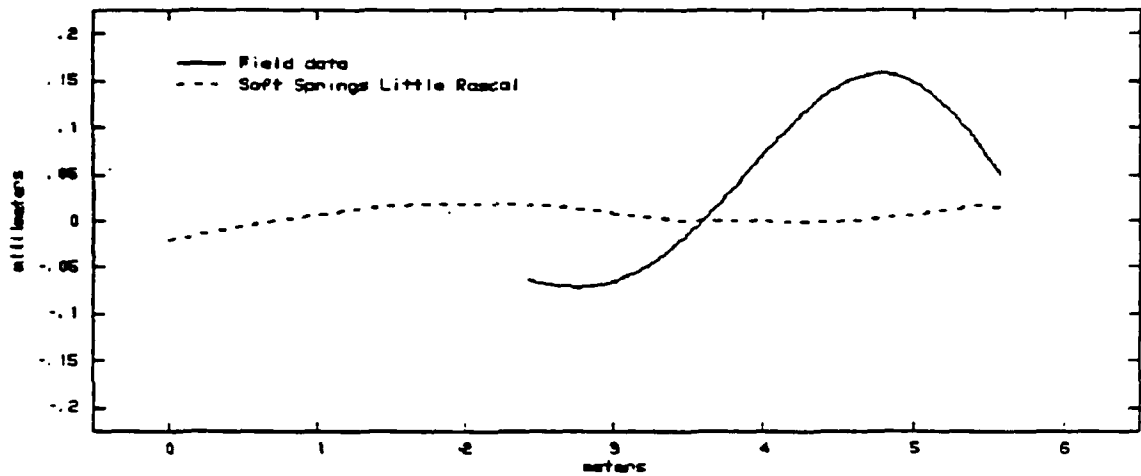


Figure 10. SOFT Springs - The Horizontal Gun Shape at Shot Exit.

How does this one particular flexible projectile model react to these three separate scenarios? There are many ways to look at the projectile dynamic response. Contact force histories, stop action snapshots of the model displacements in time and point displacement histories, pitch angles, tip-to-tail angles, cg-to-tip angles, cg-to-tail angles are just a few ways to observe the projectile response, and there are many coordinate systems in which to reference. For the sake of simplicity, projectile responses will be observed only in reference to either the projectile cg or the contact points. For example, in Figure 11. (where length is normalized) the three cases of projectile flexure are observed by holding the contact points at zero.

Shape At Shot Exit

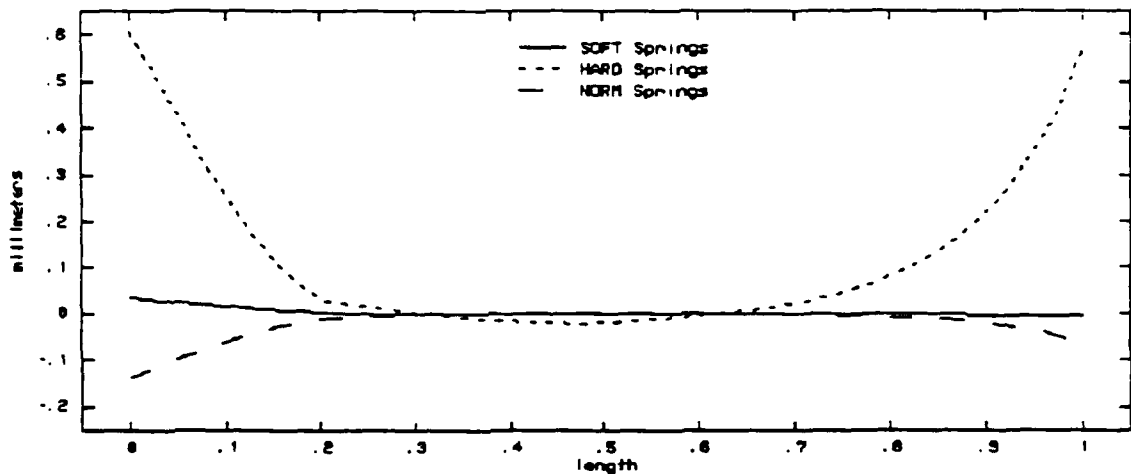


Figure 11. The Horizontal Projectile Shape at Shot Exit.

In Figures 12. and 13. are the tip and the tail displacement histories referencing the projectile model cg in the horizontal plane comparing the response of the three different cases with time zero as shot exit.

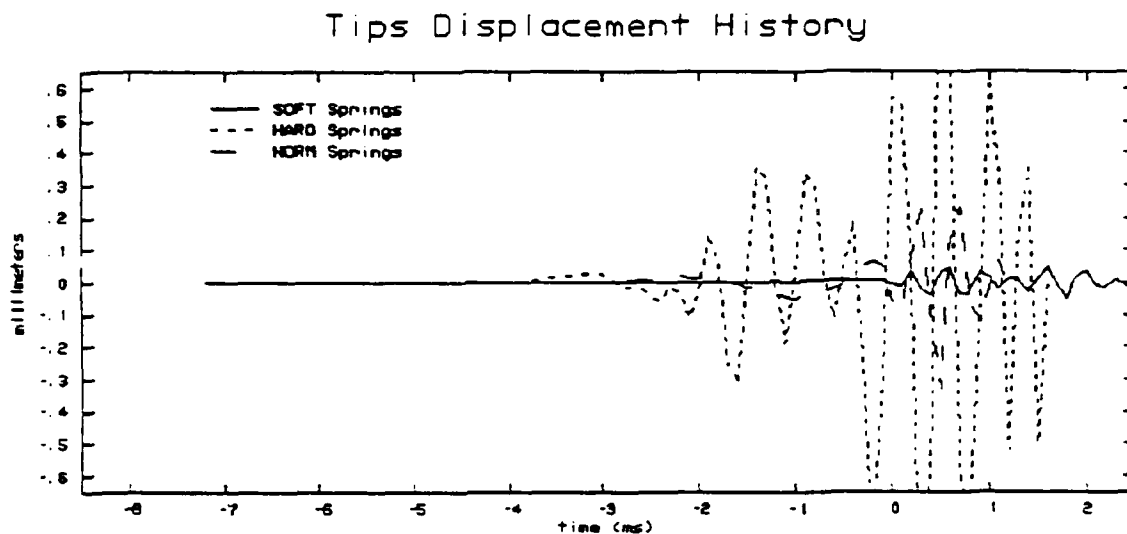


Figure 12. Projectile Tip Displacement Histories.

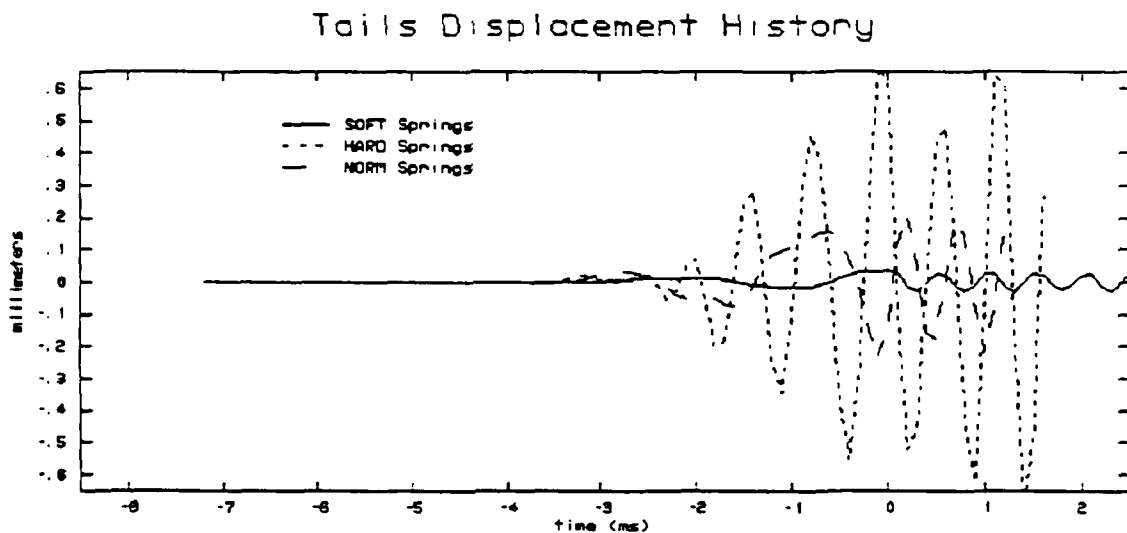


Figure 13. Projectile Tail Displacement Histories.

When observing the gun dynamics results in Figures 5. and 6., it is obvious that the HARD springs case simulation results emulate the rigid body projectile modeling accomplished under the old FORTRAN version. From the projectile modeling results in Figures 11. through 13. it can be seen that the projectile is overloaded and produces excessive vibration. On the other extreme it is obvious that the SOFT springs case is just barely loading the projectile

ERLINE, KREGEL

and barrel producing hardly any vibration. The NORM springs case simulation results look promising.

Going back to our conjecture game, the springs constants can be changed again and again to find values for the spring constants that produce gun dynamics results closely matching the experimental data. Not all the iterations on spring constants will be discussed here. Presented here will be just one other case. This case represents one half of the values used in the NORM springs case driving band and the forward bell of this projectile. Seen in Figures 14. and 15. are comparisons of the results of these gun dynamics cases.

Vertical Shape @ Shot Exit

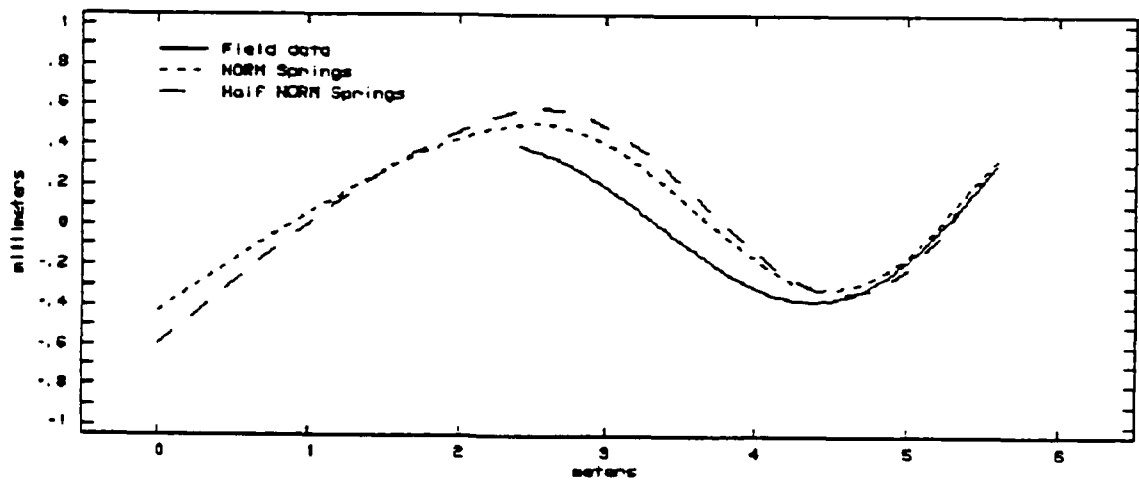


Figure 14. Two Springs Cases - Vertical Gun Shapes Compared.

Horizontal Shapes at Exit

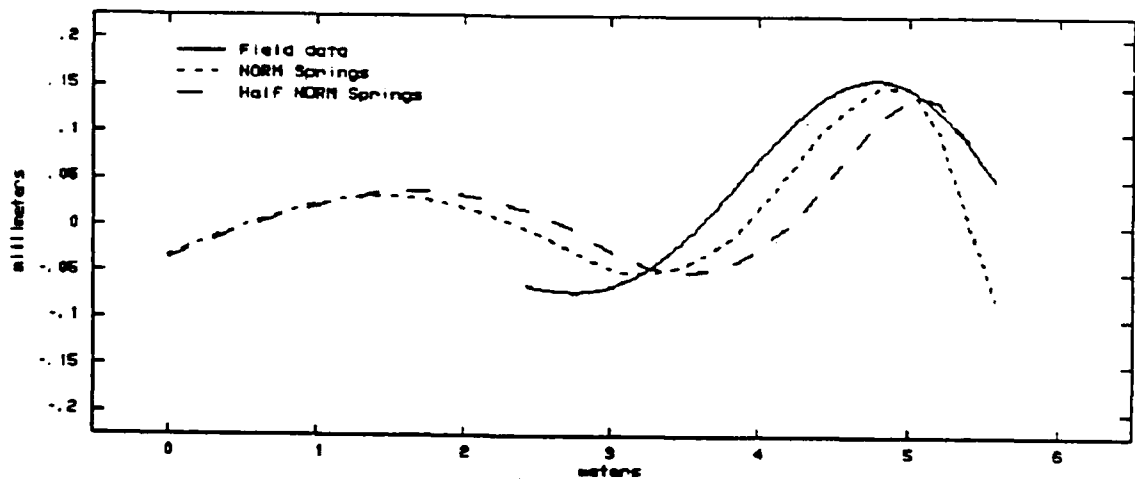


Figure 15. Two Springs Cases - Horizontal Gun Shapes Compared.

ERLINE, KREGEL

SUMMATION AND FUTURE WORK

Interestingly enough the halving of the spring constant values from the conjectured NORM case has shown gun dynamics results that appear very close to the field data. Suffice to say that the projectile's shot exit conditions are different. This indicates there is wide range of values for error if 'guesstimation' is to be the method supplying spring constants for projectiles.

In the near future it is expected that spring constants for this particular projectile shall be measured in the laboratory.

It is important to realize that for any projectile modeled in the future only the method outlined earlier on verifying the values to use for spring constants can the modeler be assured of having valid input into the Little 'Rascal' gun dynamics code. Only then can the results of the projectile dynamics be thought of in terms of precision.

In the future detailed finite element models of projectiles are expected to be generated and subjected to application of graduated static loads to obtain displacements. Also, laboratory measurements are required to verify the finite element models.

REFERENCES

1. D. Warken, K. Wolf, R. Heiser, J. Ballman, and W. Pavel, 'The Effect of Barrel Curvature and Projectile Unbalance on Excitation of Gun Vibrations', Proceedings of the Third U.S. Army Symposium on Gun Dynamics, Rensselaerville, N.Y., May 1982.
2. T. F. Erline, and M. D. Kregel, 'Modeling Gun Dynamics With Dominant Loads', BRL-MR-3638, July, 1988.
3. M. D. Kregel, E. L. Lortie, 'Description and Comparison of the 'K' Method for Performing Numerical Integration of Stiff Ordinary Differential Equations', BRL Report No. 1733, July 1973.
4. M. D. Kregel, J. M. Heimerl, 'Comments on the Solution of Coupled Stiff Ordinary Differential Equations', BRL Report No. 2769, July 1977.
5. T. P. Coffee, J. M. Heimerl, M. D. Kregel, 'A Numerical Method to Integrate Stiff Systems of Ordinary Differential Equations', BRL Technical Report No. ARBRL-TR-02206, January 1980.
6. J. O. Hallquist, D. J. Benson, 'DYNA3D User's Manual', Lawrence Livermore National Laboratory Report UCID-19677, Rev 1., 1986.

ERLINE, KREGEL

REFERENCES

7. S&D Dynamics, Inc., 'Dynamic Analysis Of The 120-mm Tank Gun', BRL-CR-576, June 1987.
8. D. A. Hopkins, 'Modelling Gun Dynamics with 3D Beam Elements', Sixth U.S. Army Symposium on Gun Dynamics, May 1990.
9. H. Gay, A. Elder, 'The Lateral Motion of a Tank Gun and Its Effect On The Accuracy Of Fire', BRL Report No. 1070, March 1959.
10. Private Correspondence with J. A. Bornstein, Ballistics Research Laboratory, Launch and Flight Division, May 1987.
11. Private Correspondence with J. Diebler, Battelle, Pacific Northwest Laboratories, Seattle, Wa. November 1989.

RABERN, BANNISTER

TITLE: FINITE ELEMENT MODELS TO PREDICT THE STRUCTURAL RESPONSE OF 120-mm SABOT/RODS DURING LAUNCH

D. A. Rabern, Ph.D.*
Staff Member, Los Alamos National Laboratory
MS G787 Los Alamos, NM 87544

K. A. Bannister, Ph.D.
Staff Member, US Army Ballistic Research Laboratory
Aberdeen Proving Ground, MD 21005-5066

ABSTRACT:

Numerical modeling techniques in two- and three-dimensions were used to predict the structural and mechanical behavior of sabot/rod systems while inbore and just after muzzle exit. Three-dimensional transient numerical simulations were used to predict the rod deformations and states of stress and strain caused by axial and lateral accelerations during launch. The numerical models include the launch tube, recoil motion, and sabot/rod system modeled as it transits the launch tube and exits. The simulated rod leaves the muzzle of the gun, and exit parameters, including transverse displacement, transverse velocity, pitch, and pitch rate are extracted from the analysis results. Results from the inbore numerical simulations were compared with previous full-scale experiments. The results of the comparisons indicated a predictive capability to model inbore three-dimensional phenomena. Two-dimensional analyses were used to model details of the structural behavior caused by the axial load environment. Methodology and results are presented for several launch environments.

BIOGRAPHY:

PRESENT ASSIGNMENT:

Dr. Rabern's present responsibilities include the numerical and experimental design and evaluation of launch and terminal ballistic performance of kinetic energy munitions.

PAST EXPERIENCE:

Dr. Rabern worked for Thiokol Corporation for three years designing, modeling, and testing tactical rocket motors. He has worked for Los Alamos National Laboratory for the past six years performing dynamic structural and hydrodynamic calculations with supporting experiments to assess inbore and terminal effects of long rod penetrators and armored targets.

DEGREES HELD:

B. S. University of Utah 1979, Civil Engineering
M. S. University of Arizona 1983, Engineering Mechanics
Ph.D. University of Arizona 1988, Engineering Mechanics

**FINITE ELEMENT MODELS TO PREDICT THE STRUCTURAL RESPONSE
OF 120-MM SABOT/RODS DURING LAUNCH**

D. A. Rabern, Ph.D.*
Los Alamos National Laboratory
Los Alamos, NM

K. A. Bannister, Ph.D.
US Army Ballistic Research Laboratory
Aberdeen Proving Grounds, MD

INTRODUCTION

Previous studies have used numerical simulations in two- and three-dimensions to characterize the structural response of sabot/rod systems during launch. Considerable effort was dedicated to axisymmetric finite element analyses to model the sabot and rod and their interface in quasi-static and dynamic simulations [1]. These calculations provide a good representation of stresses induced from the axial accelerations that occur during launch. They did not model the details of several sabot petals, tube straightness, or tube droop. More recent efforts have included using three-dimensional dynamic finite element analyses to model the axial and lateral accelerations associated with projectile launch from smooth-bore guns while the projectile was inbore [2,3]. This paper presents recent modeling techniques that extend numerical modeling capabilities in two- and three-dimensions to include inbore parameters that affect the flight path of the projectile. The analyses were focused on determining motions imparted to the projectile components during inbore travel and on understanding subsequent motions of the projectile after muzzle exit. The ultimate goals here are to ensure the structural integrity of the projectile during launch and to reduce the dispersion of kinetic energy (KE) rounds at the target. These recent code applications and methodologies are reviewed and typical results from the calculations are presented.

In sabot/rod systems the rod is very stiff in the axial direction and flexible in the lateral direction. A schematic of the M829 sabot/rod system is shown in Fig. 1. When subjected to lateral loads caused by the launch tube profile or by projectile balloting, the sabot/rod system vibrates. Artillery shells are stiff axially and laterally; vibrations in these systems contain higher frequency modes than

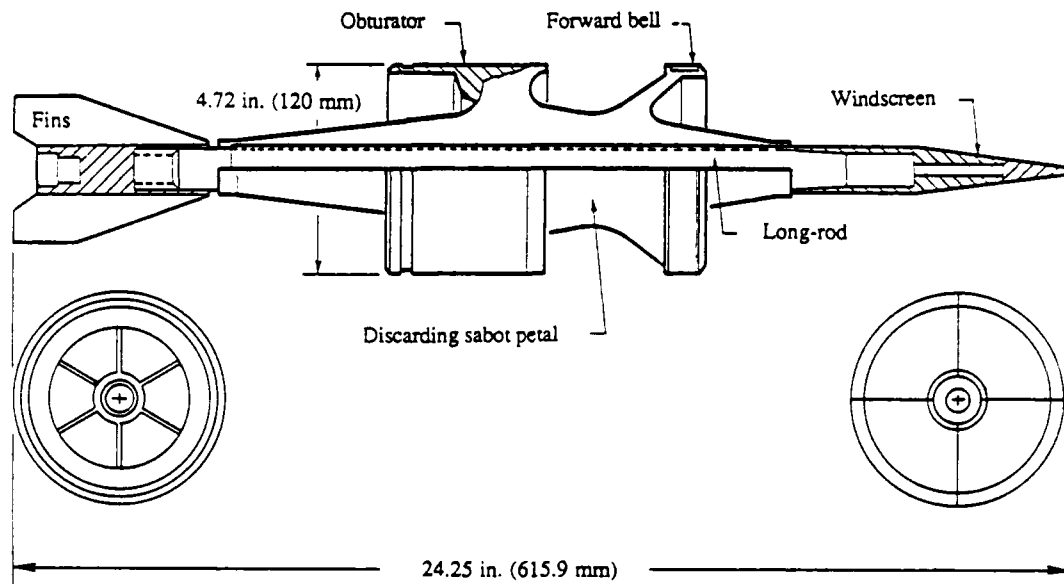


Figure 1. M829 sabot/rod schematic.

occur with the sabot/rod systems, but lateral bending is minimal. A rough estimate of peak lateral accelerations for sabot/rod systems is 1 to 10% of the peak axial acceleration, or for the 120-mm gun, about 500 to 5000 g's. This lateral acceleration is the deciding criterion for determining whether two-dimensional axisymmetric analyses or three-dimensional analyses will suffice in a specific simulation. Three-dimensional analyses, while desirable, are expensive, and they require extensive computer resources. The advantage of two-dimensional models is that very detailed modeling of sabot/rod interfaces and system components can be completed. The disadvantages are the absence of the lateral or torsional load environments and the inability to model nonsymmetric geometry, such as the discontinuity associated with sabot petals.

Several numerical analysis approaches to model the launch of sabot/rod can be used, depending on the problem, the results needed, and the manpower and computer resources available to the analyst. Beam models for predicting the axial and lateral motion of the sabot and rod have been used with success for some applications. These codes usually run on personal computers that require minimal computing resources. Two-dimensional, finite element computations that are static and linearly elastic are used to study the axial load environment associated with launch. Two-dimensional dynamic, nonlinear analyses require additional computational resources, but they include important effects caused by the dynamic load environment and by material nonlinearity. Two-dimensional rezoning is also used to model materials with large nonlinear deformations, such as obturators, during the engraving process. Simulating the dynamic axial, lateral, and torsional environments with launch tube droop, eccentric masses,

RABERN, BANNISTER

and nonsymmetric geometry requires dynamic three-dimensional finite element codes. These codes are used to model the gun and ammunition system for the duration of launch. A summary of the computational requirements for some typical inbore sabot/rod analyses is presented in Table I. This table is shown only to contrast the different analytical resources required.

TWO-DIMENSIONAL SIMULATIONS

A typical dynamic analysis of the M829 sabot/rod system in two dimensions was completed with the DYNA2D finite element code [4]. This type of analysis is used to determine the structural behavior of the sabot/rod system caused by the axial load environment. Changes in sabot geometry affect the way load is transferred to the rod. A two-dimensional dynamic analysis can be used to optimize sabot geometry to distribute the load into the rod as desired and minimize the parasitic weight of the projectile.

TABLE I
COMPUTATIONAL RESOURCES FOR INBORE SIMULATIONS

Code Type	Problem Type	Approximate Computer Run Time (hours)	Code	Computer
2D-beam	Projectile + tube	0.5	RASCAL	Zenith PC
3D-beam	Projectile + tube	1-4	SHOGUN	Apollo WS
2D finite element	Projectile	1-2	DYNA2D	Cray XMP/48
2D finite element	Projectile + tube	6	DYNA2D	Cray XMP/48
2D finite element	Projectile + tube and 1D burn code	6-7	DYNA2D	Cray XMP/48
2D finite element	Projectile + tube + obturator (rezoning)	6-12	DYNA2D	Cray XMP/48
2D finite element	Projectile + tube + obturator (rezoning) and 1D burn code	8-13	DYNA2D	Cray XMP/48
3D finite element	Projectile + tube (180-deg course mesh)	7	DYNA3D	Cray XMP/416
3D finite element	Projectile + tube (360-deg medium mesh)	10-15	DYNA3D	Cray YMP

RABERN, BANNISTER

The finite element mesh of the sabot/rod are shown in the upper half of Fig. 2. The obturator is not shown in the figure. Details of the threaded interface were not considered in this analysis. Points A, B, and C are referenced to show typical stress results from a dynamic load environment. In the same figure, the axial stress for the three locations is plotted from propellant ignition to peak pressure. At location A the rod is being pulled and the corresponding tensile stress is indicated. At location B, near the center of the rod, compressive stress is indicated. Station C, near the front of the sabot, indicates a still higher compressive stress.

The long duration of load does not excite natural frequencies in this sabot/rod system. This indicates that a static analysis with peak pressure would be a reasonable compromise from which to determine stress levels in the sabot and rod when they are subjected to an axial load environment. If the load

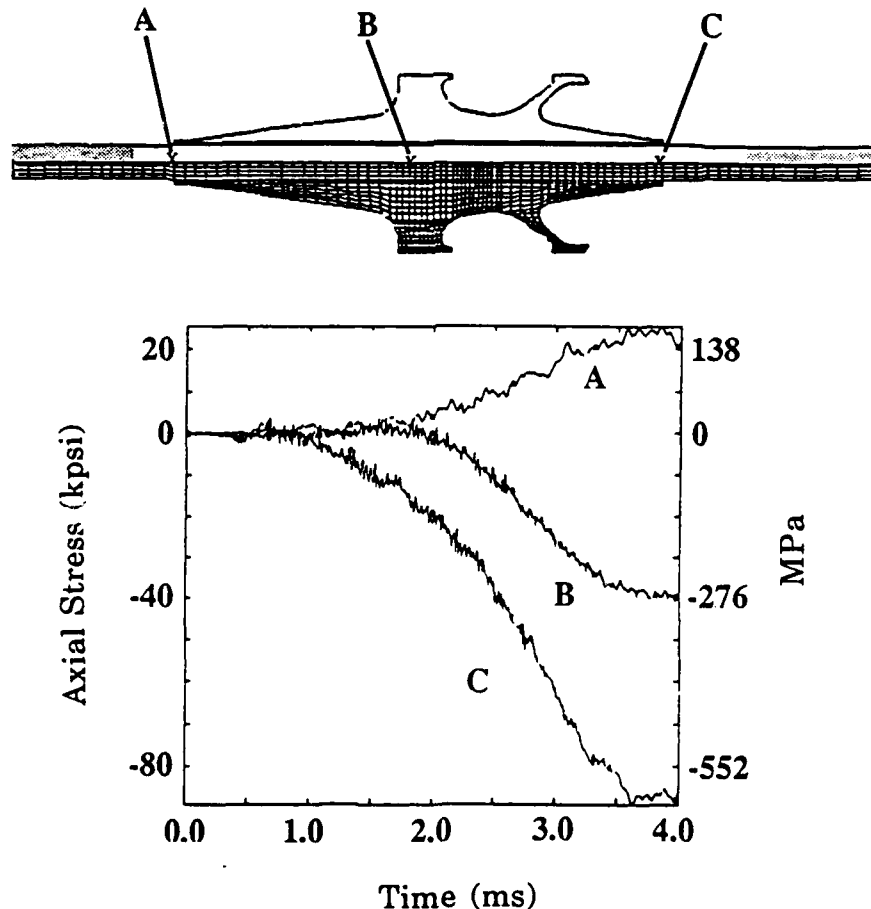


Figure 2. M829 two-dimensional finite element analysis.

duration occurs and causes natural frequencies to be excited during the launch process, a dynamic solution is required. Efforts to determine the natural frequency of the sabot/rod system are complicated by the shared boundary conditions between the sabot and rod and the sabot petal interfaces, and by the obturator and launch tube constraints. If natural frequency information is extracted numerically this will only provide data for the modeled system. Information from a finite element grid provides insufficient data to determine the actual natural frequency of a system, where the sabot can take compression, but no tension, in the hoop direction because of the sabot splits and because the sabot/rod interface takes shear loads but only minimal radial loading.

Modeling of the threaded interface is best accomplished using a two-dimensional code. A good example of this type of modeling was documented by Costello [5]. Additional modeling areas include recent efforts to model the moving pressure front that follows the projectile in the launch tube and the coupled burn codes to predict the magnitude of the pressure, coupled with the mechanical and structural displacement of the projectile as it travels down the launch tube. These unpublished options are not widely implemented and are still in the research phase.

THREE-DIMENSIONAL SIMULATIONS

At the instant of firing, gun tubes are neither perfectly straight nor rigid, so the projectile travels along a flexible curved path. Each launch tube has a unique initial path that the projectile negotiates as it transits the tube. This path changes with tube motion because of recoil, breech block eccentricity, mounting conditions, and projectile, pressure, and propellant interactions. These issues must be considered before we can adequately predict the structural and mechanical performance of sabot/rod systems during launch. These components, as well as multiple sabot petals, require a three-dimensional analysis to predict lateral accelerations, tube movement, and tube/projectile interactions.

Previous work in three-dimensional analyses [2,3] were extended to include the projectile's behavior as it leaves the muzzle of the gun. Analyses and experiments were performed to establish a methodology for predicting the structural behavior of sabot/rod systems while inbore. The sabot/rod systems and their launch environments were modeled numerically to describe in detail the structural behavior of each system as it travels down each of the launch tubes. The numerical modeling was performed to predict the stress environment and the response of the sabot/rod system. The data obtained were used to compare the structural integrity of the three separate sabot designs in three separate launch environments. A brief description of the previous work performed is introduced here to explain how that work was enhanced to include near muzzle trajectory after exiting the launch tube.

Previous Work

The M829 sabot/rod (Fig. 1) was modeled in three different 120-mm smooth-bore launch environments. The first launch tube was perfectly straight and was modeled to remove the effects of lateral loading on the sabot/rod system. The second launch tube, SN104, was used to observe the effect of minimal lateral loading on the sabot/rod system. The third launch tube, SN81, was used to observe the effects of significant lateral loads on the system. To obtain the initial launch tube profile of each tube, the launch tube was modeled with the ABAQUS [6] finite element code to determine the launch tube droop caused by gravity. Line-of-sight straightness data were superimposed on the tube droop to determine the initial launch tube profile before propellant ignition. Figure 3 presents the ABAQUS results (shown as the dashed line). The solid line represents the line-of-sight straightness for Launch Tube SN104. The addition of the lateral displacements associated with Launch Tube droop and line-of-sight straightness provides the initial tube profile (shown as the dash-dot line). Figure 4 presents the same information for Launch Tube SN81. The two launch tube profiles are contrasted in Fig. 5. Launch Tube SN104 shows minimal deviation at the end of the launch tube. In Launch Tube SN81 the projectile must negotiate a significant launch path change in the high velocity sector of projectile launch.

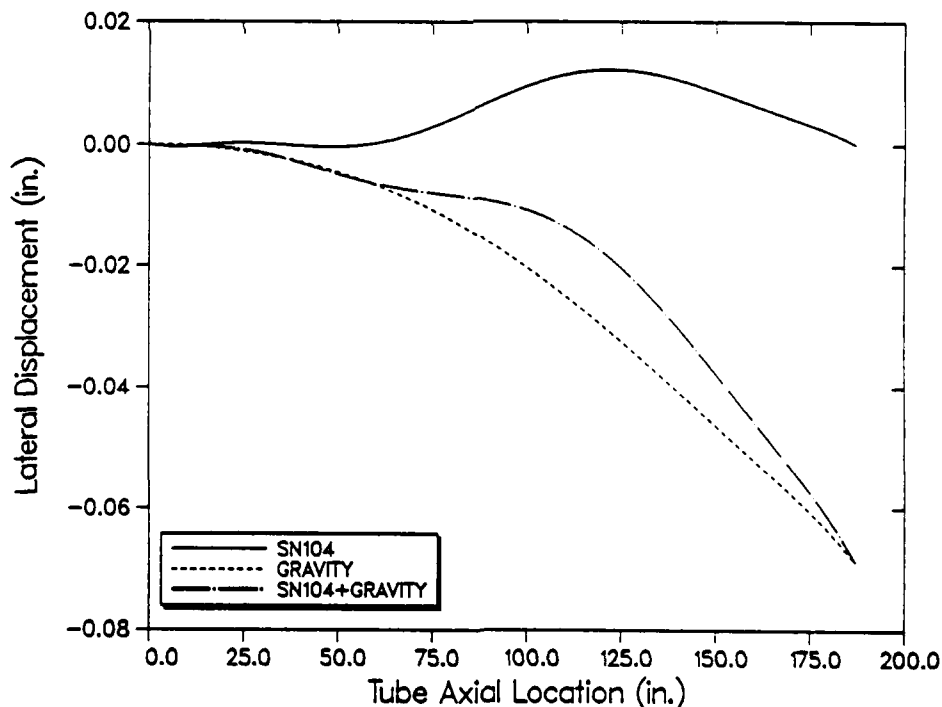


Figure 3. Lateral displacement versus axial location for Launch Tube SN104 at its initial state while under gravity loading and with the combination of the two.

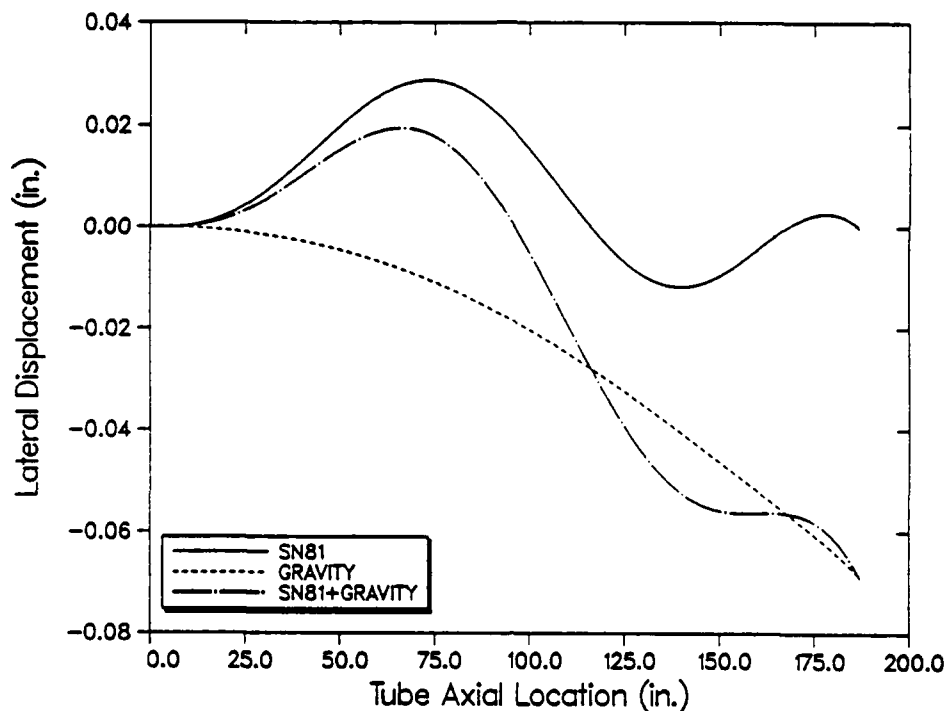


Figure 4. Lateral displacement versus axial location for Launch Tube SN81 at its initial state while under gravity loading and with the combination of the two.

These launch tubes were drawn from the US Army inventory. These profiles give an appreciation of the variability in straightness in a population of guns tubes and demonstrate the importance of considering this parameter in dynamic simulations of 120-mm gun systems. These particular launch tubes were chosen for the study for several reasons. Both launch tubes exhibit only small line-of-sight deviations parallel to the ground. This enables 180-deg three-dimensional analyses with a symmetry plane. With small changes in launch tube straightness parallel to the ground, high energy radiography equipment, which needs to be level, could be used to take radiographs of the sabot/rods through the launch tube and determine their deformed shapes caused by the launch tube lateral forcing function. Three launch environments and three M829 class sabot designs were studied numerically and experimentally to determine the launch environment and sabot design influence on inbore structural performance. The extended work presented in this paper addressed only the M829 sabot/rod in Launch Tubes SN81 and SN104.

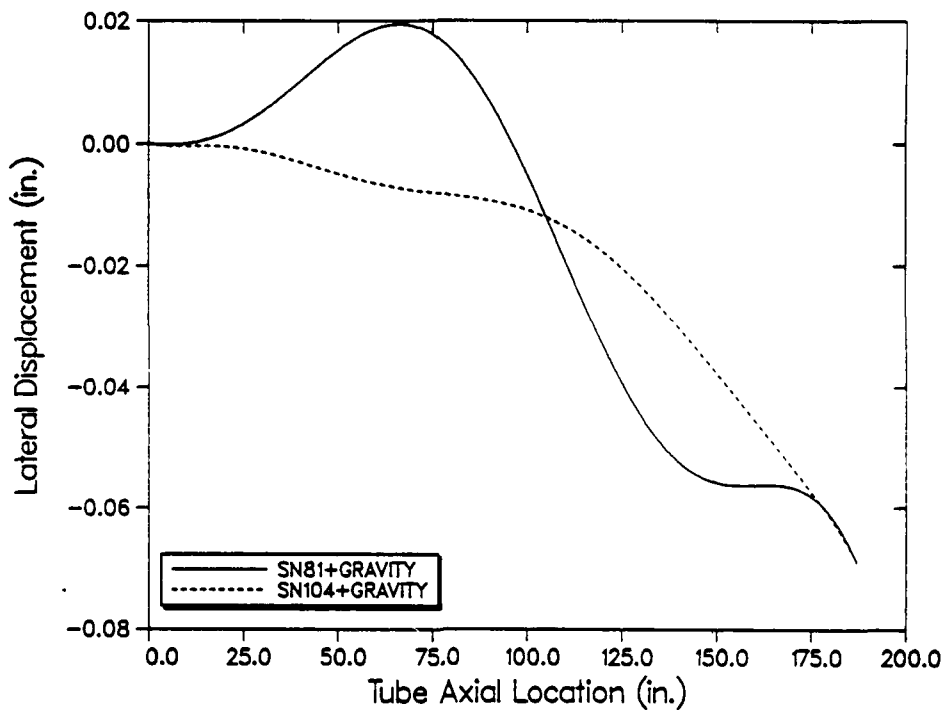


Figure 5. Comparison of lateral displacement versus axial location for Launch Tubes SN81 and SN104.

A full-scale test program was completed to determine the M829 rod deformed shape at three locations in Launch Tube SN81 and at two orthogonal stations after muzzle exit. Inbore radiography with a 2.3-MeV x-ray unit and orthogonal x-rays downrange were used to take radiographs of the sabot/rod in the launch tube and downrange [7]. Radiographs were digitized and processed to determine the centerline of the projectile at several locations inside and outside the launch tube. These data were used to benchmark numerical simulations completed earlier in the study.

DYNA3D [8], an explicit finite element code, was selected for the numerical analyses. This code has traditionally been used for dynamic transient analysis involving impact and contact surfaces. A 180-deg model, rather than a full 360-deg system, was generated. Appropriate boundary conditions were applied on the symmetry plane. The tube environment selected showed little motion normal to the constrained surface and was assessed to have small effects on the analysis results. With the 180-deg model, the problem size was cut significantly over a full 360-deg model. The M829 sabot/rod mesh in Launch Tube SN81 at time zero is shown in Fig. 6.

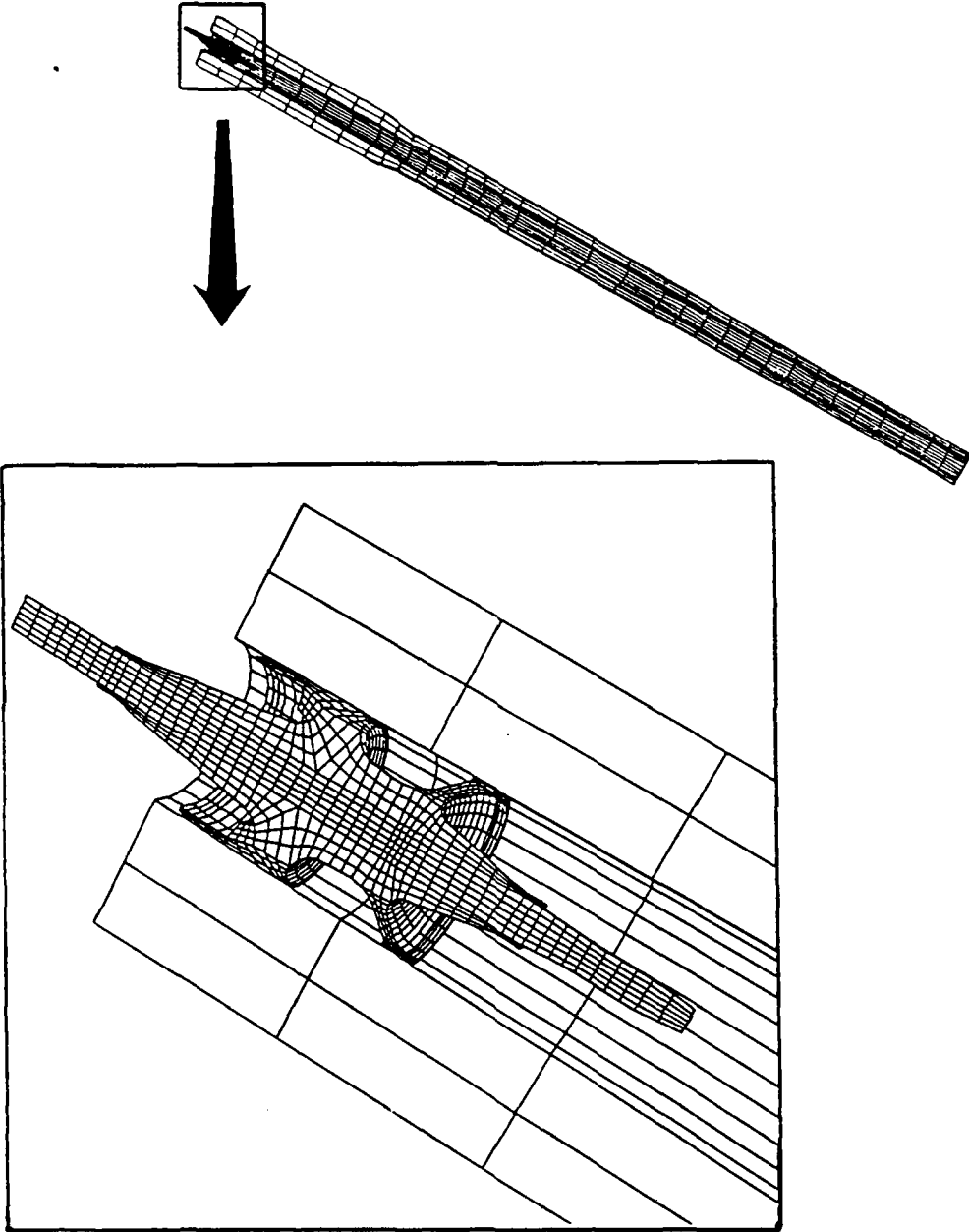
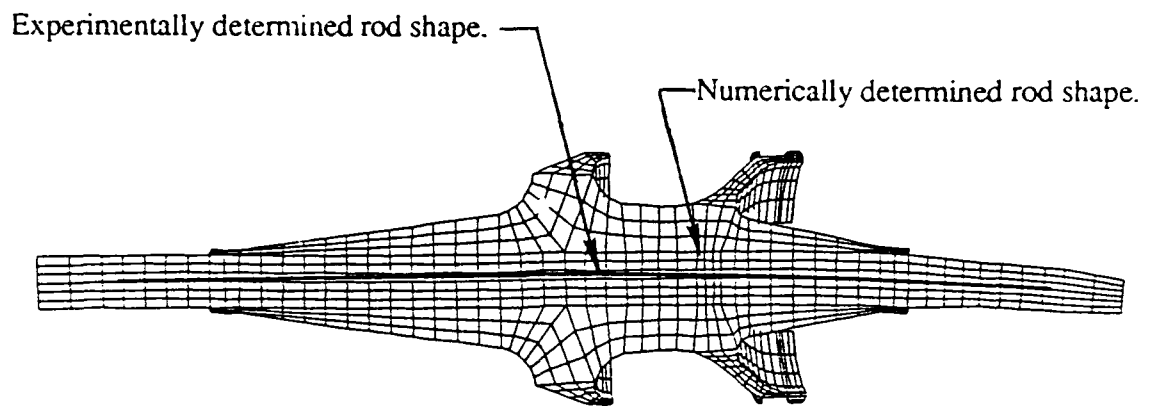
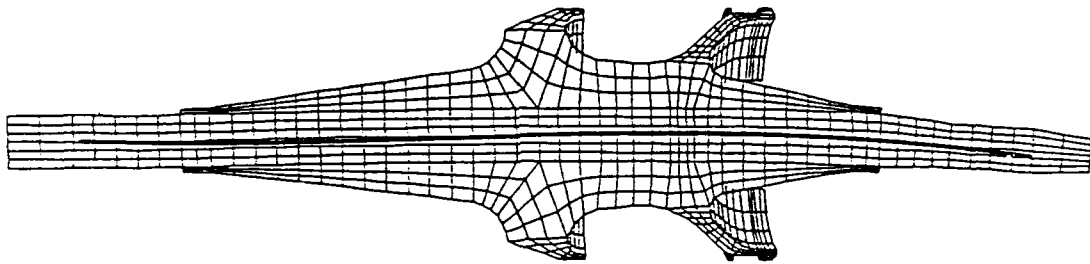


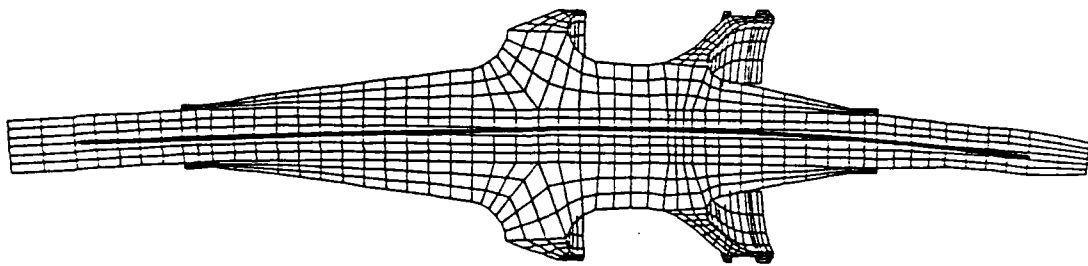
Figure 6. Finite element mesh of M829 sabot/rod system and launch tube.



Deformed rod 66 in. from launch tube muzzle.



Deformed rod 58 in. from launch tube muzzle.



Deformed rod 52 in. from launch tube muzzle.

Figure 7. Comparison of numerically and experimentally determined rod deformed shapes.

RABERN, BANNISTER

The meshes consist of approximately 7000 nodes and 5000 eight-node hexahedron elements. Six materials, three sliding surfaces, two load curves, and approximately 1000 pressure surfaces are used in each model. Although each of the models differs slightly, the meshes are relatively similar. The fin, windscreen, and launch tube were modeled with elastic material models. The obturator, sabot, and rod were modeled with a work-hardening elastic-plastic material model. The sliding surfaces occur between sabot petals, between the obturator and the launch tube, and between the forward bell and the launch tube.

Results from three experiments were compared with results from the numerical analyses. In these tests the M829 sabot/rod was used in Launch Tube SN81. The deformed shape of the rod at the centerline was calculated for each test and was plotted at the same displacement scale factor as that used in the numerical analyses. These results are superimposed on the deformed finite element mesh at the corresponding axial locations in the launch tube. Shown in Fig. 7 are the comparisons at three separate locations. The launch tube's axial locations, rather than times, were chosen to account for the small differences in velocity between the physical testing and the numerical analyses. The numerical analyses were performed with an exit velocity of 1.65 km/s; the physical experiments showed velocities between 1.67 and 1.69 km/s. Axial locations were used to compare the results. As indicated in Figure 7 the deformed pattern from testing closely matches the numerical analyses. The top comparison shows the rod 66 in. from the launch tube muzzle. The measurement is made from the tail fins of the rod. The middle comparison shows the rod 58 in. from the muzzle, and the bottom comparison shows the rod 51 in. from the muzzle. These data show that the numerical analysis deformation cycle is slightly faster than shown in the physical tests. The effect is small. The general shape of both tests and numerical analyses agree well. Table II is a summary of the tip and tail displacements referenced from the center of gravity (c.g.) of the rod from both the numerical analyses and the physical tests.

Table III shows the peak von Mises stresses that occur in each launch environment at seven selected times during the launch process. The results indicate that for launch tube SN81, the lateral loadings do not significantly affect the sabot/rod until the velocity has increased in the latter stages of launch. At this point the effect, compared with the effect obtained using the perfectly straight (PS) launch tube, develops as much 296% higher stresses because of the lateral stress environment.

Extended Work

After the study was completed, questions arose concerning muzzle exit parameters. The M829 sabot/rod numerical models were modified to include the recoil motion of the launch tube. Originally, the numerical simulations were terminated at muzzle exit (7.2 ms). The M829 simulations in Launch Tubes SN81 and SN104 were rerun to 9.0 ms so data could be extracted beyond the muzzle.

TABLE II
 COMPARISON OF TIP AND TAIL DISPLACEMENTS:
 EXPERIMENTAL TESTING VS NUMERICAL ANALYSES
 OF M829 IN LAUNCH TUBE SN81

Axial location from muzzle of gun (in.)	66	58	51
Numerical tip displacement (in.)	0.042	0.037	0.018
Experimental tip displacement (in.)	0.048	0.043	0.025
Numerical tail displacement (in.)	-0.016	0.004	0.032
Experimental tail displacement (in.)	-0.011	0.007	0.036

TABLE III
 MAXIMUM VON MISES STRESS (ksi) FOR THREE LAUNCH ENVIRONMENTS
 AT SEVEN SELECTED TIMES (s)

Time	0.0034	0.0039	0.0047	0.0053	0.0063	0.0069	0.0072
SN81	82	88	75	74	67	42	74
SN104	82	88	76	60	52	35	37
PS	82	88	76	63	37	29	25

The coordinate system for the calculations is the same as that used in the original M829 simulations. The coordinate system is shown in Fig. 8. The tube droop of the launch tube is 0.069 in. The angle between coordinate systems is 0.023° in the xy-plane.

The axial location of the sabot/rod is shown as a function of time in Fig. 9. The projectile exits the launch tube after 187 in. of travel. The simulation is terminated 293 in. from the projectile's original position or 106 in. after muzzle exit. Sabot separation and aerodynamic forces are not considered in these simulations. In reality, projectile motion will be influenced by sabot separation and aerodynamics. The axial velocity of the projectile is plotted in Fig. 10. The projectile accelerates to 5414 fps (1.65 km/s) until it exits at 7.2 ms. The velocity remains constant for the remainder of the simulation.

The average projectile lateral displacement presented in the numerical analysis coordinate system is shown in Fig. 11. The lateral displacement is calculated using several nodal traces along the axis of the rod and averaging these traces to determine the average lateral displacement of the rod for the M829 sabot/rod in Launch Tubes SN 81 and SN104. A positive lateral displacement

Numerical Analysis
Coordinate System

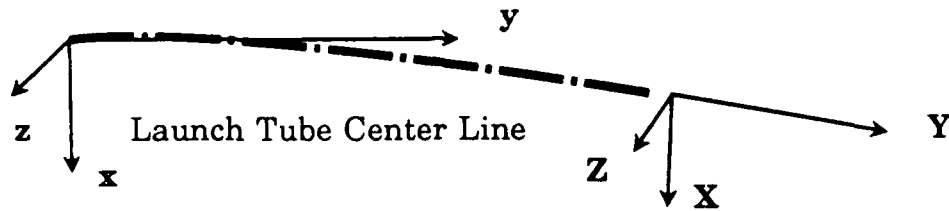


Figure 8. Analysis coordinate systems, M829 study.

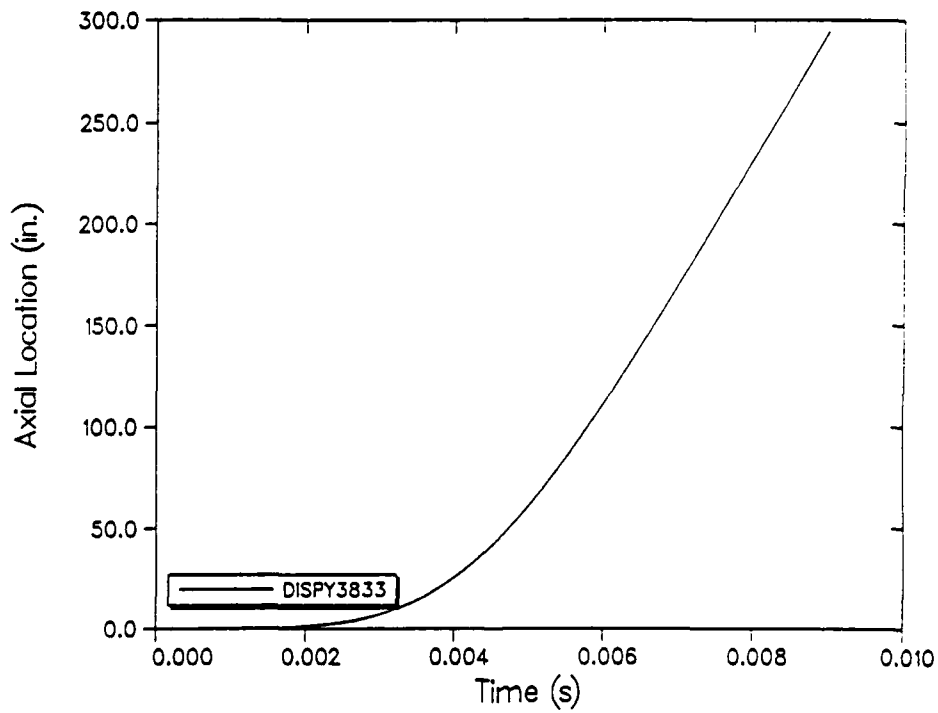


Figure 9. Axial location versus time for M829 sabot/rod.

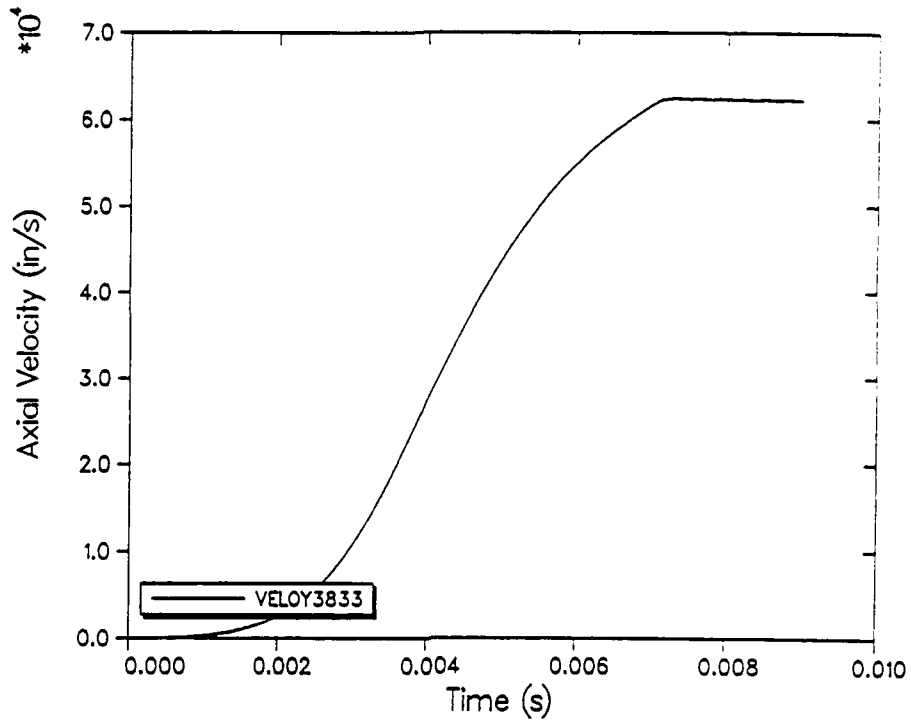


Figure 10. Axial velocity versus time for M829 sabot/rod.

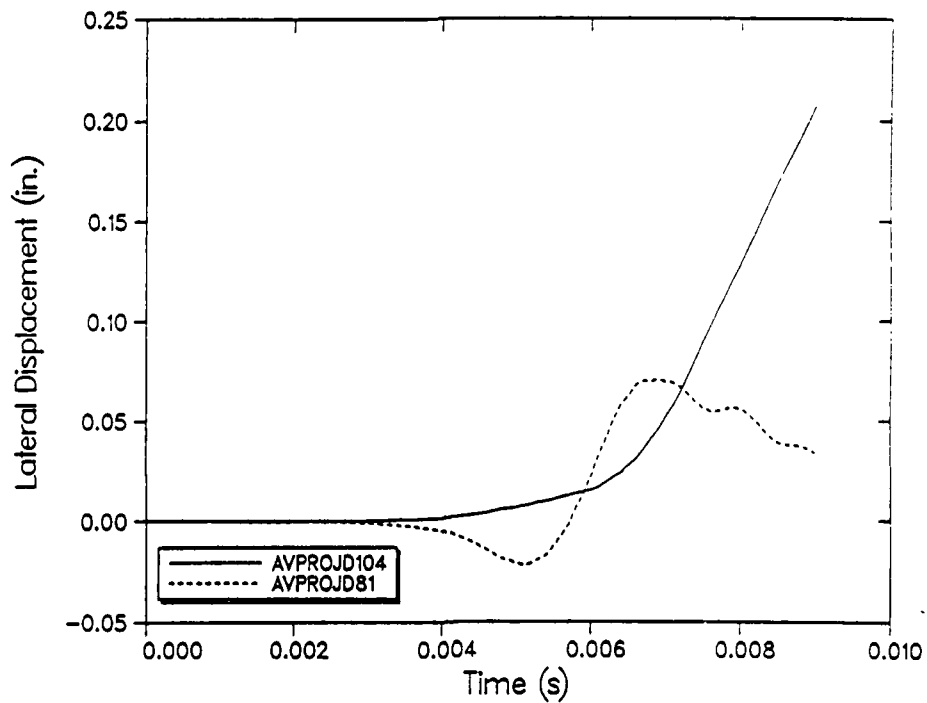


Figure 11. Average M829 projectile lateral displacement versus time for Launch Tubes SN81 and SN104.

RABERN, BANNISTER

indicates that the projectile is moving toward the ground. The lateral velocity for the two launch environments is shown in Fig. 12. This figure indicates that Launch Tube SN 81 causes an upward velocity of 23 in./s. Launch Tube SN104 produces a downward velocity of 76 in./s.

The tip and tail displacements referenced from the c.g. of the rod are shown for both launch tube environments in Fig. 13. The rigid body movement of the rod is removed by subtracting the lateral motion from the nodal traces at the tip and tail. The tip of the M829 sabot/rod in Launch Tube SN104 is plotted as the solid line, and the tail is plotted as the dashed line. The displacements are larger for Launch Tube SN81. The tip is shown as the dash-dot line and the tail as the dotted line.

The launch tube dynamics for the two cases considered are also plotted. Lateral displacement of the muzzle is shown for Launch Tube SN104 and SN81 in Fig. 14. The lateral velocity of the muzzle is shown in Fig. 15. A summary of the projectile and launch tube parameters at the muzzle exit are summarized in Table IV. The data presented are in the numerical analysis coordinate system (Fig. 8).

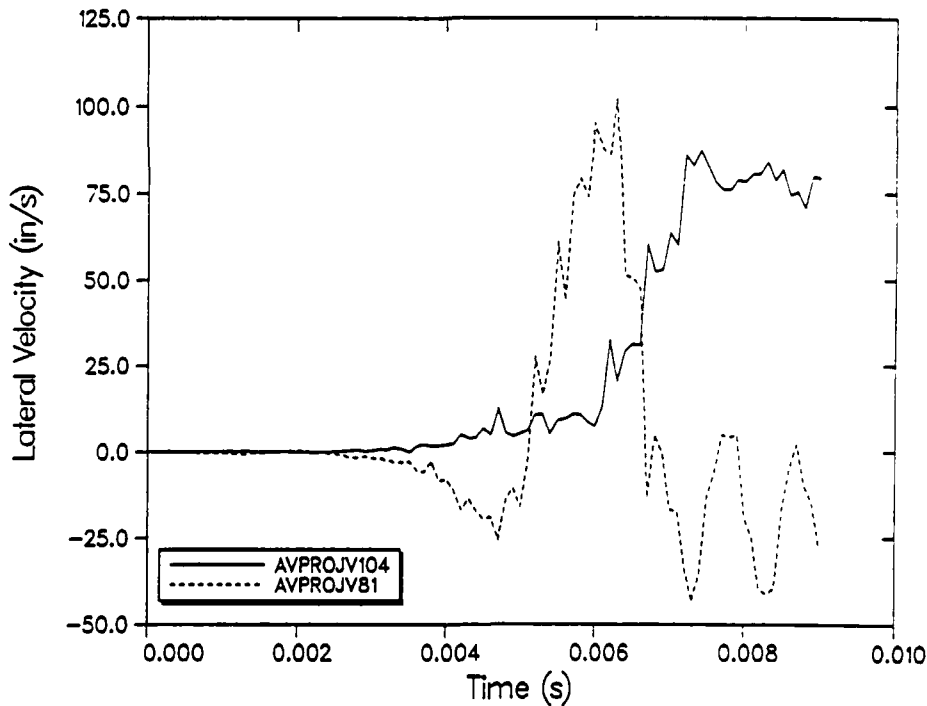


Figure 12. Average M829 projectile lateral velocity versus time for Launch Tubes SN81 and SN104.

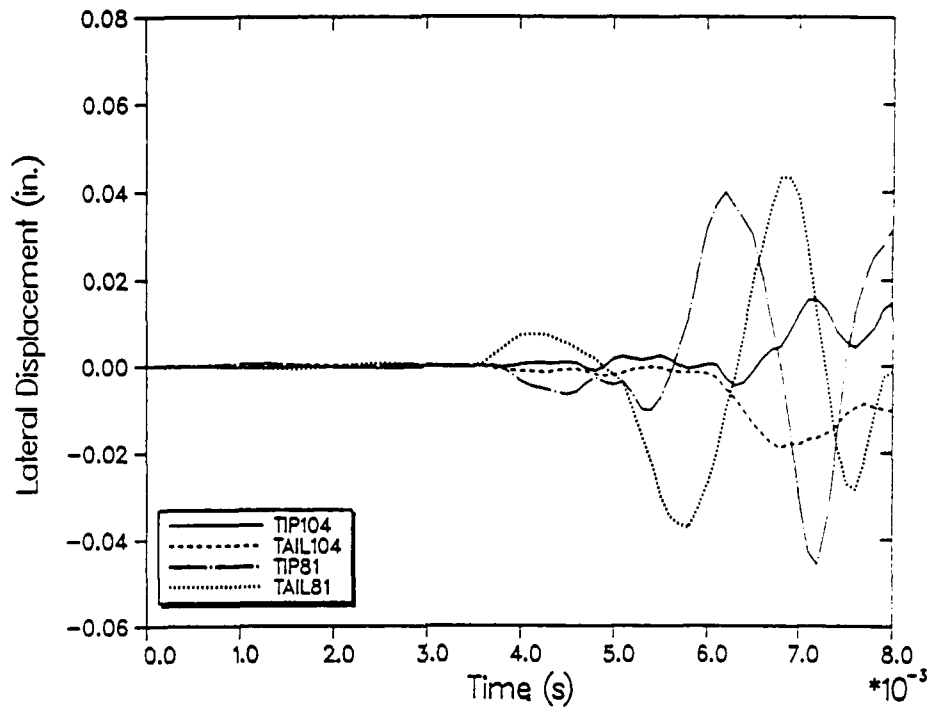


Figure 13. M829 tip and tail displacement with respect to the rod c.g. versus time in Launch Tubes SN81 and SN104.

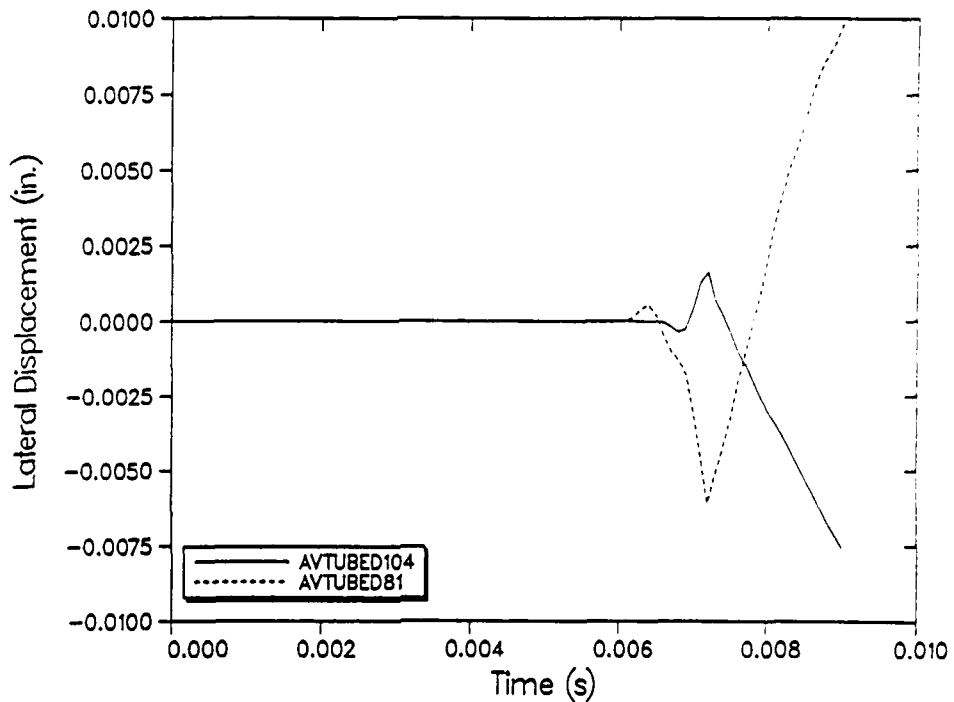


Figure 14. Average muzzle lateral displacement for Launch Tubes SN104 and SN81.

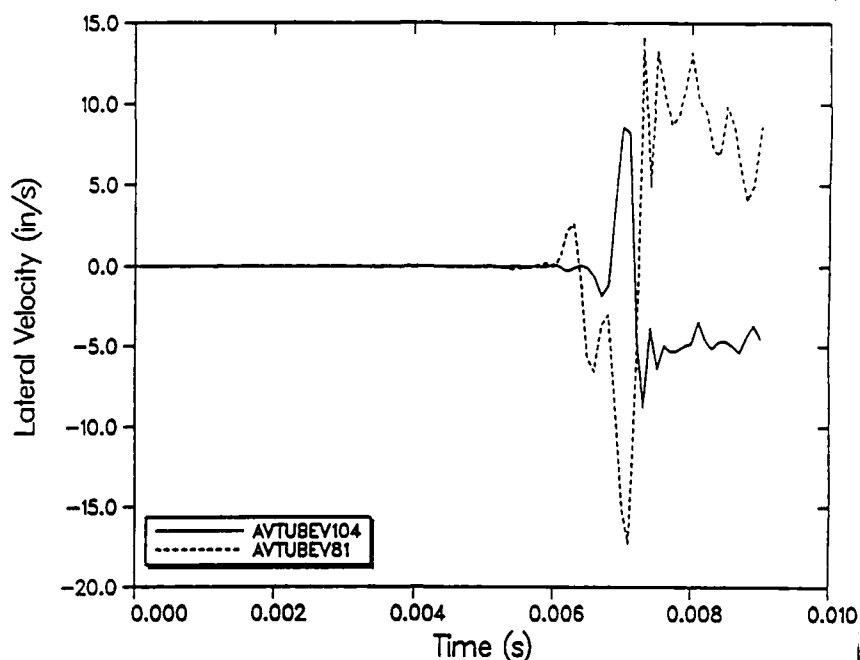


Figure 15. Average muzzle lateral velocity for Launch Tubes SN104 and SN81.

TABLE IV
DISPLACEMENT AND VELOCITY SUMMARY OF M829 SABOT/ROD
LAUNCHED FROM LAUNCH TUBES SN81 AND SN104

Launch Environment	SN81	SN104
Projectile x displacement at exit (in.)	0.063	0.069
Projectile x-velocity at exit (in./s)	-23	77
Absolute maximum rod tip x-displacement with respect to rod c.g. (in.)	0.046	0.017
Absolute maximum rod tail x-displacement with respect to rod c.g. (in.)	0.042	0.019
Rod tip x-displacement with respect to rod c.g. at exit (in.)	-0.021	0.016
Rod tail x-displacement with respect to rod c.g. at exit (in.)	0.008	-0.007
Launch tube x-displacement at projectile exit (in.)	-0.006	0.001
Launch tube x-velocity at projectile exit (in./s)	7	-5

RABERN, BANNISTER

Data presented in the tables and figures have been referenced to the xyz-coordinate system outlined in Fig. 8. Lateral velocities, pitch, and yaw are more meaningful when referenced from the launch tube's pointing angle XYZ-coordinate system. This pointing angle coordinate system was used in the experimental program. Table V presents data from the both of the launch environments in the XYZ-coordinate system for lateral velocities, pitch, yaw, pitch rate, and yaw rate. Pitch and yaw data were taken 36 in. after muzzle exit. Data from Table V indicate that the projectile from Launch Tube SN81 flew upward with a lateral velocity of 49 in./s, with a downward pitch of 0.14 deg, rotating upward at a rate of 304 deg/s. The projectile from Launch Tube SN104 moved laterally down at 51 in./s, with a downward pitch angle of 0.05° and an upward rotation of 39 deg/s. Figure 16 is a schematic of projectile motion from each launch environment.

CONCLUSIONS

Numerical tools for predicting the structural and mechanical performance of sabot/rods during launch have been used in various applications. The results have been compared with experimental data to verify their validity. Modeling techniques have evolved to include the three-dimensional analyses of sabot/rods and gun systems.

TABLE V
MUZZLE EXIT PARAMETERS IN MUZZLE POINTING ANGLE COORDINATE SYSTEM FOR THE M829 SABOT ROD IN LAUNCH TUBES SN81 AND SN104

Launch Environment	SN81	SN104
Projectile X-velocity (in./s)	49 up	51 down
Projectile pitch 36 in. from muzzle (deg)	0.14 down	0.05 down
Pitch rate 36 in. from muzzle (deg/s)	304 up	39 up

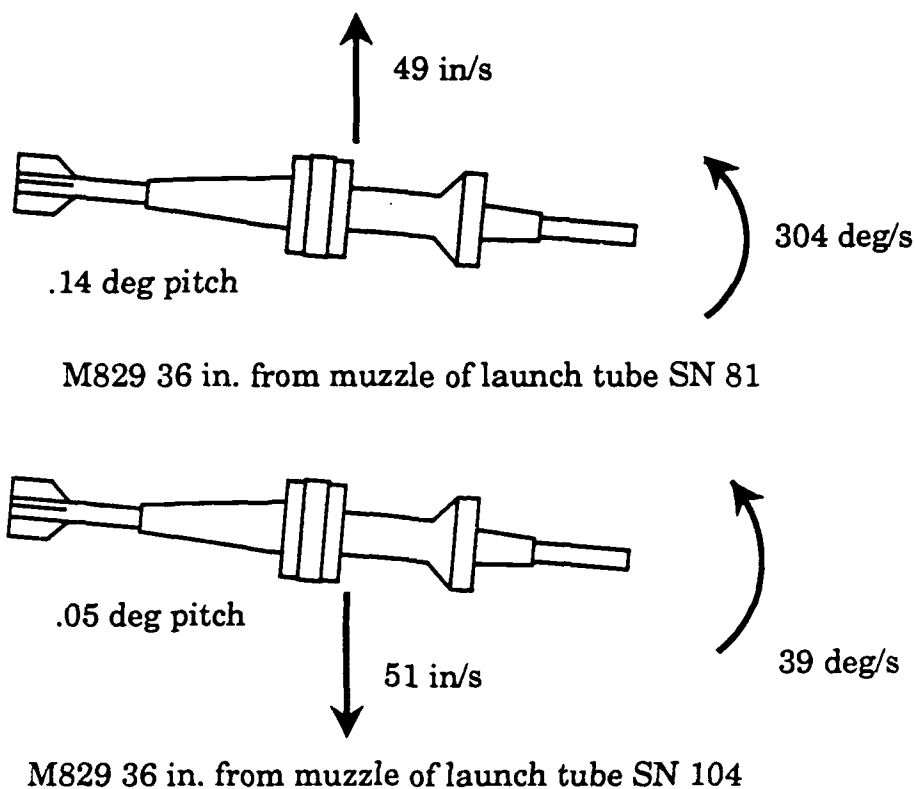


Figure 16. M829 sabot/rod motion, 36 in. after muzzle exit.

Two-dimensional finite element codes predict the axial performance of sabot/rod systems very well. Because peak pressure occurs early in projectile travel, the lateral load environment is small at this time. The projectile is moving slowly at peak pressure and has traveled only a short distance. Predicting the structural performance of the sabot/rod caused by lateral loads requires a three-dimensional analysis. The analyses needs to include seperate sabot petals, the launch tube and launch tube profile, and recoil. These analyses are well in hand but extensive postprocessing is required to make sense of the results. This is both time consuming and cumbersome, with large three-dimensional solutions. Careful evaluation of results is required to verify the validity of numerical models with complex geometry, dynamic load environments, sliding surfaces, nonlinear material response, and complex interfaces.

RABERN, BANNISTER

Future work in this area will provide more accurate solutions and greater capabilities for solving a wider class of problems. To accomplish this research in the area of sliding algorithms, code coupling with burn models and moving pressure fields are required. These efforts will enable the analyst to predict structural and mechanical behavior in gun and sabot/rod systems and will enable them to optimize their designs for lower parasitic weight of the sabot and minimal dispersion caused by projectile launch.

ACKNOWLEDGMENTS

The United States Department of Army, Department of Energy and the Ballistic Research Laboratory funded this research. The authors wish to thank L. L. Shelley for editing this manuscript.

REFERENCES

1. Drysdale, W. H., "Design of Kinetic Energy Projectiles for Structural Integrity," U. S. Army Ballistic Research Laboratory technical report ARBRL-TR-02365, Aberdeen, Maryland (1981).
2. Rabern, D. A., "Axially Accelerated Saboted Rods Subjected to Lateral Forces," Los Alamos National Laboratory report LA-11494-MS, Los Alamos, New Mexico (1989).
3. Rabern, D. A., "In-bore Structural Behavior of 120-mm Saboted Long Rods Subjected to Axial and Lateral Accelerations," in *Proceedings of the 11th International Symposium on Ballistics*, Brussels, Belgium (1989).
4. Hallquist, J. O., "User's Manual for DYNA2D -- An Explicit Two-Dimensional Hydrodynamic Finite Element Code with Interactive Rezoning," Lawrence Livermore National Laboratory report UCID-18756, Rev. 2, Livermore, California (1984).
5. Costello, E. De L., "Computational Studies on the Launching of Long Rod Penetrators," in *Proceedings of the 11th International Symposium on Ballistics*, Brussels, Belgium (1989).
6. Hibbett, Karlson, and Sorenson Inc., *ABAQUS User's Manual Version 4.5a*, Providence, Rhode Island (1985).
7. Rabern, D. A., "Axially Accelerated Saboted Rods Subjected to Lateral Forces," in *Proceedings of the 1989 Flash Radiography Topical*, Welches, Oregon (1989).
8. Hallquist, J. O., and Benson, D. J., "DYNA3D User's Manual (Nonlinear Dynamic Analysis of Structures in Three-Dimensions)," Lawrence Livermore National Laboratory report UCID-19592, Rev. 3, Livermore, California (1987).

SESSION VI:

PROJECTILES AND PROJECTILE/TUBE INTERFACE

MANNERS

TITLE: A Theoretical Study into the Effect of Sabot Stiffness on
Projectile In-Bore Motion and Launch Accuracy

N.D. MANNERS

**THE ROYAL MILITARY COLLEGE OF SCIENCE
SCHOOL OF MECHANICAL, MATERIALS & CIVIL ENGINEERING
LAND SYSTEMS GROUP
SHRIVENHAM
SWINDON WILTS SN6 8LA**

ABSTRACT:

When a gun is fired, the projectile is propelled along the barrel while the barrel itself recoils. Forces generated within the system cause both the barrel and the projectile to vibrate. Computer based mathematical models are increasingly being used for the dynamic simulation of this phenomenon, in order to study the characteristics of the motion and thus help to improve accuracy and assist in future design. One such model is the gun dynamics program suite, RAMA, which has been written at the Royal Military College of Science under contract to the Royal Armament Research and Development Establishment (Chertsey).

Many projectile parameters can influence the in-bore dynamics. This paper details a theoretical study, using RAMA, into the effects that the projectile band stiffnesses can have on it's in-bore motion and thus on the accuracy of the round.

BIOGRAPHY:

PRESENT ASSIGNMENT: Research Officer, Cranfield Institute of Technology,
modelling gun dynamics by computer simulation

PAST EXPERIENCE: Mathematical modelling, finite element stress analysis

MANNERS

A Theoretical Study into the Effect of Sabot Stiffness on
Projectile In-Bore Motion and Launch Accuracy

N.D. MANNERS
THE ROYAL MILITARY COLLEGE OF SCIENCE
SCHOOL OF MECHANICAL, MATERIAL & CIVIL ENGINEERING
LAND SYSTEMS GROUP
SHRIVENHAM
SWINDON WILTS SN6 8LA
ENGLAND

INTRODUCTION

Gun barrel vibrations are primarily caused by eccentric masses along the barrel length inducing bending moments during barrel recoil. Initial barrel curvature, such as that due to gravity sag and the non-straightness of the barrel from manufacture, produces a similar effect. As the projectile accelerates along the barrel, it is forced to follow a path determined by the profile of the bore. Both the barrel and the projectile respond to the interactive forces generated by this motion, and this causes the projectile to vibrate relative to the barrel. The in-bore balloting, together with the flexing of the barrel, can have a considerable effect on the accuracy of the round. Firstly, due to its transverse velocity, the projectile usually leaves the barrel with a different trajectory to the direction in which the barrel was originally pointing. This deviation is termed shot jump, and is a useful measure of launch accuracy. Secondly, it is known from recent experimental trials, that the pitching rate of the projectile as it leaves the barrel influences the early flight of the projectile as it aerodynamically stabilizes. The two definitions of accuracy generally used in gun dynamics are given in [1].

Using RAMA [2] to predict the in-bore projectile dynamics, a theoretical study has been made of the significance of the projectile band stiffness values in so far as they affect accuracy. This includes looking at the individual effects of the rear driving band stiffness, the front centring band stiffness, the rear driving band moment stiffness and the clearance between the front band and the barrel.

THE RAMA SUITEThe Barrel Model

The RAMA barrel dynamics modelling program simulates barrel motion by considering Euler-Bernoulli beam theory to describe the flexural vibrations, and the wave equation to describe the extensional vibrations. These equations of motion are then solved using a finite difference method. The derivation of the equations of motion is explained in [3]. Assuming that the barrel angular deflections remain small throughout, the extensional motion is given by,

$$\rho A(x) \frac{\partial^2 \eta}{\partial t^2} = \frac{\partial}{\partial x} \left(EA(x) \frac{\partial \eta}{\partial x} \right) + G \quad (1)$$

and the flexural motion is given by,

$$\frac{\partial^2}{\partial x^2} \left(EI(x) \frac{\partial^2 y(x,t)}{\partial x^2} \right) + \rho A(x) \frac{\partial^2 y(x,t)}{\partial t^2} = F_1 + F_2 + F_3 + \dots \quad (2)$$

The equations are coupled via the longitudinal external force G and the transverse external forces $F_1, F_2, F_3 \dots$. All notation used is given at the end of this report.

RAMA takes its name as an acronym of Richtmyer and Morton's Algorithm, as it is a finite difference algorithm suggested in [4] that is used to solve the flexural vibration equation (2). The algorithm used for the solution of the extensional vibration equation (1) is a similar, if more direct implicit method. It is similar to a Crank-Nicolson scheme used in solving parabolic equations. The numerical implementation of these algorithms is described in [5].

The Projectile Model

The RAMA projectile dynamics model runs interactively with the barrel model and simulates the in-bore projectile motion by determining and resolving the main forces acting upon it (see figure 1). The projectile is considered as a rigid body supported by the front and rear bands, which are represented as linear springs with parallel viscous damping (see figure 2). Assuming that the barrel angular deflections and the projectile pitch angle remain small throughout, the equations of motion representing bounce and pitch can be written as follows. For bounce,

$$m \ddot{y}_{cg} = F_r + F_f + F_p \theta \quad (3)$$

and for pitch,

$$I \ddot{\theta} = -F_r l_r + F_f l_f + F_p d + M_r \quad (4)$$

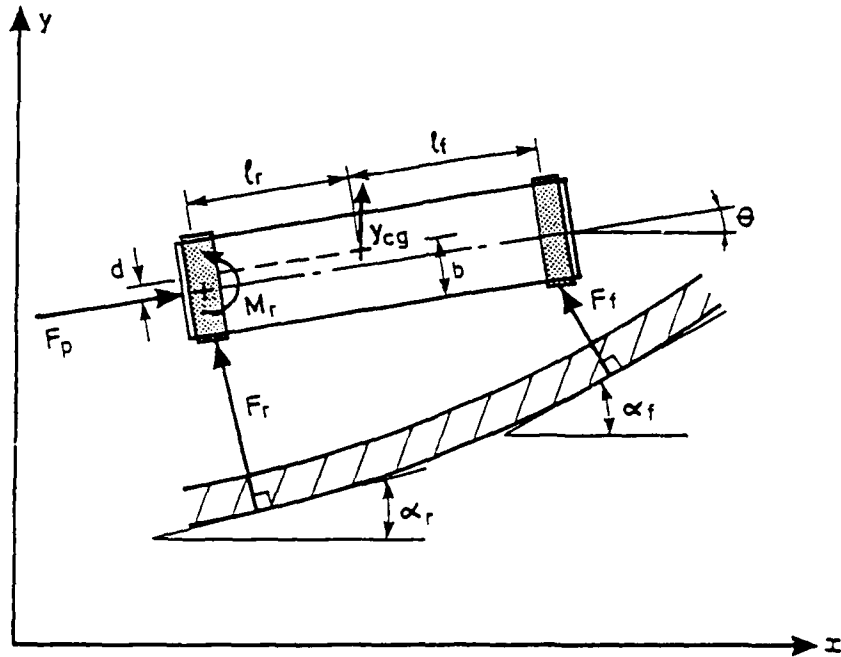


Figure 1. Projectile forces

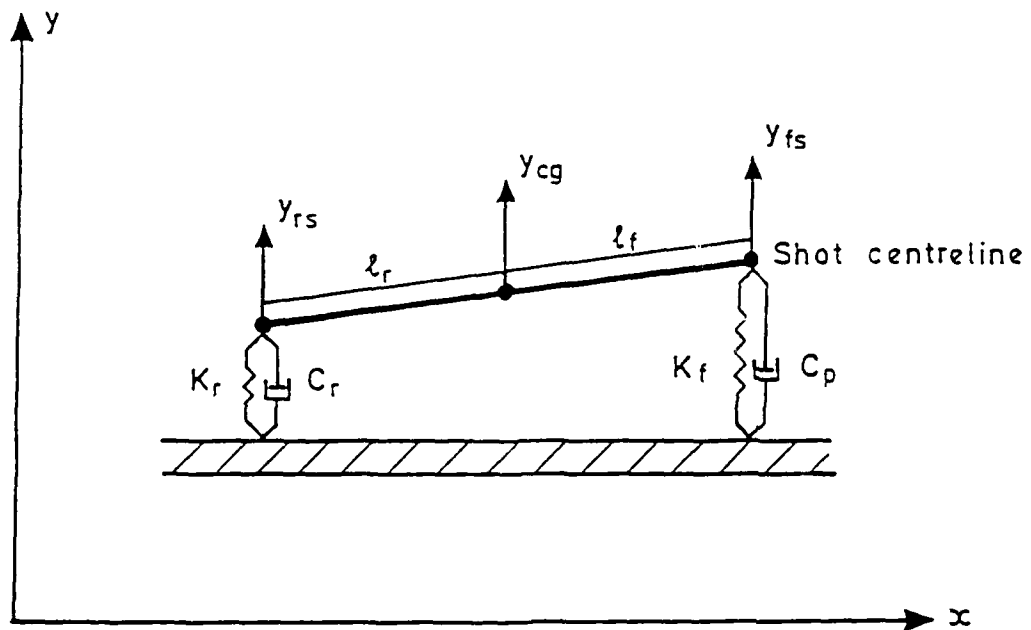


Figure 2. Projectile representation

MANNERS

where F_r and F_f are the forces at the rear and front bands respectively, F_p is the propellant gas pressure force, and F_m is the rear band foundation moment.

The rear and front band forces are the forces due to projectile/barrel interaction, and act perpendicular to the barrel tangent at the relevant band position. The linear stiffness term and viscous damping term of which they are composed, are calculated by considering the relative displacements and velocities between the projectile and the barrel in the direction in which they act. If K and C are the band stiffness and damping coefficients respectively, then the force at the band can be defined as,

$$F = -K\delta - C\dot{\delta} \quad (5)$$

Any clearance between the front band and the barrel which might occur due to limited machining capabilities and barrel wear can be modelled by effectively considering the front band stiffness and damping coefficient values as step functions. The relative displacement at a band is given by,

$$\delta = y_s - y_b \quad (6)$$

and the relative velocity can be shown to be,

$$\dot{\delta} = \dot{y}_s - \dot{y}_b - \dot{x}_s \alpha \quad (7)$$

In this equation, $\dot{x}_s \alpha$ is the vertical component of projectile velocity along the barrel which is required for the projectile to follow the barrel tangent at this point.

The pressure force affects the in-bore motion of the projectile if it is pitched or has an offset centre of mass. If pitched, a vertical component of the force is present and influences the projectile bounce. If the centre of mass is offset, a moment which influences the pitching motion is produced. Any resistance to motion along the barrel is included in the calculation of projectile acceleration, which is carried out prior to running the dynamics model. This acceleration is used to calculate the resultant force exerted on the rear of the projectile by the propellant gas pressure, which is simply given by,

$$F_p = m\ddot{x}_{cg} \quad (8)$$

The foundation moment is a restoring moment due to the rear driving band angular deformation, which is caused by the relative angular motion between the projectile and the barrel (see figure 3). Like the band forces, it is assumed to compose of a stiffness and a damping term, so that if K_m and C_m are the moment stiffness and damping coefficients respectively, the moment can be given by,

$$M_r = -K_m(\theta - \alpha_r) - C_m(\dot{\theta} - \dot{\alpha}_r) \quad (9)$$

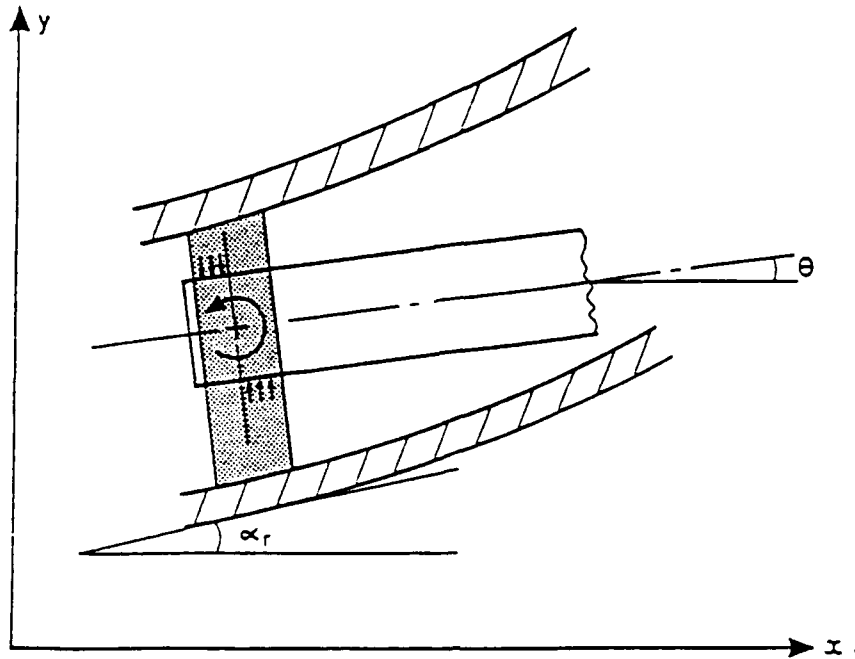


Figure 3. Rear band deformation producing foundation moment

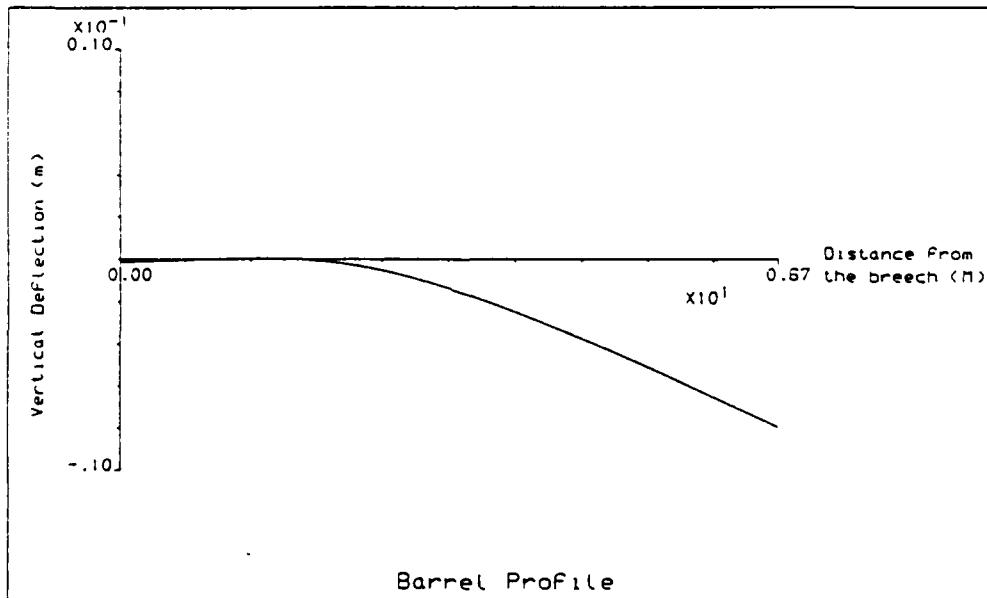


Figure 4. Straight barrel with gravity sag

MANNERS

Having defined the forces and moments, the equations of motion (1) and (2) can then be solved using a modified second order Runge Kutta technique, to give the linear and angular projectile velocity and displacement for a given time interval.

PROCEDURE

In order to allow the individual effects of the rear band stiffness, the front band stiffness, the rear band moment stiffness and the front band clearance to be studied, a reference set of data detailing the gun system and projectile parameters to be entered into the RAMA model was initially selected, and a corresponding simulation was run. These parameters were not specific to any particular gun system and projectile, but were based on realistic measured values.

The static barrel configuration used was that of a perfectly straight manufactured barrel, but with a drooped profile from the effect of gravity sag (see figure 4). A range of values for each of the band stiffnesses was selected, to reflect certain changes that might be made to the projectile design. A range of clearances at the front band which might occur in practice was also selected. Simulations were then run changing each selected value in turn, whilst keeping all other parameters constant.

Next, the static barrel profile was changed to that of a non-straight manufactured barrel, but ignoring gravity sag. The non-straightness consisted of a simple bend spread over the entire barrel length (see figure 5). The runs for each parameter change were then repeated and the results compared.

In an attempt to excite projectile in-bore motion further, the static barrel profile was then changed again. As before, gravity sag was ignored and a non-straight manufactured barrel used. This time, the non-straightness consisted of a small localized kink, about a third of the length along the barrel from the breech face (see figure 6). The runs for each parameter change were then repeated again and comparisons made of the results.

Finally, to try and separate the effects of these projectile parameter changes from any that might be produced by barrel motion specific to a particular static barrel configuration, a routine was written to enable the projectile dynamics model to be run independent of the barrel model. A selection of the above runs were then repeated. Under these circumstances, the barrel configuration with the localized kink would give the free response of the projectile within a straight barrel, having first excited it.

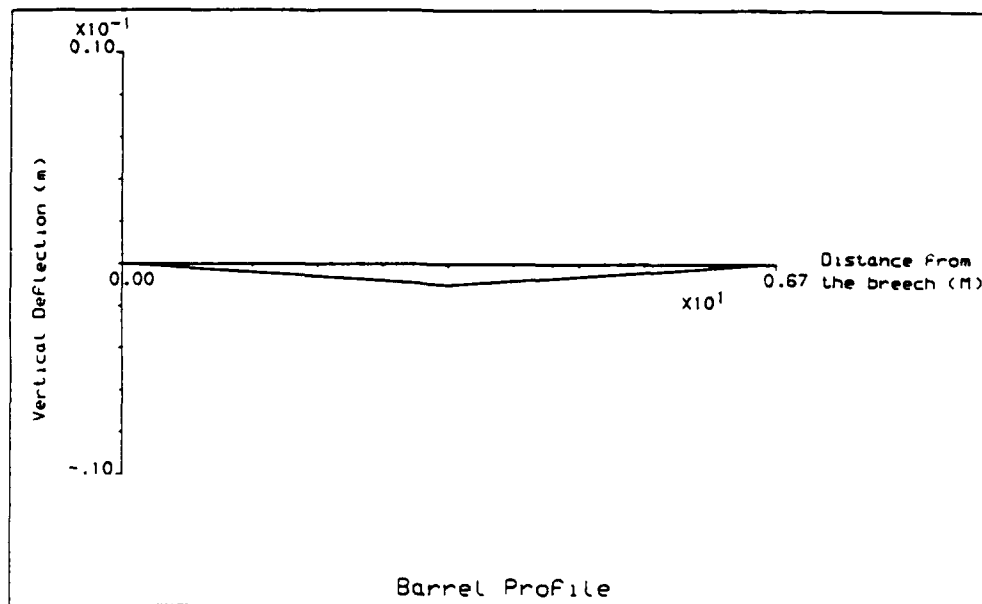


Figure 5. Non-straight barrel with bend spread over entire barrel length

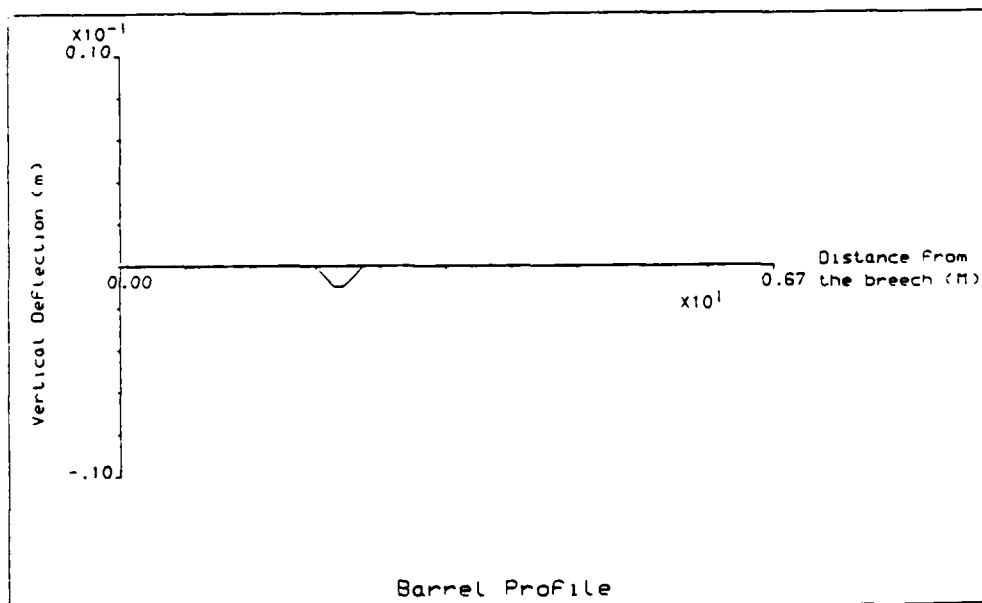


Figure 6. Non-straight barrel with localized kink

MANNERS

DISCUSSION OF RESULTS

Throughout this report, the comparisons between traces and the trends produced are discussed, and not the actual values, which would of course vary with the specification of the gun system. As stated earlier, the two main aspects of projectile motion which influence accuracy, are the jump and the pitching velocity. Jump values are only really valid as the projectile leaves the barrel, but traces for the final part of the simulation are plotted to show how it varies immediately before this time. In RAMA, projectile motion along the barrel is calculated prior to the dynamic simulation, and as this was kept the same for each run, any change in jump from one trace to another can be related to the change in the bounce velocity of the projectile.

The results obtained from the simulations using different static barrel configurations, show that barrel straightness is of major significance when considering projectile in-bore motion. Although the localized kink is probably a more severe deformity than would generally occur in practice, the increase in projectile excitement it produced was considerable, and shows that detailed investigation into the effects of barrel straightness is needed to accompany any results obtained from this investigation.

In general, increasing band stiffness would be expected to increase the frequency of the bounce and pitch in-bore vibrations. It is however advantageous to keep these vibration frequencies as low as possible, so that the projectile motion as it leaves the barrel is tolerant to small variations in exit time. It is also an advantage if the amplitude of these vibrations can be kept to a minimum, so reducing the chance of the projectile having a large value of jump and pitch velocity.

Figure 7 shows that an increased rear band moment stiffness produces a higher frequency pitching vibration, although the bounce, as seen from the jump in figure 8, does not show the same effect. This high frequency pitching is superimposed onto the general trend dictated by the barrel motion, and appears to have a greater angular velocity, until the barrel influence takes over. This is confirmed in figure 9, which gives traces from the runs using the barrel with the localized kink and not including barrel dynamics. It clearly shows that in this situation and without barrel effects, the higher rear band moment stiffness gives larger pitching velocities. It also reiterates the belief that the barrel configuration plays a major part in influencing the projectile motion. In fact under certain conditions, it was noticed that the projectile and barrel motion being out of phase can produce a damping effect, as seen in figure 10, which can significantly improve the conditions affecting accuracy. Reducing the rear band moment stiffness to give smaller pitching velocities however, appears to increase the effect that clearance at the front band has on this motion. This is seen by comparing figures 11 and 12, which show the traces for a range of clearances, at two different moment stiffnesses.

MANNERS

Figures 13 & 14, and 15 & 16 show that the influence of the rear band moment stiffness on pitch and bounce can be reduced considerably by increasing the front band stiffness. This may be due to the front band taking control of the elastic response of the projectile angular motion at higher stiffnesses. Also, as the front band becomes stiffer, the pitch/bounce couple centre moves forwards, getting closer to the centre of gravity of the projectile and therefore reducing the pitch/bounce coupling effect. Increasing the front band stiffness however, also increases the effect that clearance at the front band has on the motion. This can be seen by comparing figures 17 & 18, and 19 & 20, showing the projectile pitching velocity and jump respectively.

The effect of the rear band on projectile motion appears more difficult to analyse, although figures 21 & 22 indicate that reducing the rear band moment stiffness reduces the effect of the rear band stiffness on jump, and figures 23 & 24 seem to show that increasing the rear band stiffness reduces the effect of clearance on jump.

CONCLUSIONS

It has been suggested from previous research [6] that the rear band foundation moment is probably the dominant force on the projectile early in the ballistic cycle. This investigation has given further confidence in this theory, as it was generally found that the rear band moment stiffness had the greatest effect on the projectile in-bore motion. It was also noticed however, that this effect could be lessened by reducing the rear moment stiffness value and by increasing the front band stiffness, but both these changes tend to increase the effect of any front band clearance.

As discovered in a recently published experimental investigation into the effect of front band stiffness [7], there appears to be no simple rule for improving the accuracy of the projectile in relation to varying the band stiffnesses. Through being able to analyse these stiffnesses independently however, this theoretical study has produced certain trends which might assist in future projectile design. Overall, it appears that the projectile in-bore motion is mainly affected by the values of band stiffness relative to each other, although it is the barrel straightness which has the greatest influence.

REFERENCES

- 1) King D.W.
Definitions used in Gun Dynamics and Accuracy Research
Division note VT3/25, RARDE, Chertsey, April 1988

MANNERS

- 2) Manners N.D. and Powell S.E.
Gun Barrel Dynamics Computer Simulation (RAMA)
Documentation
RMCS Report SMMCE/LS/060/1473, November 1987
- 3) King W.P.C.
A mathematical model for gun dynamics with particular reference
to the L11A5
RMCS Report No. 82002, August 1982
- 4) Richtmyer R.E. and Morton K.W.
Difference Methods for Initial Value Problems
Interscience 1967
- 5) Smith T.F. and Powell S.E.
Gun Barrel Dynamics Computer Simulation (RAMA)
The method of solution used in the main dynamics model
RMCS Report SMMCE/LS/102/1473, March 1990
- 6) Patton E.M.
Projectile Foundation Moment Generation
4th US Army Symposium on Gun Dynamics, Florida, May 1985
- 7) Plostins P., Celmins I. and Bornstein J.
The effect of sabot front borerider stiffness on the launch dynamics of
fin-stabilized kinetic energy ammunition
11th International Symposium on Ballistics, Belgium, May 1989

NOTATION

$A(x)$	Cross sectional area of the barrel at point x .
C	Projectile band damping coefficient.
C_m	Projectile rear band moment damping coefficient.
d	Projectile centre of gravity offset in the y direction.
E	Modulus of elasticity of the barrel.
F	Projectile band force.
F_1, F_2, F_3	External transverse forces on the barrel.
F_f	Projectile front centring band force.
F_p	Resultant propellant gas force.
F_r	Projectile rear driving band force.
G	External longitudinal force on the barrel.
$I(x)$	Second moment of area of the barrel cross-section at x .
K	Projectile band stiffness.
K_m	Projectile rear band moment stiffness.
l_f	Distance from projectile centre of gravity to front centring band.
l_r	Distance from projectile centre of gravity to rear driving band.
m	Projectile mass.

MANNERS

M_r	Projectile rear band foundation moment.
t	Time.
x	Distance along the barrel measured from the breech.
\dot{x}_s	Projectile velocity along the barrel.
\ddot{x}_{cg}	Projectile acceleration along the barrel.
$y(x, t)$	Transverse deflection of barrel relative to original static position.
y_b	Transverse deflection of barrel at projectile band position.
y_{cg}	Projectile centre of gravity displacement in the y direction.
y_s	Projectile band displacement in the y direction.
\dot{y}_b	Transverse velocity of barrel at projectile band position.
\dot{y}_s	Projectile band velocity in the y direction.
\ddot{y}_{cg}	Projectile centre of gravity acceleration in the y direction.
α	Angle of barrel tangent at the projectile band position.
α_r	Angle of barrel tangent at the projectile rear band position.
$\dot{\alpha}_r$	Angular velocity of barrel at the projectile rear band position.
δ	Relative displacement between projectile and barrel at the band position.
$\dot{\delta}$	Relative velocity between projectile and barrel at band position.
η	Extensional deflection of the barrel relative to it's unstressed position.
ρ	Density of the barrel.
θ	Projectile pitch angle.
$\dot{\theta}$	Projectile pitching velocity.
$\ddot{\theta}$	Projectile angular acceleration.

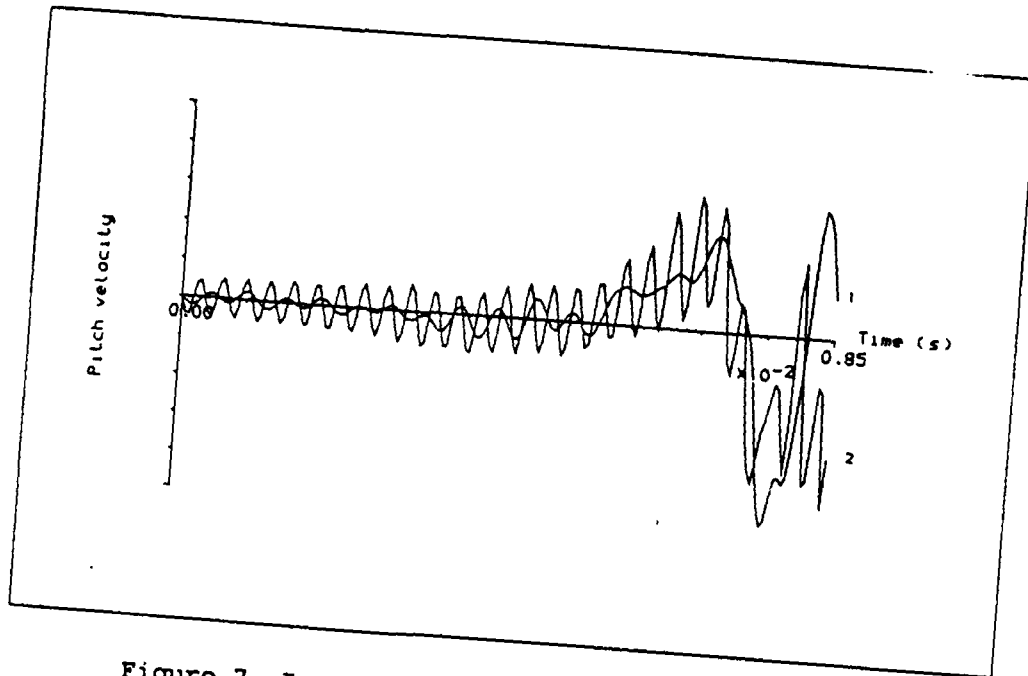


Figure 7. Increasing rear band moment stiffness

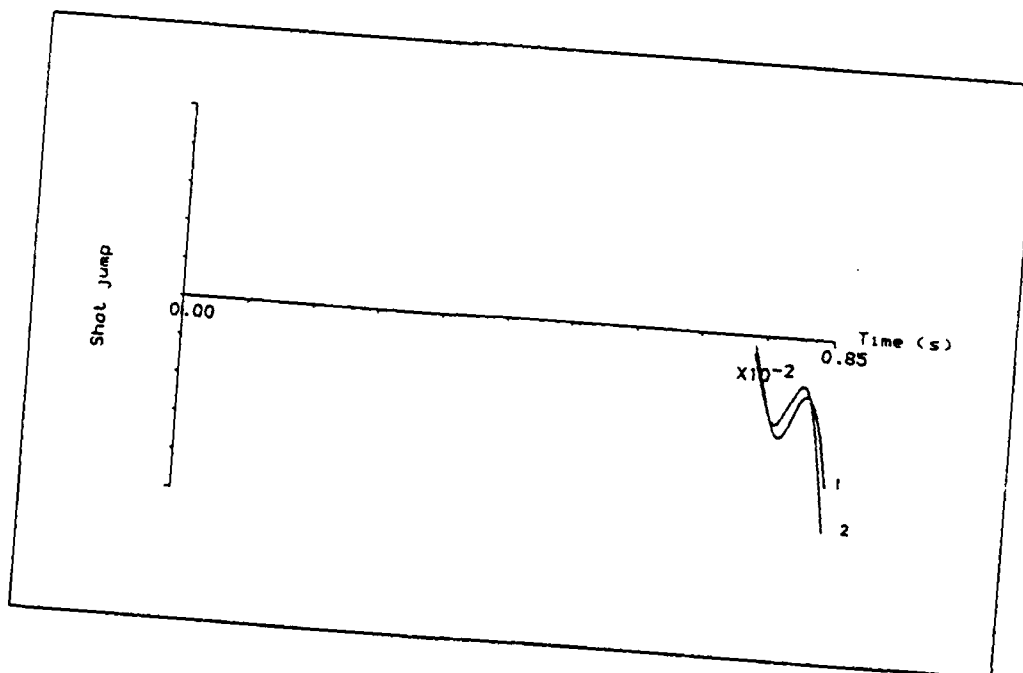


Figure 8. Increasing rear band moment stiffness

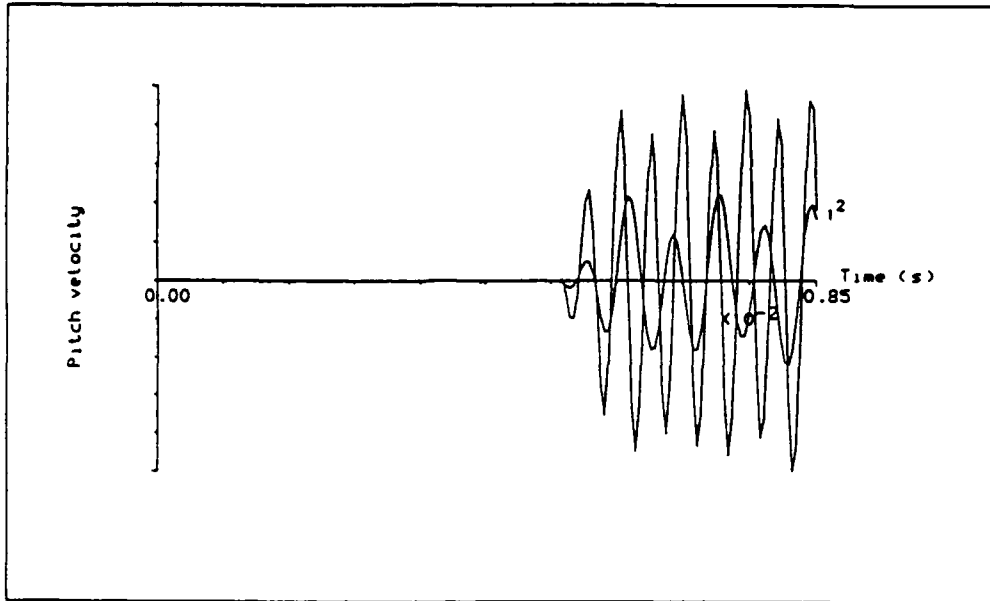


Figure 9. Increasing rear band moment stiffness - kinked barrel

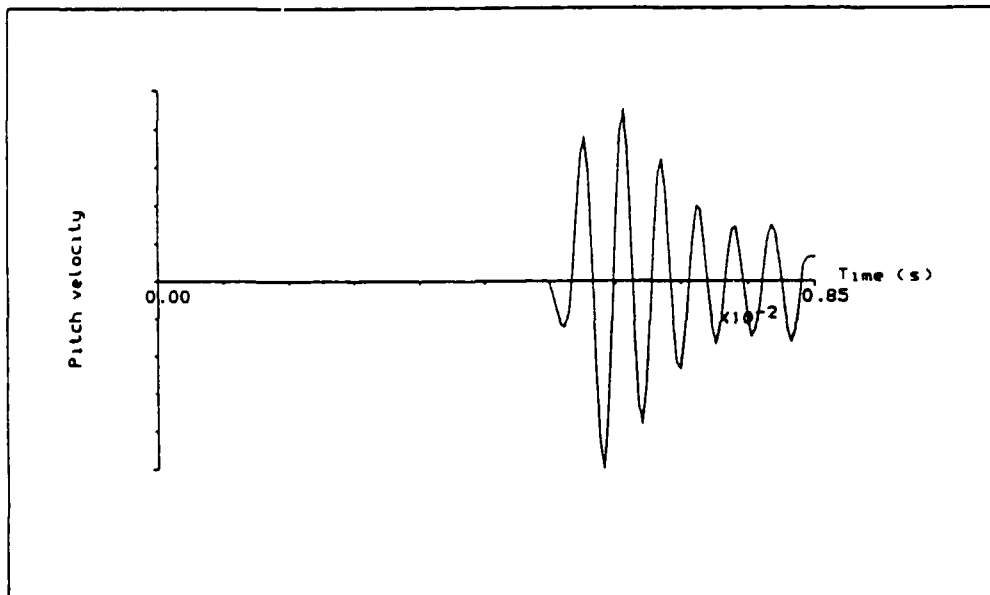


Figure 10. Damping effect due to out of phase motion

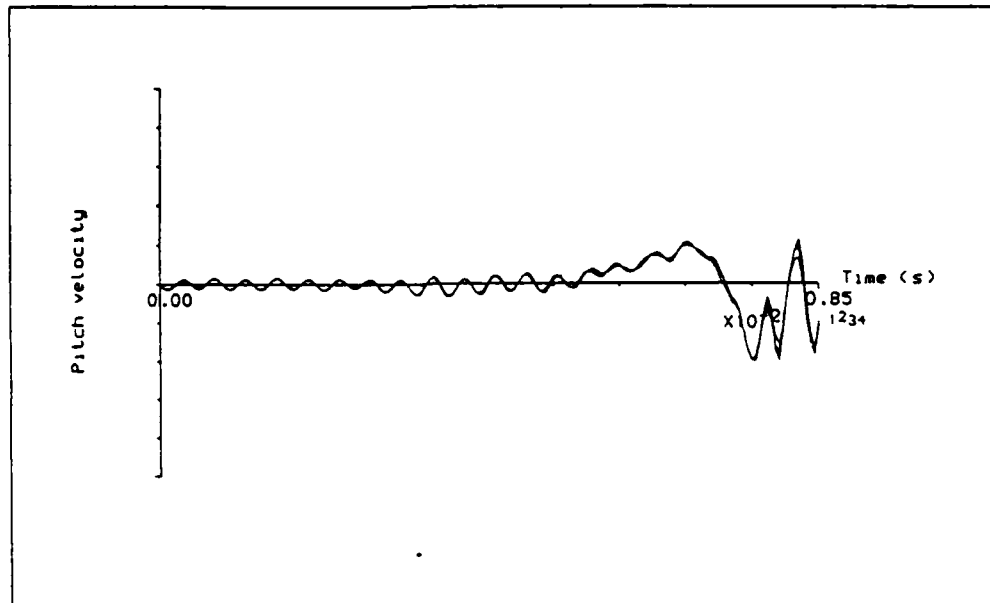


Figure 11. Increasing front band clearance with harder rear band moment stiffness

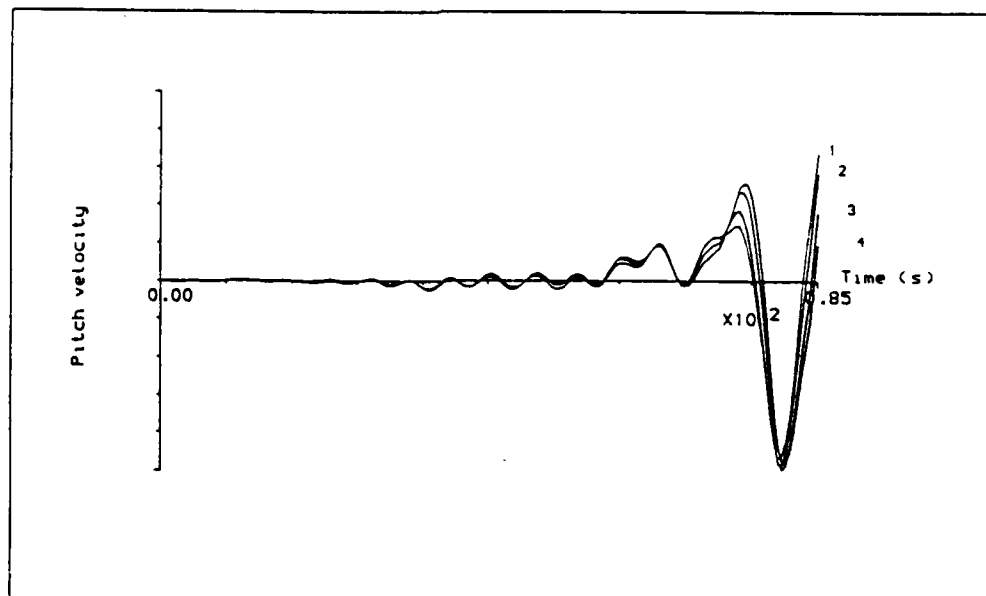


Figure 12. Increasing front band clearance with softer rear band moment stiffness

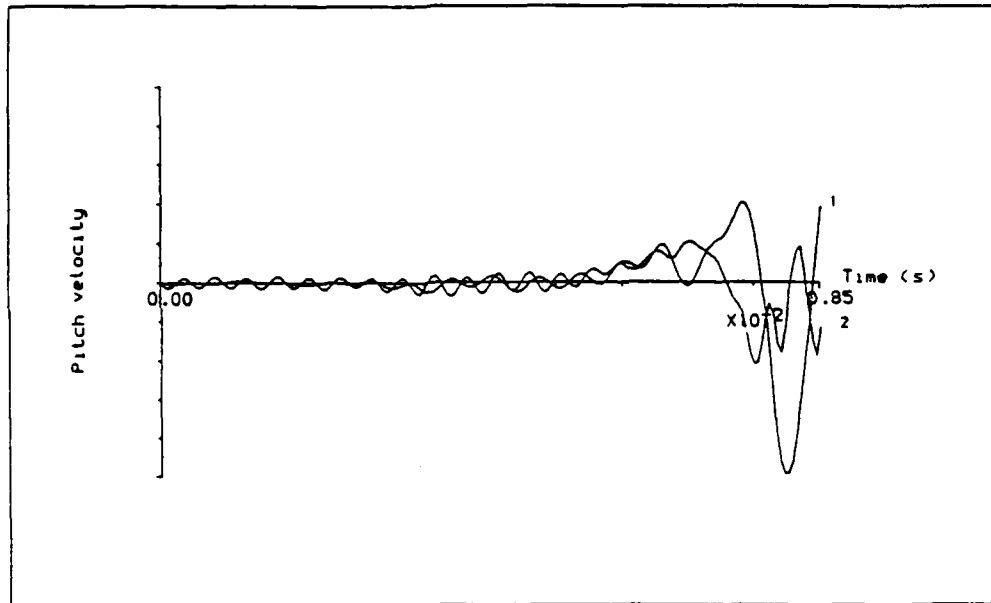


Figure 13. Increasing rear band moment stiffness with softer front band

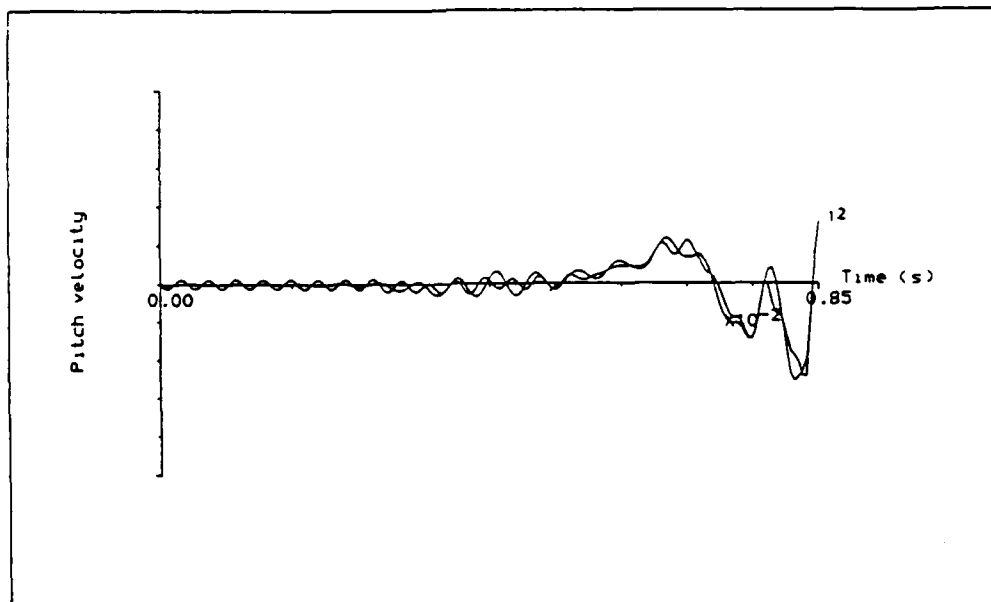


Figure 14. Increasing rear band moment stiffness with stiffer front band

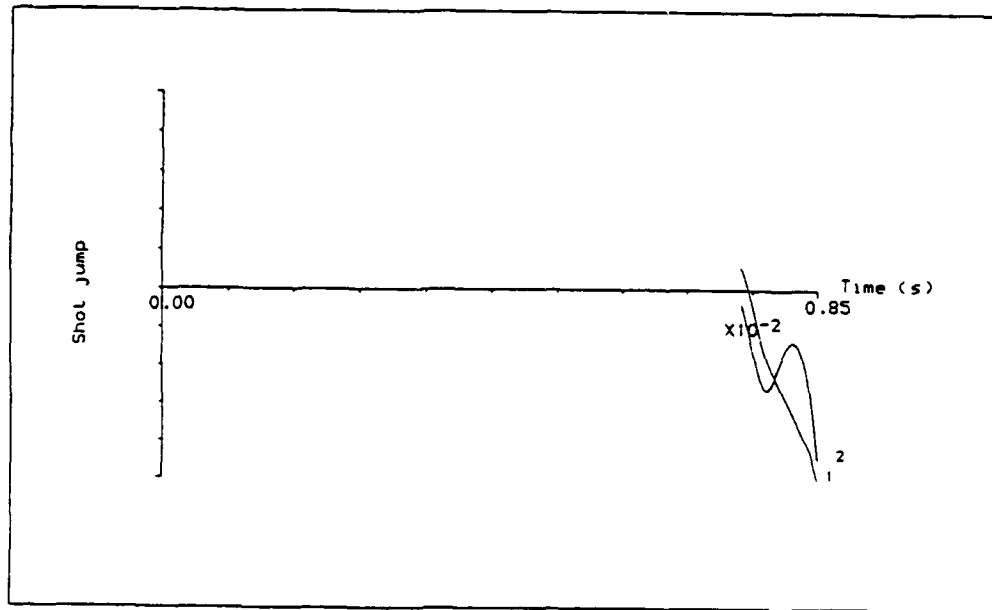


Figure 15. Increasing rear band moment stiffness with softer front band

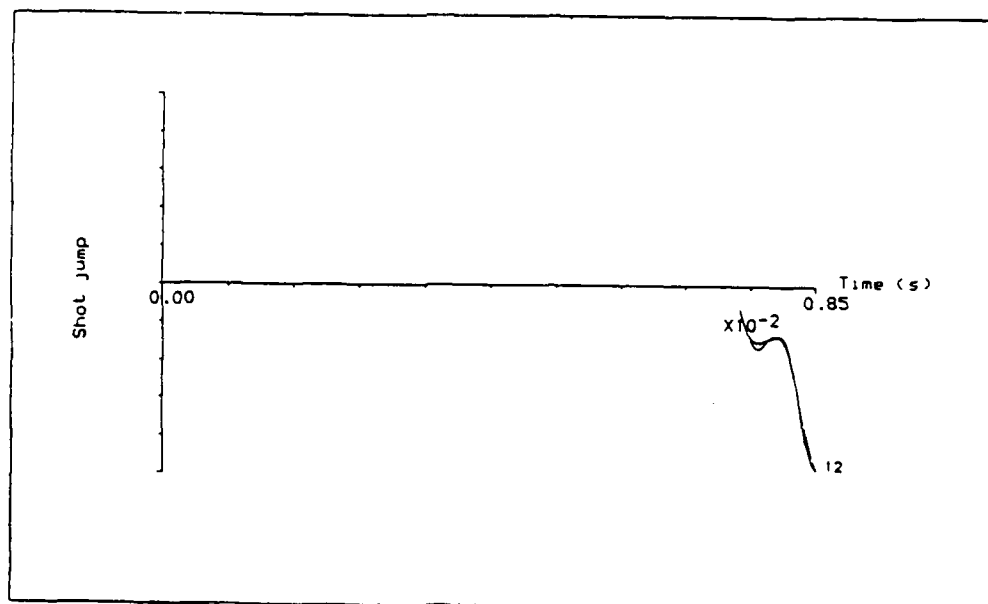


Figure 16. Increasing rear band moment stiffness with stiffer front band

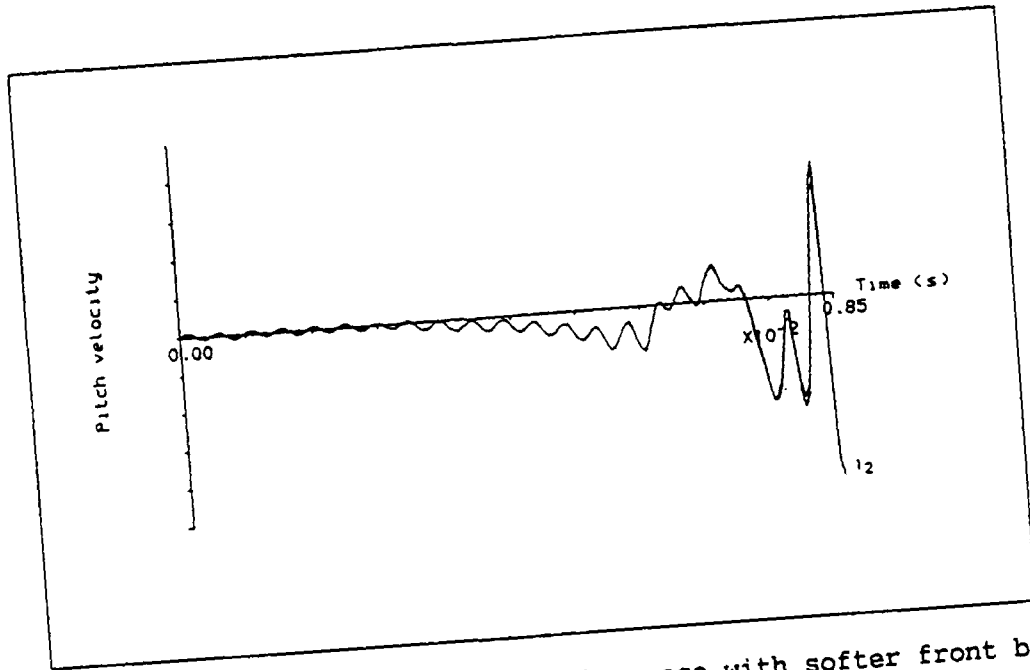


Figure 17. Increasing front band clearance with softer front band

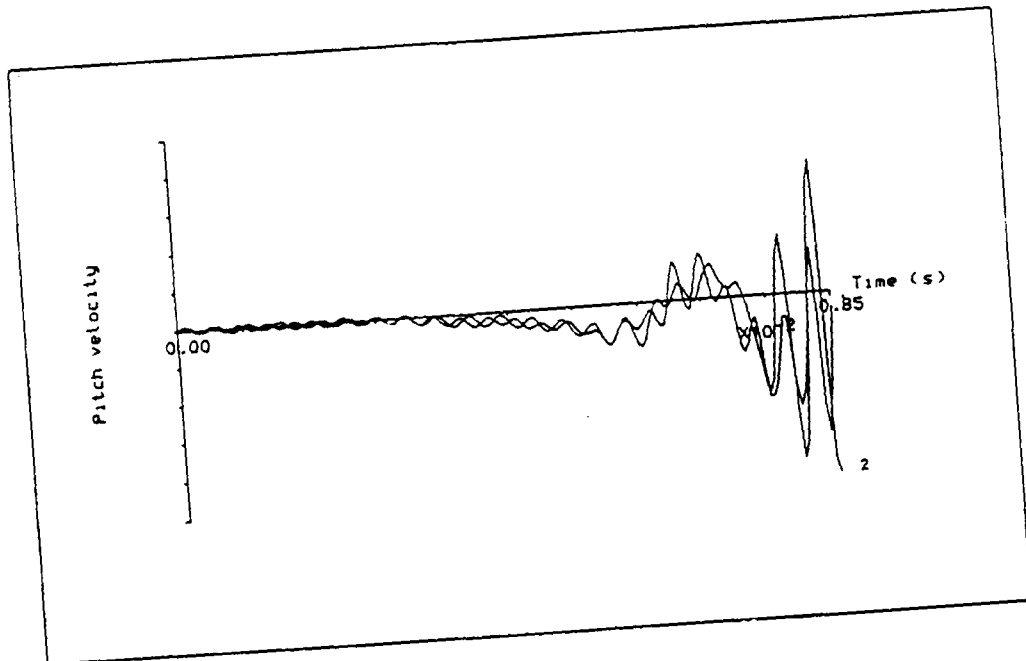


Figure 18. Increasing front band clearance with stiffer front band

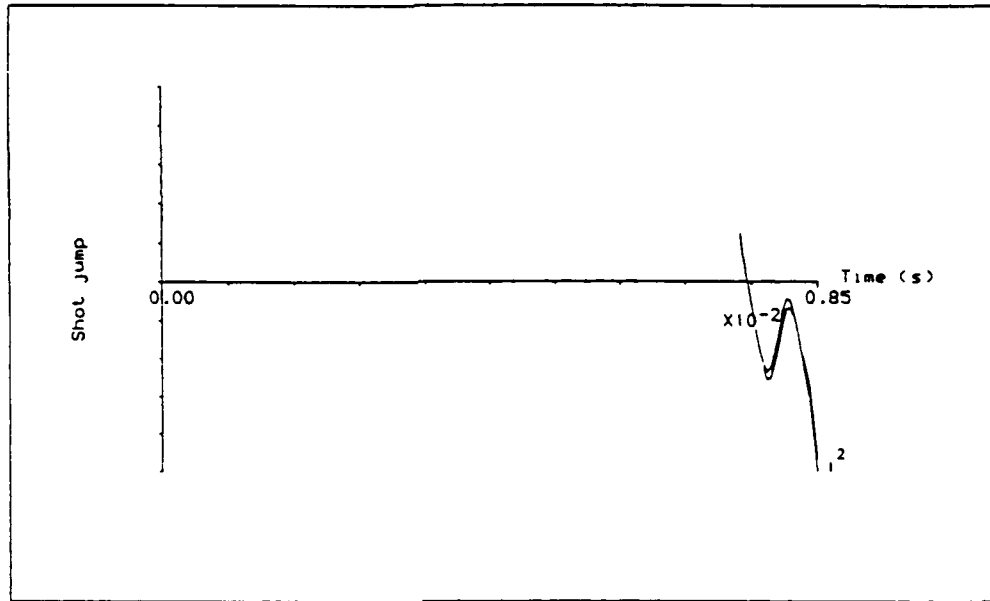


Figure 19. Increasing front band clearance with softer front band

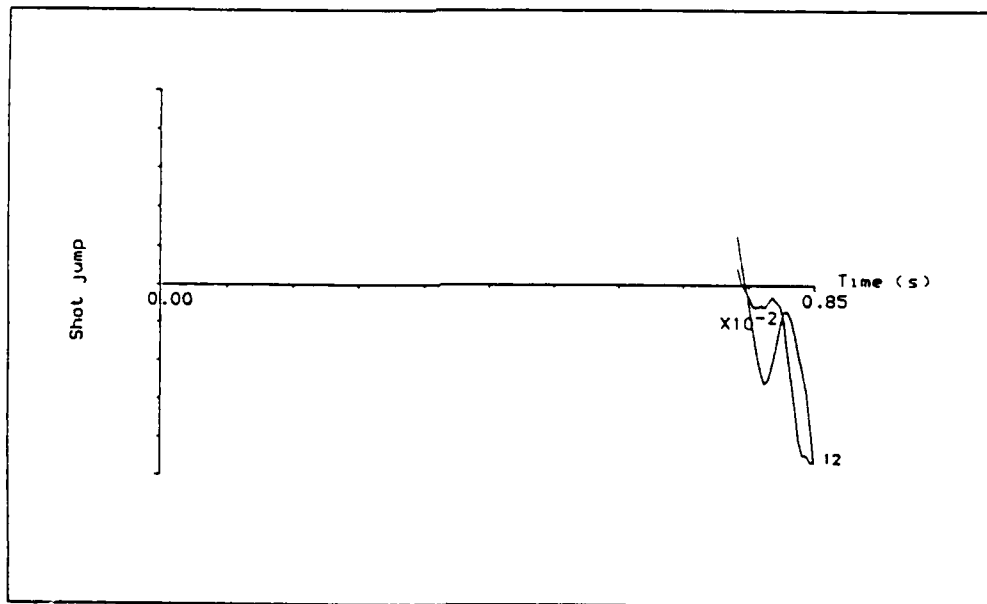


Figure 20. Increasing front band clearance with stiffer front band

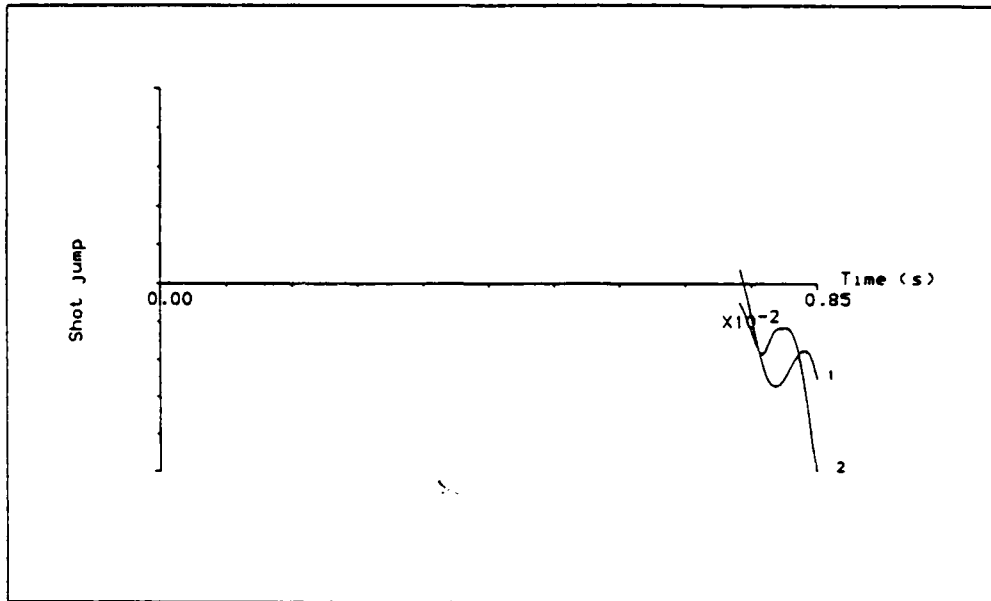


Figure 21. Increasing rear band stiffness with harder rear band moment stiffness

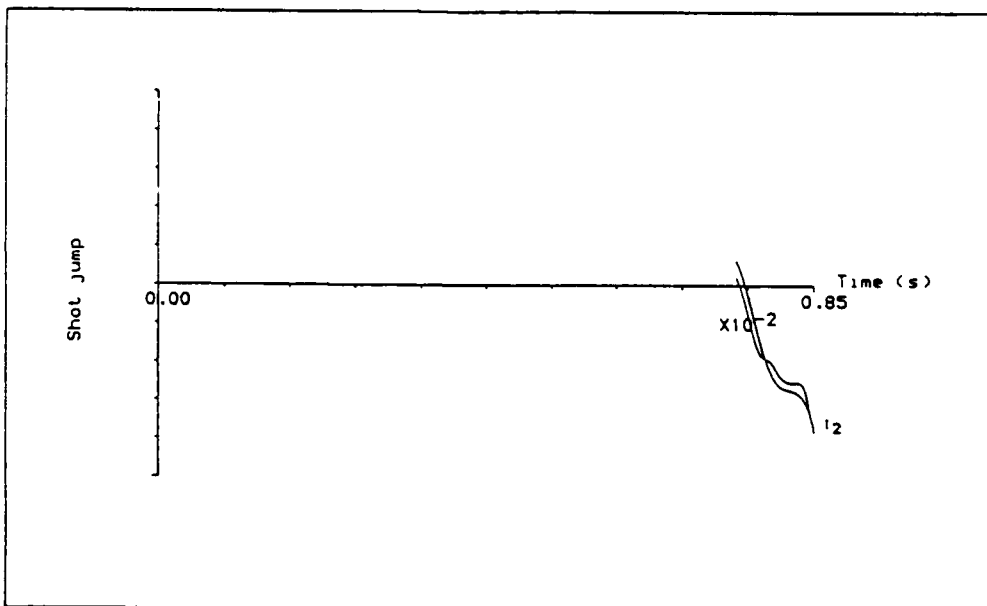


Figure 22. Increasing rear band stiffness with softer rear band moment stiffness

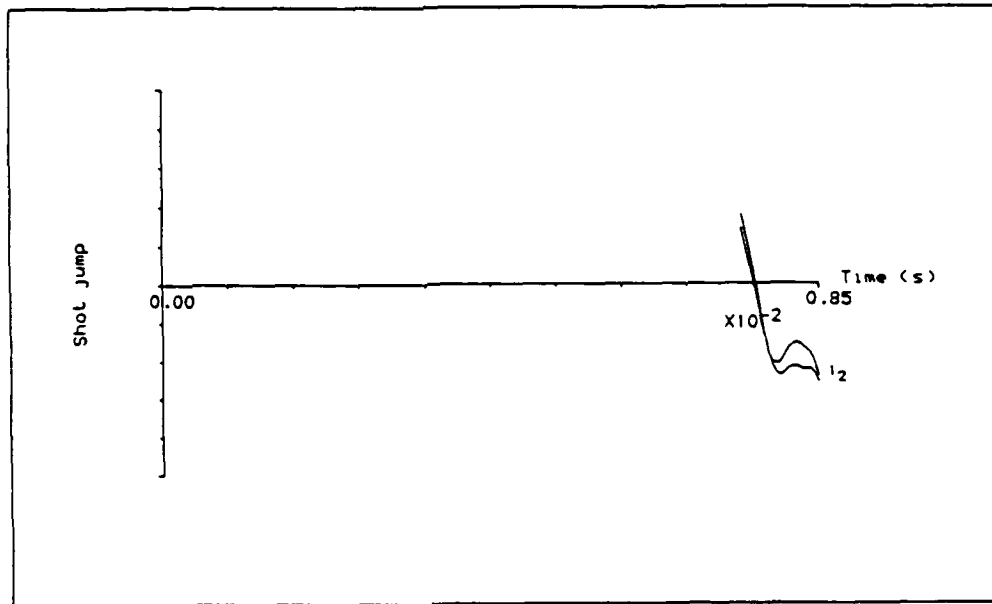


Figure 23. Increasing front band clearance with softer rear band

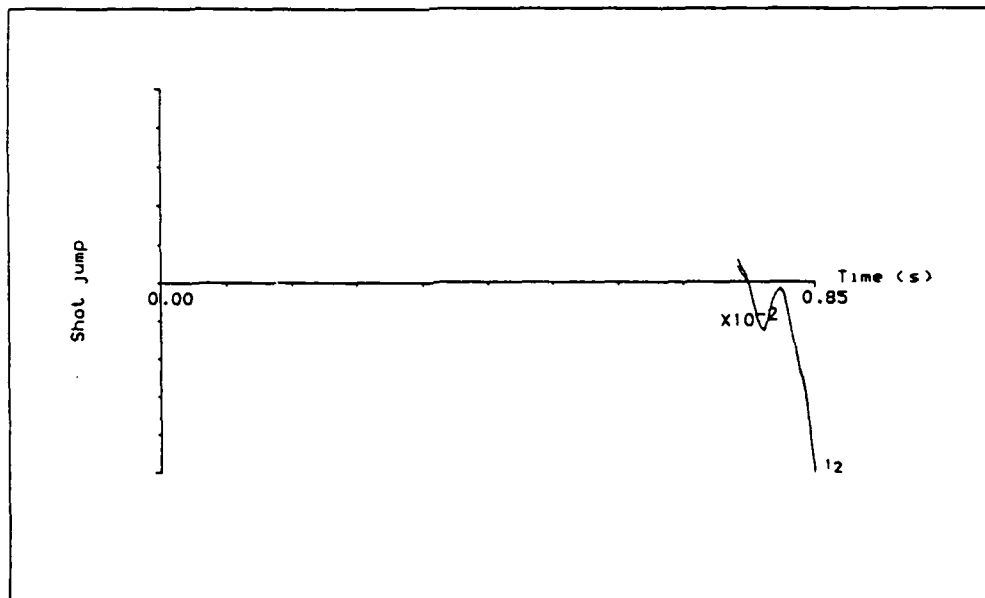


Figure 24. Increasing front band clearance with stiffer rear band

Kaste, Burton

DEVELOPMENT OF A DESIGN METHODOLOGY FOR SLIPBAND OBTURATORS

Robert P. Kaste

Larry Burton

U.S. Army Ballistic Research Laboratory

Today's standard 105-mm tank gun cannon, the M68, was designed to fire spin stabilized projectiles. Modern kinetic energy (KE) ammunitions are designed to spin at much lower rates than created by the rifling in a M68. The spin imparted by the rifling to these projectiles must be reduced to insure proper performance. This is accomplished by employing a two-piece slipband obturator. The present slipband has an inner band attached to the sabot with an outer band riding on it which serves as a rotating band. The interface between the two bands provides a slip surface which reduces the spin imparted to the projectile.

Recently, development of slipband obturator technology has been addressed by a joint DOE/DOD program. Modified obturator designs were formulated and tested, focusing on those factors believed to have the main influence on the traction at the interface of the bands, which controls spin impartation.

On-going small scale testing of 37-mm slipbanded slugs is being conducted in a modified, M3, rifled gun tube. The experimental gun's wall has been turned down to a constant thickness of 1/4 inch along the length of projectile travel to decrease its resistivity to x-ray penetration. The tube was overwrapped with a graphite fiber-reinforced epoxy to maintain the structural integrity of the tube. Results from initial testing have verified this tool's use as an in-bore spin measurement device.

This paper provides a more detailed description of the controlling slip mechanism as well as a look at the reasoning behind various modifications. The actual performance of the modified slipbands during experimental firings is presented with conclusions drawn on the merits of each design. Finally, an assessment is made on the possibility of deriving a predictive methodology for the design of slipband obturators.

Robert P. Kaste is a mechanical engineer with 11 years experience at the U.S. Army's Ballistic Research Laboratory. He is currently active in the interior ballistic performance of medium to large caliber projectiles. He has worked in the areas of in-bore structural integrity of projectiles, gun dynamics, fire control systems, design of material testing devices, and kinematics of automatic weapons. He holds a B.S. degree in mechanical engineering from Virginia Tech.

Development of a Design Methodology for Slipband Obturators

R.P. Kaste and L. Burton
U.S. Army Ballistic Research Laboratory
Aberdeen Proving Ground, MD

Rifled gun tubes impart spin to the projectiles fired through them. Traditionally projectiles were of such dimensions that high spin rates stabilized their flight. This allowed the progression from ball shaped projectiles to longer, sleeker projectile shapes which increase achievable range and accuracy. The advent of long rod projectiles brought the necessity for a different type of stabilization. These projectiles are fin stabilized and while they still spin, they must be spun at much lower rates than the spin stabilized projectiles. In order to fire both classes of projectile from the same gun, some mechanism was required to provide the correct spin to the respective projectile.

An understanding of the mechanism for imparting spin to a projectile leads toward a method of altering spin of the projectile. A spin stabilized projectile has a rotating band of either metal, usually lead, copper, brass, or plastic which is securely attached to the projectile. The lands of the rifling in the gun tube engrave into the rotating band and force the projectile to follow the path of the rifling as it traverses the length of the barrel. Obturation, or sealing, is achieved by the interference fit of the soft band with the inner surfaces of the gun tube. Sometimes additional sealing is required and an obturator is added to the projectile. This may be a rubber seal added to the base of the projectile.

A method used to reduce the spin of a projectile is the slipband obturator. The paradox of this design is that the element which engages the rifling must both seal the combustion gases from escaping by or through the projectile while being disconnected enough not to impart its full rotation to the projectile body. Never the less, such a band was developed and successfully implemented on the M735 fin stabilized discarding sabot kinetic energy projectile. This slipband, developed at Picatinny Arsenal in the late 1960's and early 1970's, consists of an inner sealing band made of polypropylene and an outer obturator made of nylon 6/6.

In recent years the development of long rod kinetic energy projectiles created a resurgence of interest into the mechanism and design of slipband obturators. The Ballistic Research Laboratory (BRL) felt the importance of understanding the

mechanism great enough to warrant a moderate study effort into the phenomenology. Through prior interactions with the Department of Energy's Sandia National Laboratory in Livermore, CA (SNLL) the BRL knew of their interest and ongoing work in the area of obturation and torsional impulse. A Department of Army-Department of Energy-Memorandum of Understanding (DOA-DOE-MOU) was established to study the issue of slipband technology.

SNLL had been performing significant work both in dynamic response finite element modelling of copper obturator bands and on experimental studies of the strain and extrusion process of copper bands as they made the transition through the gun's forcing cone and the constant diameter of a smooth-bore gun tube.[1][2] Large efforts were made to increase their computational abilities to study a nylon obturator band. This required continuation on code work which included 2-D rezoning capabilities to refine and redefine the finite element mesh due to the large deformations encountered by the extruded band materials. It also required the establishment of material properties for the plastics which were used in the slipband obturator.

Dan Dawson of SNLL studied the properties of many plastics and combinations of plastics which may be considered for use in this application.[2] He found that the polypropylene and nylon combination already in use was one of the best of those he studied. In addition he studied the use of several different lubricants applied to the plastics and their effect on the static and dynamic friction at their interface. The slipband obturator design in current production includes the use of a silicon lubricant.

Many characteristics of polymer properties were studied by Wendell Kawahara at SNLL.[3] He has modelled and experimentally studied the affects on materials' mechanical behavior of temperature, moisture, and rates of loading.

Paul Nielan of SNLL worked on the development of a computer code called BANDSLIP which is used to predict the exit spin velocity of a projectile given the base pressure input to the projectile, the initial geometric conditions of the obturator within the gun tube, and the mechanical and thermal properties of the band materials.[4] This predictive code is based on the following theory.

The band geometry and interference with the projectile body and gun tube wall creates an initial condition called band pressure. The material selection and temperature define a coefficient of friction within the band assembly. The combination of the forces acting on the interface of the inner and outer band and the coefficient of friction of the interface, control the amount of torque which may be transmitted to the projectile body from the gun barrel's rifling. The code assumes the inner band does not rotate on the projectile body and the outer band must follow the path of the rifling. There are two surfaces within the band configuration where torque may be transmitted. The radial surface's ability to transmit torque is largely controlled by the

band pressure which compresses the surfaces together. The base pressure controls the force on the front surface interface. A diagram of these surfaces is shown in Figure 1.

The code predicts the progression for torque transmission of the nylon/polypropylene slipband. Initially, band pressure and the friction coefficient are great enough to transmit sufficient torque for the projectile to rotate at the rate of rifling. Evolving gas causes increased base pressure which accelerates the projectile linearly and therefore also rotationally while it increases the normal force on the front surface and decreases the normal force on the radical surface. The outer obturator band is assumed to seal against the gun wall. Gas pushes between the inner sealing band and the outer band and relieves the force between the bands due to band pressure. As the projectile is forced down the gun bore the rifling forces the outer band to rotate at the twist rate of the rifling. For a while full torque is transmitted between the bands, but eventually the radial surfaces are separated and no torque is transmitted there. If the surfaces can not transmit the full torque imparted by the rifling to the accelerating projectile, slippage begins. The heat generated by the slippage increases the temperature of the interface until the polypropylene melts. Polypropylene has a much lower melting temperature than nylon. If the surfaces are not in contact or one of the surfaces has melted, the ability to transmit torque is assumed to cease. At this time the projectile continues to accelerate linearly down the gun tube, but has reached its terminal rotational velocity.

This theory matches up generally well with evidence from actual gun firings. Slipband obturator components found after sabot discard reveal the inner surface of the outer band often is in an as-machined condition.[5] All that typically remains of the front surface of the inner band is a small nub. The outer, or obturator, band is often forwardly and rearwardly extruded. This correlates with SNLL's other findings on obturators both analytically and experimentally. The predicted trend that rounds fired at 120 F should reach lower spin rates than those fired at 70 F which should be lower than those fired at -20 F has not been seen to hold true. The code's predictions are based on the longer time necessary for the heat generation to raise the materials from their initial temperature to their melt temperatures. It does not account for different band pressure values due to the thermal expansion of the materials in the band, gun, or the projectile. The geometric differences in the size of the components could be inputted, but this does not automatically affect the value of the band pressure.

In fact, two unknown inputs into the prediction are band pressure and the coefficient of friction. Reasonable values have been established as inputs, but they are based on empirical understanding of the system. The code has the ability to generate families of values of both band pressure and coefficient of friction which will result in predicted values of exit spin rate.

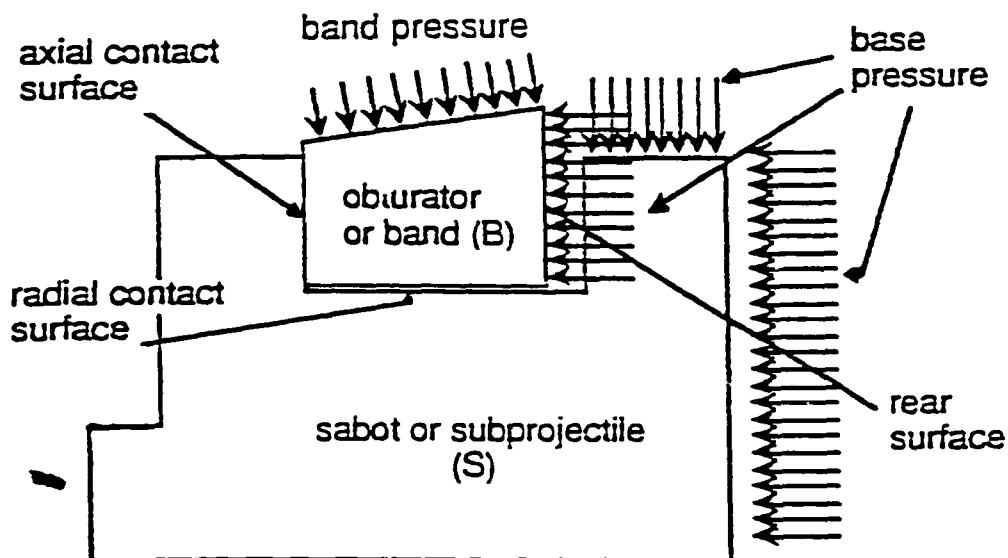


Figure 1 BANDSLIP modelling considerations.

An example of this is shown in Figure 2. Knowledge of any two of these parameters will allow determination of the third.

The theory is however quite useful and believable in making design considerations for slipband obturators. The selection of materials can be used to alter the coefficient of friction which controls the initial condition of spin up and the melting temperature which will control the final spin rate if slippage occurs. Geometric considerations in the design affect the initial band pressure and the interval of time for the base pressure to reduce the band pressure's component in torque transmission. The geometry also controls the rate at which the loading on the front surface will generate heat and cause melt to occur.

BRL has and is performing a series of gun firing tests which are designed to study the slipband obturator.[6] A useful tool which was developed is a 37-mm rifled gun tube which was machined down to a 1/4 inch wall thickness over the region of projectile travel and then overwrapped with graphite/epoxy to provide structural support. This allows the projectile to be observed through the bore using 450 keV flash x-rays, which are available in one of BRL's indoor ranges. This technique was used to determine the in-bore rotation of the projectile as it traverses the tube. Copper rotating bands were shown to rotate at the rate of the rifling and a slipband design based on the band used on M735 projectile was shown to limit the rate of rotation of the projectile body to about 10 percent of that of the rifling as seen in Figure 3. At the time of this writing the only band modifications that have been tested are in the interference of the fit between the inner and outer bands. These differences were quantified as a torque required to rotate the outer band on the projectile. Using a constant initial condition in a test jig, the torques available for testing were measured to be between 0 and 9.5 inch-pounds. Results of these tests given in Figure 4 show the spin varying from 2 to 12 percent of full spin. A more comprehensive and controlled test of varying the interference fit of the band components is ready to be implemented.

The U.S. Army Armament Research, Development, and Engineering Center (ARDEC) designed a series of tests using 105-mm slugs, which were performed by the Combat Systems Test Activity (CSTA) at Aberdeen Proving Ground, to study various slipband configurations. Unfortunately, sparse resources limited the extent and perhaps usefulness of this testing. The various designs considered are shown in Figure 5. The rationale behind the various designs and modifications are as follows.

1. "M833" band - "J band" also used on the M735 projectile used as a base line indicator.
2. "STANDARD" band - Band currently in use. It has twice as much material on the front lip of the inner band than the "M833". This is to ensure that polypropylene is not consumed before muzzle exit. This has not been verified. This band was used as a base line indicator.
3. "PETROLEUM GREASE" band - "STANDARD" band but substituted

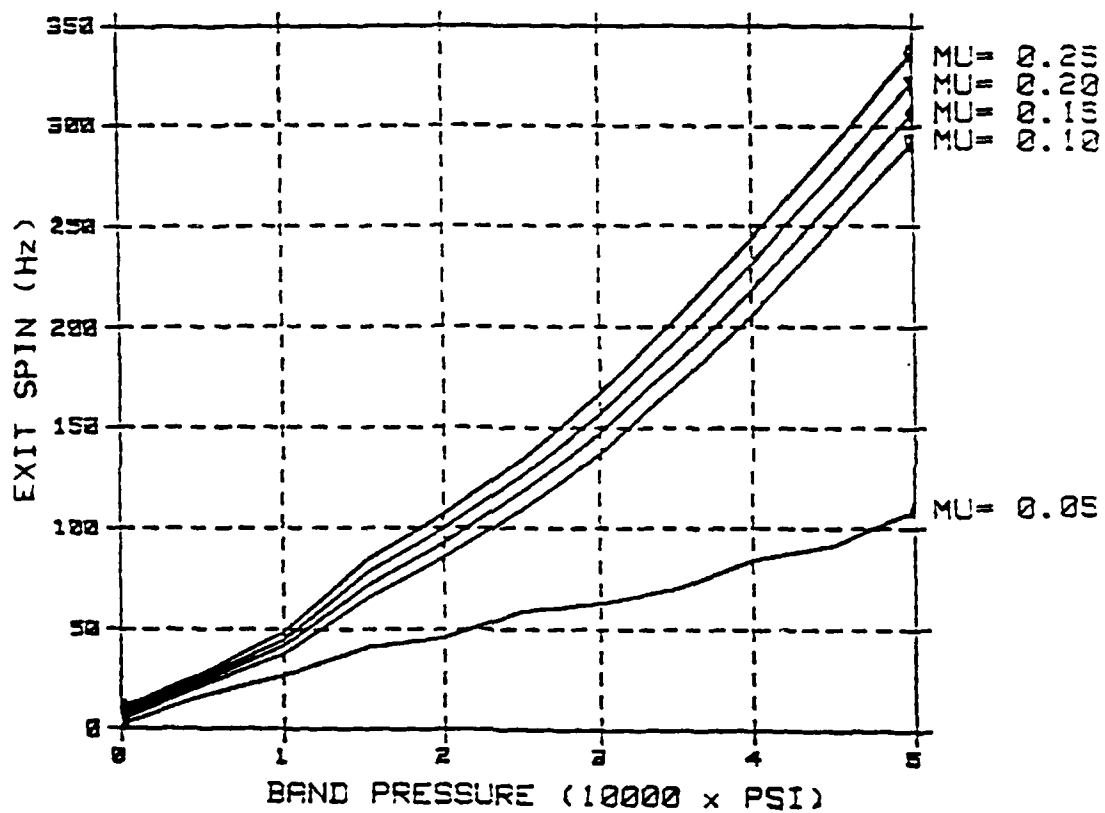


Figure 2 Family of exit spins for slug projectiles predicted by BANDSLIP.

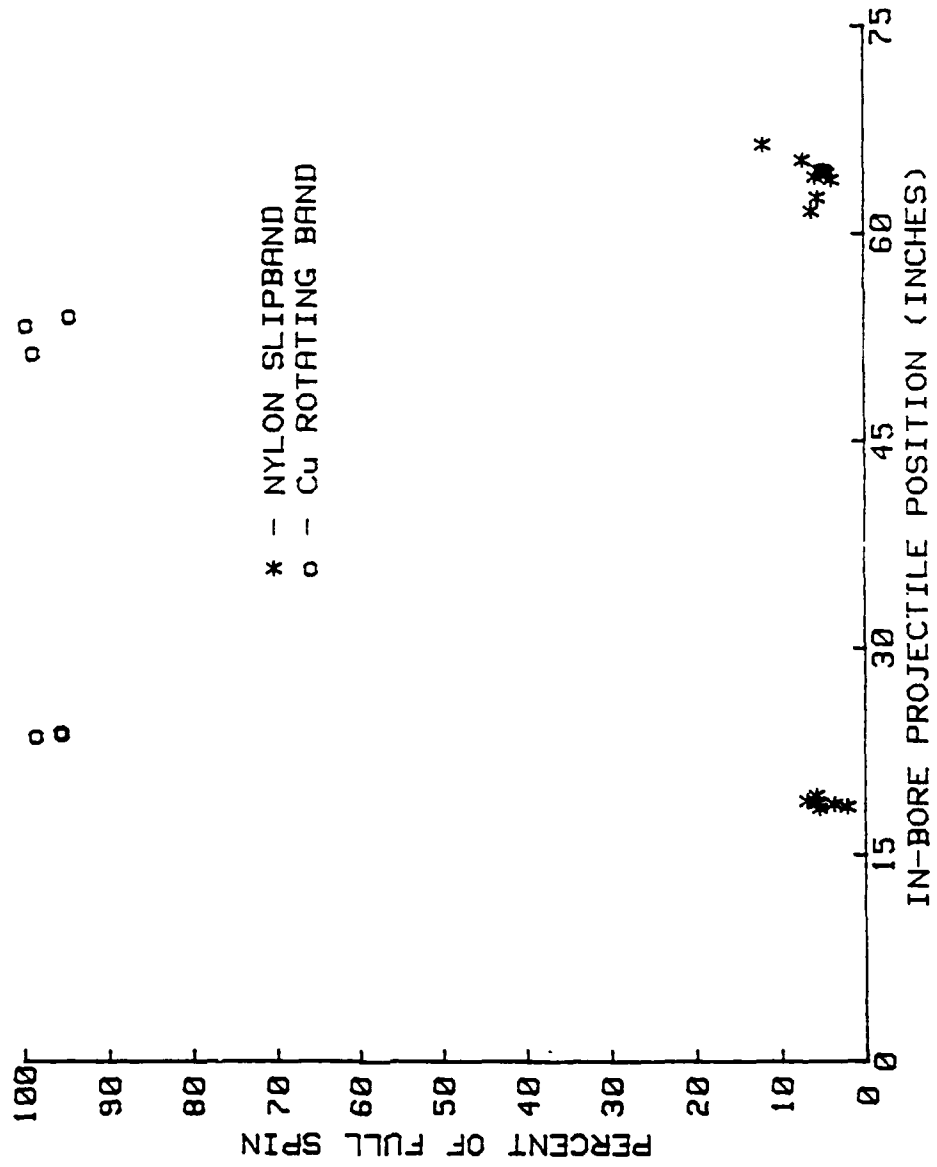


Figure 3 Experimental results of through-bore radiography study of slugs with copper rotating bands and slipband obturators.

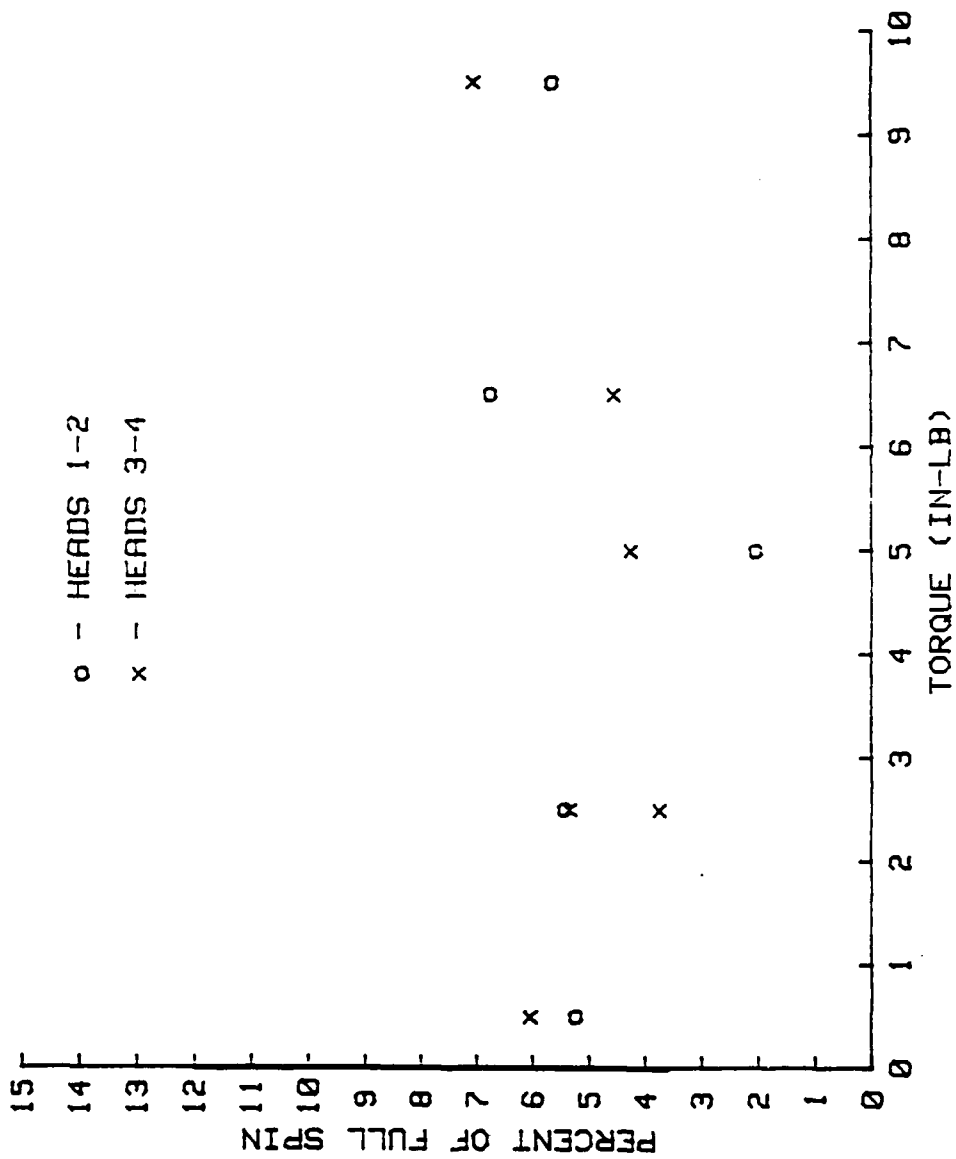


Figure 4 Results of torque sensitivity tests in 37-mm gun.

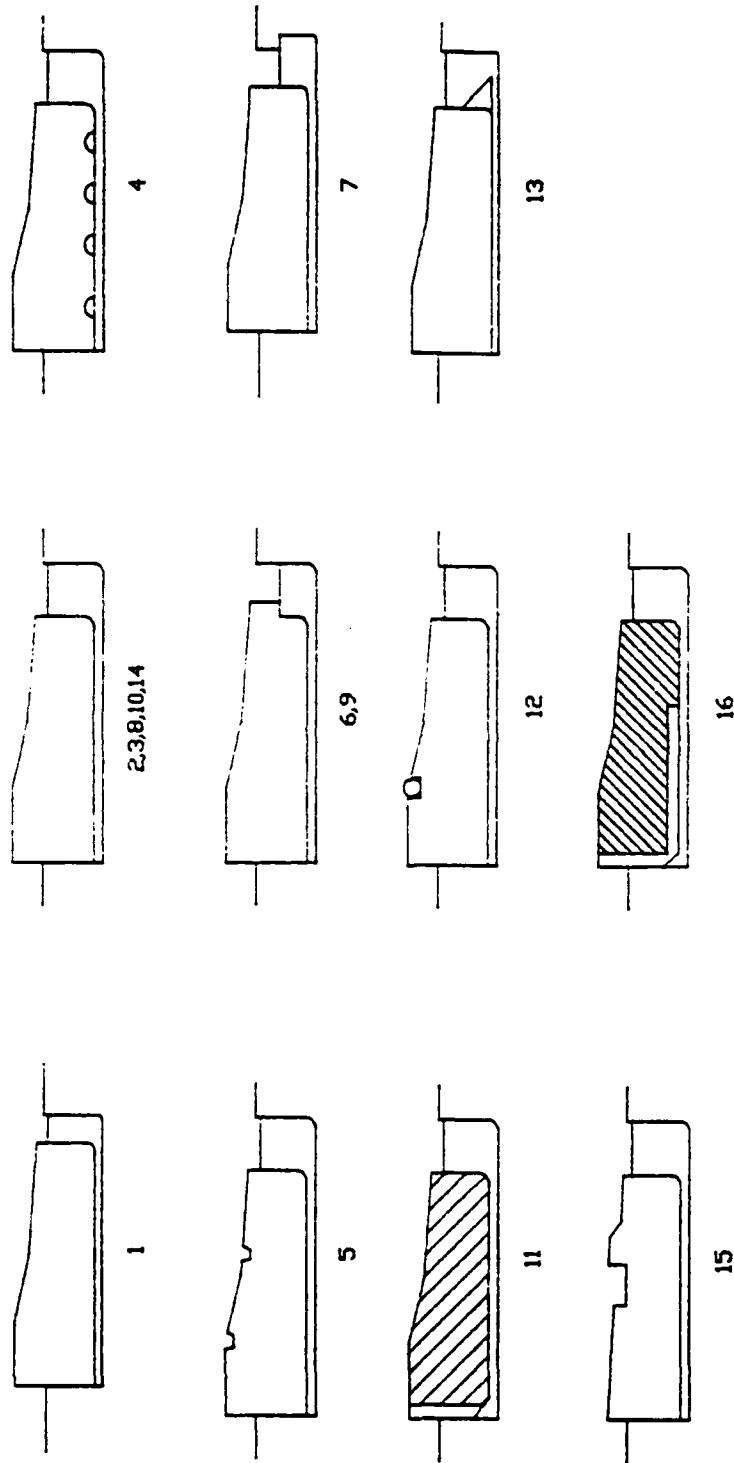


Figure 5 Band configurations tested on slug projectiles.

petroleum grease for the silicon lubricant currently used. Laboratory investigations showed this grease may reduce the static friction coefficient of this system. Its use was to see if this lowered coefficient of friction would lower the threshold of slippage during the early phase of motion, before base pressure creates a clearance between the band components.

4. "CIRCUMFERENTIAL GROOVES" band - "STANDARD" band with circumferential grooves cut into the underside of the obturator band to promote the "air bearing effect" of the gases between the band components.

5. "CANNELURE GROOVES" band - "STANDARD" band with cannellure grooves cut into outer surface of the obturator band to reduce band pressure by changing the initial contact positions of the band with the gun tube wall and by creating stress relief for compressed obturator.

6. "OVERHANGING OBTURATOR" band - Forward surface of the inner band is standard thickness, but reduced in height. Obturator is cut back in front to overhang the inner band. This is to entrap the molten layer of polypropylene as it is formed, creating a more effective bearing and extending the life of the molten polypropylene bearing.

7. "OVERHANGING SABOT" band - Creates a entrapment system for the molten layer as in the previous band but maintains the original amount of material of the "STANDARD" obturator band, although not as effective in preserving the molten layer as it is first generated.

8. "TIGHT STANDARD" band - Same band as "STANDARD" but processing of the installment is adjusted to create a tighter fit after installment.

9. "OVERHANGING OBTURATOR WITH PETROLEUM GREASE" BAND - Investigated to determine affect of the different lubricant on the "OVERHANGING OBTURATOR" which showed to be effective.

10. "LARGER ID" band - Material was removed from the inner diameter of the "STANDARD" obturator to reduce band pressure by reducing the interference of the band between the gun tube wall and projectile body.

11. "'SANDIA'" band - Based on a design by SNLL which was intended to more freely allow gases to infiltrate between the band components while maintaining the proper location of the obturator. Sixteen grooves were to be cut into the obturator surfaces. Radial grooves in the rear surface were .05 to .06 inches deep with a radius of about .03 inch. Longitudinal grooves in the inner surface were .04 to .05 inches deep with a radius of about .03 inch. However, the original design broke during installation. The longitudinal slots on the inside radial surface of the obturator were eliminated and the resulting band was used. The operational intent of the design is to quickly reduce band pressure and initiate slippage.

12. "O-RING" band - Not originally designed to reduce spin, this band was included as a form of the "CANNELURE GROOVE" concept with added obturation during initial pressurization provided by

the O-ring.

13. "NOTCHED SEALING BAND" band - Uses the shown effectiveness of the reduced front surface contact in the overhanging concepts. This design was conceived to exploit the reduced area and increase the slipping velocity by increasing the radius of the contact area. The design should also provide entrapment of the molten layer.

14. "REDUCED OD" band - The reduced outer diameter of the obturator was intended to reduce the interference with the gun wall and projectile .

15. "520T" cannellure groove band - A band design from Chamberlain Corp. which had shown to be effective in prior testing was evaluated. Reduced band pressure by allowing space for material flow, but improved obturation design over the "CANNELURE GROOVES" warranted its inclusion.

16. "SANDIA MOD" band - A band based more closely to SNLL's original concept was tested. Twelve longitudinal and radial grooves were used with radii of .100 inch cut .015 to .020 inches deep into both surfaces.

Designs one through seven were tested in the first test series. Designs two, six, and eight through thirteen were tested in the second series. Designs one, two, and fourteen through sixteen were tested in part three of the testing. Lack of resources precluded the reevaluation of design 7 which required modification to sabot. Sample sizes were groups of 5 in the first two test series and groups of three in the third of the series.

Using one way analysis of variance reveals the following from this data. The velocity means for slugs with band design one fired in tests one and three are different. However, the velocities determined for band design two are considered to be equivalent in all three tests. Likewise, the velocities determined for band six are equivalent in tests one and two. Designs with velocities less than the standard band (2) are 5, 10, 11, 13, 14, 15, and 16.

The chamber pressure means for band design one were also determined to be different between tests one and three. The difference correlates with the difference found in velocity. Once again means for band designs two and six were determined to be equivalent in their respective tests. Chamber pressures that can be considered less than standard (2) are 10, 11, and 15.

Band designs one, two, and six all were found to have equivalent spin values between their respective test groups. Spins that were found to be higher than the standard band (2) were designs 1 and 14.

Using this analysis, it is difficult to determine the differences in variability between band designs. All values determined for band designs two and six were found to be equivalent statistically. Likewise spin values for design one were found to be equivalent between tests one and three. However, the scatter in data produces large standard deviations when combining data from the different tests. Pooling the data between tests

results in apparent improvement in variability for all designs as compared with design 2, which was evaluated in all three tests. Clearly this is an artifact of the small populations and the occasion to occasion variability of the data available.

Unfortunately this forces more subjective evaluations from the available data. Pressure and velocity results are indications of a band design's obturation performance. They may, however, be indicators of resistance to engagement with the rifling and compression through the forcing cone of the gun. Data collected in the tests includes high speed photography of a view looking into the bore of the gun. These records provide information on the obturation on the projectile. Many of the band designs which yielded lower pressures and velocities were not shown to have provided poor obturation as evidenced by photography of little or no flashes of light while the projectiles were in-bore. The projectiles could not be recovered, so physical data on obturator leakage and wear were lost. The photographic evidence infers the conclusion that the in-bore resistance to travel was reduced. In future testing, propellant charges for projectiles using these bands should be adjusted to determine spin rates at equivalent velocity and chamber pressure.

The one way analysis of variance test reveals that only designs one and fourteen result in an increase in spin as compared to design two. The spin produced by design one could be expected to be greater than standard (2) from the theory explained previously. The increase in spin due to design fourteen is not so easily explained. On the surface one might expect design fourteen to behave like design ten. Both result in a thinner obturator band which should reduce band pressure and ease the infiltration of combustion gases, however, the overall results are different. Velocities are lower for both than standard, but only band ten has lower chamber pressure (and thereby presumably lower base pressure). Design ten has equivalent spin as standard but design fourteen has greater spin. However, it might be noted that design ten does have greater spin than design two in the test in which both were actually fired and the spin for fourteen is borderline equivalent to two in the overall comparison. The pressure for design fourteen is marginally equivalent to that of design two, shading towards being lower than two.

If one concludes that designs 10 and 14 may be in fact equivalent in having provided reduced velocities and pressures with greater spin than standard, is there a rational explanation for this? Yes, if the reduced chamber pressure and projectile velocity were caused by combustion gases flowing over the obturator. Reduced base pressure and pressurization from above would allow the band pressure to remain high, transmitting more torque to the projectile and increasing spin rate. If reduced chamber pressure and velocity were caused by reduction of in-bore resistance to travel and obturation was maintained the spin rate would be expected to be equivalent or lower than that of a standard banded projectile. It could be possible that obturation

is occurring in an unconventional fashion. Gas leakage over the top of the obturator during the initiation of pressurization could force the obturator down creating a seal with the inner or sealing band. Later, when the obturator has travelled completely through the forcing cone, it could obturate properly against the gun wall. Exclusion of combustion gas from between the bands would prevent the decrease in the normal force in the radial contact region thereby increasing the spin rate.

Tables 1 through 3 present the data from the three tests. The error bands for each design are plotted between the mean \pm $1/2$ (standard deviation). The complete data sets from each of the three tests are shown. The one way analysis of variance includes these data and uses a pooled standard deviation and the number in the sample population to reflect upon the independence between data sets. Using this analysis the spin behavior of design two is considered equivalent in all three tests.

Several results of modifying the standard obturator can be seen at least qualitatively. It appears as though the strength of the obturator or the support provided to the obturator is at a critical value. In all cases where material has been removed and left a region unsupported, designs 4, 5, 11, 13, and 16, a reduction in velocity occurred. Design 6 which has material removed, but provides support to this region does not show this reduction. Design 12 where material is removed but is somewhat supported by the addition of the O-ring shows some reduction in velocity but not to the same degree as the other designs. Even designs 11 and 16, where one would not expect a significant reduction of support in the obturator show reduced velocity. While design 15 also shows reduced velocity and it has unsupported regions, its design is not as closely based on the standard design as the others.

The results from the designs tested all provide agreement to the basic theory of spin generation of BANDSLIP. Reducing the torque carrying ability of the band system through alteration of the coefficient of friction or reduction of band pressure reduces the rate of spin of the projectile as it exits the gun. Analysis of the data from these tests have led to a better understanding of the operation of the slipband obturator and towards another generation of design.

Features which are important to a slipband obturator system are:

A low coefficient of friction between the slipping surfaces.

The ability to limit torque transmissivity via reduction of the normal force between slipping surfaces or reduction in coefficient of friction (shear load transmission). This class of design provides these features through gas infiltration between the band components and through one component of the slipping interface becoming molten.

If a material is to be sacrificial there must be enough material or a mechanism to insure this material survives throughout the entire travel through the gun tube.

TABLE 1 BAND PERFORMANCE IN SPIN

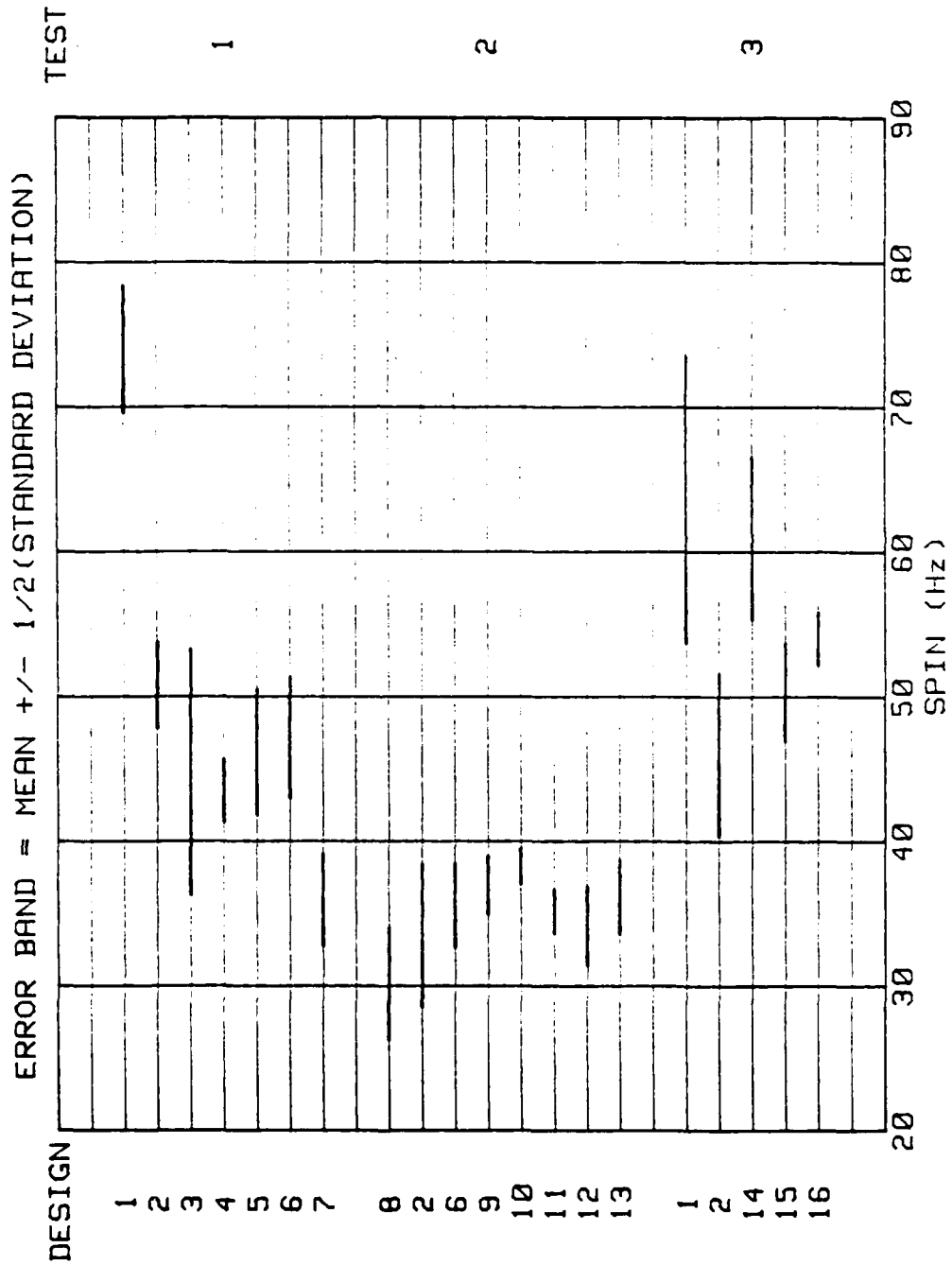


TABLE 2 BAND PERFORMANCE IN VELOCITY

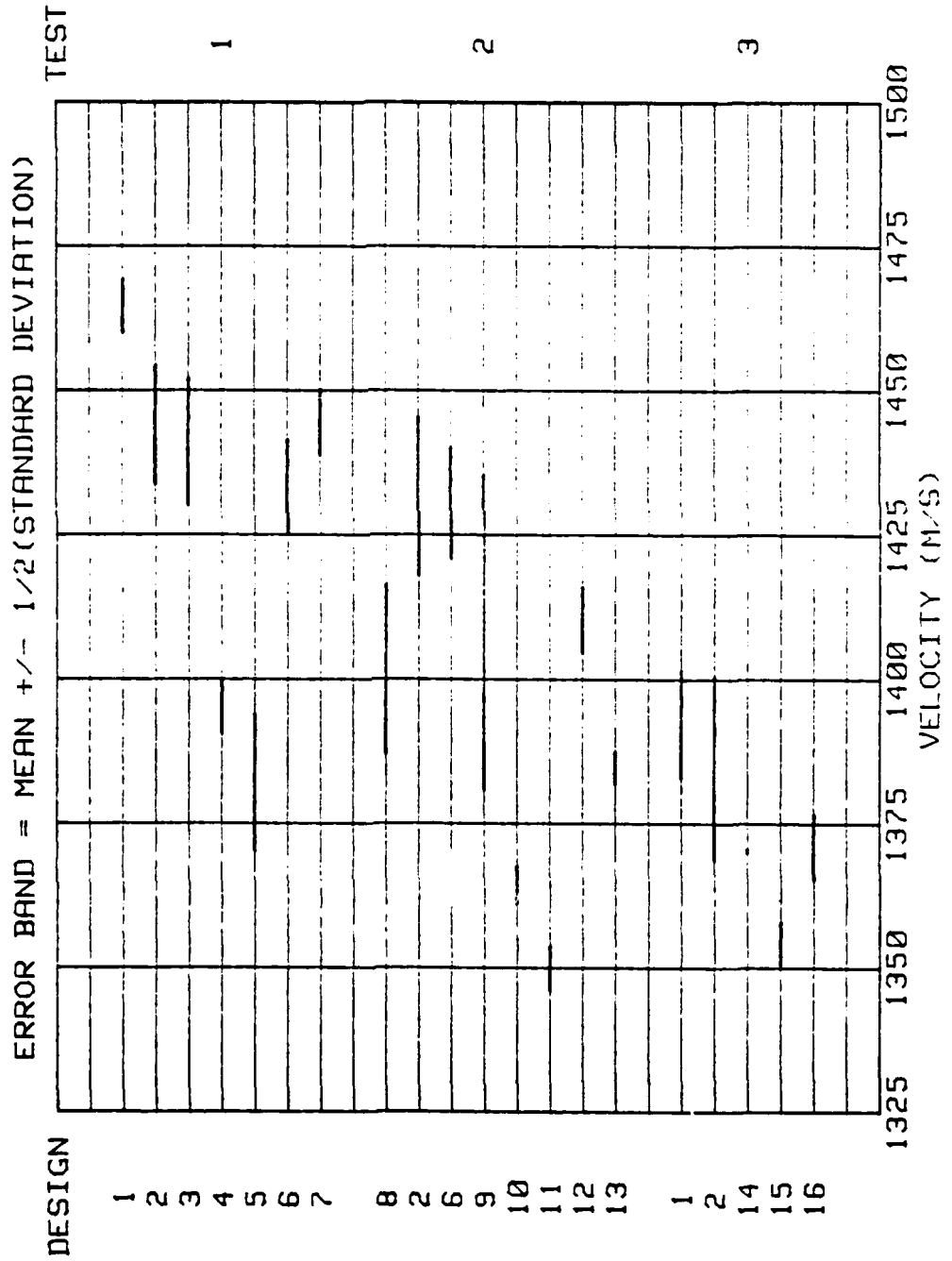
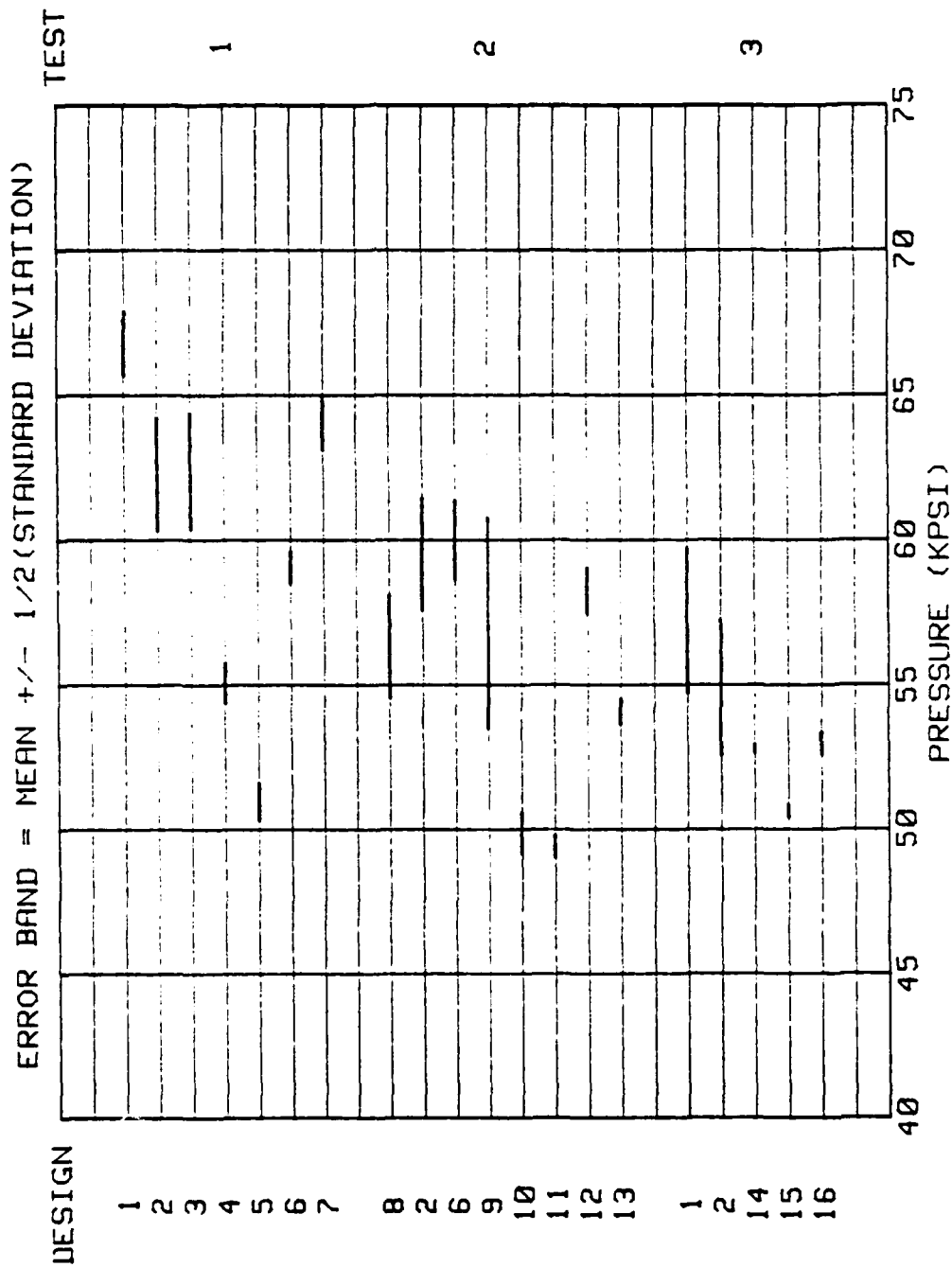


TABLE 3 BAND PERFORMANCE IN PRESSURE



The obturator must have sufficient strength and be of proper design to provide good obturation against the gun wall throughout the ballistic cycle without increasing the normal force between projectile and the obturator or preventing other mechanisms from reducing the normal force.

In order to use purely analytical methods to create obturator designs which provide optimum ballistic performance including spin, more complex models are necessary. The model would have to be able to calculate band pressure as a function of geometrical interference and loading due to changing geometry as the obturator passes through the forcing cone and base pressure rise. It would have to determine which interfaces act as seals and which do not as a function of time and travel. Band pressure would be treated as a gradient rather than a nominal value as currently implemented. A more complete modelling of temperature effects would also be needed to account for thermal expansion effects or at least these factors must be accounted for before geometry and material property inputs are put into the code. The effect of loading rate and humidity on the material properties would also need to be incorporated. Inclusion of all these factors could provide not only a technique for analytical obturator design but also a method to find causes for round to round variability within a design. Development of such a tool is not an impossible task, but one that has yet to be achieved.

References

- [1] P.E. Nielan, K.J. Perano, W.E. Mason, "ANTIPASTO - An Interactive Mesh Generator and Preprocessor for 2 Dimensional Analysis Programs", SAND90-8203, April 1990.
- [2] K.J. Perano, "Minutes of the February 25, 1988 DA/DOE Program Review Meeting"
- [3] W.A. Kawahara et.al. "Temperature, Moisture, and Strain Rate Effects on the Compressive Mechanical Behavior of Nylon 6/6", SAND88-, January 1988.
- [4] P.E. Nielan, G.A. Benedetti, "Spin Rate Prediction for Projectiles with Slipping Obturators, Including the Effects of Friction Heating", Sandia National Laboratories, to be published.
- [5] C.D. McCall, B.P. Burns, "Investigation of M735 KE Projectile Slip Obturator Behavior", BRL-MR-3716, Dec 1988.
- [6] L.W. Burton, R.P. Kaste, I.C. Stobie, "A Technique for Measurement of In-bore Projectile Spin", BRL-TR- 3037, Sept 1989.

Benson, R. - Benson, W. - Sorenson

TITLE: A METHODOLOGY FOR DESIGNING PROJECTILE INTERFACES TO
SURVIVE WORN GUN TUBE LAUNCHING
by * RICHARD C. BENSON, WILLARD R. BENSON, TOM SORENSON
BEACON TECHNOLOGY, INC., 8 Grover Rd., Dover, N.J. 07801

ABSTRACT:

The issue of component integrity of projectiles fired from worn gun tubes has been a major area of concern over the past 20 years. The importance has escalated as projectile design has become more complex. This report offers a new model that characterizes the torsional impulse that occurs during the early motion of a projectile into the worn rifling. The model is confirmed by experimental results obtained in instrumented 155mm gun/projectile firings.

Also included in the computer model is the analysis of friction coupled payload loads carried within the projectile. It includes the analysis of cargo slippage treating both static and sliding friction. Slippage is permissible provided the cargo comes up to full spin rate prior to muzzle exit. A slipping interface which recovers can be beneficial since it limits the rotational acceleration pulse delivered to the slipping unit. These issues are addressed and a rationale for the design of component interfaces is offered.

BIOGRAPHY:

Richard C. Benson is a professor of mechanical engineering at the University of Rochester and vice president of Beacon Technology, Inc. (BTI). He received a B.S.E. in mechanical and aerospace Science from Princeton University in 1973, an M.S. in mechanical engineering from the University of Virginia in 1974, and a Ph.D. in mechanical engineering from the University of California, Berkeley. From 1977 to 1980 he worked for Xerox Corporation as a technical specialist/project manager. In 1980 he joined the University of Rochester, and in 1983 he joined BTI. In 1984 Dr. Benson received the Henry Hess Award, given annually, if warranted, by the American Society of Mechanical Engineers for the outstanding technical paper by a young author.

Benson, R. - Benson, W. - Sorenson

A METHODOLOGY FOR DESIGNING PROJECTILE INTERFACES
TO SURVIVE WORN GUN TUBE LAUNCHING
by

*DR. RICHARD C. BENSON,
PROFESSOR of MECHANICAL ENG.
UNIV. OF ROCHESTER
ROCHESTER, NY 14627

WILLARD R. BENSON, PRES.
BEACON TECHNOLOGY, INC.
8 GROVER ROAD
DOVER, NJ 07801

THOMAS SORENSON
BEACON TECHNOLOGY, INC.
8 GROVER ROAD
DOVER, NJ 07801

TABLE OF CONTENTS

Introduction

Analysis

Two Delta Spin-up Model
Slip Mechanics
Acceleration vs. Time Curve

Determining δ and Δ

Tactical Round Analysis

Interface Slipping

Design Considerations

References

INTRODUCTION

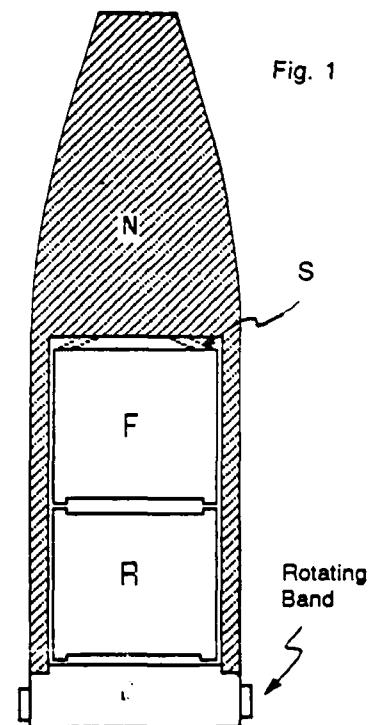
Over the past twenty years, a great deal of interest and effort has been devoted to understanding the rotational dynamics of a projectile traveling down a worn rifled gun tube. The rotational acceleration spike that occurs after a few inches of travel and considerably before peak acceleration has been known to cause:

- * Threaded and pinned joints to fail.
- * Kinetic energy penetrators to slip within their sabots resulting in inadequate angular muzzle momentum to insure stable flight.
- * Projectiles to explode within the gun tube due to the high explosive slippage within the shell body.
- * Fuzes to slip their time settings.

New more complex projectiles such as SADARM, APM and the like have many interfaces that will be subjected to the rotational acceleration spikes associated with their projection through a worn gun tube. It follows that the various interfaces must be appropriately analyzed to insure integrity and to preclude catastrophic failure. This requires a knowledge of the applied loads.

This paper offers a method to characterize the rotational acceleration spike that results due to the linear travel and "spin up" that occurs prior to fully engaging the rifling of a worn gun tube. Further, it offers a method to analyze and to evaluate the result of any slipping that may occur at a friction interface.

A typical cargo carrying projectile will have 2 or more contained sub-projectiles or munitions and several friction interfaces some of which may also use pins or keys. The Beacon Technology, Inc. (BTI) computer code treats up to 10 interfaces each with their own coefficient of friction. For the purpose of this paper, the configuration shown in figure 1 will be analyzed. The shell consists of a base B with a rotating band attached; Shell N; two contained canisters, F and R; and spring S between the forward canister F and the Shell N. The spring is primarily used to keep the payload snug during the dynamics associated with transportation and handling, and the spring's allowed displacement is such that the "set back" of the shell N less the spring force goes through base B. In a like manner, the set back of canisters and spring, plus the spring force, goes through base B at the interface between R and B.



ANALYSIS

Two Delta Spin-Up Model

In an unworn gun tube the relationship between the angular rotation θ and linear displacement x can be expressed as

$$\theta = Kx, \quad \dot{\theta} = K\dot{x}, \quad \ddot{\theta} = K\ddot{x} \quad (1)$$

where K is the constant associated with the twist of the rifling. In a worn gun tube the projectile will travel a distance $x = \delta$ before any angular spin begins, i.e. at $x = \delta$ the following conditions exist

$$\theta = \dot{\theta} = \ddot{\theta} = 0. \quad (2)$$

Not until the projectile has traveled a distance $x = \Delta$ does the projectile become fully engraved with conditions

$$\theta = Kx - \theta_{1ag}, \quad \dot{\theta} = K\dot{x}, \quad \ddot{\theta} = K\ddot{x}. \quad (3)$$

The θ_{1ag} offset recognizes the fact that although the projectile eventually reaches full angular velocity and angular acceleration, it does not rotate through the same total angle as in the unworn tube.

The "two delta spin-up model", proposed by Beacon Technology, Inc. (BTI) is a simple polynomial curve-fit that will take the unspinning projectile at position $x = \delta$ to fully engraved conditions at position $x = \Delta$. We approximate

$$\theta = C_0 + C_1y + C_2y^2 + C_3y^3 + C_4y^4, \quad (4)$$

where

$$y = (x - \delta) / (\Delta - \delta), \quad (5)$$

and $C_0 \dots C_4$ are constants determined by the boundary conditions in equations (2) and (3) and

$$C_0 = C_1 = C_2 = 0, \quad C_3 = K(\Delta - \delta), \quad C_4 = -K(\Delta - \delta) / 2 \quad (6)$$

Thus while $\delta < x < \Delta$ the following expressions govern the "spin-up" of the projectile

$$\theta = K(\Delta - \delta)(y^3 - y^4/2) \quad (7)$$

$$\dot{\theta} = K(3y^2 - 2y^3)\dot{x}, \quad (8)$$

$$\ddot{\theta} = K(3y^2 - 2y^3)\ddot{x} + [6K / (\Delta - \delta)](y - y^2)\dot{x}^2 \quad (9)$$

The rotation lag is found by evaluating equation (7) for $x = \Delta$ and subtracting from Kx to give

$$\theta_{1ag} = K(\Delta - \delta) / 2 \quad (10)$$

An illustration of function (9) is shown in Fig. 2. The dashed curves indicate nominal conditions in an unworn gun tube. The most important observation to be made is that there will be a large "spike" in $\ddot{\theta}$ as the projectile comes up to speed. This, in turn, creates an impulse torque on the projectile that is greater than that experienced at the same point in a new tube. This impulse torque will increase the loading on the rifling band and most likely accelerate the wear process. It also has the potential of causing slippage or breakage of internal components in the projectile.

The $\ddot{\theta}$ spike (λ_1 , see fig. 2) has been investigated by a number of authors using various models [refs (1), (5), (6), (7), (8), (9), (10), (12)]. The torque during the "transition" or "clutch-up" distance $\Delta - \delta$ is, in fact, a highly complicated function of the worn gun tube profile, and band strength and shape. To conduct an analysis of the actual dynamics of the rotating band engraving is beyond the scope of this paper.

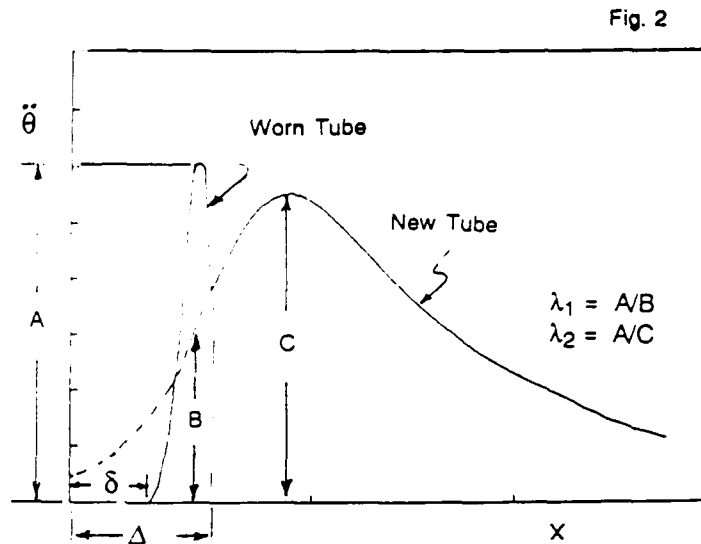
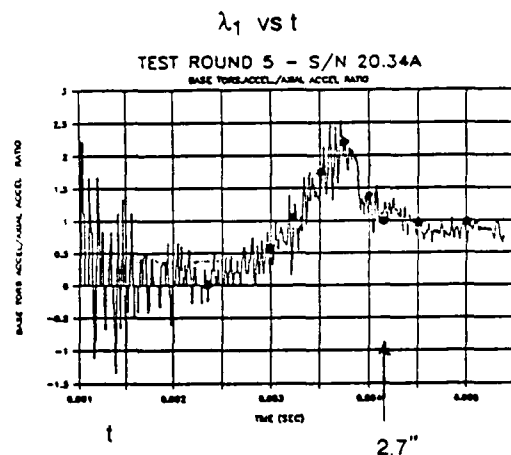


Fig. 2

Fortunately, a great deal of instrumented experimental firings have been conducted with worn gun tubes, and this data may be used to test the reasonableness of the empirical "two delta" model of this paper. Figure 3 shows λ_1 , the experimentally measured ratio for base angular acceleration divided by the rotational acceleration expected from a new tube ($K\dot{\omega}$) along with calculated points using the "Two Delta Spin-up Model" plotted against time. Details for the test are given in Ref 14. The two delta fit is quite good and sufficient for evaluating the response of the projectile system.

Slip Mechanics

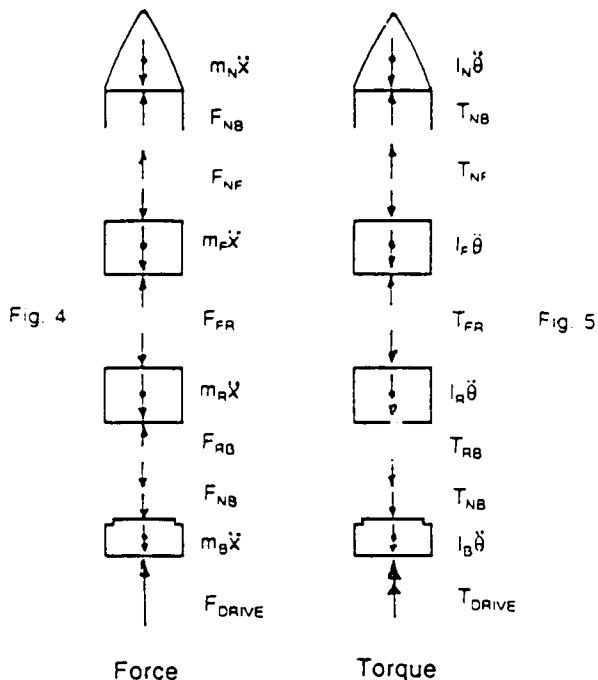
The worn gun tube torque spike raises concern about internal loads and dynamics of the projectile. A particular concern is that components may slip relative to one another causing damage to the cargo or inferior flight dynamics after leaving the gun. To further study these possibilities we have create a mathematical model, and used it to simulate conditions that lead to slip. This is admittedly a very simple model, but one that we believe is useful for qualitative assessments.



• Calculated Two Delta Spin-up points

Fig.3

Free Body Diagram



Figures 4 and 5 show a free-body diagram for forces and torques passing through a four component projectile that consists of a: base (B), nose (N), front can (F), and rear can (R). The nose attaches to the base and encloses the two cans. Driving the whole projectile is a force F_{DRIVE} and torque T_{DRIVE} that are both known from pressure-time data and the preceding spin-up analysis. Internal forces are denoted by the symbol F , and a double subscript denoting the interface of interest (e.g. nose to front can is F_{NF}). A similar notation is used for torques (e.g. T_{NF}). Component masses are denoted by m with a subscript, and mass moments of inertia are denoted by I with a subscript.

The system as presented is statically indeterminant. We can solve for all forces in terms of the nose/front-can reaction force

$$\begin{aligned}
 F_{NB} &= m_N \ddot{x} - F_{NF} \\
 F_{FR} &= m_F \ddot{x} + F_{NF} \\
 F_{RB} &= (m_R + m_F) \ddot{x} + F_{NF} \\
 F_{DRIVE} &= (m_B + m_N + m_R + m_F) \ddot{x} = m_{Total} \ddot{x} \quad (11)
 \end{aligned}$$

Similarly, we can solve for all torques in terms of the nose/front-can reaction torque

$$\begin{aligned}
 T_{NB} &= I_N \ddot{\theta} - T_{NF} \\
 T_{FR} &= I_F \ddot{\theta} + T_{NF} \\
 T_{RB} &= (I_R + I_F) \ddot{\theta} + T_{NF} \\
 T_{DRIVE} &= (I_B + I_N + I_R + I_F) \ddot{\theta} = I_{Total} \ddot{\theta} \quad (12)
 \end{aligned}$$

Each of the equations above has an inertial set-back part (e.g. $m_N \ddot{x}$, $I_N \ddot{\theta}$) and a part due to the reaction at the nose/front-can interface (e.g. F_{NF} , T_{NF}). The nose/front-can interface has a spring preload on the order of 4,000 pounds. This is quite small in comparison to the "G" forces that occur during firing, and it suggests that we can ignore F_{NF} and T_{NF} in the equations above. This would render the system statically determinant and

far easier to analyze. We will make this assumption, however, it should be noted that the validity depends not only on the smallness of the initial preloading of F_{NF} and T_{NF} , but also on the dynamic value that develop during firing. Stated in other words, we are assuming that almost all inertial set-back (force and torque) of the nose is transmitted directly to the base, and little is passed through the cans.

We now consider the possibility that the nose will slip relative to the base. We use a simple friction model. Slip occurs if the following inequality occurs

$$T_{NB} > r_{NB} \mu_{NB} F_{NB} \quad (13)$$

where r_{NB} is the radius of the nose/base interface, and μ_{NB} is the static coefficient of friction. The right hand side may be interpreted as the static torque limit that the base may transmit to the nose. Prior to slip (if it occurs at all) the nose spins at exactly the same angular velocity as the base which drives it, i.e.

$$\dot{\theta}_N = \dot{\theta}_B = \dot{\theta} \quad (14)$$

where $\dot{\theta}$ is found from the preceding spin-up analysis. Once slip begins between the nose and base, then we shift to a sliding friction model. The torque at the interface immediately drops to

$$T_{NB} = r_{NB} \mu_{NB}^d F_{NB} \quad (15)$$

where μ_{NB}^d is the dynamic coefficient of friction at the interface. We have typically assumed that the dynamic coefficient is one third the static value; $\mu^d = \mu/3$. With slip occurring, the nose will no longer rotate at the same angular velocity as the base. Instead, the nose rotation is found from integrating

$$I_N \ddot{\theta}_N = T_{NB} \quad (16)$$

through time. Because of its direct engagement with the gun tube, the rotation rate of the base is assumed to be unchanged during component slip

$$\dot{\theta}_B = \dot{\theta} \quad (17)$$

where, again, $\dot{\theta}$ is the value dictated by normal rifling or by the spin-up model of this paper.

Slip can also switch back over to stick. If $\dot{\theta}_N$ catches up with $\dot{\theta}_B$, we cease integrating equation (16), and lock the two spin rates together as in equation (14). It is also possible for the rear can to slip against the base. The equations governing the slip and stick are identical in form to (13) ... (17), but with a subscript "R" replacing "N" in all cases. Nose/base and rear-can/base are the two most likely interfaces for slip. Other interfaces could slip, such as the front-can/rear-can, but are less likely.

The algorithm of the BTI simulator may be summarized as follows: Pressure-time data is input or curve-fit, and the axial motion of the projectile is determined. This determines the set-back forces at all interfaces. The rotation of the projectile base is then determined by the normal rifling ratio or by the spin-up model of this paper. This determines the inertial torques that must be maintained at the interfaces.

If static friction limits are not exceeded than all projectile components are assumed to rotate at the exact same rate as the base. If static friction limits are exceeded, then components are allowed to rotate relative to each other. The angular acceleration is determined by classical rigid body dynamics with driving torques limited by the dynamic coefficients of friction. Slipping ceases whenever a forward component (usually the nose or rear can) catches up to the angular velocity of the rear component (usually the base) driving it. Integration in time is done by a predictor/corrector numerical method.

As noted earlier, this is a simple model of value in qualitative assessments. Further work should be directed towards more detailed modelling of the stick/slip mechanics of the interfaces, and in determining the influence of loads from the front-can/nose interface.

Acceleration vs Time Curve

Six test rounds were fired with a PXR-6297 + 16 oz. propellant charge conditioned to 145°F in order to achieve PIM (Permissible Individual Maximum Pressure). Acceleration vs time was determined for the first 8 inches of travel using the collector cup, wires down the gun tube method.

The early portion of the acceleration/time curve can be represented for analytical convenience by the equation

$$\ddot{x} = At^2 + B$$

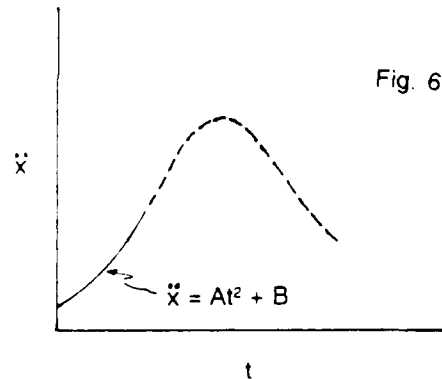
as illustrated in Figure 6. The complete \ddot{x} vs time curve would also include the dashed portion. The BTI code is being up graded to include the complete curve. For the purpose of this paper, the expression $\ddot{x} = At^2 + B$ is sufficient since it adequately represents the early travel of the projectile which includes the $\ddot{\theta}$ spike of interest. In fitting the experimental data, a good value for A and B for the heavier test round is

$$A = 1.2 (10^{11}) \text{ in/sec and } B = 0$$

and for the lighter tactical round

$$A = 1.386 (10^{11}) \text{ in/sec and } B = 0$$

The important region of concern is during the first few seconds of travel. Unfortunately, some computer codes do not model this region very well. Quite frequently, arbitrary values of shot start pressure are used. The principal reason for most all computer codes is to determine maximum pressure and muzzle velocity with little if any concern about the early time phase of propulsion. A proper torsional impulse evaluation requires acceptable \ddot{x} vs time data as an input.



Determining δ and Δ

The instrumented test projectiles were fired from Yuma gun tube #S/N 29226 which was in the 4th quarter of wear. Typical results of integrating acceleration data are shown in Figure 7. This implies a reasonable value of δ and Δ for the experimental

round to be $\delta = .3$ inches and $\Delta = 2.7$ inches.

The input conditions for the BTI computer model of the experimental rounds are shown in Table 1. The friction resisting torque capability of the shell body with the base is shown as the upper curve of Figure 8. Since the driving torque shown by the lower curve of Figure 8 remains below the upper

curve, the shell body does not slip relative to the base. A no slip condition was also predicted for the contained cans. The rotational acceleration spike is reproduced in Figure 9 and the calculated value are plotted on the same curve as the experimental results in Figure 10. The worn gun tube spin up velocity $\dot{\theta}$ is shown on Figure 11 along with the spin up velocity that would result from a new tube.

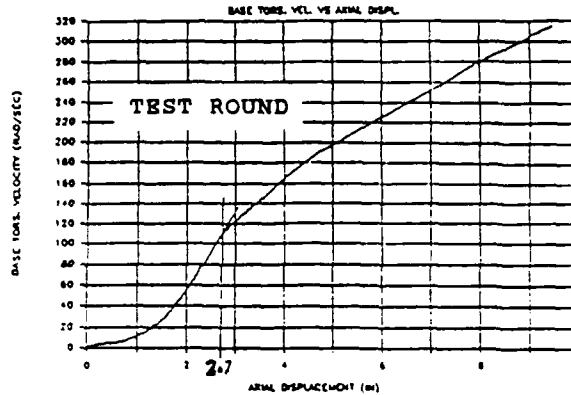


Fig. 7

TABLE 1.		TEST ROUND	TACTICAL ROUND	
Weight-Nose	=	36.60	25.96	1b
Weight-Base	=	18.93	13.53	1b
Inertia-Nose	=	206.19	177.63	1b-in
Inertia-Base	=	124.72	92.83	1b-in
Friction N/B	=	0.54	0.54	
Friction N/F	=	0.12	0.12	
Friction Ratio	=	0.33	0.33	
Radius-N/B	=	2.94	2.94	in
Radius-N/F	=	1.41	1.41	in
Pre-Load	=	4000.00	4000.00	1b
Stiffness Ratio (0-1)	=	1.00	1.00	
Free-Run Dist	=	0.30	0.30	in
Spin-Run Dist	=	2.70	2.70	in
Gun Tube Length	=	200.00	200.00	in
Rifling Const	=	0.0515	0.0515	rad/in
Weight-CanF	=	32.70	33.14	1b
Inertia-CanF	=	155.08	169.00	1b-in
Friction-F/R	=	0.54	0.54	
Radius-F/R	=	2.71	2.71	in
Weight-CanR	=	27.94	27.94	1b
Inertia-CanR	=	145.08	145.08	1b-in
Friction-R/B	=	0.54	0.54	
Radius-R/B	=	2.705	2.705	in

TEST ROUND, BASE ROT ACC VS TIME

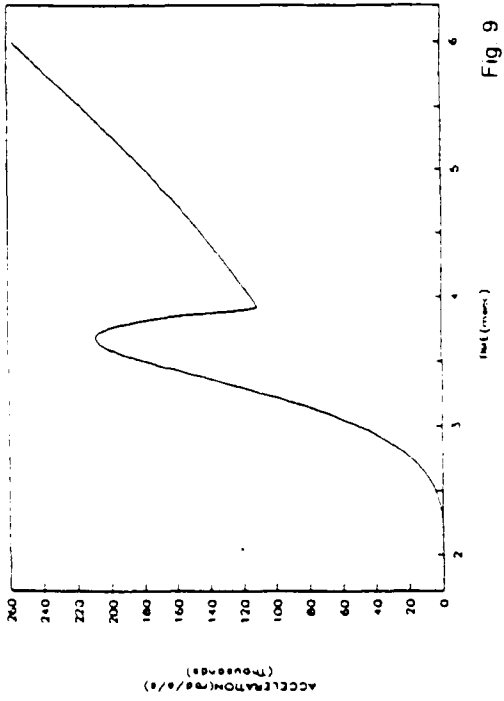


Fig 9

NOSE/BASE TORQUE

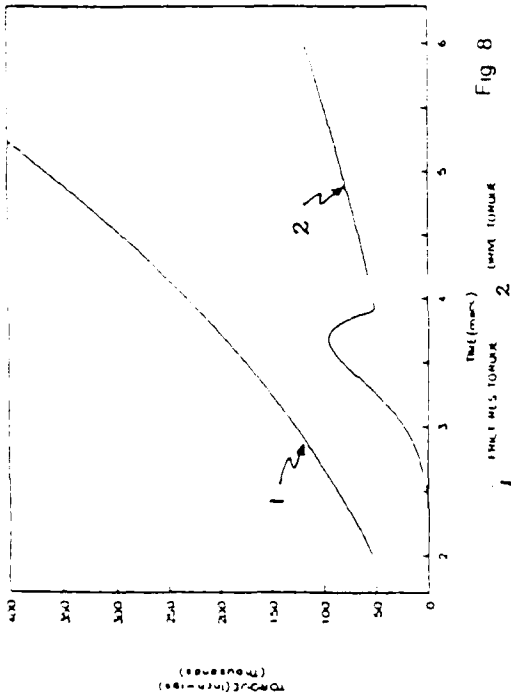


Fig 8

ROTATIONAL VII VS TIME

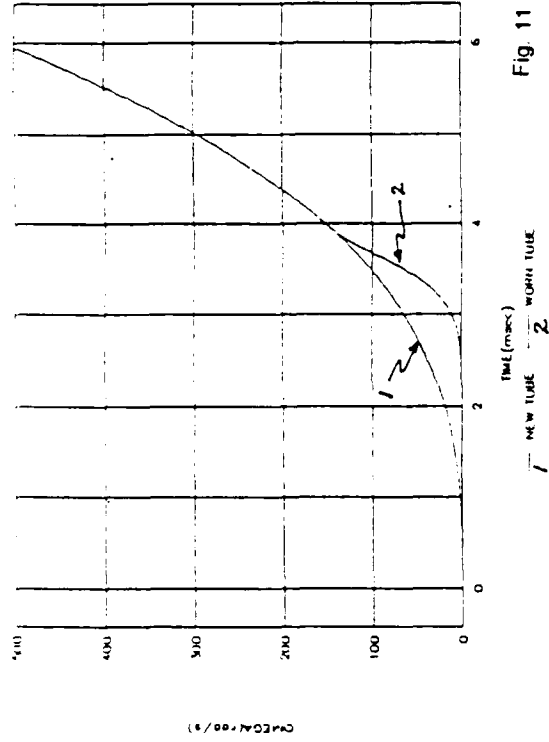


Fig 11

TEST ROUND 5 - S/N 20.34A

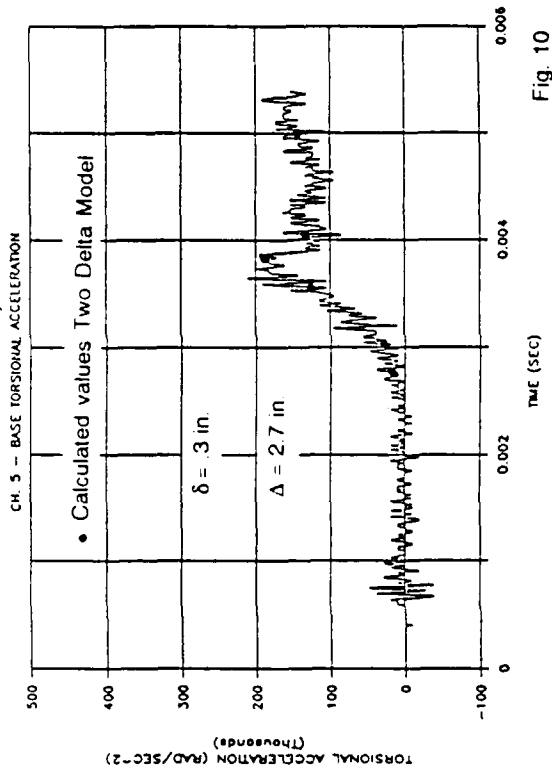


Fig 10

In the case of the test round the polar moment of inertia is 630.91 lb. in.² vs 587.46 lb. in.² for the tactical round. This is a 7.4% increase. The experimental round was also 15.4% heavier than the tactical round. (The rotating bands are the same for both rounds).

One would expect the tactical configuration to come up to spin in a shorter time period due to its lesser inertia. It would also impact the rifling at a higher velocity. As a result, one would expect a higher $\ddot{\theta}$ max.

For the same δ and Δ .

$$\ddot{\theta} \text{ max (experimental round)} = 1.933 (10^5) \text{ rad/sec}^2.$$

$$\ddot{\theta} \text{ max (tactical round)} = 2.077 (10^5) \text{ rad/sec}^2.$$

or a 7.4% increase.

The input values of the tactical round are shown in Table 1. The torque results for the nose/shell body are shown in Figure 12 which implies that the shell body does not slip relative to the base. This is also true of the contained canisters. The $\dot{\theta}$ vs t is shown in Figure 13 and the $\ddot{\theta}$ spike in Figure 14.

The above calculations were based on a δ of .3 inches and a Δ of 2.7 inches. This resulted in a $\ddot{\theta}$ max of 2.077 (10^5) rad/sec² for the tactical round. The peak $\ddot{\theta}$ at the peak Gs of 15,000 is 3(10^5) rad/sec². The value λ_1 associated with the $\ddot{\theta}$ spike is approximately 2.0.

The friction μ needed to preclude slipping in a new tube using a threaded joint and assuming no help from the threads is

$$\mu \geq \frac{I\ddot{\theta}}{M\ddot{x}_r} \quad \text{or} \quad \mu \geq \frac{KI}{Mr} \quad (18)$$

where M = set back mass
 I = polar moment of inertia
 K = rifling constant
 r = radius to friction surface

for the shell body

$$\mu = \frac{.0515(177.63)}{25.96(2.94)} = .12$$

for the canister F

$$\mu = \frac{.0515(169)}{33.14(2.705)} = .097$$

for the canister R

$$\mu = \frac{.0515(169 + 145.08)}{(33.14 + 27.94)(2.705)} = .098$$

For a λ_1 of 2.0 the required friction for no slip would be

shell/base	=	.240
canister P / canister R	=	.194
canister R / base	=	.196

For design purposes, a λ_1 of 2.0 is not adequate since not all worn gun tubes are alike and a given worn gun tube changes. In addition, if slipping does occur, a sliding coefficient of friction should be used. The static coefficient of friction for the experimental and tactical interfaces indicated above was determined to be .54 (knurled surfaces were used).

The extensive work of reference 12 indicated that for various tubes at various wear levels λ_1 ranged from 1.29 to 2.12 and λ_2 from .37 to 1.56. The gun tube used in this study had a λ_1 of approximately 2.0 and a λ_2 of .68 at the time of testing.

Figures 15, 16 and 17 offer some insight to the variability problem of worn gun tubes.

In the experimental work of references 12 the clutch up distance $(\Delta - \delta)$ varies from .85 to 5.1 inches for the worn tubes studied. It is also implied that a Δ greater than 8 inches would be the condemnation level of a worn tube.

Figures 15, 16 and 17 which employ the Two Delta model indicate that a rotational acceleration spike is likely in a new tube. This was also found to be true in the study of reference 12. A $\ddot{\theta}$ spike in a new tube should not be detrimental if δ is 0, the peak $\ddot{\theta}$ of the spike is low even though the λ_1 value could be high. The band would deform somewhat and spin up would occur at a value much less than the length of the band. Slippage in a new tube would depend on the friction, the preload, and shot start conditions all of which are controllable.

As the tube wears and δ increases, and assuming a minimum $(\Delta - \delta)$ of .85 inches or greater, the portion of the curves of Figure 15, 16 & 17 that apply are to the right of the dashed line $(\Delta - \delta) = .85$.

It would be interesting to determine δ and Δ as a tube wears in order to better establish the operational curve (dashed line) for Figures 15, 16 and 17. The T point on the curves indicate the condition of the tube used in this study.

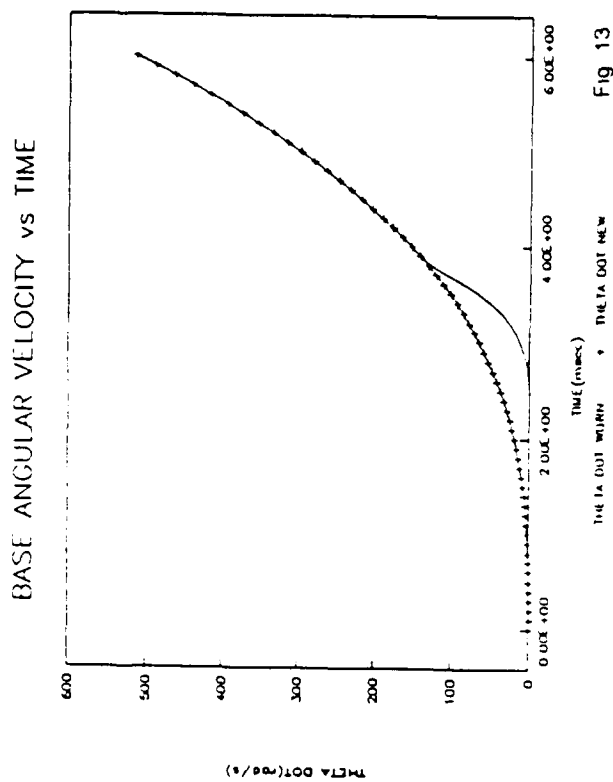


Fig 12

BASE ANGULAR ACC vs TIME

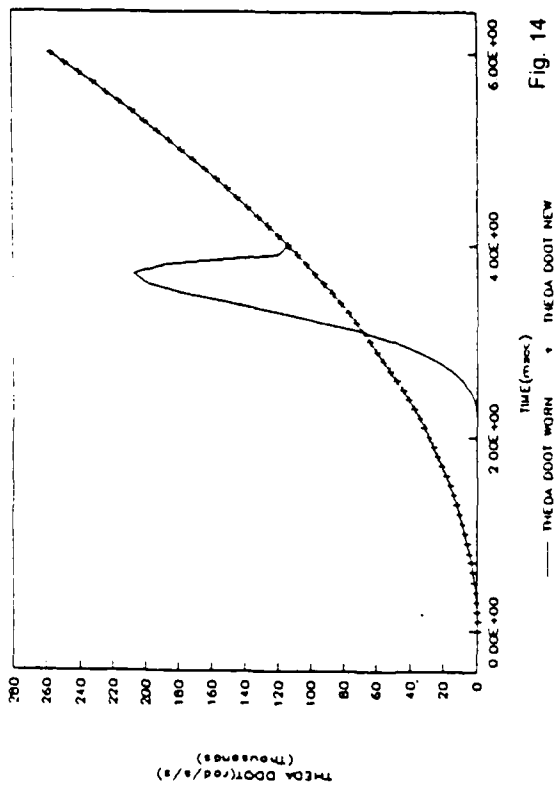
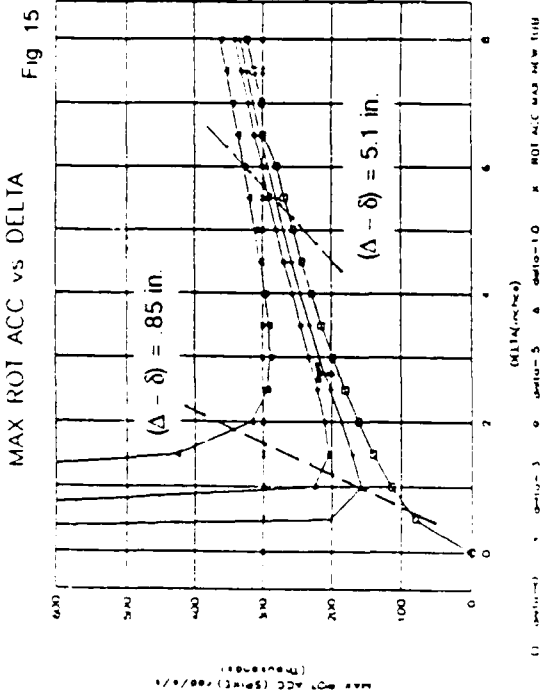
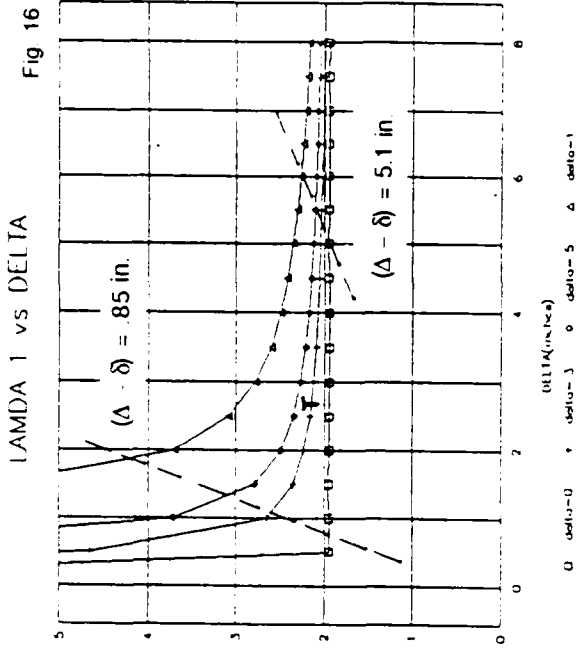


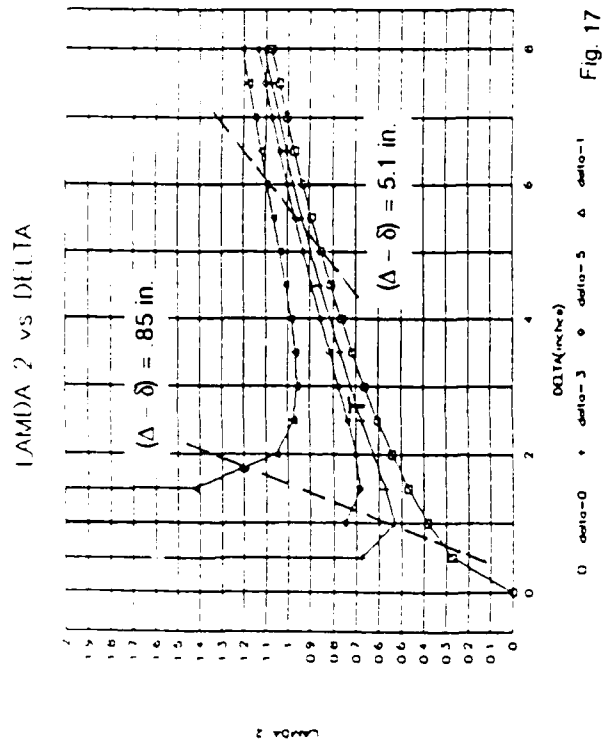
Fig 13

TACTICAL ROUND CONDITIONS



WORN GUN TUBE TRENDS

T = Condition of worn gun tube



Interface Slipping

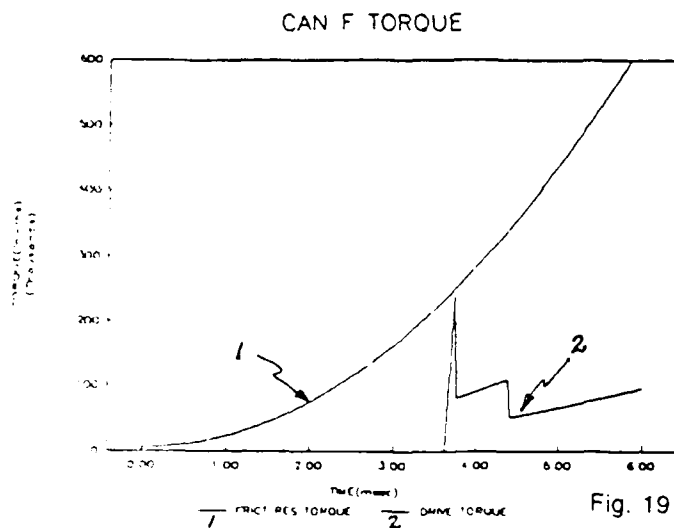
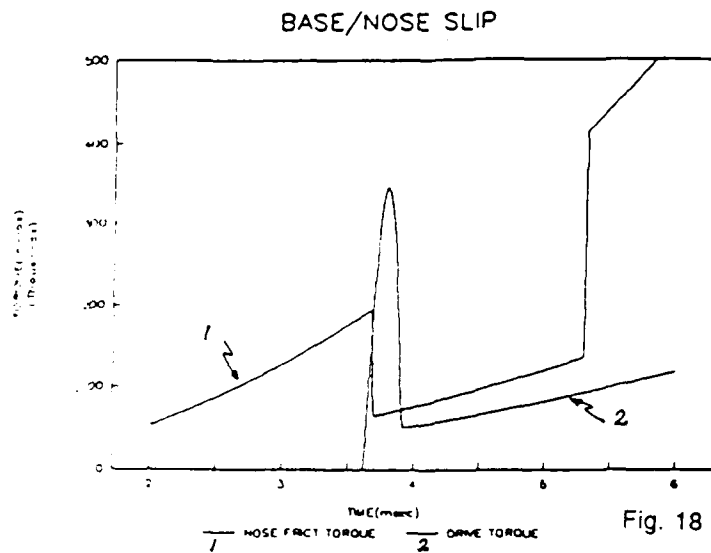
The λ_1 value determines if a friction interface will slip. If it does, a sliding coefficient of friction should be used. From reference 15, at very high relative velocities, (100 inches/sec) the kinetic coefficient of friction for mild steel or medium steel could be 1/3 of the static value. With a new tube and a small δ and Δ , the interface could slip but the relative velocity would be low and the coefficient of friction would be close to the static value.

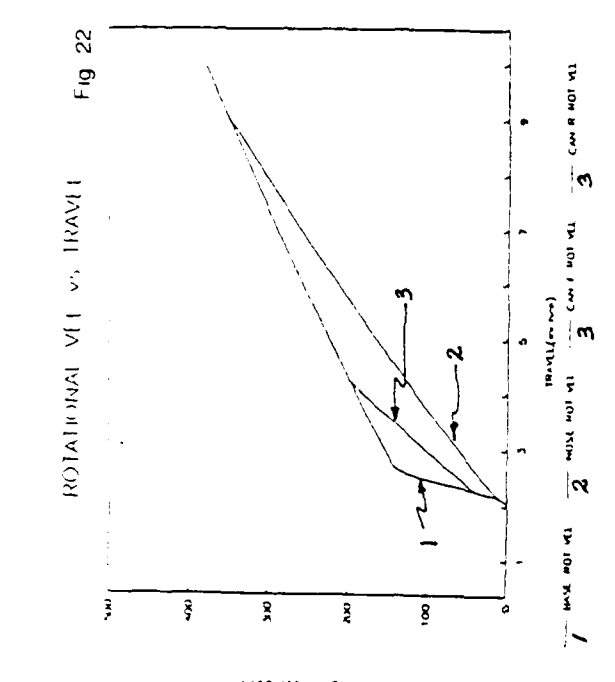
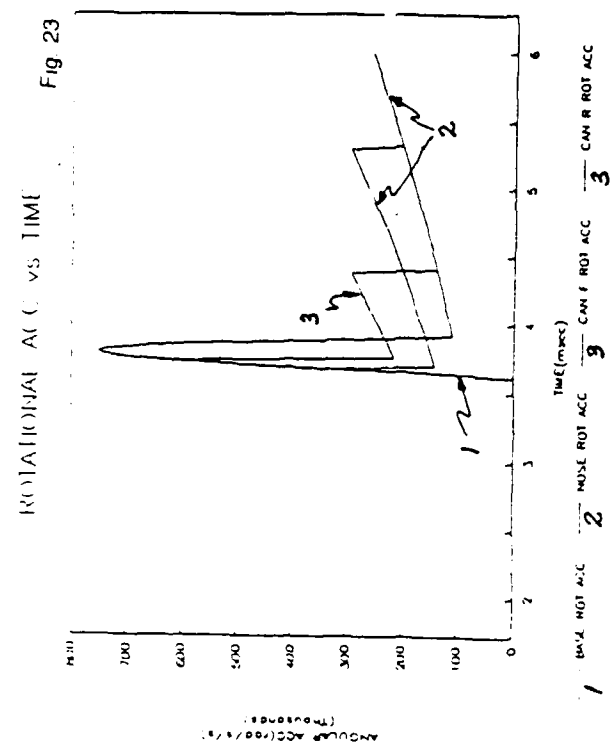
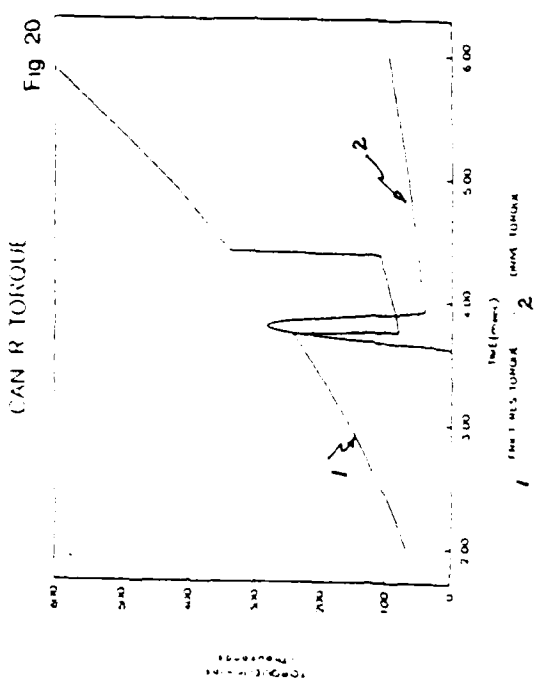
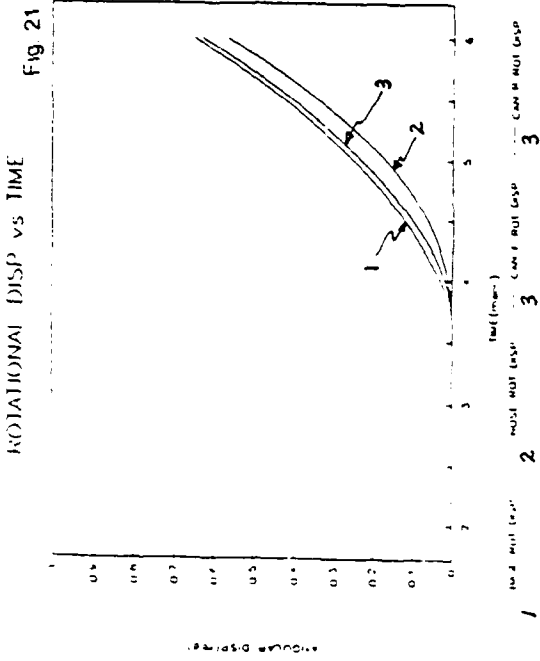
For the experimental and tactical round treated in this report, knurled interfaces were used and a friction coefficient of .54 was determined and used. To assess the results of any slippage, a kinetic coefficient of friction of .54/3 was used as a conservative approach.

For the worn gun tube that was used, the λ_1 value of 2.0 was not great enough to induce slippage.

In order to examine the effects of slippage, a δ of 2.0 inches was used together with a Δ of 2.7 inches. Results are shown in Figures 18 through 23. The nose slips relative to the base 4.76 degrees prior to catching up to the base. It was estimated that a 20 degree slip could be tolerated without stripping the threads of the nose/base joint. Can R slips 2.46 degrees as does Can F on top of Can R. The θ lag is shown in Figure 21 and the θ history in Figure 22. Figure 23 shows how the θ pulse is reduced in value on the canisters as a result of slippage, which in turn reduces the rotational spike effects on any components within the canisters.

In the analytical analysis, the inertial effects of any slipping component is replaced by its frictional resistive torque.





Design Considerations

This analysis coupled with the results of other studies, suggests the following good design practices:

1. To prevent any adverse effects of slippage, the static friction of any interface should be $\geq \alpha \frac{K_I}{M_r}$ where a suggested value of α should be 3.5 or greater.
2. For structural integrity considerations, a $\ddot{\theta}$ value of 1.5 times $\ddot{\theta}_{\text{max}}$ at \ddot{x} should be sufficient. ($\lambda_2 = 1.5$)
3. Any pinned or keyed joint should treat the friction capabilities of the joint to preclude over design (e.g. too many pins, etc.).
4. λ_1 values are likely to be < 2.5 and ≈ 2.0
5. The weakest link should be an element that would not result in catastrophic failure. It's better to have a canister slip as compared to its high explosive filler.
6. The computer model and design approach presented in this report coupled with the experimental results of ref. 12 offer an approach to evaluating the behavior of projectiles in various worn gun tube environments and can be used to assess the effects of new propellant charges relative to projectile/worn gun tubes performance.

References

Reference List of Reports and Papers on the Effects of Free Run and/or Worn Gun Tube Environments on the Axial and Rotational Dynamics of a Projectile Propelled from a Gun Tube.

1. W. R. Benson, "Comments on the Effect of Free Run on the Integrity of Projectile Joints and Projectile Subsystem Response", Internal Report, ASD, LCWSL, US Army ARRADCOM, February 1977.
2. Author Unknown, "Root Cause Analysis of Safety Certification Test Failures on the 8 inch, XM650E5 RAP Projectile", Picatinny, May 1977.
3. G. A. Benedetti, "Estimates for a Minimum Coefficients of Static Friction Required at the Rocket Motor - Bulkhead Interface Joint for the W79", Note to D. J. Bohrer (Sandia), 12 May 1977.
4. G. E. Bubb, "Experimental Investigation of Free Run on 8 Inch Projectiles" 25-28 April 78 Meeting of DEA-G-1060, NSWC, Dahlgren, VA.
5. A. E. Schmidlin, "Computer Simulation of Projectile Motion in a Gun Tube with Free Run" 4th International Symposium on Ballistics, Monterey, California, 17-19 October 1978.
6. M. Kornhauser, "Preliminary Analysis of the Effects of Rotating Band Engraving and Free Run on Angular Accelerations and Bond Pressures" Report for Picatinny Arsenal, 15 May 1979.

7. G. A. Benedetti, "Measurements of Torsional Impulse and Projectile Balloting for Artillery Fired Projectiles Using In-Bore Telemetry", Presented to NATO NAAG Panel IV, Surface-to-Surface Artillery, April 21-25, 1980.
8. A. E. Schmidlin, "Torsional Impulse in Gun Launched Projectiles", Technical Report ARLCD-TP-80037, Dover, NJ, March 1981.
9. G. A. Benedetti, "Measurement of Torsional Impulse and Projectile Balloting for Artillery Fired Projectiles Using In-Bore Telemetry", Presented to 3rd U.S. Army Symposium on Gun Dynamics, May 11-14, 1982.
10. G. A. Benedetti, "Measurement of Torsional Impulse for Artillery Fired 155mm Projectiles Using In-Bore Telemetry", Presented to the 3rd Quadrilateral Ballistics Working Group, Fort Halstead, Kent, United Kingdom, April 22-23, 1982.
11. D. E. Wayne, "NATO FH70 Cannon Tube Wear Versus Torsional Impulse Study for Artillery Fired 155mm Projectiles", Sandia National Laboratories, September 1, 1982.
12. Lapetina, Miller and Chung, "Torsional Impulse Study for Artillery Fired 155mm Projectiles", SNLL, HDL, ARDEC, Undated (1982 or later).
13. G. A. Benedetti, "Dynamic Response of a Beam Subjected to Gun Launch Accelerations", Sandia National Laboratories, SAND 83-8206, April 1983.
14. SMI Report "Torsional Impulse Measurements on a 155mm Test Round", August 1989.
15. Marks Mechanical Engineering Handbook (8th Edition).

TITLE: Comparison of Computed and Measured Jump of 120mm Cannon
E. M. Schmidt*, D. S. Savick, D. H. Lyon, and P. Plostins
U. S. Army Laboratory Command
Ballistic Research Laboratory
Aberdeen Proving Ground, MD 21005-5066

ABSTRACT: The output from codes describing various stages of the launch of a fin-stabilized sabot projectile are compared with experimental data. The predictions are coupled and used to predict the fall of shot on target. Based upon the contrasts between data and theory, areas requiring further examination are suggested.

BIOGRAPHY:

PRESENT ASSIGNMENT: Chief, Fluid Physics Branch, Launch and Flight Division, Ballistic Research Laboratory

DEGREES HELD: B.S., M.S. and Ph.D., Polytechnic Institute of Brooklyn

COMPARISON OF COMPUTED AND MEASURED JUMP OF 120MM CANNON

E. M. Schmidt, D. S. Savick, D. H. Lyon, and P. Plostins
U. S. Army Laboratory Command
Ballistic Research Laboratory
Aberdeen Proving Ground, MD 21005-5066

1. INTRODUCTION

One of the ultimate goals of launch dynamic modeling is to predict the impact of a round on target. Once this is achieved, the sensitivity of impact to variations in initial conditions can be studied for the purpose of analyzing bias and dispersion. The launch process is complex, consisting of a sequence of coupled mechanical and gas dynamic interactions leading up to free flight of the projectile. Considerable effort has been expended to develop computer codes which describe a particular portion of launch; however, these models have not been coupled so that a direct comparison can be made of their ability to actually predict the total perturbation to the projectile trajectory. This paper will examine available models and present results of a preliminary attempt to use them in predicting actual holes on targets.

Upon propellant ignition, both the projectile and gun tube begin to accelerate. The tube is not perfectly straight. It has curvature associated with manufacturing, gravity, and firing dynamics. It is distorting under the moving pressure pulse and in response to the projectile, the mounting system, and its own geometric asymmetries. The projectile moves at high velocity along this distorted path and is subject to a gross lateral, balloting motion upon which is superimposed flexural or vibrational modes. At the muzzle, the projectile disengages from the moving tube in stages, as first the front bell of the sabot passes out of the tube followed by the rear bulkhead. Subsequently, the round passes through the reverse flow region of the muzzle blast, during which the sabot discard commences. Both mechanical and aerodynamic interactions occur between the sabot components and the projectile as the restraining bands fail and the sabots begin to first rotate off and then lift away from the flight body. Once clear of the blast and sabot discard regions, the projectile enters free flight where its motion is reasonably well understood.

The launch dynamics have been estimated using codes available at the Ballistic Research Laboratory (BRL). The gun and projectile in-bore dynamics are computed using both the RASCAL [1] and SHOGUN [2,3] codes. Muzzle blast loadings are approximated analytically [4]. Sabot discard dynamics are calculated using the AVCO Sabot Discard model [5]. Finally, the free flight trajectory deflection is analytically determined [6]. Each model is coupled to its logical predecessor which supplies initial conditions.

Data taken in firings of a set of 120mm cannon provide an experimental basis for comparison. Three different cannon, Tubes Number 84, 85, and 104, have been shown to produce distinct bias in the fall of shot (Fig. 1). The plot shows the centers of impact of a number of M866 rounds fired from these cannon. Even when mounted on different tanks, this clear, tube dependent signature was reproduced. It should be mentioned that the tubes were preproduction prototypes and are not representative of currently fielded systems. However, these tubes were deliberately selected since their strong bias provides a clear discriminator against which the prediction of launch dynamics models may be tested. In addition, the static characteristics and dynamic responses of the cannon and projectile have been measured in detail. These will form the initial conditions and basis for comparison with theory.

2. EXPERIMENTAL DATA

The round tested was the M866, a fin-stabilized, sabot (3 segment) training projectile launched at a velocity of 1680m/s from the 120mm, M256 cannon. Data were taken on three different cannon, Tubes Number 84, 85, and 104. The cannon were tank mounted.

The experimental arrangement is shown in Figure 2. The cannon is instrumented with linear variable displacement transducers (LVDT), eddy probes and strain gages to measure the x,y,z displacement of the tube during the firing event [7,8]. When the projectile exits the tube, its motion is observed at two separate locations along the trajectory using orthogonal flash radiographs [9]. The x-ray images contain fiducials which have been surveyed along the initial cannon line of fire prior to the shot. The first set of three stations obtains orthogonal radiographs at 0, 1.8 and 3.6m from the muzzle. The projectile c.g. position and angle of attack are measured at each station and used to define the projectile linear and angular velocity at the midpoint, i.e., 1.8m. At this point, the projectile is just emerging from the muzzle blast and still has the sabot components in mechanical contact. The second set of three stations are located at 8.5, 10.3, and 12.1m from the muzzle. These define the projectile dynamics at the 10.3m station where the sabots have completely discarded and the round is in unconstrained free flight. The projectile then enters the BRL Transonic Range where its motion is measured over 250m of the trajectory. Finally, it impacts upon a target at 985m.

The instrumentation is surveyed, prior to each shot, into a coordinate system which is based upon the line of fire. This permits each set of data to be related to the next and the launch process can be reconstructed out of its component parts, Fig. 3. The plot shows the target plane with the actual measured impact given by the closed symbol. The vector construction of open symbols represents the extrapolation of the measured launch dynamics into the target plane. As can be seen from the comparison of the open and closed circles, the extrapolation is fairly accurate. The first vector, gives the difference between the static gun pointing angle (0,0) and the dynamic

pointing angle at shot exit (triangular symbol). The gun crossing velocity is divided by the projectile launch velocity and added to the pointing angle (inverted triangle). If the projectile moved perfectly with the tube, suffered no subsequent loads, and did not yaw, it would be expected to follow a trajectory characterized by this departure angle. The data show this is not the case.

The diamond symbol gives the lateral c.g. velocity measured at the 1.8m x-ray station divided by the launch velocity. The dashed line is the vector difference between this point and the gun dynamic components. It is taken to represent the mechanical disengagement impulse seen by the projectile. This includes in-bore rigid body and vibrational loads, the separation effect, muzzle blast, and the initial stages of sabot discard. Obviously, this data point includes some interesting dynamics. It would be valuable if improved experimental techniques could be developed to give better resolution of these processes. Some progress [10] is being made to obtain such data, but much remains to be done.

The square symbol gives the lateral c.g. velocity measured at the 10.3m x-ray station divided by the launch velocity. The dashed line is the vector difference between this point and the 1.8m x-ray. It represents the sabot discard impulse imparted to the projectile over the interval. The angular motion of the projectile is also important since it leads to a trajectory deflection, termed aerodynamic jump [6]. Using the angular velocity measured at the 10.3m station, the aerodynamic jump is vectorially added to the linear velocity providing closure with the predicted or extrapolated point of impact. The accuracy of this process is typically 0.2mrad. The data presented in Figure 3 is important since it forms the basis for comparison between theory and experiment in the subsequent sections.

3. THEORY

A. GUN AND PROJECTILE DYNAMICS: Two different models were selected for comparison, RASCAL [1] and SHOGUN [2]. Both have been documented and were made available to the current authors for use.

(1) RASCAL: "Little Rascal" is a two-dimensional finite element model which employs a direct transient analysis approach. The code was developed by Kregel and Erling of the Ballistic Research Laboratory (BRL). Both the barrel and projectile are modeled utilizing a series of equally spaced cylindrical elements, nodes of which are assigned equivalent mass and spring stiffness values. Inertial forces as well as barrel flexure forces can then be calculated using this simplified description. Flexure at each node is approximated by a second order difference method. This also allows bending forces to be computed. Nodal accelerations caused by these forces are integrated once with respect to time to obtain nodal velocities, and again to yield displacements. Forces, in addition to those produced by flexure of the barrel, are present from pressure effects, mounting characteristics and

projectile/barrel interactions. All forces are then integrated by a predictor-corrector technique stabilized by a numerically stiff ordinary differential equation solver.

Both the barrel and projectile models can contain up to 40 elements each. The breech is also simulated by cylindrical elements and included in the barrel model; however, an offset mass calculation is performed to account for the breech center-of-gravity location. The trunnion and elevation stations are modeled using estimated linear spring supports with clearances. No counterrecoil force due to either the recoil spring or the recoil piston are included in the present model. The projectile model is supported, as it proceeds down the dynamic barrel centerline, by two linear springs, one which represents the sabot forward bell and the other the rear bulkhead. Lastly, the code does not permit clearances between the forward bell and gun tube.

The "Little Rascal" program has been shown to provide barrel motion that agrees fairly well with experimental results for various gun systems. In addition, it gives the user overall ease of modeling and well explained input files, while maintaining a relatively fast computation time (6 minutes on a PC). However, the normal mode shapes and natural frequencies can not be extracted and the analysis only considers one plane at a time, meaning that no out-of-plane coupling is treated. If this coupling is judged important, a more complete modeling approach must be undertaken. This approach would include the out-of-plane coupling effects due to the breech center-of-gravity location, gun tube/recoil mechanism interface and projectile motion induced by gun tube curvature.

(2) SHOGUN: In order to address these effects, a 6 degree-of-freedom model, called Dynacode-G/P [3], was developed by Soifer and Becker of S³D Dynamics under contract to BRL. Since the structure of the code made changes in tube and projectile difficult, Hopkins [2] developed the Shogun code based upon the approach of Dynacode-G/P. Shogun was written in a modular fashion to allow easy changes among gun system components.

Shogun models the components as axisymmetric, linear-tapered, Bernoulli-Euler beams. The method incorporates a consistent mass finite element approach along with normal mode summation. The nodal masses can be visualized as being connected through springs with stiffnesses determined by the finite elements. This allows the resulting equations to be written in the form

$$M\ddot{x} + Kx = F(x,t) \quad (1)$$

By setting $F(x,t)=0$ these equations can be solved for the normal modes of vibration which include the rigid body modes, yielding eigenvalues and eigenvectors which, in turn, can be used to transform equation (1) into a set of uncoupled second order differential equations. Interface characteristics

are required in order to characterize the forces between the gun system components. The resulting equations are solved utilizing a variable time-step, 4th order Runge-Kutta solver.

The program is coded in Fortran and is currently running on both a Cray-XMP and Apollo workstations. A typical Cray run requires 30 seconds. Presently the code has only tabular output, although a graphical post-processor is under development. A user definable clearance between the sabot bell and gun tube is used to simulate balloting.

B. MUZZLE BLAST: Using the approach of Schmidt, Fansler, and Shear [4], the influence of muzzle blast upon the projectile linear and angular velocities was shown to be negligible for this case.

C. SABOT DISCARD MODEL: Under contract to BRL, the AVCO Systems Division developed a code [5] to predict sabot discard aerodynamics. The code is semi-empirical in nature using data collected in wind tunnel tests [11] to provide insight into the nature of the flow over the sabot components and projectile. It was the initial intent of the work to simply treat the process of symmetric sabot discard; however, it was extended to the case of asymmetric discard which is of interest in the present study.

The code calculates the forces and moments acting on the projectile and sabot components. If the initial dynamics of these bodies is not symmetric, there will be a disturbance to the flight path of the penetrator. Two types of interactions are considered. One is the contact, or mechanical, interaction that occurs as the sabot pivots off the projectile. The other is the aerodynamic interaction due to the sabot shock waves impinging on the projectile.

The code requires input descriptions of the projectile inertial and aerodynamic characteristics, the sabot geometry and inertial properties, the location of the sabot relative to the projectile, and the initial dynamic state of the sabot and projectile. This last set of data is taken from the output of the Rascal and Shogun codes. Since these codes do not treat the sabot segments independently, the assemblage was given the linear and angular velocities directly from the in-bore models. No attempt was made to describe the effect of elastic decompression of the sabot segments following release from the tube. This could change the initial dynamics of both the sabot components and the projectile.

The code is written in Fortran and is compatible with most operating systems. Input data are read from a file containing the required parameters and projectile characteristics. The results are output to a master file and a number of subfiles containing specific parts of the sabot trajectory data. These subfiles are formatted in a manner that is convenient for plotting packages.

D. FREE FLIGHT DYNAMICS: The Sabot Discard Code provides values of the projectile linear and angular velocity at 10.3m from the muzzle. The linear velocity gives a direct trajectory deflection relative to the initial firing line, while the angular velocity is used to compute the aerodynamic jump using the standard relationship [6]:

$$\theta = [I_y/mD^2][C_{l\alpha}/C_{m\alpha}]\alpha' \quad (2)$$

4. COMPARISON BETWEEN EXPERIMENT AND THEORY

A. GUN DYNAMICS: Both Rascal and Shogun were configured for the 120mm, M256 system firing the M866 projectile through gun tubes SN 84, 85 and 104 (except for Shogun which had no tube 84 file). The physical properties of the code projectile models along with actual measured values are listed in Table (1). Rascal values, calculated using the maximum of 40 elements, result in lower launch and flight masses when compared to measured values. On the other hand, the Shogun projectile model computes values within several percent of the measured.

Table 1. Comparison of Physical Properties

	Measured	Rascal	Shogun
Projectile Mass (kg)	2.73	2.09	2.73
Proj + Sabot Mass (kg)	5.45	4.65	5.43
c.g. (m from base)	.0213	.0220	.0223

There are large differences between the two codes regarding values used for spring constants on the sabot front bell and rear saddle, Table 2. It is not known how the Shogun constants were obtained, however, the Rascal numbers resulted from a combination of static experiments and finite element calculations. Therefore, more confidence lies in these values.

Table 2. Sabot Spring Constants

	Rascal	Shogun
Front Bell (lb/in)	5.7E+4	2.0E+7
Rear Bulkhead (lb/in)	4.3E+5	1.6E+8

The two codes do a reasonable job of predicting the tube dynamics, Fig. 4-6. The plots show the dynamic deflection of the tube centerline at the time of shot exit. The muzzle is located at the zero station. The experimental data extend back along the tube until it enters the mantlet of the tank. In the vertical plane, the magnitude and shape of the deflection are captured.

There are some differences near the mantlet location which may reflect more a problem in the data than in the codes. The horizontal deflections reveal some interesting differences between the tubes. Tube 84 points to the right at the time of shot exit while Tube 85 points to the left (+ is right, - is left). Tube 104 has very little slope. It is very encouraging that the Rascal code picks up these differences. Essentially the only input changed from tube to tube is the centerline profiles. The Rascal predicted response to this change is in excellent agreement with experiment. Unfortunately, Shogun computations have not yet been made for Tube 84 so this comparison can not be made.

At the instance of shot exit, the gun pointing angle and crossing velocity are of interest since they represent the possible dynamic state of an ideal projectile, Fig. 7 and 8. Again the comparisons are relatively good. Rascal predictions are indicated by the nomenclature R84, R85, and R104, giving the code and tube number. Similarly, Shogun calculations are represented by S85, and S104. Rascal predicts the correct variation between the tubes and does an excellent job in depicting Tube 85. With respect to the gun crossing velocity (divided by the projectile launch velocity), the magnitude of this parameter is quite a bit smaller than the pointing angle, Fig. 8. The codes correctly predict the magnitudes of the angles, but do not agree between themselves or with the data as to the orientation.

B. PROJECTILE DYNAMICS: Both the linear and angular velocity are of interest, Fig. 9 and 10. The figures show the measured and computed projectile dynamic state at a distance of 1.8m from the muzzle. Since the muzzle blast effect is negligible and the computed sabot discard perturbation is small at this location, the theoretical results are essentially the muzzle states predicted by the two codes. As can be observed, the comparison between calculation and experiment is not as good as for gun dynamics. With the projectile linear velocities, the codes predict roughly the correct magnitudes, but the orientations are somewhat off. However, a tendency to cluster toward the second quadrant is reproduced.

For the angular rates, Rascal overpredicts the magnitudes and absolute orientations. Rascal does produce a relative orientation that is similar to measured data. The Shogun prediction of angular rate is reasonable for Tube 104, but is incorrect for Tube 85. The orientation is opposite to that observed and the magnitude (47.0rad/s) is greater than measurement by a factor of four. It is probable that this difference is due to the relative sabot stiffnesses between the two codes (Table 2). It is apparent that improved estimations are required of the structural characteristics. In addition, a more complete description of the separation process to include elastic decompression of the components would be worthwhile.

C. SABOT DISCARD: The computed total asymmetric pitching moment on the projectile generated as a result of initial angular rates typical of the Rascal outputs are plotted in Figure 11. Four cases are plotted for initial angular rates of +/- 2rad/s and +/- 17rad/s. The former correspond to launch

from Tube 104, while the latter are representative of Tube 85. The sign convention refers to the relationship between the angular velocity and the sabot interface orientations. Positive sign means that the projectile is yawing such that the nose is moving upward toward the centerplane of the top sabot component (the M866 has three components). Negative sign means that the projectile is yawing such that the nose is moving downward toward the interface or crack between the two bottom components. Since the up or down directions are really arbitrary, this result indicates that there is a different sensitivity to the sabot discard impulse depending upon the orientation of the interfaces between components. For the 17rad/s case, this translates into a difference of 0.5mrad depending upon whether the projectile is yawing into a sabot segment or into a crack between them. It should be possible to design a test to demonstrate the existence of this variable response.

The change in linear velocity due to the sabot discard impulse is plotted in Figure 12. Only the Rascal code was considered due to the large differences between measured and computed angular rates with Shogun. The data are widely scattered and it is difficult to pick out a central tendency. The predicted magnitudes are in rough agreement with measurement.

The total angular velocity is presented in Figure 13. The predictions continue to overestimate the measured values. The relative orientation between Tube 84 and 85 is reproduced; although, the absolute orientation is not captured.

D. TARGET IMPACTS: The computed dynamics can be summed to produce an estimate of the trajectory deflection angles. These are plotted against the measured impacts in Figure 14. The predicted values are not in good agreement with the experiment; however, this was not totally unexpected. This study was intended to be a first attempt at integrating the available models to estimate the launch disturbance and to identify possible areas for improvement in modeling. The fact that the models do show significant differences between the tubes is encouraging. Again, the Rascal code is the basis for predicting the gun/projectile dynamics. Between tubes, the only difference was in the description of the centerline curvature. The models indicate that this results in a distinction between tubes. The data also reflect this behavior. It is interesting that the diagonal nature of Tube 85, 104, and 84 is reproduced; although, the slope of the predictive diagonal is at right angles to the experiment.

5. SUMMARY AND CONCLUSIONS

A comparison between predicted and measured gun launch perturbations is given. Both component and total perturbations are investigated. It is found that the gun dynamics are reasonably well modeled by the Rascal and Shogun codes. However, the projectile dynamics are not as faithfully reproduced. In particular, projectile angular rate after separation from the tube is not in good agreement with experiment. It is apparent that improved techniques to estimate the in-bore structural characteristics of sabot projectiles is required. In addition, the details of separation from the tube need to be included in models. The experimental data taken in this region are also lacking. Very little data is available describing the in-bore motion of these projectiles and the separation dynamics have not been adequately described.

The sabot discard analysis produced the interesting result of showing an impulse imparted to the projectile that depends upon the relative orientation between the angular velocity and sabot interface (crack) orientation.

When the outputs of the various models were summed to predict target impact, there was good news and bad news. The good news was that there was a clear discrimination between different gun tubes with roughly correct magnitudes. The bad news was that the predictions did not reproduce the same direction as the experiment. This may not be catastrophic if relative sensitivities are of interest.

6. REFERENCES

- [1] T. F. Erline, "Flexible Projectile Modeling using the Little Rascal Gun Dynamics Program", 6th U. S. Army Symposium on Gun Dynamics, Tamiment, PA, 14-17 May 1990.
- [2] D. A. Hopkins, "Modeling Gun Dynamics with Three-Dimensional Beam Elements", 6th U.S. Army Symposium on Gun Dynamics, Tamiment, PA, 14-17 May 1990.
- [3] M. T. Soifer and R. S. Becker, "Dynacode-G/P and Its Application to the 120mm Tank Gun", 5th U. S. Army Symposium on Gun Dynamics, Rensselaerville, NY, 23-25 September 1987.
- [4] E. M. Schmidt and K. S. Fansler, "Trajectory Perturbations of Fin-Stabilized Projectiles due to Muzzle Blast", AIAA Journal of Spacecraft and Rockets, Vol. 14, No. 6, June 1977, pp 339-344.
- [5] D. Siegelman, J. Wang, and P. Crimi, "Computation of Sabot Discard", CR-00450, Ballistic Research Laboratory, APG, MD, February 1983.
- [6] C. H. Murphy, "Free Flight Motion of Symmetric Missiles", R-1216, Ballistic Research Laboratory, APG, MD, July 1963.

- [7] J. A. Bornstein, T. F. Erline, B. T. Haug, D. A. Hopkins, "Investigations on the Dynamics of Tank Guns," Proceedings of the 11th Annual Symposium On Ballistics, Brussels, Belgium, 9-11 May 1989.
- [8] J. K. Biele, "Gun Dynamics Effects on Jump of Smooth-Bore Tank Guns", 8th International Symposium on Ballistics, Orlando, FL, 23-25 October 1984.
- [9] J. A. Bornstein, I. Celmins, P. Plostins, and E. M. Schmidt, "Launch Dynamics of Fin-Stabilized Projectiles", AIAA Atmospheric Flight Mechanics Conference, Boston, MA, August 1989.
- [10] D. A. Rabern, "In-Bore Structural Behavior of 120mm Saboted Long Rods Subjected to Axial and Lateral Accelerations", 11th International Symposium on Ballistics, Brussels, Belgium, 9-11 May 1989.
- [11] E. M. Schmidt, "Wind Tunnel Measurements of Sabot-Discard Aerodynamics", AIAA Journal of Spacecraft and Rockets, Vol. 18, No. 3, May-June 1981, pp 235-240.

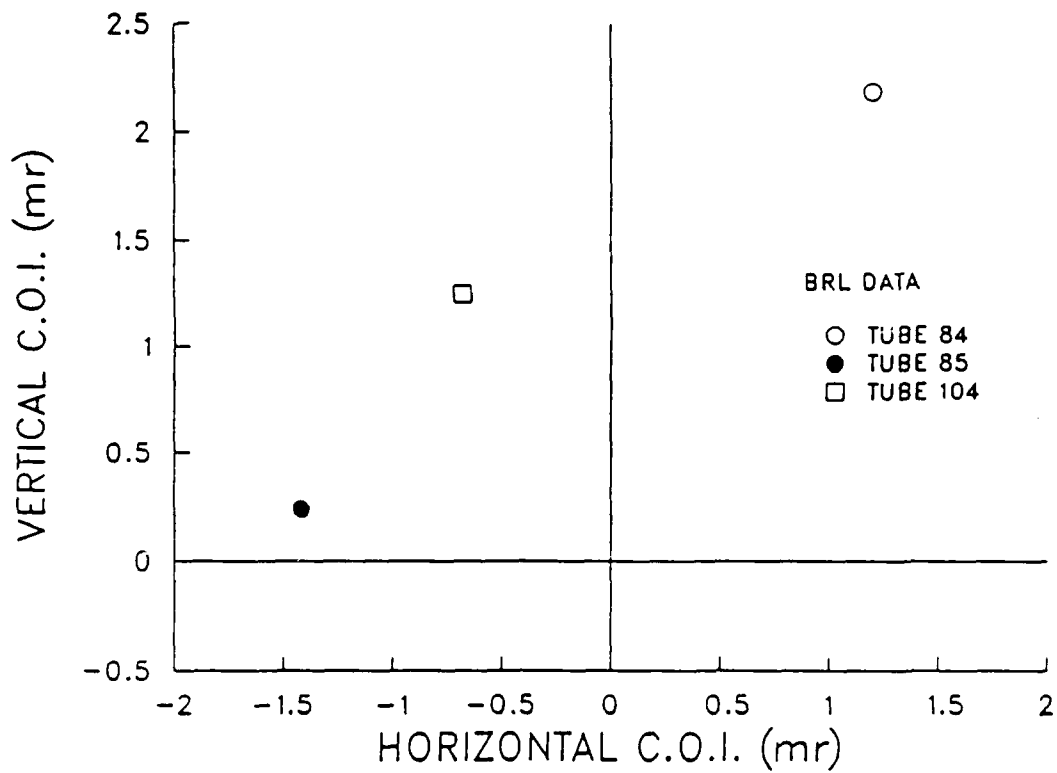


Figure 1. Group Centers of Impact for Three Tubes

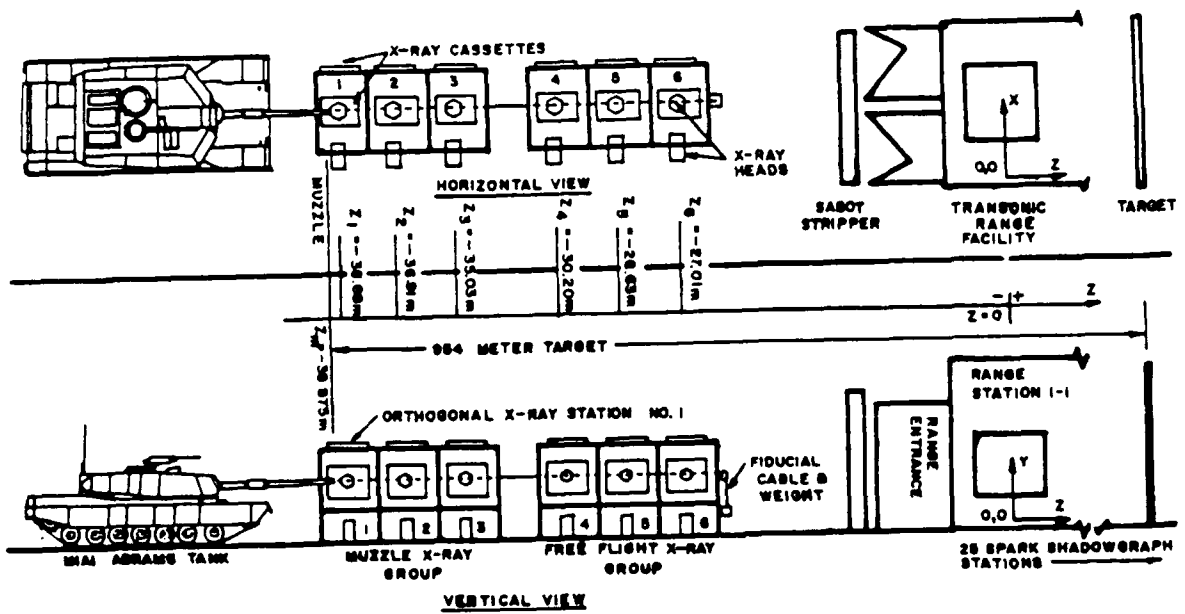


Figure 2. Experimental Arrangement

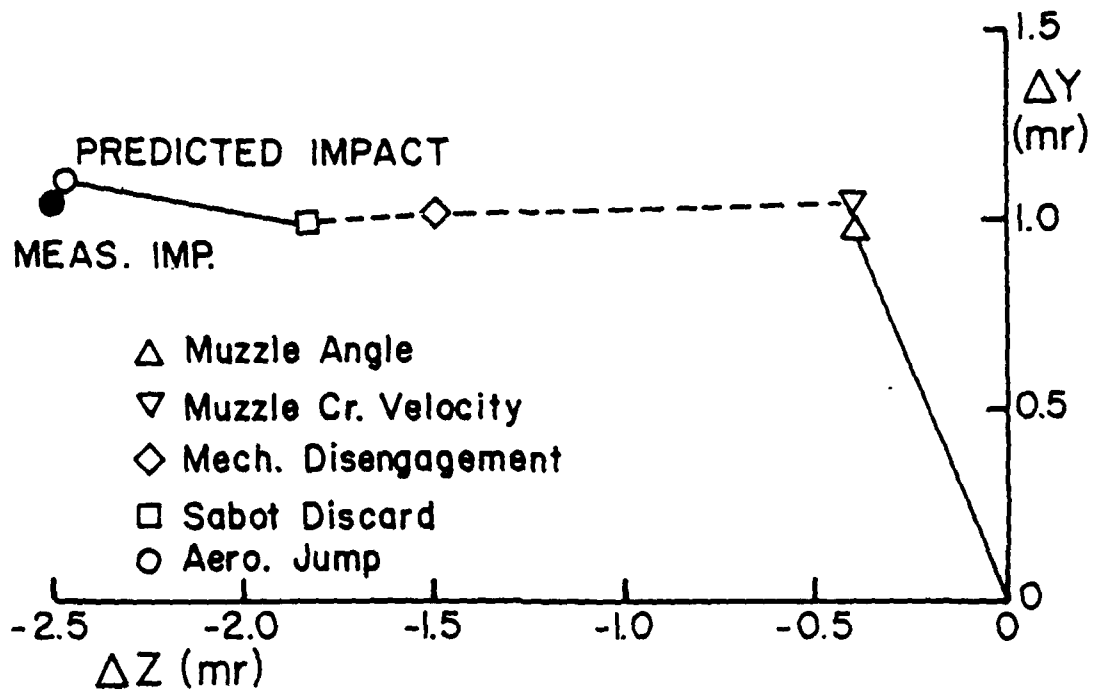


Figure 3. Launch Disturbance Closure Diagram

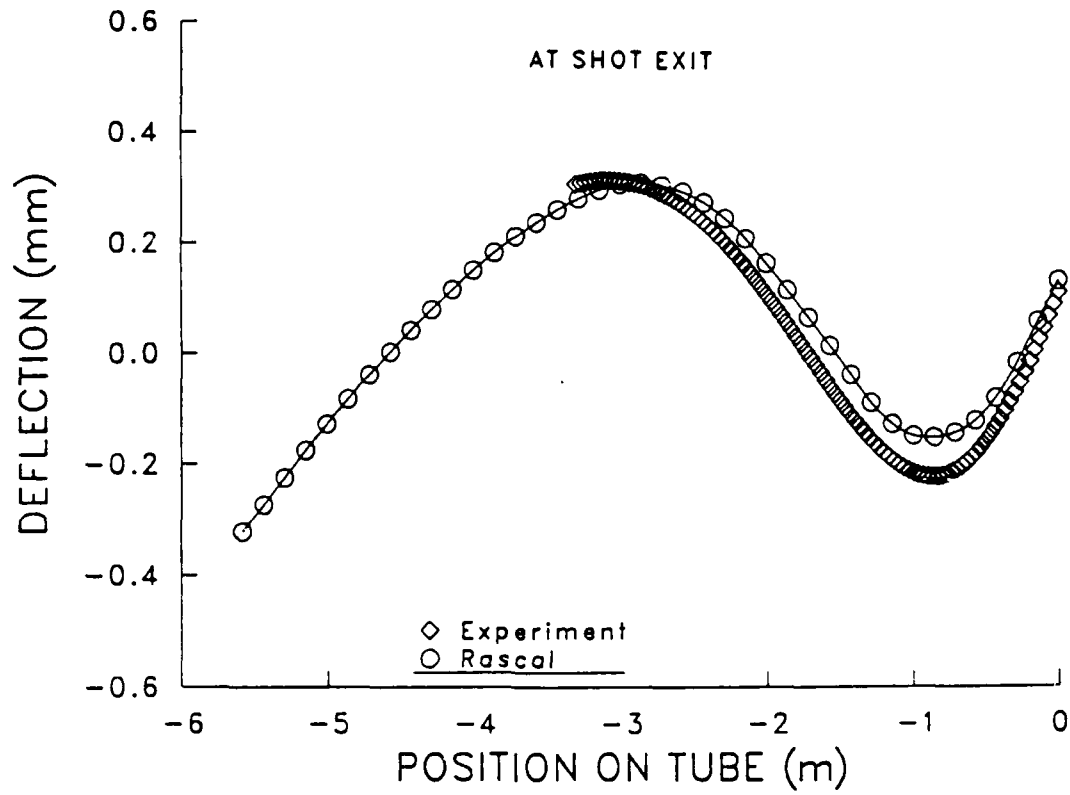


Figure 4a. Vertical Centerline Deflection, Tube 84

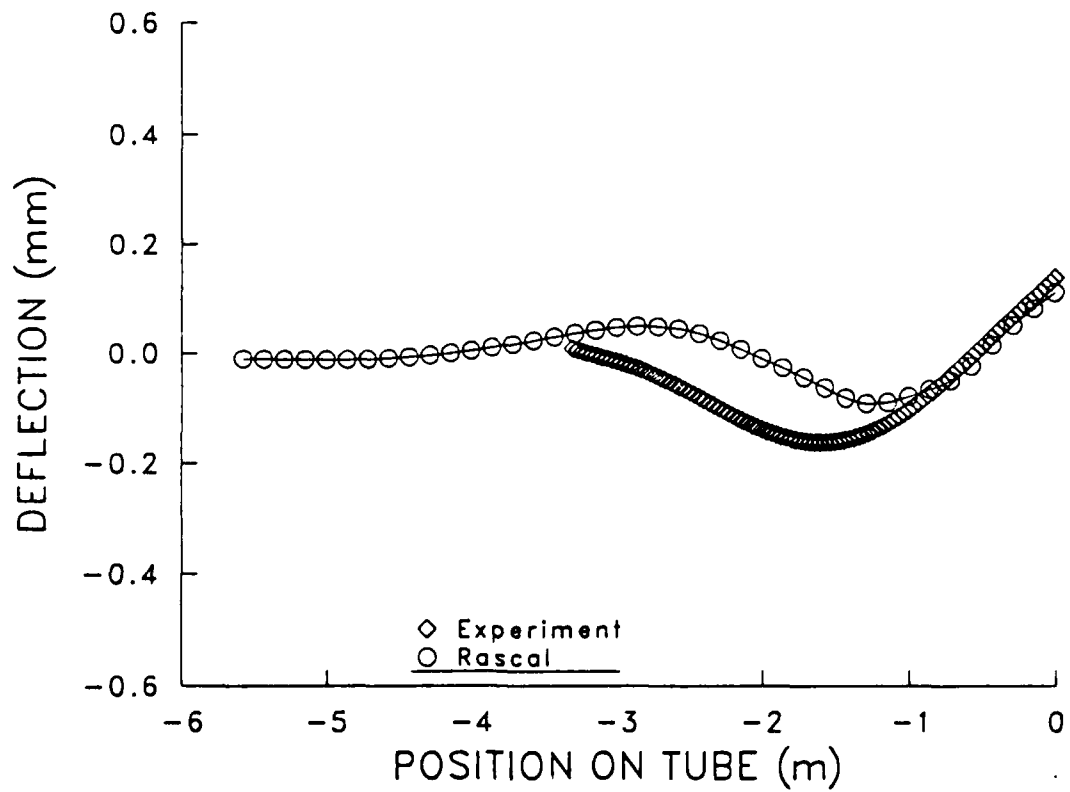


Figure 4b. Horizontal Centerline Deflection, Tube 84

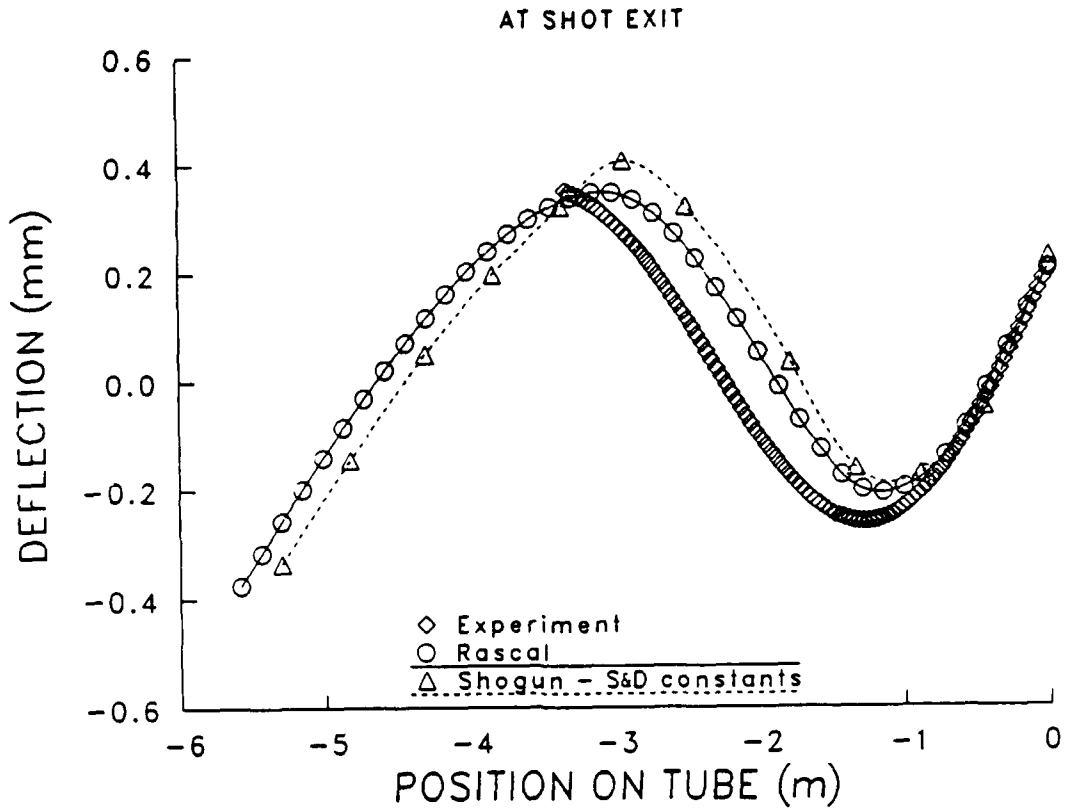


Figure 5a. Vertical Centerline Deflection, Tube 85

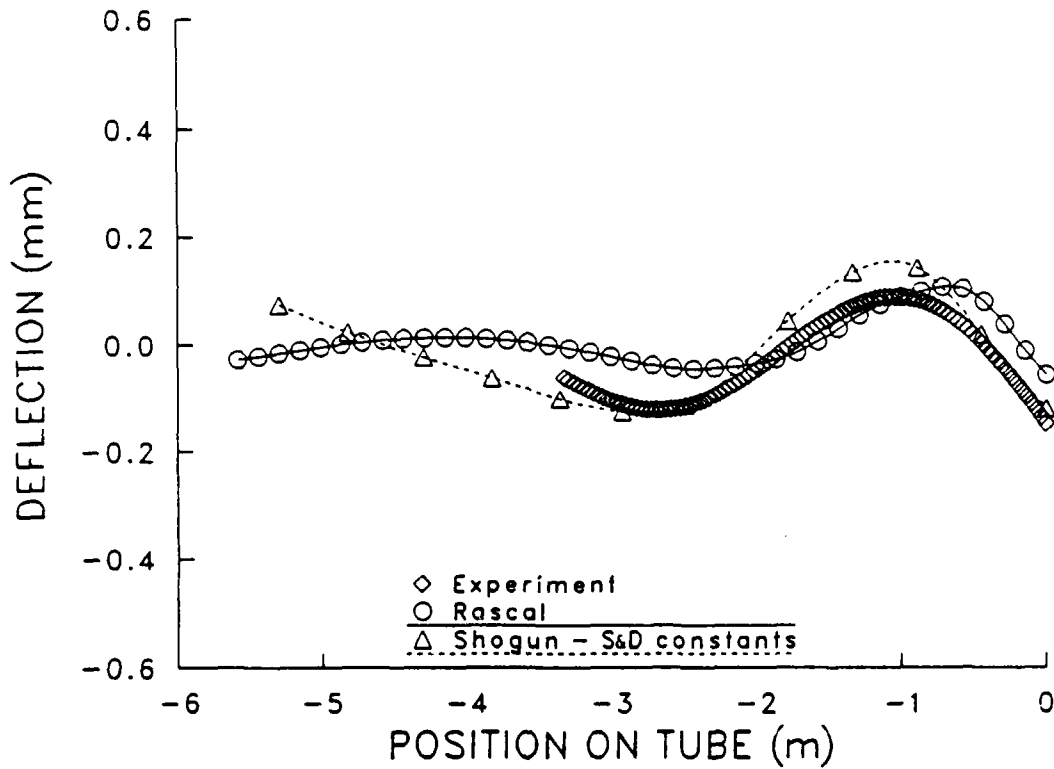


Figure 5b. Horizontal Centerline Deflection, Tube 85

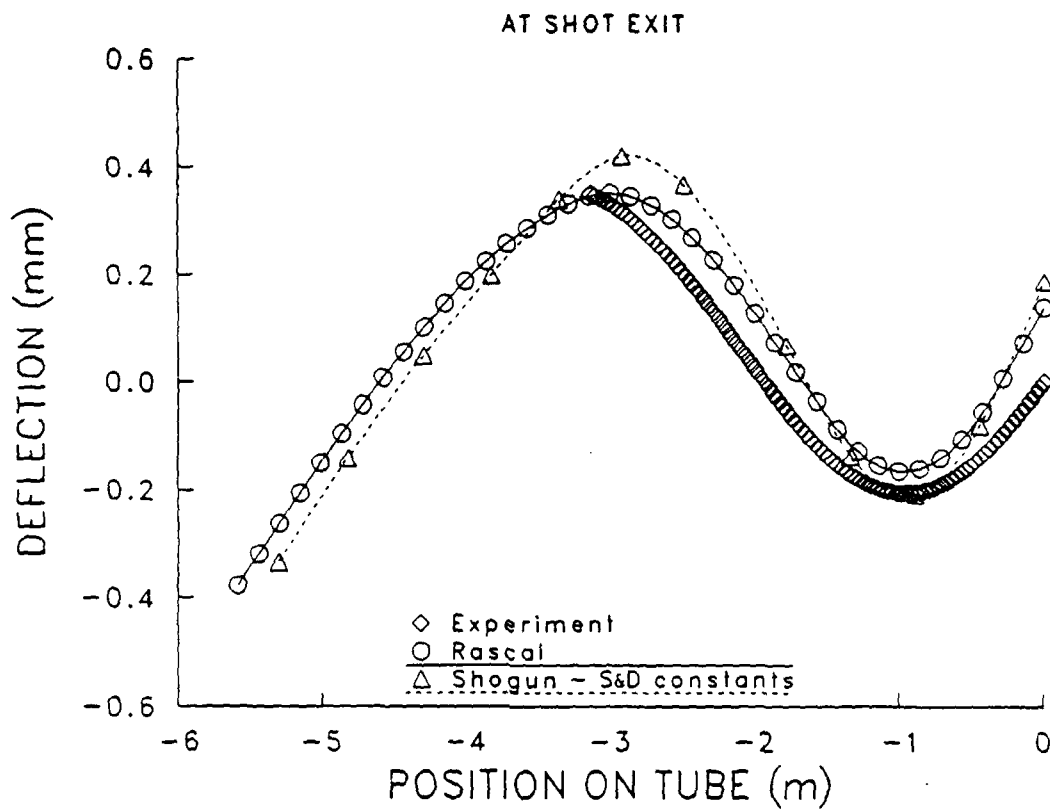


Figure 6a. Vertical Centerline Deflection, Tube 104

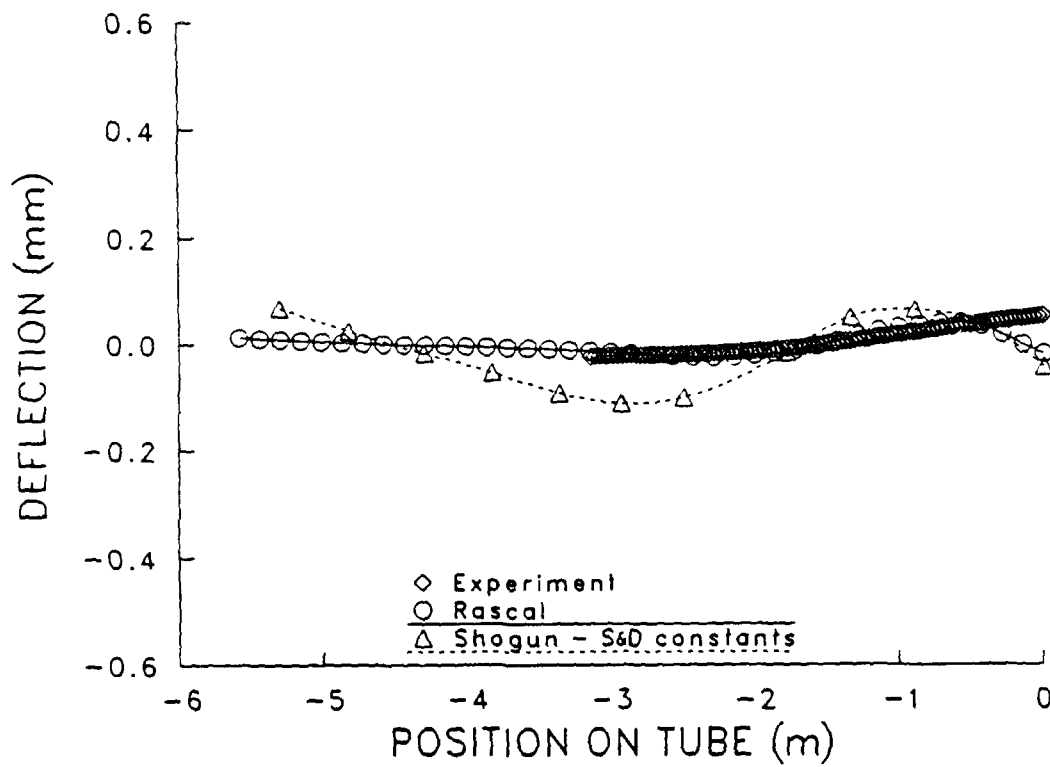


Figure 6b. Horizontal Centerline Deflection, Tube 104

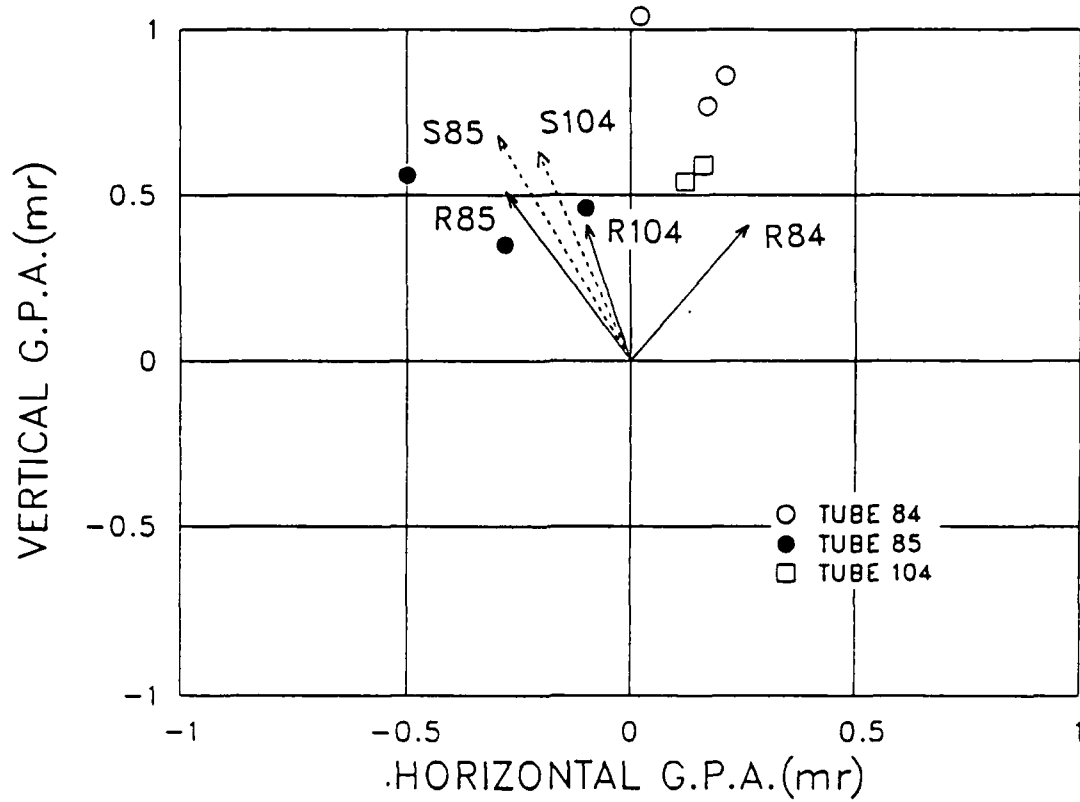


Figure 7. Muzzle Pointing Angle at Shot Exit

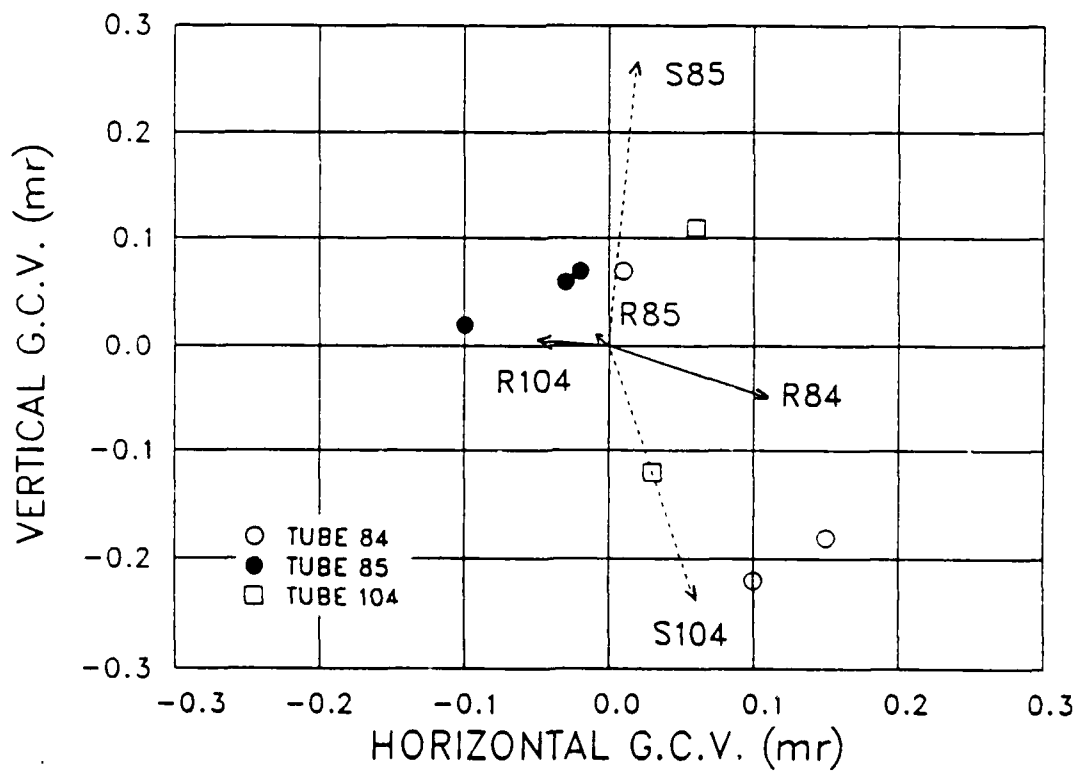


Figure 8. Muzzle Crossing Velocity at Shot Exit

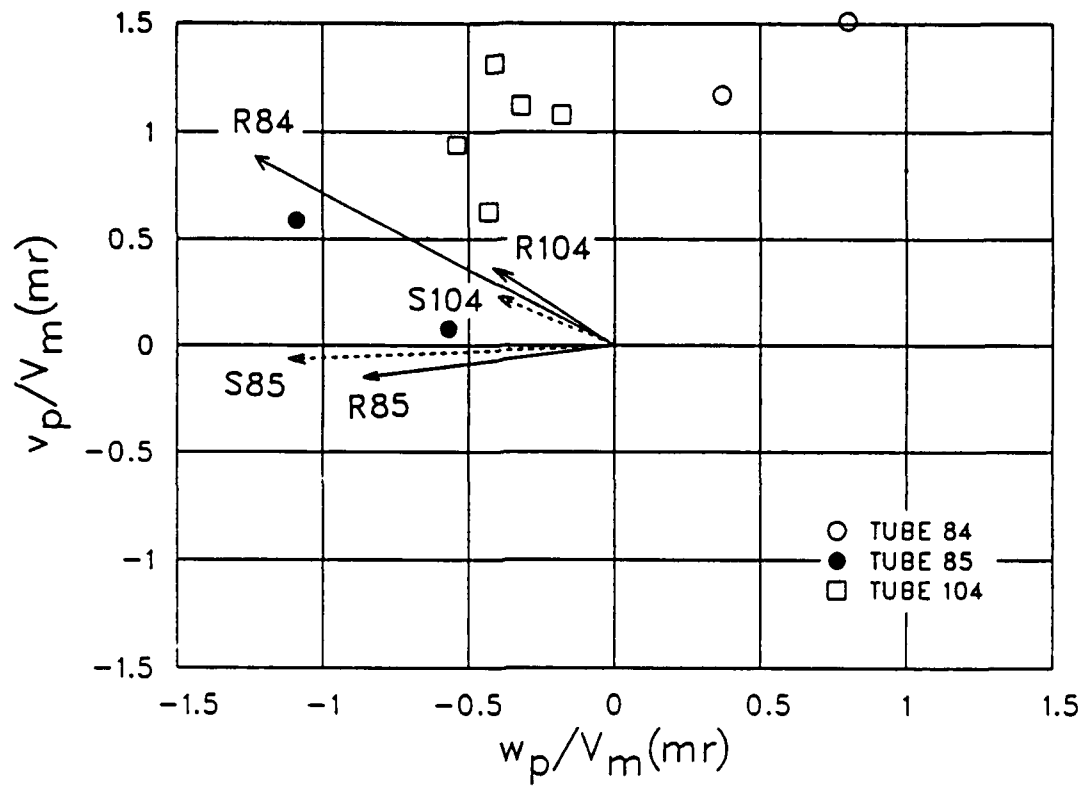


Figure 9. Projectile c.g. Velocity 1.8m outside Muzzle

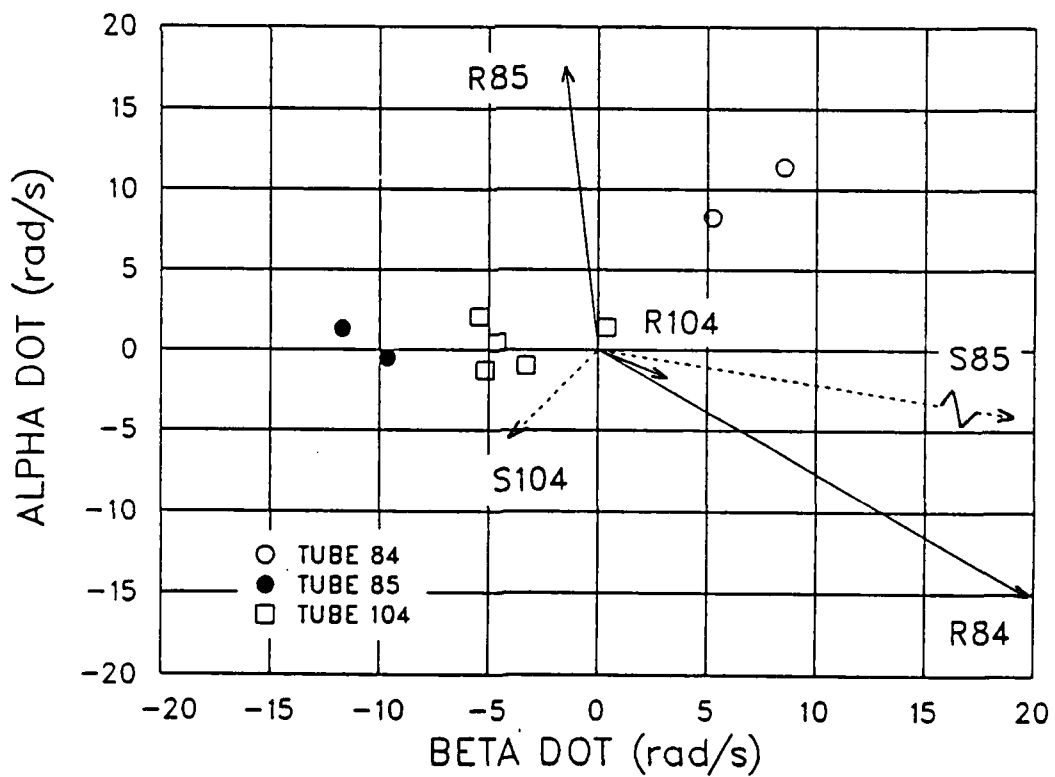


Figure 10. Projectile Angular Velocity 1.8m outside Muzzle

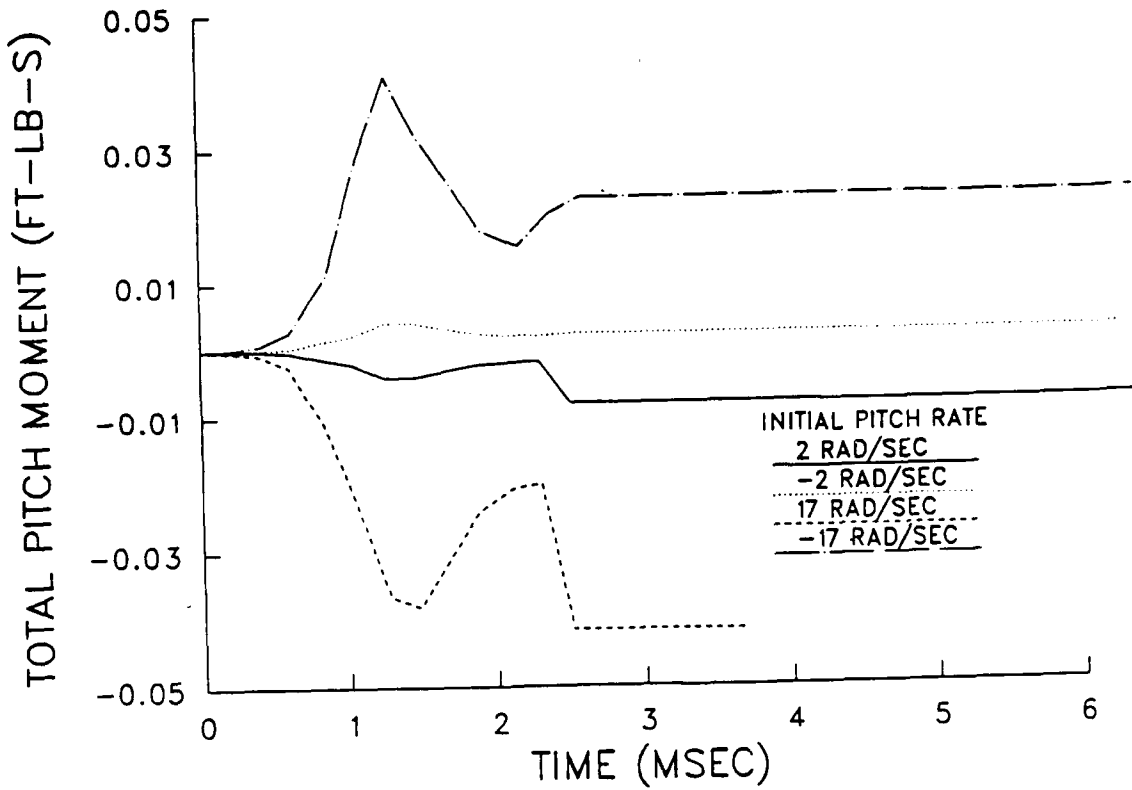


Figure 11. Total Asymmetric Sabot Discard Angular Impulse

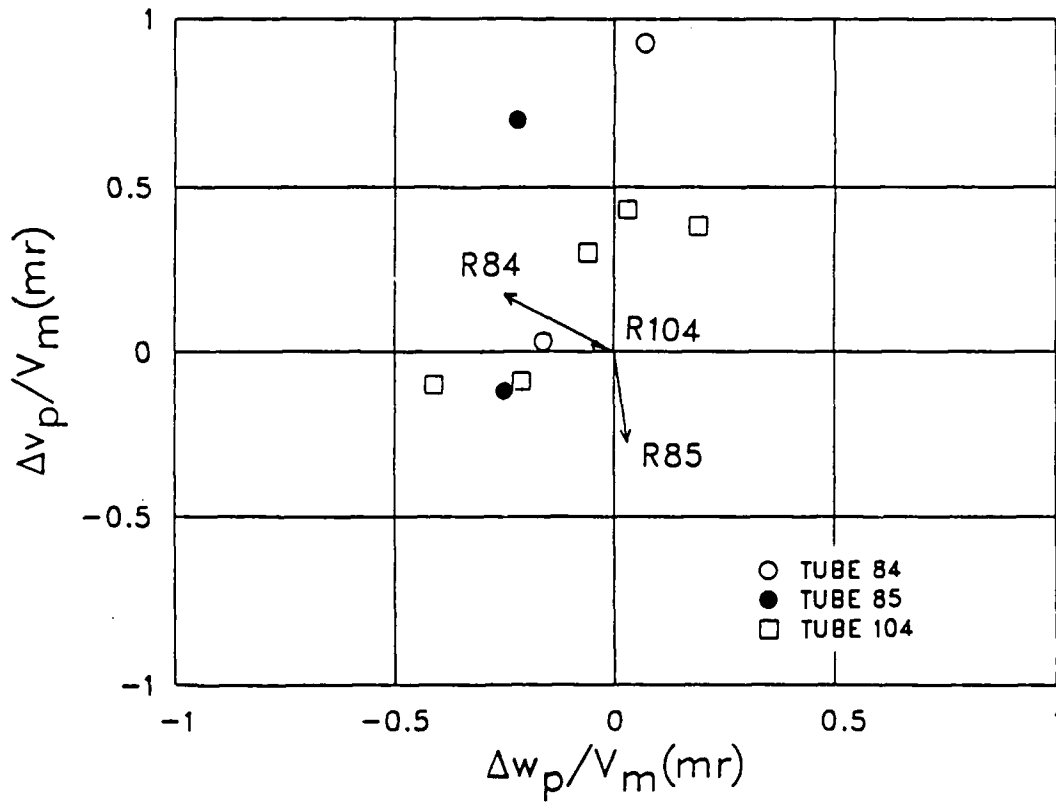


Figure 12. Change in Projectile c.g. Velocity due to Sabot Discard

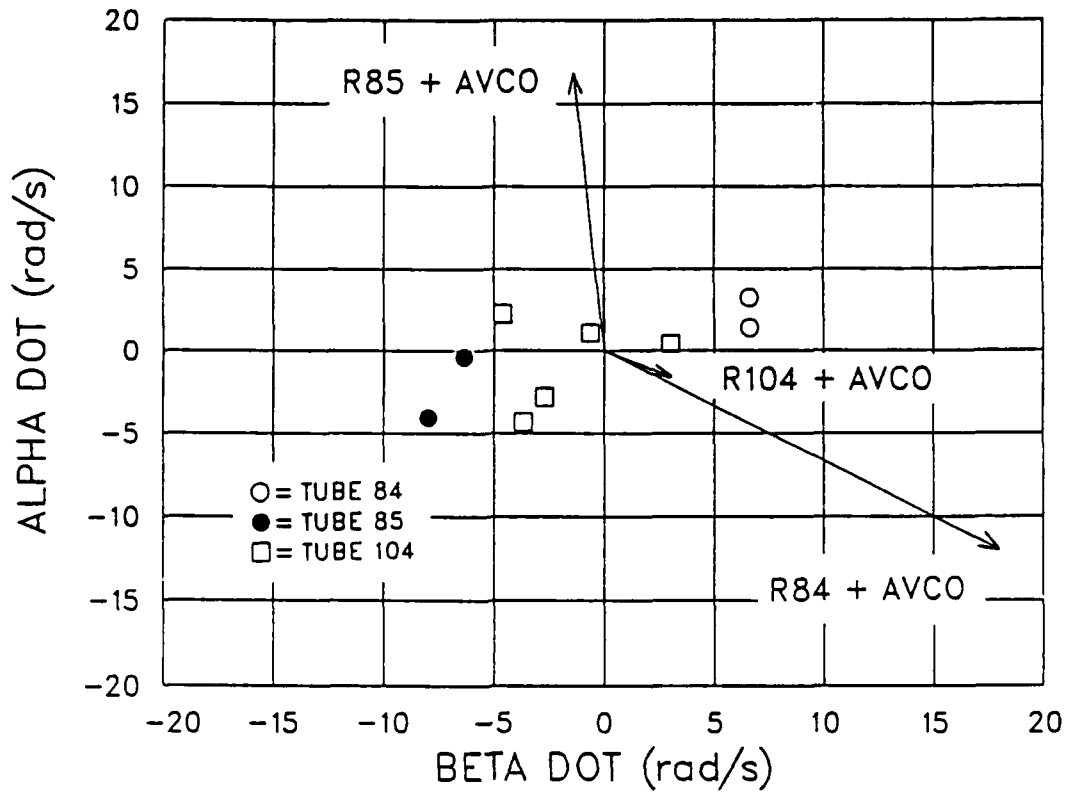


Figure 13. Projectile Angular Velocity at 10.3m from Muzzle

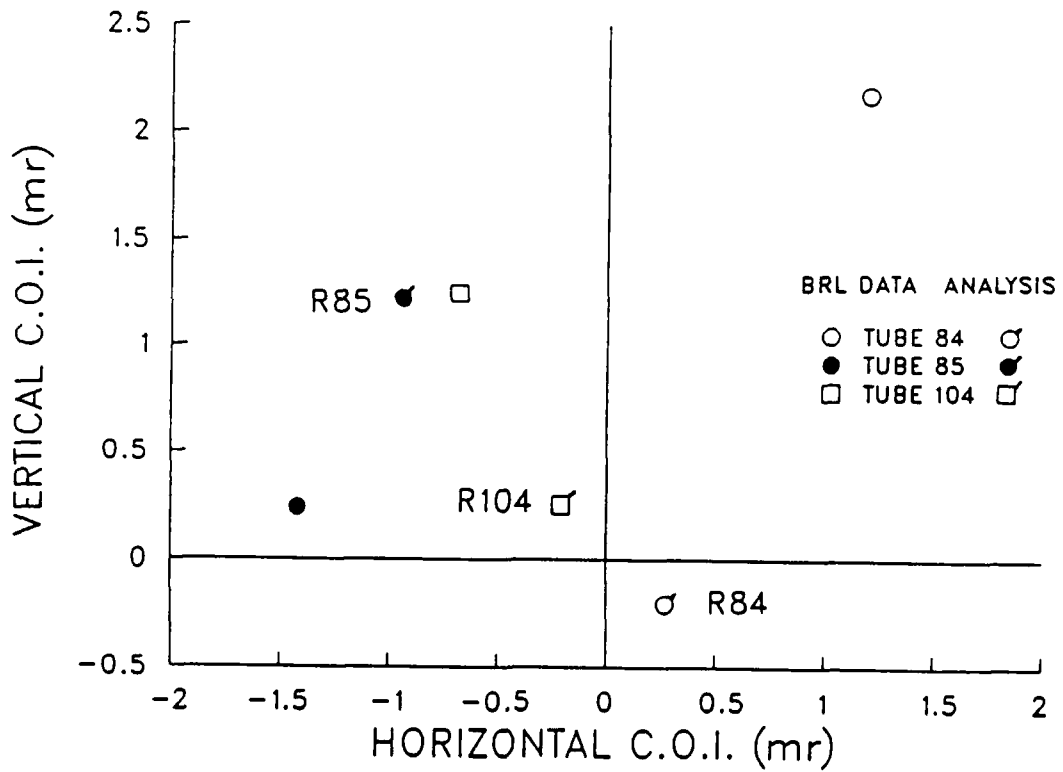


Figure 14. Comparison of Measured and Predicted Impacts

THE FIFTH U.S. ARMY SYMPOSIUM
ON GUN DYNAMICS

THE THEORETICAL MODELLING OF THE DYNAMICS OF INITIALLY NON-STRAIGHT BARRELS
USING FINITE DIFFERENCE TECHNIQUES

*S.E. Powell

Royal Military College of Science
School of Mechanics, Materials and Civil Engineering.
Land Systems Group
Shrivenham, Swindon, Wiltshire, SN6 8L, England.

P.H.G. Penny

Royal Armament Research and Development Establishment
Chobham Lane, Chertsey, Surrey KT16 0EE, England.

ABSTRACT

Computer based mathematical models are playing an increasingly important role in the search for greater tank gun accuracy. One such model is the gun dynamics program suite RAMA which has been written at RMCS under contract to the Royal Armament Research and Development Establishment (Chertsey).

The simulation is based on equations derived from the Euler-Bernoulli beam theory, to describe the transverse vibrations in the vertical plane, and from the wave equation to describe the longitudinal vibrations caused by recoil. These equations are solved using an implicit finite difference method.

To begin the dynamic simulation with a non-straight barrel it is necessary that, when the barrel is in the required initial position, the shear and bending forces at each node sum to zero. To achieve this the initial values of displacement, slope, curvature and change in curvature are calculated so that the stresses in the model are in equilibrium before the firing sequence begins. The analysis is arranged so that the static configuration of the barrel is calculated separately from the dynamic simulation.

Three methods are available to do this: Firstly, the calculation of the barrel profile from a given configuration as a beam supported at the cradle bearings under gravity, secondly, the specification of a deflection and slope of the barrel at the muzzle, with the program calculating the barrel profile, and thirdly, the input of the initial barrel profile as a series of ordered pairs.

In addition to a comparison between experimental results and theoretical predictions for a simple recoiling beam with an offset mass, selected gun barrels were measured and simulated by the computer program. Predicted changes to the transient response of the gun barrel are presented and discussed in this paper, whilst further trials results are presented in a companion paper by Penny and Perry.

BIOGRAPHY

PRESENT ASSIGNMENT: Research Officer, Royal Military College of Science.
DEGREES HELD: B.A., M.Phil.

Copyright (C) Controller, Her Majesty's Stationery Office, London 1987.

THE THEORETICAL MODELLING OF THE DYNAMICS OF INITIALLY NON-STRAIGHT
BARRELS USING FINITE DIFFERENCE TECHNIQUES

S.E. POWELL

ROYAL MILITARY COLLEGE OF SCIENCE
SCHOOL OF MECHANICAL, MATERIALS AND CIVIL ENGINEERING
LAND SYSTEMS GROUP
SHRIVENHAM, SWINDON WILTSHIRE, SN6 8LA, ENGLAND

P.H.G. PENNY

ROYAL ARMAMENT RESEARCH AND DEVELOPMENT ESTABLISHMENT
CHOBHAM LANE, CHERTSEY, SURREY, KT16 0EE, ENGLAND

1) INTRODUCTION

Over the last fifteen years RARDE (formerly MVEE), has undertaken a number of investigations into tank gun accuracy. The early work concentrated almost entirely on firing trials and these trials identified a number of physical parameters that were shown to have an effect on the gun system accuracy (elevation backlash, muzzle reference mass offset, barrel droop). It should be noted that in this context the gun system comprises the complete gun together with its ammunition, mounting, recoil system, and the elevation and traverse mechanisms; it does not include the sighting, fire control or gun control servo-systems. One result of this work was that the 'Chieftain' tank firing APDS could be 'fleet zeroed' after measuring barrel droop and setting the other mechanical parameters. This saved considerable ammunition, range time and money.

A little under ten years ago it became apparent that a computer simulation of the physical processes associated with gun firing could help considerably in our understanding of the various interactions that occurred between parts of the system during the gun firing impulse; only the end result was seen at the target during the firing trials! The mathematical model that was developed at RMCS, uses a finite difference representation of the differential beam equations and has been reported in previous papers [1,2]. A number of features have been improved over the years, for example the internal ballistics model, barrel gravity droop and the cradle bearing representation. The current programme of enhancements is scheduled to add a number of features that are now considered necessary, (see Figure 1). Whilst the existing analytical methods are considered suitable for these developments, it is considered that ultimately, if gun components use composite materials in a manner such that their directional properties become significant, then dynamic, non-linear finite element or boundary element analysis methods will probably be required.

The one parameter that has consistently been identified as being the largest single contributor to variations in gun accuracy, is that due to the barrel. This is both in terms of barrel to barrel movement of the Mean Point of Impact, (for example after a barrel change), and also ammunition serial consistency. Recently some excellent trials work in the United States, reported to us through The Technical Co-operation Programme, identified projectile strike coordinates with certain barrel features. Whilst the U.S. 120mm M256 barrel and the U.K. 120mm L11 barrel are dissimilar in many respects (length, mass, rifling, breech mass and mounting type), it was considered that some additional firing on an existing U.K. gun accuracy investigation could possibly confirm some of the U.S. results with a different gun system.

It is probably true to say that, to date, the measurements taken during firing trials have led the analysis techniques, in that careful measurement has shown effects that cannot be modelled by the current computer programs. Where the existing computer programs have been of considerable benefit is in assisting our understanding of the relationship between cause and effect. This paper is concerned with the procedures adopted for taking measured data from real gun barrels, how that data is processed into a form capable of being used by the computer simulation program, and an explanation of the resulting predictions given for initially non-straight gun barrels when compared with some experimental results.

A more detailed report of the experimental firing results from four selected 120mm gun barrels is given in a companion paper [3], although the barrel data is included here for illustrative purposes. Since the companion paper may not always be read in conjunction with this work, it should be pointed out that the barrel data given in this paper is for four selected barrels covering an un-typical range of 'in-service' equipment. The data should not be viewed as being representative of current equipment; indeed one barrel exceeds the current production tolerances by some margin!

2) BARREL MODELLING THEORY

2.1) Overview of the finite difference model

The computer based model which is described in this paper was developed under contract to RARDE (Chertsey), by the Mathematics and Ballistics department at the Royal Military College of Science. A further contract to enhance the program suite and to provide full testing and documentation, was placed with Land Systems Group RMCS in October 1985.

This section gives a brief updated description of the mathematical basis of the finite difference model described in reference [1], followed by a description of the present computer code.

When a gun recoils any eccentric masses along its length will induce bending moments due to their inertia. The primary eccentricities are due to the breech and the muzzle reference sight. Bending moments will also be induced by off axis masses due to curvature of the barrel, for instance that caused by gravity droop. The effect of the shot on the barrel may also be significant but is not considered here.

The extensional and flexural vibrations of the barrel are modelled by considering an Euler-Bernoulli beam in a frame of reference which is constrained to rotate about a fixed point 'O'. Assuming that the angle θ remains small throughout, the extensional and flexural equations of motion are:

$$\rho A \frac{\partial^2 \eta}{\partial t^2} = \frac{\partial}{\partial x} \left(EA \frac{\partial \eta}{\partial x} \right) + G \quad (1)$$

$$\frac{\partial^2}{\partial x^2} \left(EI \frac{\partial^2 y}{\partial x^2} \right) + \rho A \frac{\partial^2 y}{\partial t^2} - \frac{\partial}{\partial x} \left(\frac{\partial y}{\partial x} T \right) = F_1 + F_2 + F_3 \quad (2)$$

where

$$G = - \rho A \frac{\partial^2}{\partial t^2} (\theta y) - \frac{\partial}{\partial x} \left(\frac{\partial y}{\partial x} \frac{\partial S}{\partial x} \right) - \theta \frac{\partial S}{\partial x} - \left(\theta + \frac{\partial y}{\partial x} \right) k(x, t) y(x, t) \quad (3)$$

$$F_1 = \frac{\partial}{\partial x} \left(\frac{\partial y_s}{\partial x} T \right) \quad (4)$$

$$F_2 = \theta \frac{\partial T}{\partial x} - \rho A \left[(x + \eta - X_0) \ddot{\theta} + 2 \dot{\eta} \dot{\theta} + \ddot{\eta} \dot{\theta} \right] \quad (5)$$

$$F_3 = k(x, t) y(x, t) \quad (6)$$

and the initial static position of the barrel is given by,

$$\frac{\partial^2}{\partial x^2} \left(EI \frac{\partial^2 y_s}{\partial x^2} \right) = - \rho A g + k(x, 0) y(x, t) \quad (7)$$

Let the bearings be of length l_1, l_2 and have moduli of elasticity k_1, k_2 . Then the elastic foundation function $k(x, t)$ has the form

$$k(x, t) = \begin{cases} 0 & 0 \leq x < d_1 - n \\ -k_1 & d_1 - n \leq x \leq d_1 + l_1 - n \\ 0 & d_1 + l_1 - n < x < d_1 + l_1 + d_2 - n \\ -k_2 & d_1 + l_1 + d_2 - n \leq x \leq d_1 + l_1 + d_2 + l_2 - n \\ 0 & d_1 + l_1 + d_2 + l_2 - n < x \leq L \end{cases} \quad (8)$$

Each bearing exerts a moment on the cradle due to its reaction with its mounting. This moment is given by

$$M(t) = - \int_0^L (x + n - X_0) k(x, t) y(x, t) dx$$

Therefore the equation of motion of the cradle is given by

$$I \ddot{\theta} = M + s(\theta, \dot{\theta})$$

where $s(\theta, \dot{\theta})$ is the stiffness function representing the elevating gear impeding the motion of the cradle. This is fully defined in [1].

The breech mass and the mass of the muzzle reference sight are considered to be rigidly attached to the barrel. The boundary conditions for equations (1) and (2) are then derived by considering the breech and muzzle mass. These equations are described in reference [1], where the driving force for the system and its implementation in the code are also discussed.

The scheme used to calculate a numerical approximation to the solution of the system of equations (1) and (2) is based on an implicit algorithm suggested in reference [4].

The filestore of the RAMA suite of programs has been re-designed so that the same version of the suite can be run at both RARDE and RMCS establishments, an overview of the current system is given in figure 2. Operation of the model is controlled by program RAMAMENU which provides the user with a menu from which to drive the system. RAMAMENU supervises creation or amendment of the Weapon Data file. It also supervises the running of the programs HMSOV3, DROOP and RAMA. Each of the program or data files in figure 2 is discussed below.

The Control file contains a title and the names of the Weapon Data file, the Static Configuration file and the Internal Ballistics file. It also specifies the length of time over which the system is to be modelled, the time step, the variables which are to be

'plotted' on the line printer, a smoothing factor' (which is used to minimise rounding errors in the matrix manipulations), the number of mesh points, whether the cradle is moving, the elevating gear backlash factor, whether terminal graphics are required, whether an output file is required and, if so, the time step to be used for the output data.

The Weapon Data File contains the majority of the parameters used by the model, for instance the modulus of elasticity and density of the barrel material. It also holds specifications of the cradle, the recoil system and the elevating mechanism, and of any mass eccentricities along the recoiling mass. The barrel external diameters are given at various distances from the breech and can describe both sudden changes in diameter and gradual tapers.

HMSOV3 is an internal ballistics program which generates the pressure/time profile and the shot travel/time profile and stores them in the Internal Ballistics file. This file is generated in one of two ways. The first, where only limited data is available assumes a simple shot start pressure. The other uses a full shot engraving model.

The Ballistics Program file contains the information required by HMSOV3 which includes gun parameters, resistance parameters, primer parameters and the charge parameters.

The Internal Ballistics file holds the details of the internal ballistics variables needed by the RAMA Dynamic Model. It contains the following columns of data. Time, breech pressure, shot pressure, shot position (measured from the shot start position), shot velocity, shot acceleration and shot resistance. These are followed by the data required to calculate breech pressure due to venting gas after shot exit.

The suite is arranged so that the static configuration of the barrel is calculated before the dynamic simulation begins. Either of two separate programs can be used to do this. Program DROOP calculates the initial barrel gravity droop profile using data from the Weapon Data file, and stores the information in the Static Configuration file. DROOP gives the user two options: First, to allow the calculation of the barrel configuration as a beam supported at the cradle bearings, under gravity. Or second, to specify the deflection and slope of the barrel at the muzzle, and allow the program to calculate the barrel profile. INPRO is a new program which has been added to the suite to allow the user to specify the initial barrel profile as a series of ordered pairs. It is more fully described in section 2.2.

The Static Configuration file contains the following columns of data which describe the static configuration of the barrel. Position along the barrel, vertical deflection, slope, curvature and the first derivative of the curvature. The file can be used by the dynamic modelling for any number of runs which require that particular configuration of the ordnance.

Before the dynamic simulation begins, the dynamic modelling program splits the barrel into a number of elements, using the number of mesh points specified in the Control File. It also calculates the initial values of vertical deflection, slope and curvature at each mesh point. The program reads values from the Static Configuration file. It then uses quadratic interpolation to give the required values at each mesh point.

Program RAMA provides the dynamic modelling. Gun motion can be monitored at a terminal during a run.

The output data from the RAMA dynamic modelling is stored in a file, in the present model the following data is stored. Time, breech longitudinal acceleration, cradle rotation, breech deflection, muzzle deflection, muzzle slope, muzzle vertical velocity, force on the rear bearing and force on the front bearing. Using this file a plotting program can be used to produce a number of different traces.

Each time the RAMA Dynamics Modelling program runs it produces a file which is suitable for printing on a line-printer. The file contains a listing of the Control file, a listing of the Weapon Data file, the number of iterations used, the length of a barrel increment, the time increment used and certain shot exit information. Optionally it also holds 'graphical output' for printing on the line-printer, of muzzle deflection, muzzle slope, vertical muzzle velocity, breech deflection and cradle rotation.

An extensive programme of improvements to the computer code is currently being undertaken, see Figure 1, and a timescale for various 'work packages' has been agreed. Large portions of the code have already been rewritten in a structured form, using ANSI standard FORTRAN 77 for added inter-machine portability, and supplied with extensive documentation. Additional graphics programs have been written, to enhance the presentation of current output, and to be easily amendable to supply traces of the additional output that is planned.

2.2) The intromission of initially non-straight barrels to the model

This section describes the program INPRO, which has been added to the suite to allow the user to specify initial barrel profiles. The program prompts the user to input ordered pairs representing the profile of the central axis of the barrel. It outputs a Static Configuration file which is compatible with the RAMA dynamics program. To be compatible the output file is required to contain the values of slope and curvature, as well as the value of vertical deflection at each position along the barrel. The first derivative of curvature is not used by the dynamic model and therefore has been ignored.

Two different methods can be used to calculate slope and curvature. In the first method, the first derivative at the first point (breach end) is estimated as the slope of the line between the first and second points. The second derivative at this point is therefore zero. The first derivative at an 'inner point' is estimated by fitting a parabola through the point and the points either side of it, and using the slope of this parabola at the 'inner point'. The second derivative is calculated by differentiating the equation of the parabola twice. The first derivative at the last point (muzzle end) is estimated as the slope of the line between the last and penultimate points.

This method has the advantage of plotting a curve through every data point, but has the disadvantage that experimental errors are not smoothed out. It was therefore decided to provide a second option, which fits a 'best fit' parabola to the data points using the least squares method, and uses the equation of this parabola to give values for X, Y , and the first and second derivatives of Y with respect to X .

The program described above was used, with the rest of the RAMA suite, to predict the results of experimental trials. The predictions, which were produced using the method of fitting a curve through each measured point, are compared with the experimental results in section 4.

3) EXPERIMENTAL TECHNIQUES

3.1) A simple experimental apparatus

An experimental apparatus was designed to provide data to test the theoretical barrel curvature routine. The apparatus (Fig 2) consisted of a .76 m x .0048 m dia. steel rod which could just run freely through two brass bushes. These were held in aluminium uprights which were bolted to an aluminium base plate.

The base plate was positioned on a bench and the rear end of the rod was connected via a wire to a 362 gm mass. An impulse was produced by dropping the mass from the height of the base plate, so that the wire, when taut, ran over a pulley which was positioned to the rear of the base plate. The mass was dropped 834 mm before the wire became taut. The mass then accelerated the wire and rod for 40 mm before hitting the floor.

An accelerometer was fitted to the rear of the rod. Signals from the accelerometer were filtered at a low pass value of 400 Hz. 'Muzzle' motion was measured by a proximity transducer placed underneath the beam and 40 mm from the initial position of the front end.

The experimental procedure involved measuring the beam profile in the vertical plane at six places using a Vernier rule, dropping the mass to produce an impulse on the rod and recording the results using 'Datalab' DL902 transient recorders. Data was then transferred to an HP9836 computer for storage and display. Different barrel profiles were created by securing lead masses to the 'muzzle'. Three different configurations were used; with no added muzzle mass, with a 10g mass added and with a 30g mass added. For each configuration several readings were taken to ensure repeatability. Results from the simple experimental apparatus are discussed in section 4.1.

3.2) Investigations using full scale barrels

An existing U.K. tank gun programme had selected four tank gun barrels for investigation [3]. All four barrels had been measured for straightness and concentricity according to the usual U.K. measurement procedures [5], but excluding the normal wear correction. The straightness results are shown in figures 4 and 5, however, the angular measurements commonly recorded in the U.K. have been converted into the linear measurements more common in the U.S. The sign convention applied to the data is shown with the figures.

With regard to the barrel straightness measurements, the readings are subject to an overall error of $\pm 0.08\text{mm}$; this is mainly due to difficulties with repeatability. After firing, propellant combustion products lodged in the bore can prevent the optical target from seating properly and hence introduce a false reading.

The straightness data for the four barrels was used as input for the program 'INPRO'. A curve that passed within $\pm 0.05\text{mm}$ of all the barrel straightness readings would be considered to lie within the measurement error and therefore acceptable. The predicted results from the computer simulation runs using the real barrel data are given in Section 4.2.

4) DISCUSSION OF EXPERIMENTAL RESULTS AND COMPARISONS WITH THE THEORETICAL MODEL

4.1) Results from the simple experimental apparatus

An example acceleration trace for the simple experimental apparatus is given in Figure 6. Figure 7 shows the muzzle displacement recorded for the same test, along with the theoretical prediction, which was produced using the technique of fitting a curve through every measured point. The traces stop abruptly because after accelerating for 40mm the rod was pulled clear of the measuring transducer. The theoretical traces were smoother than the experimental traces but predicted accurately the slope and amplitude of the displacement.

4.2) Results from the full scale barrels

The predicted vertical muzzle deflections for each of the four barrels are given in Figure 8. The associated predicted muzzle slopes, in the vertical plane, are given in figure 9. Figure 10 shows the predicted horizontal deflections whilst figure 11 shows the slopes in the horizontal plane.

From figure 4 it can be seen that the vertical bend, for three of the barrels, is relatively close together compared with the fourth (barrel NG12212). This is reflected in the theoretical predictions (figure 8) which show that the trace for barrel NG12212 is some distance away from the traces for the other barrels. Similarly in the horizontal, barrel NG12212 is straighter than the other barrels and this is reflected in a lower predicted horizontal displacement (figure 10). In the horizontal, barrels NG694 and NG6654 are relatively close together, whilst barrel NG987 bends in the opposite direction, this is again reflected in the theoretical results. In the vertical the effects of gravity on the motion of the barrels swamps the effects due to out of straightness.

The results from the firings using each of the four barrels are plotted in figure 12. It can be seen from this figure that the serial to serial variations are much smaller than the barrel to barrel variations, suggesting that the barrel effects are dominant. The theoretical model does not predict barrel to barrel effects of this magnitude, however, it is interesting that the straightest barrel gives Mean Points of Impact closest to the calculated point of impact.

The present study provides strong experimental evidence that barrel characteristics have a significant effect on the Mean Point of Impact of the shot. Previous work has shown that shot/barrel interaction is important [6,7], and this study suggests that the study of barrel motion alone will not accurately predict the effects of barrel straightness.

5) CONCLUSIONS

For a simple accelerating beam test the computer model gave good predictions. However when used with 'live' data the experimental results were not accurately predicted. It is believed that this is primarily due to the absence of shot effects in the model and the lack of cross coupling between the horizontal and vertical models.

A substantial effort is now being made to produce a full three dimensional model which will include the effects of the shot. Further experimental investigations into bore straightness are being carried out. Usually only nine or ten data points are taken when measuring barrel profiles. It has been recommended that extra readings are taken close to the ends of the barrel. This is because the greatest error in the curve fitting is likely to be in these regions. If a greater number of points are measured a more sophisticated curve fitting routine could be required, this would probably use a cubic B spline method. The technique of fitting a higher order polynomial through the data has been rejected.

This is because the method could introduce inaccuracies, and also because the variable distances between data points, that this technique would require for greatest accuracy, would make the physical measuring more complicated.

6) ACKNOWLEDGEMENTS

We would particularly like to acknowledge all the careful work undertaken by the staff of Mr George Rawlinson of Defence Quality Assurance, and Mr David Haugh of RARDE (Fort Halstead)

7) REFERENCES

- 1) King W.P.C. Pagan G. and Thomas M.D.
A model for tank gun movements during firing using an implicit difference numerical algorithm.
3rd US Army Symposium on Gun Dynamics, Rensselaerville, NY, May 1982.
- 2) Penny P.H.G. and King W.P.C.
The predicted effect on 'gun jump' due to changes in gun cradle bearings and gun barrel stiffness.
4th US Army Symposium on Gun Dynamics, Riviera Beach, Florida, May 1985.
- 3) Penny P.H.G. and Perry J.A.
An account of some experiments undertaken to correlate measured gun barrel features with the movement of serial mean points of impact.
5th US Army Symposium on Gun Dynamics, Rensselaerville, NY, September 1987.
- 4) Rickmeyer R.E. and Morton K.W.
Difference methods for initial value problems.
Interscience 1967.
- 5) Unpublished MOD report.
- 6) Powell S.E.
A simple theoretical model of shot/barrel interaction within a smooth bore gun.
4th U.S. Army Symposium on Gun Dynamics, Riviera Beach, Florida, May 1985.
- 7) King W.P.C. and Thomas M.D.
The effects of barrel curvature on gun jump.
TTCP KT6 Workshop ,RARDE (Fort Halstead), September 1984.

7) NOTATION

- $A(x)$ = Cross sectional area of the barrel at point x .
 d_1 = Distance from the breech to the rear of the rear bearing.
 d_2 = Distance between the front of the rear bearing and the rear of the front bearing.

- E = Modulus of elasticity of the barrel.
 g = Acceleration due to gravity.
 $I(x)$ = Second moment of area of the barrel cross-section at x .
 k_1 = Stiffness of the rear bearing.
 k_2 = Stiffness of the front bearing.
 $k(x,t)$ = Elastic foundation function for the bearings.
 l_1 = Width of rear bearing.
 l_2 = Width of front bearing.
 L = Length of the barrel.
 S = Lateral force in the barrel.
 t = Time variable.
 $T(x,t)$ = Tension in the barrel at point x at time t .
 x = Distance from the breech along the barrel.
 X = Distance from the breech to the trunnions.
 $y(x,t)$ = Transverse deflection relative to the original static position.
 $y(x)$ = Original static position of the barrel.
 ρ = Density of the barrel.
 $\theta, \dot{\theta}, \ddot{\theta}$ = Angle, angular velocity and angular acceleration of the cradle about the trunnions.
 $\eta(x,t)$ = Extensional deflection of the barrel relative to its unstressed position.

'RAMA' ENHANCEMENTS

To introduce into existing gun dynamics computer program:

- the ability to model non-straight barrels using real data
- to model shot/barrel interaction and shot dynamics
- to further improve the cradle bearing model
- to introduce a flexible cradle
- to make the program fully three dimensional
- to introduce vehicle inputs at the trunnions and elevating/traverse gear

Figure 1

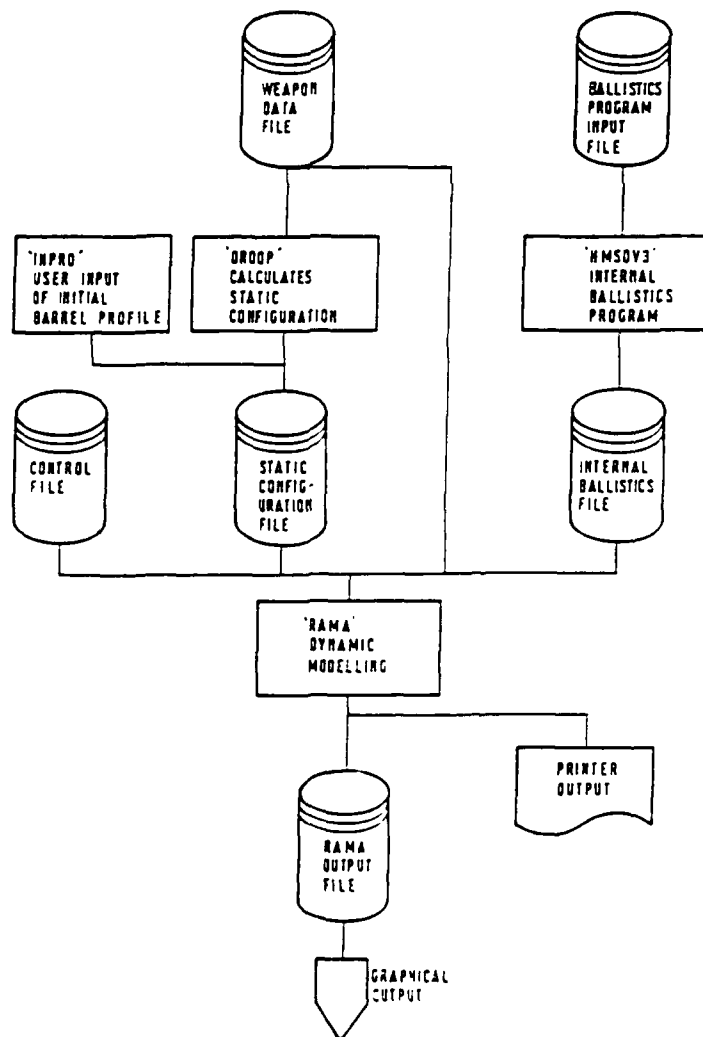
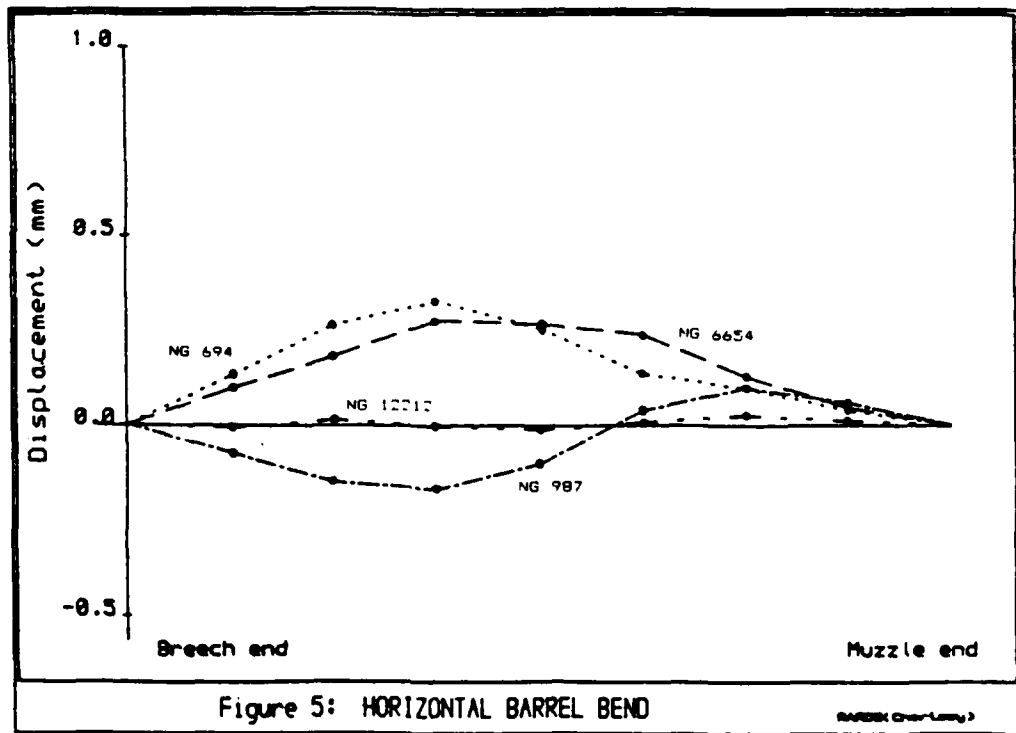
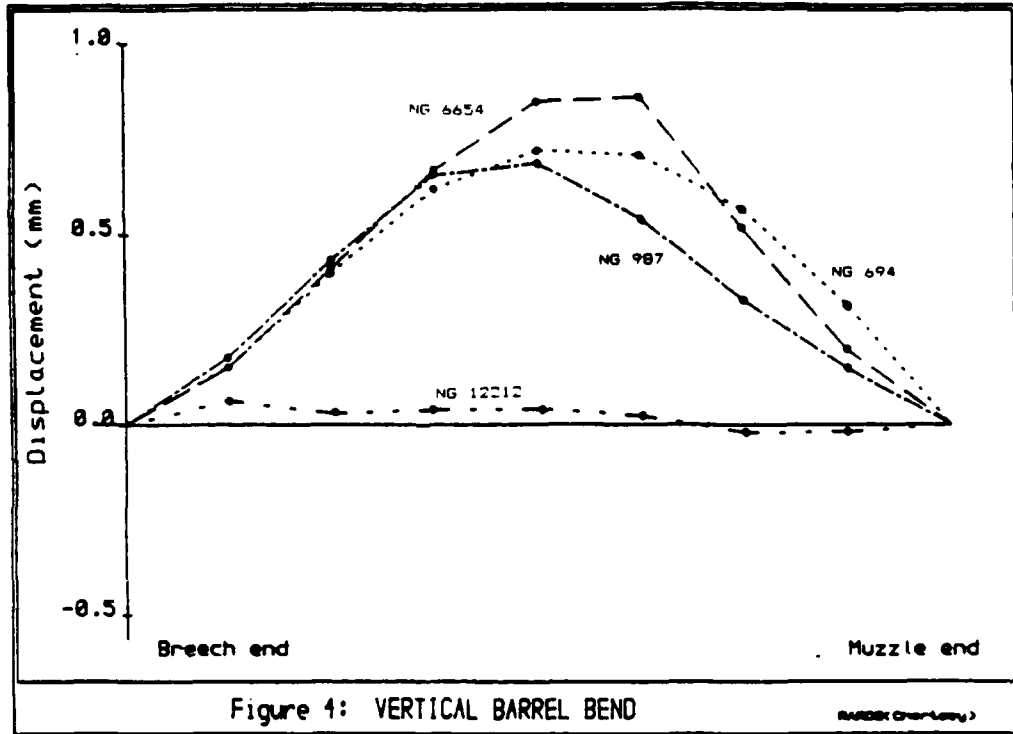
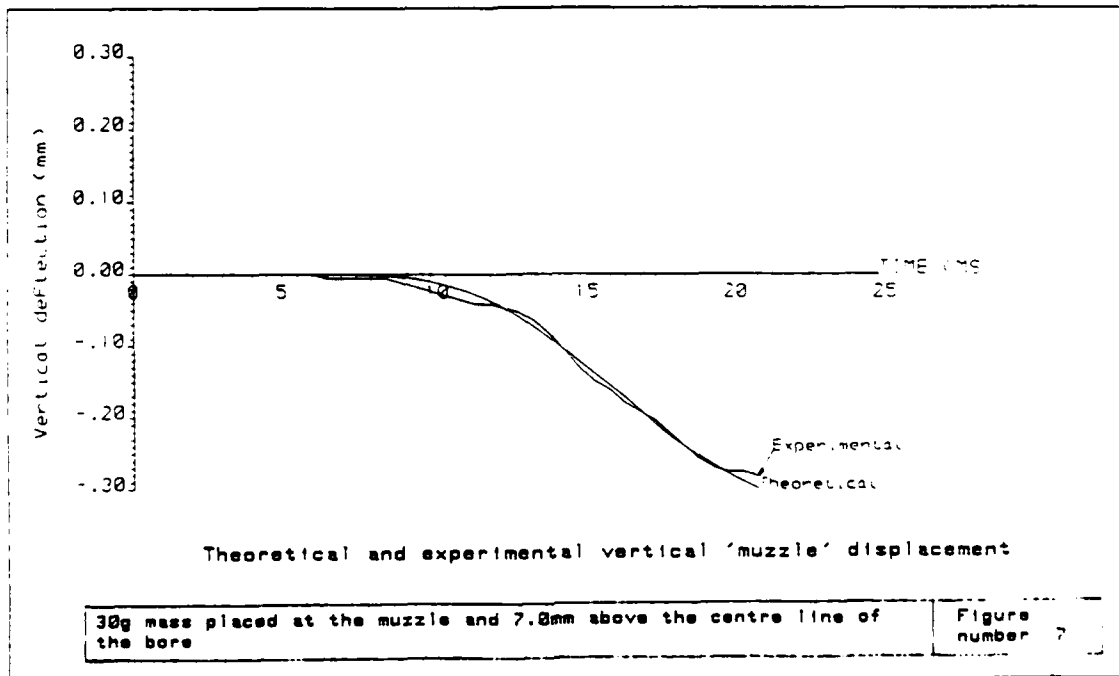
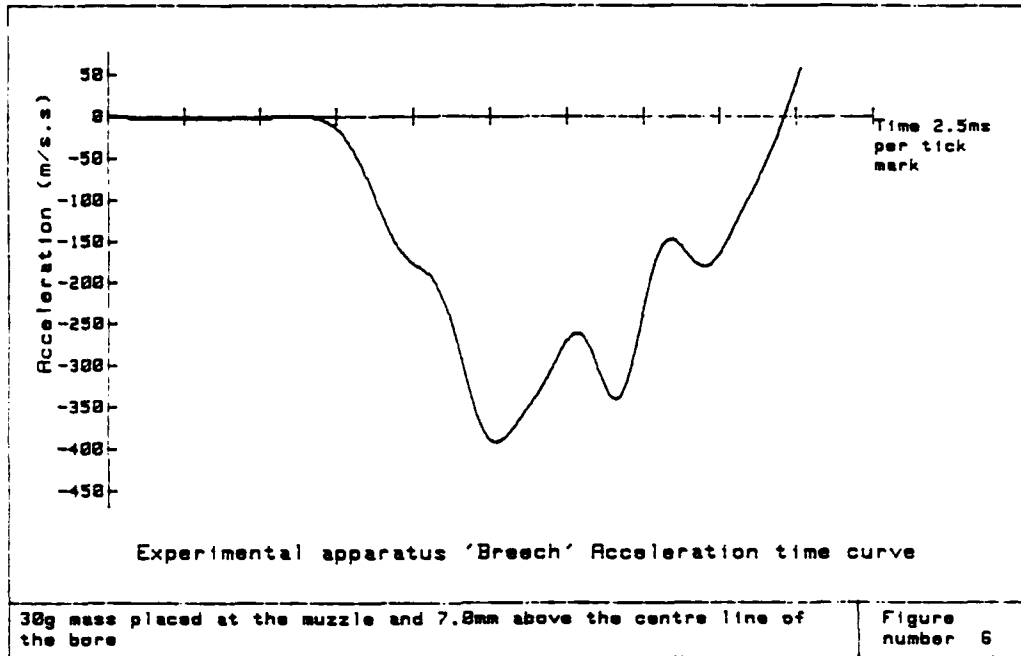


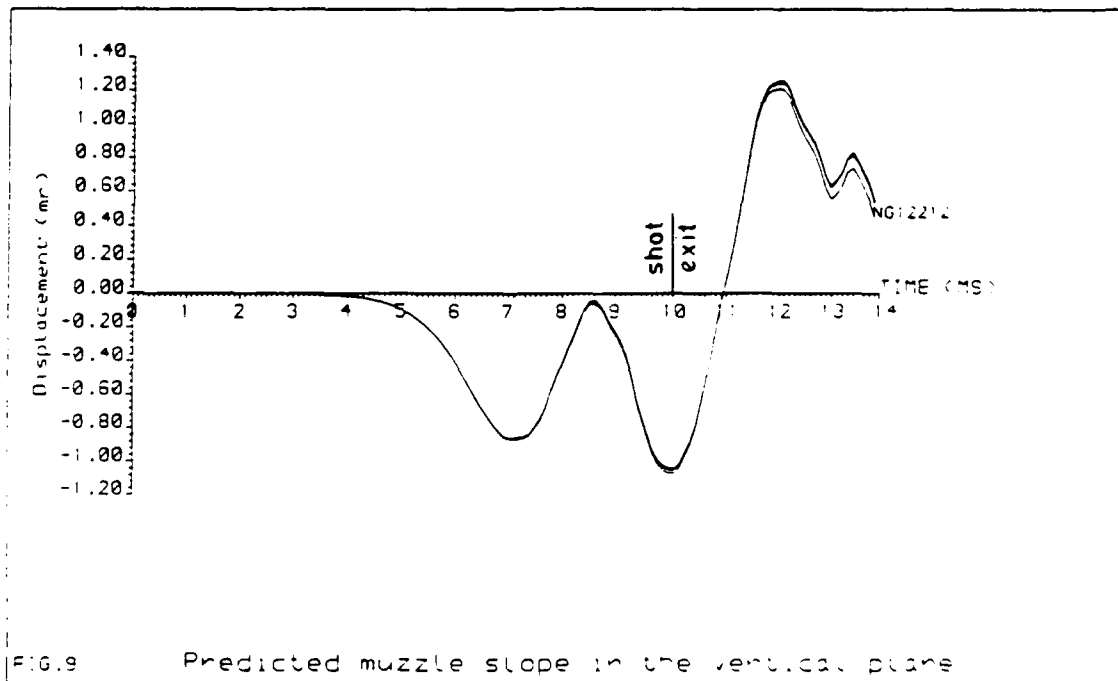
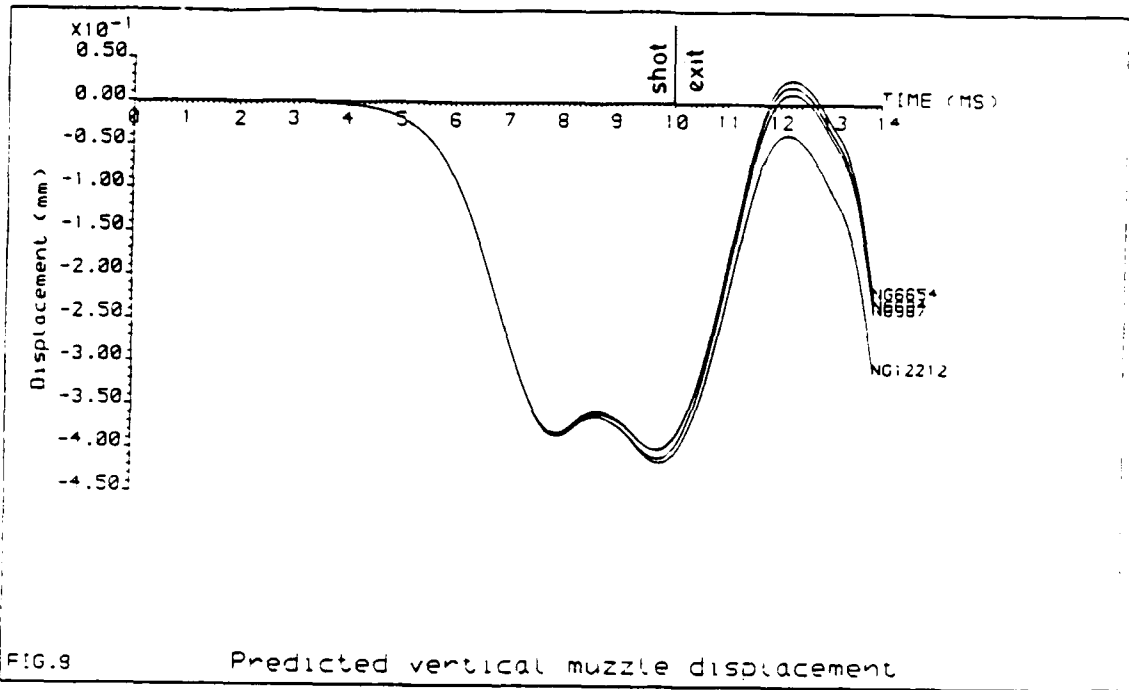
FIGURE 2 SYSTEM OVERVIEW

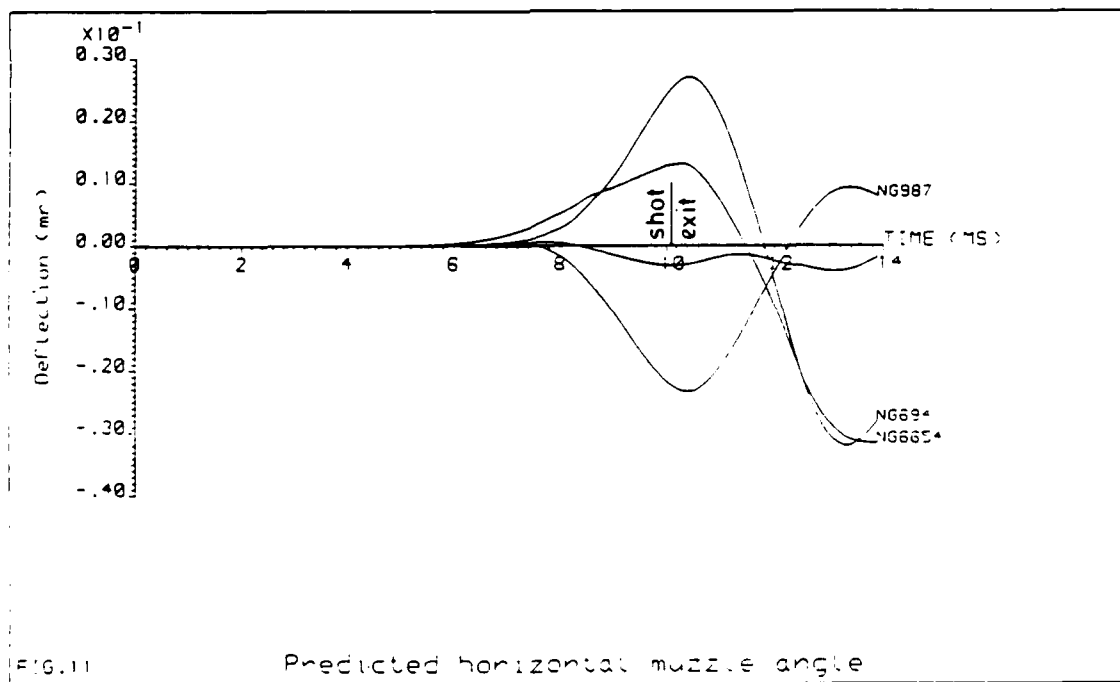
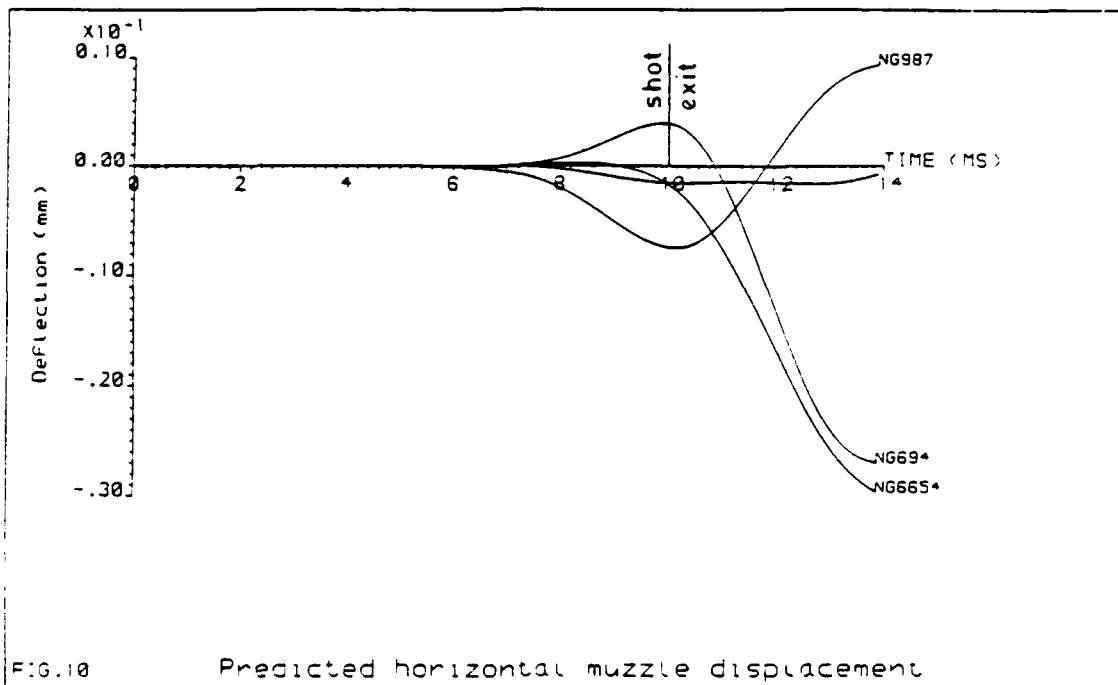


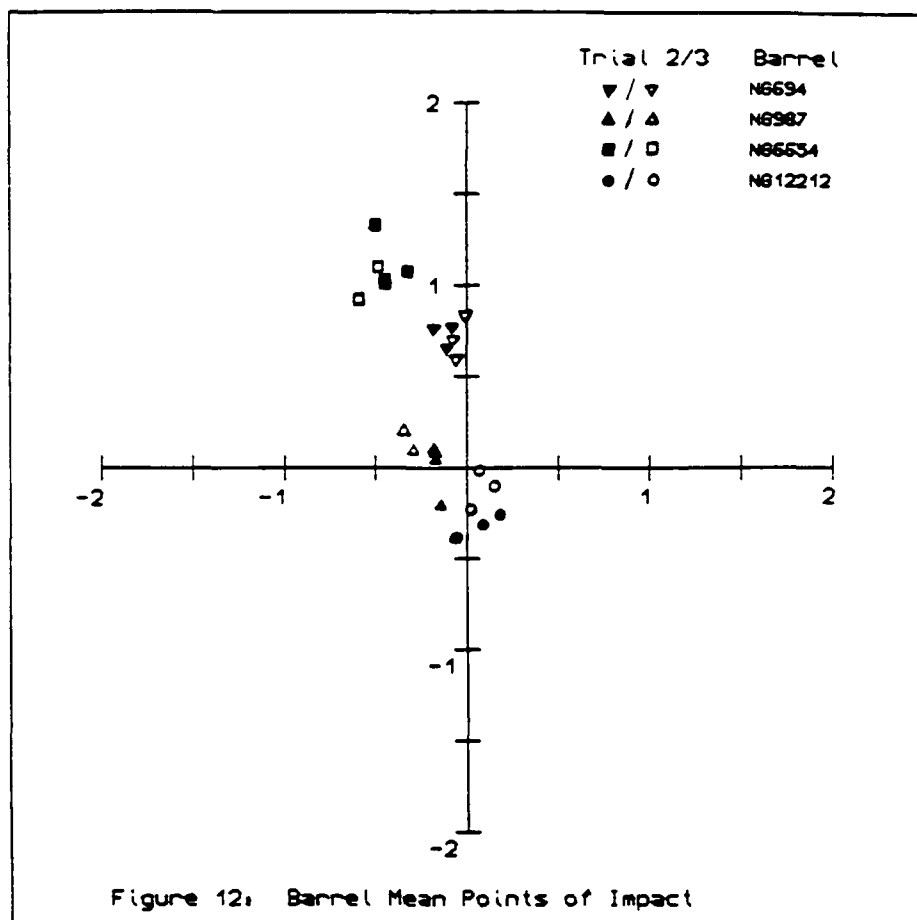
FIGURE 3 THE SIMPLE EXPERIMENTAL APPARATUS











Polcyn and Cox

TITLE: The Adaptation of NASTRAN for Three-Dimensional Gun Dynamics Problems
M. A. Polcyn
P. A. Cox
Southwest Research Institute
6220 Culebra Road
San Antonio, Texas 78284

Modifications have been made to COSMIC NASTRAN to make it more suitable for gun dynamics type problems. The approach taken was to provide for the computation, by NASTRAN, of the interior ballistics and tube-support interactions. The calculations are made based on input of the projectile parameters, breech pressure, projectile axial motions and the tube support parameters. Another goal of the program modifications was to provide, in a single NASTRAN module, all of the variables necessary for calculation of the interior ballistics parameters. This will allow other users an opportunity to write and program their own gun dynamics forces with a minimum of DMAP alters.

Calculations were made with NASTRAN for comparison with previous calculations made with the two-dimensional code, GUN2D. Also, parameter studies were made to show the affect on tube motions produced by different breech force models, Bourdon forces and axial accelerations coupled with lateral displacements. The NASTRAN changes and instructions for use of the modified code are documented in a final report.

BIBLIOGRAPHY

Present Assignment: Research Engineer, Department of Energetic Systems, Southwest Research Institute

Past Experience: Research Assistant, Case Western Reserve University

Degrees Held: BSCE and MSCE, Case Western Reserve University

THE APPLICATION OF NASTRAN TO THREE-DIMENSIONAL GUN DYNAMICS PROBLEMS

* M. A. Polcyn
P. H. Cox
Southwest Research Institute
San Antonio, Texas

INTRODUCTION

The COSMIC version of NASTRAN[1] has been applied to gun dynamics problems by Simkins[2], but input to the program proved to be very cumbersome. As a result of this experience, it was felt that to routinely apply NASTRAN to gun dynamics problems, modifications to the code, or to the input preprocessors, would be required. Two approaches were feasible. One was to create new preprocessors to compute the proper input files for NASTRAN. Another approach was to imbed code in NASTRAN for calculating the nonlinear forces directly, using input which is based on conventional descriptions of the gun and projectile. The second approach was taken in this work, and the results are reported herein.

To determine the best strategy for modifying NASTRAN, we utilized the services of Mr. Tom Butler, a NASTRAN specialist. Mr. Butler was able to help by: (1) quickly instructing us on the use of NASTRAN dummy modules (DUMMODS), (2) identifying the storage locations in NASTRAN for the data needed to calculate the gun dynamics forces, and (3) teaching us the procedures for reading and writing NASTRAN internal files. The following modifications to NASTRAN were selected as the simplest approach for implementing the necessary changes:

- Modify Rigid Format 9 (RF 9)
- Write two DUMMODS for gathering and transferring data to the TRD module
- Modify the TRD module (actually replace it with a new DUMMOD) to add the nonlinear gun dynamics forces
- Use standard NASTRAN provisions for all input

NASTRAN MODIFICATIONS

New NASTRAN Input Data

Standard NASTRAN input provisions are used for all input in the gun dynamics problem. Most of the input is common to dynamics problems in general. This includes such data as:

Polcyn and Cox

- node numbers
- nodal coordinates
- element connectivity
- element properties
- damping
- concentrated masses
- time integration parameters
- time-dependent forces

In addition, specialized input is required to compute the gun dynamics forces (as they are computed in this modified version of NASTRAN) and these data are input using the direct table input (DTI) provision. Additional data are required in the following categories:

- Gun Tube Parameters
- Projectile parameters
- Projectile-tube Friction parameters
- Tube support parameters

The individual parameters in each category are described in a subsequent section, "USER'S GUIDE TO THE NEW PROVISIONS."

"DUMMOD for Gathering NASTRAN Internal Data

In NASTRAN, several data blocks are built and passed to the TRD module; however, the solution of gun dynamics problems requires that additional data, part of which is input by the user and part of which is generated within NASTRAN, be passed to TRD. This module, called DUMMOD2, was developed to collect element input data and internally generated data, organize it, and write it to a single output file. DUMMOD2 was added to RF 9 by means of a DMAP alter. The "call" statement for the module is:

```
DUMMOD2 EQEXIN, USET, GPDT, EST, , , , /SWRI1, , , , , /$$$$$$$$$
```

The dummy module consists of the subroutine DUMOD2 (spelled with only one "M") and the subroutine swriin2. Both subroutines are given in Reference 3.

The data collected and reformatted by DUMMOD2 are:

- external-internal node number pairs
- degree-of-freedom (dof) numbers (active)
- nodal coordinates
- element connectivity
- beam element data

Nodal coordinates, element connectivity and beam element data are the same as input to the program. The dof and internal node numbers are generated internally by NASTRAN.

DUMMOD for Collecting the New Input Data

This module, called DUMMOD3, was developed primarily to collect the "new input" to NASTRAN which is required for the gun dynamics calculations. It also reads the output file from DUMMOD2 and combines it with the new input data on a single output file.

The new data are passed into NASTRAN through the direct table input provision. DUMMOD3 reads the input tables and writes the data, along with the output from DUMMOD2, to a single output file. All input to the new TRD module can now be brought in through one input data block, the only available data block left in DUMMOD1 which replaces the TRD module.

A call to DUMMOD3 is added to RF 9 by means of a DMAP alter. The "call" statement for the dummy module is:

```
DUMMOD3 SWRI1,GUNTUBE,PRJCTL.FRICT,TUBSUP,,,/SWRI2.....,/////////$
```

The dummy module includes not only the subroutine DUMMOD3 but also subroutine swriin1, which actually reads the input data and writes it to the output file, outfil. Reference 3 contains listings of these subroutines.

DUMMOD to Replace the TRD Module

TRD is the module in NASTRAN that computes the solution to transient problems. The dummy module written to replace it, called DUMMOD1, is the same as TRD except for the way in which the nonlinear forces are calculated. Changes to the module were:

1. The NLFT data block was changed to NLGUN, which corresponds to the output data block from DUMMOD3.
2. The parameter NLFTP was changed to NLGUNP.
3. Subroutine TRD1D was replaced with subroutine GUNLD, which calls the gun dynamics force routines.
4. Subroutines to calculate the dynamic forces on the gun, patterned after those in GUN2D[4,5], were added to the module.

The name changes in items 1, 2, and 3 were made only to emphasize the changes to the program and to show where they occurred. Replacement of TRD1D with GUNLD, and the addition of the subroutines to calculate the forces, were major changes. Two subroutines are called from GUNLD: IBFORC, which calculates the nonlinear forces on the gun tube produced by the projectile motions, Bourdon effects, and axial accelerations; and SUPR, which calculates the tube-support interaction forces. Additional subroutines are called from IBFORC and SUPR.

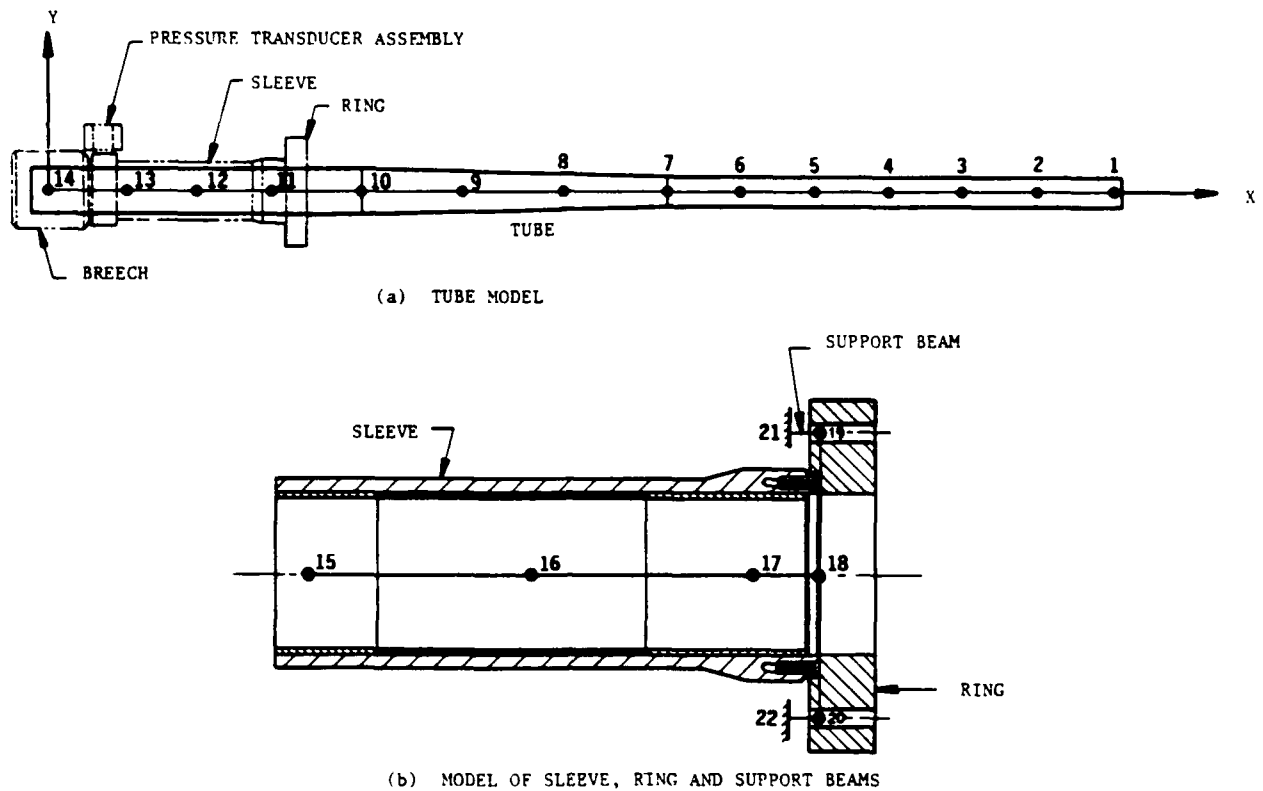


Figure 1. Finite Element Model of the SwRI Gun

They are:

```

IBFORC.....PROMO
              FAB
              FLAGR

SUPR.....FLTS
    
```

Descriptions of subroutine GUNLD, and the subroutines called from GUNLD to calculate the nonlinear gun dynamic forces are given by Cox and Polcyn [3].

NASTRAN 2-D CALCULATIONS

Modifications were made to NASTRAN in two steps. First a two-dimensional version was developed: i.e. the subroutines added to calculate the gun dynamics forces were two-dimensional. Calculations were made with the 2-D version of NASTRAN for comparison with earlier results obtained with the program GUN2D[4,5]. The gun model used for these calculations (Figure 1) was the 1/5.25th scale model of the 105 mm M68 tank gun previously tested and

analyzed by Cox and Hokanson[4]. Excitation to the model was provided by measured breech pressure and calculated projectile axial motions. Projectile axial motions were calculated from the measured breech pressure and were consistent with measured time and velocity at projectile muzzle exit. Certain model parameters were held constant in all 2-D calculations. They were:

- no gravity droop
- clearances at the tube supports
- contact stiffness values
- initial tube curvature in the x-y plane
- tube offsets from the support center line at the support points

Small Breech Mass Eccentricity

Calculations were performed with NASTRAN to duplicate earlier GUN2D results. In addition to the model parameters listed above, the following program features were constant in these calculations:

- unbalanced breech force applied in its instantaneous direction
- no balanced breech forces
- no Bourdon forces
- axial acceleration effects based on initial tube position only

NASTRAN results were computed for an integration time step of 0.0000025 sec; whereas, GUN2D results were computed with an integration time step of 0.000005 sec out to 1.0475 ms and 0.0000025 sec thereafter. GUN2D has an automatic time step reduction feature; whereas, COSMIC NASTRAN does not.

Figure 2 compares the tube lateral displacements at the muzzle. There are slight variations in the signature of the displacements, but the magnitudes differ by less than 5% at all points in time out to muzzle exit (approximately 1.75 ms). Tube recoil, compared in Figure 3, gives differences less than 0.04%. Finally, Figure 4 shows the impact forces at the front support computed by the two programs. The magnitudes are similar except for the first large negative spike that occurs in the NASTRAN results. When this spike is neglected, the other spikes (caused by interaction between the tube and the support), are in good agreement in time and in fair agreement in magnitude. Relative to the GUN2D values, the spike at 1.0 ms is +14% higher in the NASTRAN results and the spike at 1.14 ms is 14% lower in the NASTRAN results.

Varying the integration time step produced some interesting changes in the support reaction forces. Figure 5 shows the effects of larger time steps on the front support reaction. Doubling the time step to 0.000005 sec. changed the magnitude of the spikes. Doubling it again to 0.00001 sec changed the magnitude even further and caused the first spike to reverse in sign. We now believe that the integration time step may have been too large in GUN2D (with the integration scheme used) to properly resolve the initial spikes in the interaction forces; however, we doubt that the contact forces at the

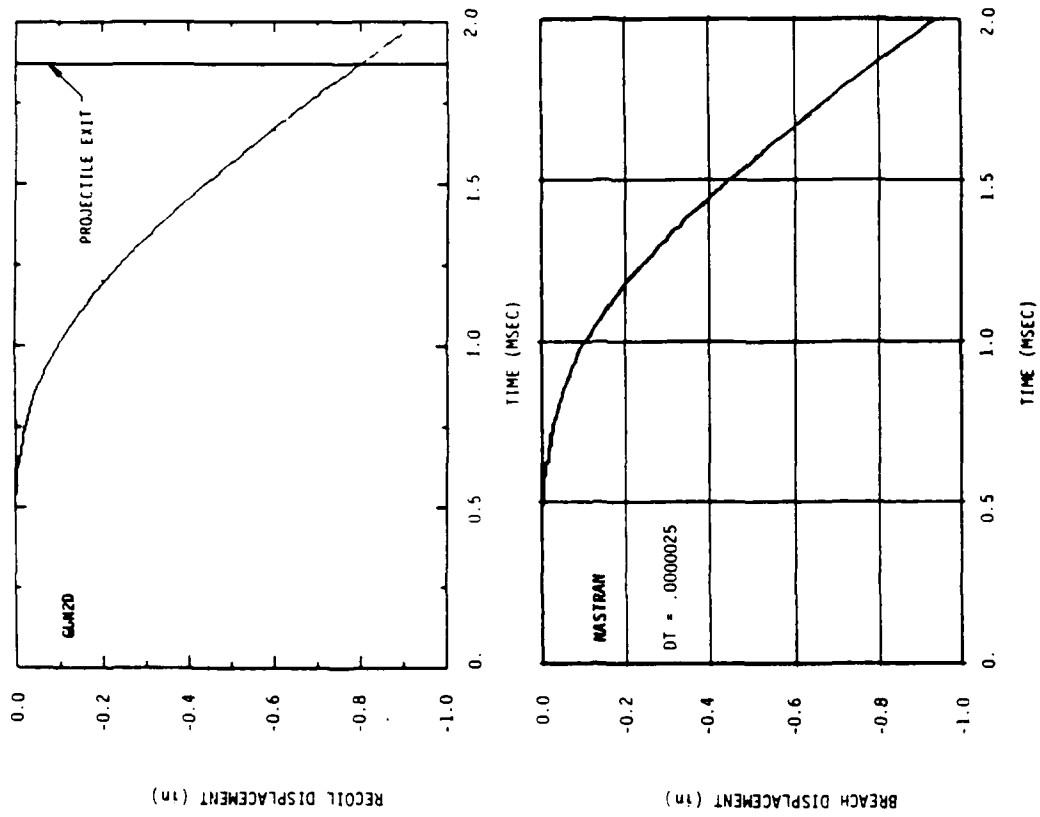


Figure 2. Comparisons of Muzzle Displacements

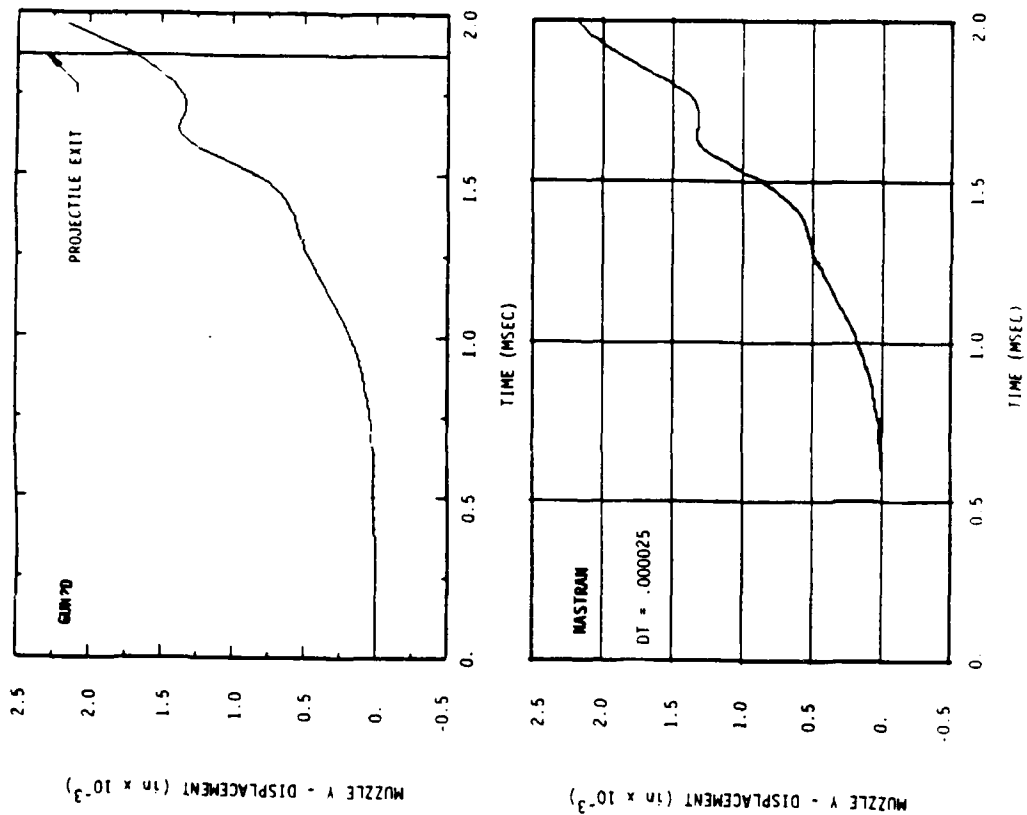


Figure 3. Comparisons of Tube Recoil

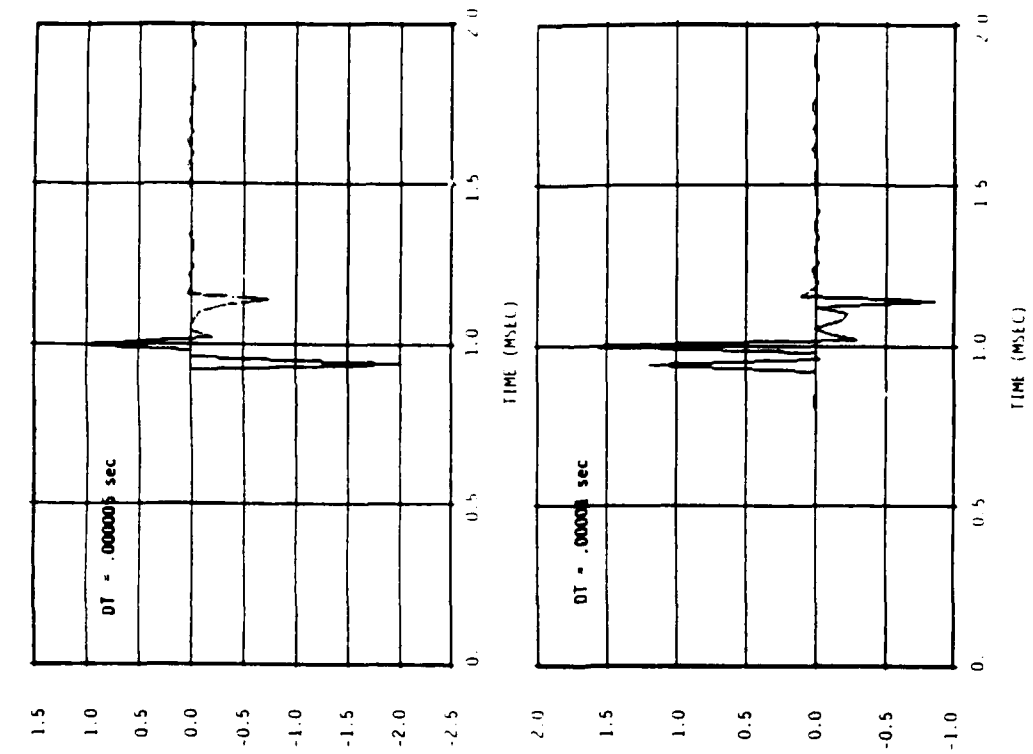


Figure 4. Comparisons of the Front Tube Support Reaction Forces

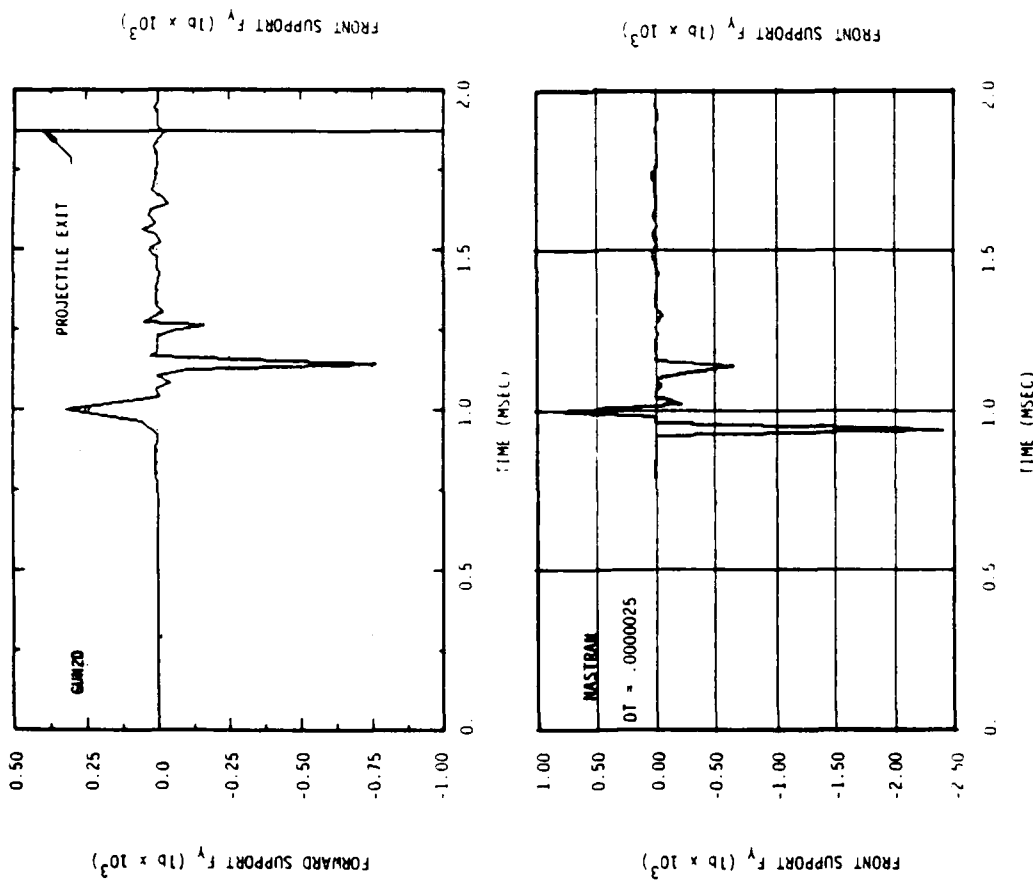


Figure 5. Effect of the Integration Time Step on NASTRAN Forces at the Front Tube Support

supports will ever agree closely. They are too sensitive to the integration scheme used by the programs and to the integration time step. The effect on muzzle displacements produced by changing the time step were small. Only subtle differences were apparent in the displacements for the three different time steps investigated. As would be expected, the differences in the recoil motions were even less.

Large Breech Mass Eccentricity

Tube motions were calculated with NASTRAN for a large breech mass eccentricity. These calculations were made with the same model except that:

- the positive breech mass eccentricity was increased from 0.0145 inches to 0.1752 inches
- the tube was straight (initial curvature removed)

Muzzle displacements obtained with NASTRAN and GUN2D are given in Figure 6. The signatures are similar, but peak displacements differ by 20 %. Although the differences are larger than we expected, we could not attribute them to input errors. As for the comparisons with a small breech mass eccentricity, we believe that different numerical solution procedures account for most of the differences that we have observed between NASTRAN and GUN2D.

NASTRAN 3-D CALCULATIONS

Once the three-dimensional gun dynamics forces had been added to NASTRAN, calculations were made for comparison with the two-dimensional results. The comparisons were made to examine the differences that are produced by three-dimensional versus two-dimensional modeling. In addition, calculations were made to show the effects produced by modeling the breech forces in different ways, adding Bourdon forces to the code, and adjusting the lateral loads produced by the tube axial accelerations as the tube displaces from its initial position. Calculations were also made for the Watervliet Arsenal 30 mm gun based on information provided in Reference 6. Results for the Watervliet model will not be addressed in this paper because they are not of general interest, but they are available in Reference 3.

The gun model used for the 3-dimensional calculations was the same as for the two-dimensional model, except that curvature and tube offsets from the supports were added in the x-z plane for some of the calculations, and the physical descriptions of some parts of the model are slightly different in 3-dimensions than in 2-dimensions. This was particularly true in the mounting structure for the sleeve. For this reason, exact correlation was not expected between the 3-dimensional and 2-dimensional results even when we attempted to make all loading and model parameters the same in both calculations.

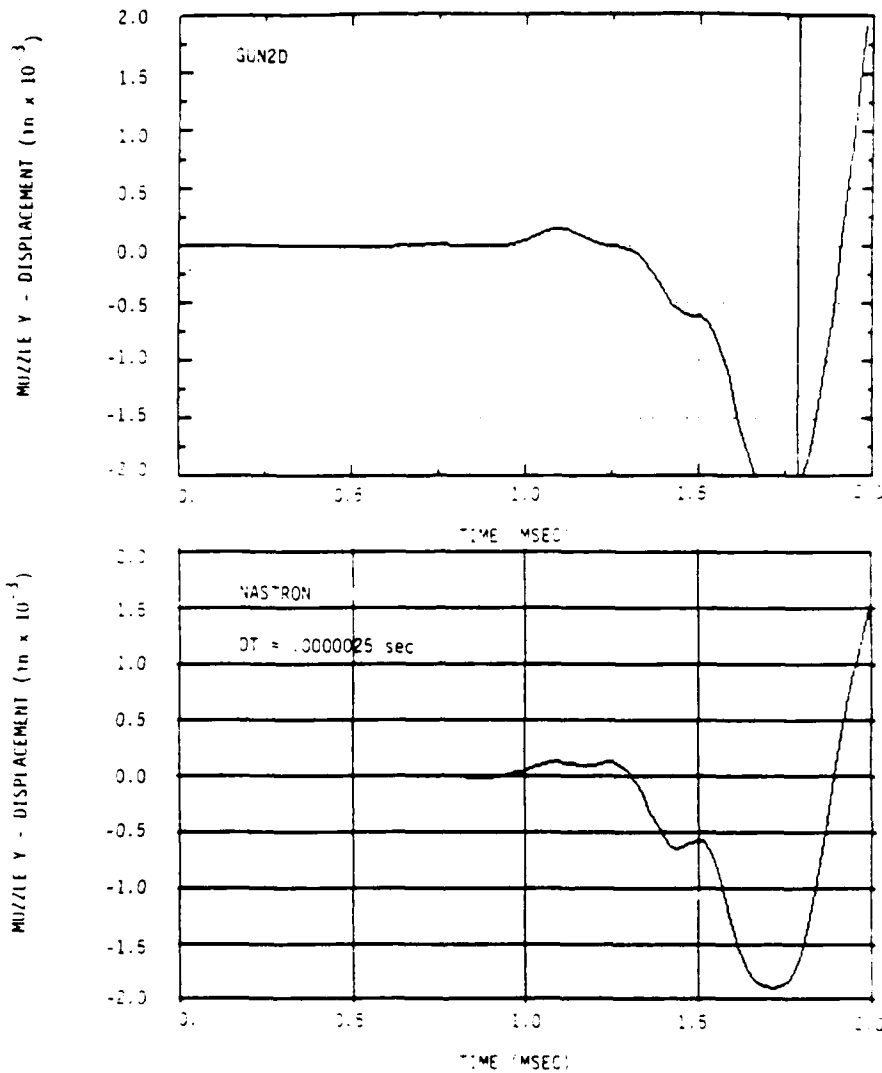


Figure 6. Muzzle Displacements for a Straight Tube and a Breech Mass Eccentricity of 0.1752 Inches Above the Tube Axis

Results with the 2-D Gun Model

Figures 7 and 8 show the results obtained in 3-D calculations when only x-y curvature and y-offsets of the tube from the supports, are included. Figure 7 gives muzzle y-and z-displacements and Figure 8 gives the front tube support interaction forces in the y and z planes. By comparison with the results in Figures 2 and 4, we see that the results are only slightly changed. This is to be expected since there is very little excitation in the x-z plane for this case. The differences in the vertical (y) direction are due to the fact that the 2-D and 3-D models of the gun are not exactly the same.

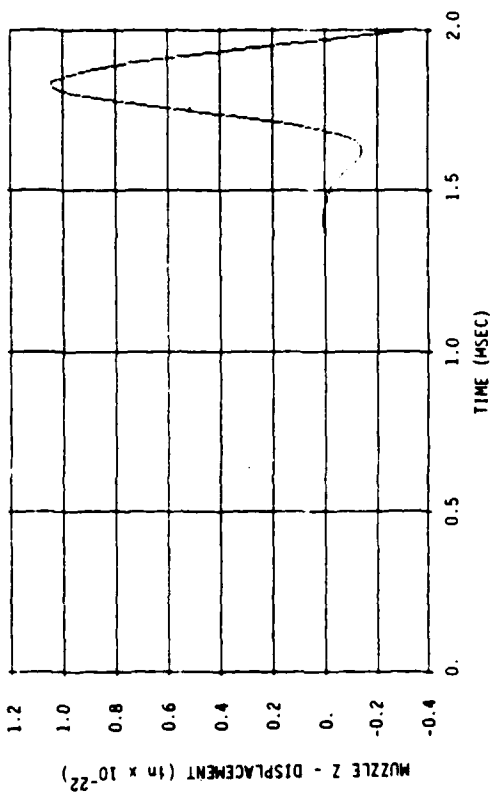
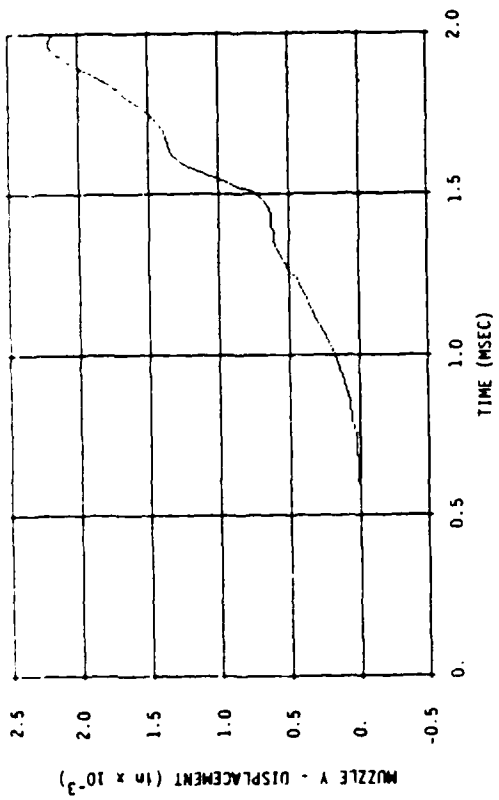


Figure 7. Muzzle Displacements: 3-D Gun Model with Initial Curvature and Tube Offsets at the Supports in the X-Y Plane

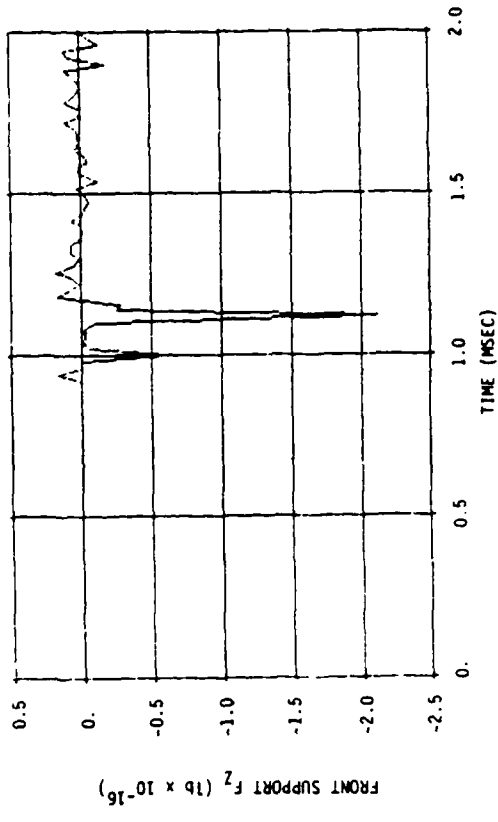
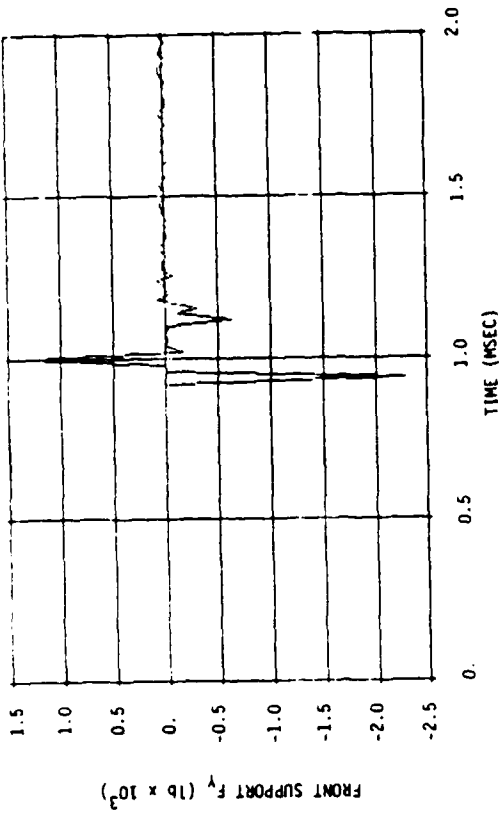


Figure 8. Front Support Reactions: 3-D Gun Model with Initial Curvature and Tube Offsets in the X-Y Plane

Results with a 3-D Gun Model

Introducing curvature and tube offsets at the supports in both the x-y and x-z planes (a realistic 3-D model) gives the results in Figures 9 and 10. For this case sharply increased displacements are observed in the x-z plane. In addition, the x-z motions have affected motions slightly in the x-y plane as seen by comparing Figures 9 and 10 with Figures 7 and 8. While the differences are not great, there is obviously some cross coupling between the two planes, produced by torsion and by interactions at the supports. For a rifled barrel, the cross coupling should be greater because of the contribution of gyroscopic moments from the spinning projectile.

A Look at Different Breech Force Models

Because breech forces provide strong excitation to the gun, the way they are modeled can be important. In GUN2D, only the unbalanced breech force was applied to the tube, and it was applied in its initial direction throughout the calculation. There is clearly a balanced force that acts in the breech region also. It acts over an area equal to that of the breech face less the minimum area of the bore. While it does not contribute to the tube recoil, it acts to stretch the tube in the chamber region. In addition, as the tube moves during firing, the instantaneous direction of the breech forces change.

Three-dimensional calculations were made with NASTRAN to examine the effects on tube response of modeling the breech forces in different ways, namely,

1. unbalanced breech force in a fixed direction
2. unbalanced breech force in its instantaneous (variable) direction
3. unbalanced and balanced breech forces acting in their instantaneous directions.

The calculations revealed that the three different methods of modeling the breech force changed the muzzle displacements by less than 1% in the plane of primary response. In the lateral plane, displacements were initially insignificant (less than 1×10^{-20} inches). The percentage changes in this plane were higher, but the displacements remained insignificant. Support reaction forces showed similar changes. Complete results are given in Reference 3.

Bourdon Forces and Axial Acceleration Effects

Bourdon forces and axial acceleration effects were found to be small in two-dimensional calculations by Cox and Hokanson[4]; however, for completeness, the forces produced by these effects were added to NASTRAN, and their effects in three-dimensional calculations were examined. The gun model used for the calculations was the same as used in the breech force study and both balanced and unbalanced breech forces were applied.

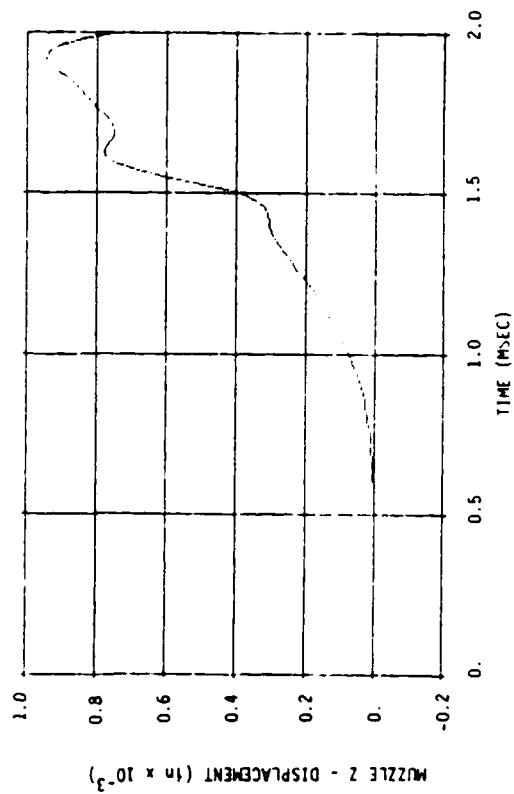
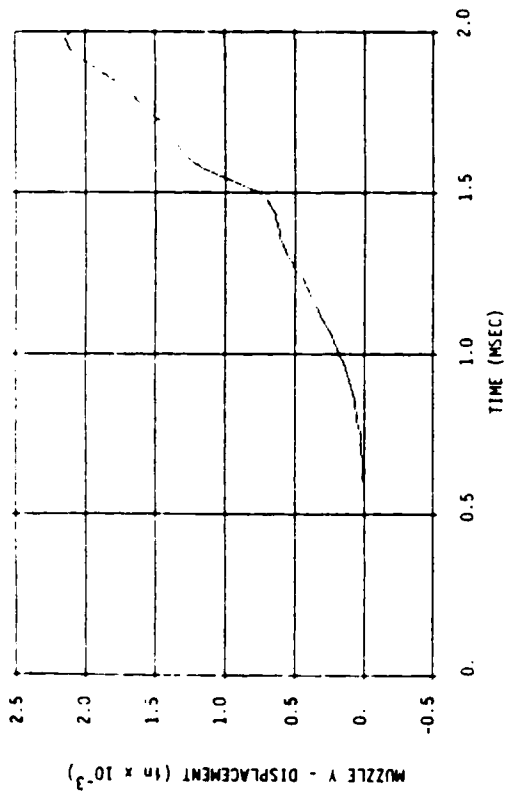


Figure 9. Muzzle Displacements: 3-D Model with Initial Curvature and Tube Offsets at the Supports in the X-Y and X-Z Planes

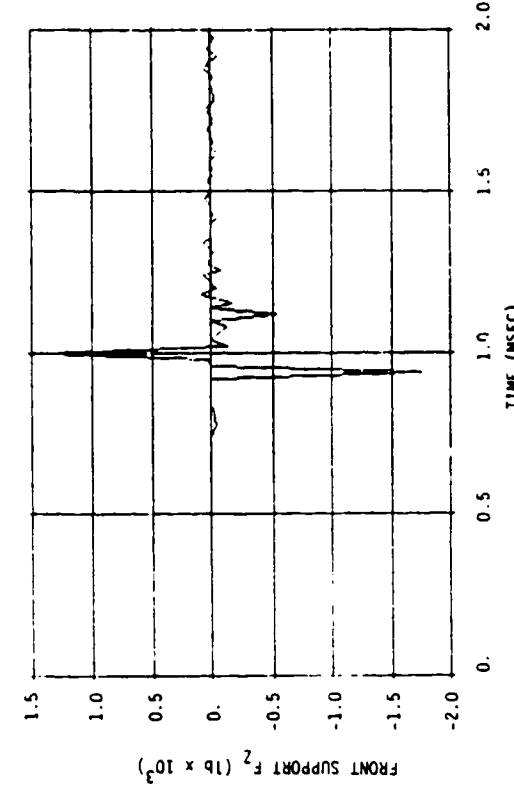
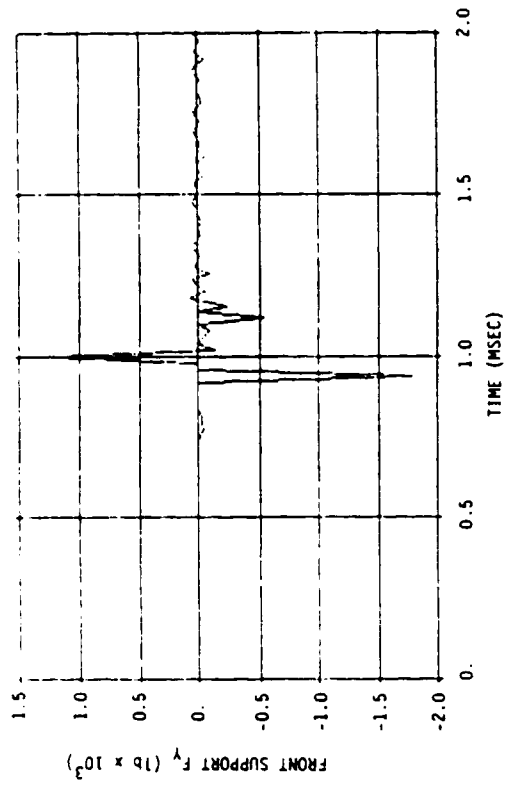


Figure 10. Front Support Reactions: 3-D Model with Initial Curvature and Tube Offsets at the Supports in the X-Y and X-Z Planes

Bourdon Forces--Bourdon forces are those created by internal pressure on a curved tube that act to straighten it. In a gun tube these forces are a function of the breech pressure, and they act from the breech face to the aft rotating band on the projectile. NASTRAN calculations were made with and without Bourdon forces to examine their effect on the tube response. As for the breech models, only slight differences could be detected in the principal muzzle displacements or support reaction forces [3]. The changes were less than 1%.

Axial accelerations--Axial accelerations (along the x-axis), when coupled with lateral displacements (from the x-axis), create forces that act to return the tube to the x-axis. Thus, the effect of axial accelerations is to lift the muzzle of a drooped tube. This effect can be accounted for by putting initial tube curvature or droop in the gun model as initial displacements from the x-axis. However, the "axial acceleration effects" are constant throughout the calculation, unless tube displacements from the initial position are accounted for in their calculation.

Adjustments to the axial acceleration forces were added to NASTRAN to examine the effects of these forces on the tube behavior. The differences were insignificant for both displacements and forces in the plane of the primary response. Although minor changes in the signature of the displacements were detectable, the differences were less than 1%. Complete details are given in Reference 3.

USER'S GUIDE TO THE NEW PROVISIONS

Modeling Requirements

Standard NASTRAN input cannot fully describe a model for gun motion analyses. Additional information concerning the gun tube, the projectile, friction between the projectile and the gun tube, and tube support parameters is also required, and is input using the Direct Table Input (DTI) provision in NASTRAN. The sections which follow describe the input requirements and model limitations. A detailed description of the format for the NASTRAN data cards is not provided in this report; the user should refer to the NASTRAN User's Manual[1]. Any set of consistent units can be used, but in English units mass must be expressed as weight divided by gravity.

Geometry

The model geometry is input using the standard NASTRAN input provisions. Data cards required and limitations to the model are as follows:

- **GRID cards** - to define nodal points of the model. Grid point 1 must be at the muzzle and grid point numbers must increase uniformly and monotonically toward the breech. Grid points of the supports and other attachments follow the breech node. The muzzle must lie at

the more positive end. Due to array dimensions, the model is limited to 200 degrees of freedom and 40 grid points. These limits may be increased by increasing the dimensions of arrays f, d, v, a, sili, silj, am, od, ood, ipp, iqq, x1, x2, x3, and itt. Directions for modifying the code are presented in a later section.

- **MAT1 card** - defines material properties of the gun tube.
- **PBAR and CBAR cards** - defines element connectivity and stiffness properties. Only BAR elements may be used to describe the gun tube. Element 1 must be closest to the muzzle and element numbers must increase uniformly and monotonically toward the breech. Due to array dimensions, the model is limited to 40 elements. This may be increased by increasing the dimensions of arrays aj, ey, sk, ri, ro, and cphi.

Masses

Nodal masses are input using CONM2 cards. Breech mass eccentricities are also input on these cards. Because masses are read directly from the generated mass matrix, it should be possible to use the CONM1 cards or to allow generation of the mass matrix by specifying a mass density on the MAT1 card. Use of the later approach will require the use of one of the concentrated mass cards to define breech mass eccentricity. Although these alternate approaches have not been tested, no problems are expected.

Time Dependent Forces

The nonlinear gun tube forces are calculated in the program. However, the breech force is input with the NASTRAN dynamic load input capabilities using TLOAD1, DLOAD, DAREA, and TABLE1 cards. The breech force input should be calculated as the internal pressure multiplied by the breech area and should be directed toward the breech (the force should be negative). The modified program will adjust this force by applying lateral forces so that the actual breech force is applied in the instantaneous direction of the breech. Also, the force at the breech will be offset by balancing forces acting in the positive direction in the breech region.

Nonlinear Forces

Specialized input is required to compute the nonlinear gun dynamics forces in the modified version of NASTRAN. These data are input using the Direct Table Input (DTI) provision. The following additional data are required:

Gun tube parameters

- E and G --- elastic and shear moduli of the tube
- twist ----- tube rifling

- pload ----- preload of the recoil spring on the recoiling parts.
- jnbrch ---- external node number of the breech
- jnpld ----- external node number of the preload application point
- iradflag -- flag turning tube radial expansion on/off (1/0)
- ibourd ---- flag turning Bourdon forces on/off (1/0)
- iaxacc ---- flag turning axial acceleration forces on/off (1/0)
- ri(i) and ro(i) - inside and outside radii of the gun tube at element i. The radii must be input beginning at element 1 and increasing uniformly and monotonically.

Projectile parameters

- rbrch - inside radius at breech
- xmp --- projectile mass
- xjmp -- projectile rotary inertia about the spin axis
- zjmp -- projectile pitching inertia about the c.g.
- ecc --- eccentricity of the projectile mass from the tube centerline
- bzero - initial angular position of the mass eccentricity
- xcg --- initial position of the projectile c.g. along the tube
- ydsp, xdsp - displacement-time pairs for projectile travel along the tube (up to 100 pairs)
- yvel, xvel - velocity-time pairs for projectile travel along the tube (up to 100 pairs)
- yacc, xacc - acceleration-time pairs for projectile travel along the tube (up to 100 pairs)

Friction parameters

- vc, r - parameters in the projectile-tube friction equation
- grav -- gravity constant
- fcoef - constant friction coefficient
- pcoef - constant for computing projectile base pressure
- yfrf, xfrf - friction-displacement pairs for displacement dependent friction (up to 100 pairs)

Tube support parameters

- jsp - external node number of support
- clr - radial tube-to-sleeve clearance at the supports
- y0 -- initial y-offset of the tube relative to the centerline of the supports
- z0 -- initial z-offset of the tube relative to the centerline of the supports
- fs -- viscous damping coefficient at the supports
- ac, bc - constants in the contact force-reaction equations for the supports

Job Control

Data cards must be included in the data deck to control the analysis. These include cards for output requests, plotting requests, load case selection, constraint selection, and time step selection. Most of these cards are in the case control deck. Also, input must be included to perform the DMAP ALTER's which include the modifications to NASTRAN to perform gun dynamics analyses. These cards are described in detail in the following section. For a complete discussion of case control in NASTRAN, the user should refer to the NASTRAN User's Manual.

Data Card Descriptions and Formats

The input using standard NASTRAN data cards will not be described in this users guide; rather, the user should consult the NASTRAN User's Manual. In this section, the cards used to utilize the DMAP ALTER's which modify NASTRAN for gun dynamics problems will be described in detail. Also, the format of the DTI cards which must be used will also be described. Sample input decks are provided in Reference 3.

DMAP ALTER's

In order to use NASTRAN for solving gun dynamics problems, alterations must be made to rigid format 9. One DMAP ALTER must be included to gather the necessary data. A second alter must be used to replace the transient solution module (TRD) with the modified version of TRD (DUMMOD1). The following data cards must be included in the executive control deck for each problem being solved:

```

APP      DISPLACEMENT
SOL      9.0
ALTER    55
DUMMOD2  EQEXIN, USET, GPDT, EST, , , , /SWRI1, , , , , / , , , , , $
DUMMOD3  SWRI1, GUNTUBE, PRJCTL, FRICT, TUBSUP, , , /SWRI2, , , , , / , , , , , $
ALTER    125, 125
DUMMOD1  CASEXX, TRL, SWRI2, DIT, KDD, BDD, MDD, PD/UDVT, PNLD, , , , ,
NOE, NONCUP, NCCL, ISTART, , , *DIRECT* , , , $
ENDALTER
    
```

The APP and SOL cards call the proper rigid format (RF 9) to perform a transient dynamic analysis. The remaining statements modify the rigid format for gun dynamics problems. The ALTER 55 card inserts the DUMMOD2 and DUMMOD3 modules into rigid format 9 after line 55. DUMMOD2 gathers the standard NASTRAN input data from data blocks EQEXIN, USET, GPDT, and EST and writes the required data to a data block named SWRI1. DUMMOD3 gathers the data from SWRI1 and writes this data and the data input with the DTI cards to another data block named SWRI2. Note that the data input with the DTI cards is stored in data blocks named GUNTUBE, PRJCTL, FRICT, and TUBSUP. The ALTER 125, 125 card replaces the standard NASTRAN module TRD with the modified module (named

DUMMOD1). The data block names, GUNTUBE, PRJCTL, FRICT, TUBSUP, SWRI1, and SWRI2, may be any name so long as the name is used in a consistent manner from the DTI cards to the above DMAP ALTER cards.

Direct Table Input

Four data blocks are generated using the Direct Table Input (DTI) capabilities of NASTRAN. These data blocks contain additional information describing the guntube (named GUNTUBE), the projectile (named PRJCTL), guntube-projectile friction (named FRICT), and the tube support conditions (named TUBSUP). The names of the data blocks may be any name as long as they are used in a consistent manner throughout the input data.

All input data cards, including the DTI cards, have ten, eight character fields per line. Each set of DTI cards contains the input for a single data block. The first field for each DTI card contains the word "DTI", and the second field contains the name of the data block. The first card for each data block is a header card. The third field of this card contains a zero (0) and the fourth field contains the number of logical records in the data block. Following this card, one card (which may be one or more lines if required) is given for each record. The third field contains the record number and the remaining fields contain the data. Fields one and ten are used to indicate that the card is continued on a following line.

The formats for the DTI cards required for the modified version of NASTRAN are given in Table 1. The symbol, +***, is used to tie cards together which must be continued on more than one line. The symbol must be unique for each pair of lines which must be continued. The procedure for Direct Table Input is discussed in detail in the NASTRAN User's Manual[1].

Procedures For Including Modifications to Nastran

In order to run the modified version of NASTRAN, the new and modified subroutines must first be incorporated into the executable version of NASTRAN. Portions of this procedure must also be followed in order for the user to include additional changes to the code. Compiling and linking the NASTRAN computer code is accomplished by running two of several command files which are provided with the NASTRAN package. The files of interest are RECOMP.COM and LINK07.COM.

RECOMP.COM is used to compile the modules which consist of the modified subroutines to be included in the NASTRAN code. The .OBJ files which are created are included into the NASTRAN object library, NASTRAN.LIB. The

Table 1. Format for DTI Cards

DTI +***	GUNTUBE ENDREC	0	2							+***
DTI +***	GUNTUBE iradflag	1	e	g	twist	pload	jnbrch	jnpld		+***
DTI +***	GUNTUBE ri(3)	2	1	ri(1)	ro(1)	2	ri(2)	ro(2)		+***
+***	...	ro(3)	ri(4)	ro(4)	ri(5)	ro(5)	ri(6)	ro(6)		+***
+***	(repeat as necessary)				+***
+***	...	i	ri(i)	ro(i)	ENDREC					
DTI +***	PRJCTL ENDREC	0	4							+***
DTI +***	PRJCTL xcg	1	rbrch	xmp	xjmp	zjmp	ecc	bzero		+***
DTI +***	PRJCTL ydsp(4)	2	ydsp(1)	xdsp(1)	ydsp(2)	xdsp(2)	ydsp(3)	xdsp(3)		+***
+***	...	xdsp(4)	ydsp(5)	xdsp(5)	ydsp(6)	xdsp(6)	ydsp(7)	xdsp(7)		+***
+***	(repeat as necessary)				+***
+***	ydsp(i)	xdsp(i)	ENDREC					
DTI +***	PRJCTL yvel(4)	3	yvel(1)	xvel(1)	yvel(2)	xvel(2)	yvel(3)	xvel(3)		+***
+***	...	xvel(4)	yvel(5)	xvel(5)	yvel(6)	xvel(6)	yvel(7)	xvel(7)		+***
+***	(repeat as necessary)				+***
+***	yvel(i)	xvel(i)	ENDREC					
DTI +***	PRJCTL yacc(4)	4	yacc(1)	xacc(1)	yacc(2)	xacc(2)	yacc(3)	xacc(3)		+***
+***	...	xacc(4)	yacc(5)	xacc(5)	yacc(6)	xacc(6)	yacc(7)	xacc(7)		+***
+***	(repeat as necessary)				+***
+***	yacc(i)	xacc(i)	ENDREC					
DTI +***	FRICT ENDREC	0	2							+***
DTI	FRICT	1	vc	r	grav	fcoef	pcoef	ENDREC		
DTI +***	FRICT yfrf(4)	2	yfrf(1)	xfrf(1)	yfrf(2)	xfrf(2)	yfrf(3)	xfrf(3)		+***
+***	...	xfrf(4)	yfrf(5)	xfrf(5)	yfrf(6)	xfrf(6)	yfrf(7)	xfrf(7)		+***
+***	(repeat as necessary)				+***
+***	yfrf(i)	xfrf(i)	ENDREC					
DTI +***	TUBSUP ENDREC	0	2							+***
DTI +***	TUBSUP ENDREC	1	cir(1)	y0(1)	z0(1)	fs(1)	ac(1)	bc(1)		+***

Polcyn and Cox

```
DTI      TUBSUP      2  clr(2)  y0(2)  z0(2)  fs(2)  ac(2)  bc(2)  +***  
+***      ENDREC
```

NOTE: Spaces between lines are for clarity only and are not used in the actual input deck.

modules and corresponding subroutines which contain the modifications are as follows:

<u>Modules</u>	<u>Subroutines</u>
DUMMOD2	DUMOD2 SWRIIN2
DUMMOD3	DUMOD3 SWRIIN1
DUMMOD1	DUMOD1 TRD1AS TRD1CS GUNLD IBFORC PROMO FLAGR SUPR FLTS FAB

The new and modified subroutines are described in Reference 3 RECOMP.COM must be run for each of the above modules.

The executable for NASTRAN consists of 15 executable files, NAST01 through NAST15. Therefore, there are 15 command files which must be run to link the entire code. The modifications to the code are contained only in NAST07.EXE. To include the modifications in the code, only one of the command files must be run, namely LINK07.COM.

CONCLUSIONS AND RECOMMENDATIONS

The conclusions from this work are:

1. It is feasible to modify NASTRAN to include the calculation of the nonlinear forces in gun dynamics problems.
2. The modifications made to NASTRAN permit the solution of gun dynamics problems by inputting to the program the physical

Polcyn and Cox

- parameters of the gun and projectile and the forcing functions.
3. Input for gun dynamics problems is easily accomplished using standard NASTRAN input provisions.

We recommend that the work be continued, with the goal of having a rigid format in NASTRAN accepted by COSMIC for gun dynamics problems. To accomplish this goal will require improvements to the present code, to include, for example, a better projectile model and the removal of some of the current input restrictions. In addition, the code must be carefully checked and used successfully by other members of the gun dynamics community.

REFERENCES

1. "The NASTRAN User's Manual," NASA SP-222(07), June 1985.
2. Simkins, T.E., "Transverse Response of Gun Tubes to Curvature-Induced Load Functions," Proceedings of the Second U.S. Army Symposium on Gun Dynamics, held at The Institute of Man and Science, Rensselaerville, NY, 19-22 September 1978.
3. Cox, P.A. and Polcyn, M.A., "The Adaptation of NASTRAN for Three-Dimensional Gun Dynamics Problems," prepared for the Benet Weapons Laboratory, U.S. Army Research and Development Center, by Southwest Research Institute under Contract No. DAAA22-B6-C-0200, September 1987.
4. Cox, P.A. and Hokanson, J.C., "The Influence of Tube Support Conditions on Muzzle Motions," Final Report, prepared for the U.S. Army Research Office by Southwest Research Institute under Contract No. DAAG29-79-C-0037, SWRI Project 02-5622, August 1982.
5. Cox, P.A. and Hokanson, J.C., "Muzzle Motions of the M68 105mm Tank Gun," Contract Report ARBRL-CR-00418, prepared by Southwest Research Institute, San Antonio, Texas, March 1980.
6. Letter from G. Albert Pflieg1, Benet Weapons Laboratory, Watervliet Arsenal, to P.A. Cox, Southwest Research Institute, dated 7 July 1987.

PENNY, PERRY

TITLE: AN ACCOUNT OF SOME EXPERIMENTS UNDERTAKEN TO CORRELATE MEASURED GUN BARREL FEATURES WITH THE MOVEMENT OF SERIAL MEAN POINTS OF IMPACT.

F H G PENNY and J A PERRY

ROYAL ARMAMENT RESEARCH AND DEVELOPMENT ESTABLISHMENT
CHERTSEY, SURREY, KT16 0EE, UNITED KINGDOM.

ABSTRACT:

For many years now the results of gunnery trials have shown that movements of the Mean Point of Impact of ammunition serials can be correlated with changes to major mechanical items within the weapon system. With the earlier types of kinetic energy projectile the ballistic dispersion was sufficiently large that movements of serial Mean Points of Impact, due to equipment changes, were often masked by the general movement of the MPI due to serial differences in the dispersion pattern.

With the introduction of the fin stabilised type of kinetic energy ammunition, the inherent ballistic dispersion has been significantly reduced, amongst other factors, and the variability of the Mean Point of Impact introduced due to physical changes to the gun system mechanics, now has a discernable effect on gun system accuracy. The manner in which parts of the gun system contribute toward a system bias is obviously of interest since improvements to gun accuracy could be obtained. Recent firing results indicate that changes to specific features of the gun barrel can have considerable effects. A limited firing programme was authorised in order to confirm these reported effects.

The paper describes the results of firing trials from a tank and a firing stand for four gun barrels selected from British Army use. The barrels were selected as covering the range of variability experienced by the Army whilst 'shooting-in' nearly five hundred tanks. The barrel parameters chosen for investigation were bore straightness and concentricity with the external diameter. The paper explains the methods used for barrel measurement and details the experimental procedures and measurements taken during the firing trials from both the tank and firing range stand. A comparison between the features measured from the four selected barrels and the significance of the movements in serial Mean Points of Impact is made and the basis of further full scale firing experiments discussed.

BIOGRAPHY:

PRESENT ASSIGNMENT: MBT Weapon Systems Division, RARDE (Chertsey),
Surrey, KT16 0EE, UK.

DEGREES HELD: BSc, PhD - City University, London, UK.

Copyright (C) Controller, Her Majesty's Stationery Office,
London 1987.

PENNY, FERRY

AN ACCOUNT OF SOME EXPERIMENTS UNDERTAKEN TO CORRELATE
MEASURED GUN BARREL FEATURES WITH THE MOVEMENT OF SERIAL
MEAN POINTS OF IMPACT

P H G Penny and J A Ferry
Royal Armament Research and Development Establishment,
Chertsey, Surrey, KT16 0EE, United Kingdom.

1. INTRODUCTION

The variability of gun barrel droop has been recognised as a source of tank gun inaccuracy since 1944; however, the first serious attempt to relate the dynamic behaviour of the gun to tank gun accuracy in the United Kingdom was initiated in 1962. The 'PRODIGAL' series of trials used modified 105mm L7 tank guns to investigate the effects of different cradle bearings and cradle bearing positions. Although the 'PRODIGAL' trials used straightforward analysis methods and had relatively simple instrumentation equipment, they did reveal that attention to the mounting arrangements could improve accuracy and reduce the variability of gun jump. They also emphasized that the gun and its mounting should be considered as a single system.

Little further gun accuracy work was undertaken until the 'GIFT-HAT' series of trials were initiated in 1971. These trials used the 120mm L11 tank gun and a spin stabilised APDS kinetic energy projectile. The trials revealed that high maintenance standards were necessary for a gun system to remain repeatably accurate and a number of parameters were shown to contribute toward the variability of gun jump; in particular, barrel droop and elevation system backlash, stiffness and friction [1]. In addition, the APDS shot for the later trials was modified to improve sabot separation and this further reduced dispersion at the target.

It was appreciated that an understanding of the dynamics involved with gun firing could aid the development of the gun system and could improve future tank guns. Instrumentation began to be developed for measuring gun system variables close to the muzzle and a programme of analysis was initiated that has resulted in the computer simulation programs 'RAMA' and 'SHOCK-AID'.

2. CURRENT SITUATION

There are two common ways of equipping a tank fleet with a new gun or ammunition system. The first, and preferred method, is to be able to fit any gun to any tank

PENNY, PERRY

without loss of accuracy or the need to 'shoot-in'. This is known as adopting a 'fleet zero'. This method also allows the gun to be fired in reversionary modes without loss of accuracy. The second method, operationally acceptable but possibly expensive, is to characterise the barrel after manufacture and to feed the characterising parameters of the barrel into the fire control system on installation: 'Shooting-in' is one such method of characterisation. Unfortunately, if this procedure is adopted reversionary firing modes using ballistic graticules become more complicated or less accurate.

The United Kingdom, in common with a number of other nations, started using a fin stabilised kinetic energy projectile a few years ago. Analysis of the data from the ten barrels used for the Range and Accuracy trials for this projectile, showed what was considered to be an unacceptable spread of serial Mean Points of Impact (MPI's). This was particularly marked in the vertical plane and it was considered that, if these ten barrels were typical of production, the UK would have to start to 'shoot-in' each tank with a serial of ammunition. The situation was reassessed after approximately one hundred tanks had been 'shot-in'. This confirmed the range of MPI's in both line and elevation and the necessity of continuing to 'shoot-in' UK tanks. A scatter plot of the Commission Firing MPI's for approximately six hundred UK tanks is shown in Figure 1.

A decision to investigate the apparent problem of variable accuracy was made and it was proposed that a solution be sought such that a 'fleet zero' could, once again, be applied to UK tank guns.

3. EXPERIMENTAL PROGRAMME

For the initial phase of the programme it was decided that four barrels would be selected from the Commissioned tank fleet of the British Army of the Rhine (BAOR), and that these barrels would be chosen on the basis of MPI's near the extreme edge of the scatter plot shown in Figure 1, (one from each quadrant). In addition, the tanks had to have had no further major work undertaken on them since being Commissioned. Those barrels selected are shown in Figure 2. The barrels were to be re-fired in BAOR to confirm their behaviour before being removed from the tank and sent back to the UK for detailed measurement. Following measurements for straightness and wall thickness variation undertaken by the Defence Quality Assurance Product Support Division at Woolwich Arsenal, the barrels were to be range fired first from another tank and then from a firing stand.

PENNY, PERRY

It was argued that if the variable accuracy was due to the barrel, then this should generally be repeated in different installations and that we ought to be able to correlate some physical barrel parameter(s) with the relative positions of the MPI's. In addition, if we were then able to account for these parameters within our computer simulation programs we could recommend measurement or manufacturing changes which could possibly reduce the variability experienced. A companion paper by Powell and Penny details some of the analytical work [2].

Since the initial firing on Phase 1 of the programme was to be undertaken fairly quickly little instrumentation was used. The trial confined itself to careful measurement of the existing equipment, careful control of the build of each installation and a closely written trials specification. A later Phase 2 of the programme was to carry more instrumentation and special hardware.

4. MEASUREMENT AND ANALYSIS

When the barrels were refired in order to confirm their behaviour, it was noted that the MPI's had shifted considerably, (see Figure 2). Before the trials in the UK commenced the barrels were carefully measured for straightness and wall thickness variation according to standard UK procedures [3]. The results are given in Tables 1 to 4 and polar plots of barrel straightness and wall thickness variation are shown in Figures 3 and 4. The angular measurements recorded in the UK have been converted into linear measurements more common in the United States. The sign convention applied to the data is given with the tables and, with regard to the wall thickness variation measurements, it should be emphasized that the measurements were taken over the standard thermal paint finish.

The repeatability of the wall thickness measurements is within 0.1mm whilst, from previous experience, the variability of the paint thickness is typically less than 0.1mm. It can be seen that even if the errors are considered to be cumulative, barrel NG6654 undoubtedly has an eccentric bore. Indeed an eccentricity of this magnitude has not been recorded before!

With regard to the barrel straightness measurements, the readings are subject to an overall error of $\pm 0.08\text{mm}$; this is mainly due to difficulties with repeatability. After firing, propellant combustion products lodged in the barrel bore can prevent the optical target from seating properly and hence introduce false readings.

The same gun mounting was used for all the UK tank and stand firing and some care was taken to ensure that the anti-rotation key (required in a rifled barrel), and the continuous engagement key (used to maintain alignment of the breech opening mechanism

PENNY, PERRY

during recoil), were adjusted to obtain the same clearance figures. The cradle bearing-to-barrel clearances were measured and noted for each barrel, and each barrel bore was inspected before and after a serial was fired.

Whilst the Commissioning and re-firing serials undertaken in BADR used ten round serials it was considered that, with the small ammunition dispersions currently being experienced, a seven round serial could be used for the subsequent UK trials with little effect on the MPI position. Prior to each serial two 'warmer' APDS rounds were fired and each serial was terminated with an eighth round which had a copper crusher gauge inserted in the propellant to monitor gun chamber pressure. Projectile velocity was measured using sky screens and strike coordinates and meteorological conditions were recorded. A low cross-wind limit of 5m/s was insisted upon as a precaution against significant down-range wind variation. In addition, whilst a firing rate of approximately one round every ten minutes was requested the serial had to be aborted if an interval exceeding thirty minutes occurred. After one serial was completed a second was not allowed to start until the gun chamber and chase temperatures had cooled to within 5 C of the ambient air temperature. On only two occasions were two serials completed within one day.

The strike coordinates were analysed using standard statistical methods with Normal distributions assumed. From target strike coordinates a Mean Point of Impact and vertical and horizontal standard deviations were calculated for each serial. In addition to the measured tangent elevation and aim-off, was added the ballistic figures for the meteorological conditions measured and standard jump and throw-off figures. From these calculations the measured MPI could be placed relative to an expected point of impact. Although a Frank-Grubb's test was used to detect outliers or 'wild-rounds', the MPI figures shown include all rounds.

5. DISCUSSION OF RESULTS

The MPI results are shown in Figure 5. These results include the serials from each of the four barrels investigated, when fired from both a tank and a firing stand.

It can be seen that the MPI's for a particular barrel are fairly close to one another on the three occasions that a specific equipment was fired and that there is almost no difference between the tank and firing stand results. It can also be seen that the MPI's fall distinctly into groups associated with each barrel, although the standard deviations obtained from the firing stand tended to be a little larger than those from the tank.

PENNY, FERRY

Generally the UK trial results gave smaller occasion to occasion movements of the MPI position than those experienced between Commissioning and re-firing in BAOR. In addition, the MPI figures obtained in BAOR when the selected barrels were re-fired gave results more in agreement with the later UK controlled trials.

The straightest barrel (NG12212), has not proved to give a more consistent MPI position than some of the other barrels selected, although its serial MPI positions are fairly close to the expected point of impact. We do not know, as yet, what features of the barrel control the movement of the MPI position. The programme is continuing with a barrel rotated through 90 increments and a number of special barrels are to be produced to a new specification. More instrumentation will be used in the second phase of the programme and we are also continuing to examine our current data in more detail. There is much yet to be explained!

6. CONCLUSIONS

The MPI positions appear to be largely determined by the barrel. For the four barrels investigated, the MPI's on a number of occasions have been shown to give a distinct and repeatable pattern, regardless of the installation from which they have been fired.

The MPI positions from the closely controlled trials do not compare very well with the results obtained from the Commissioning firing.

We cannot state what physical parameters of the barrel determine the MPI positions, but further analytical and experimental work is being undertaken.

7. ACKNOWLEDGEMENTS

We would particularly like to acknowledge all the careful work undertaken by the staff of Mr George Rawlinson of Defence Quality Assurance, and Mr David Haugh of RARDE (Fort Halstead).

8. REFERENCES

[1] Unpublished MoD report.

[2] Powell S.E. and Penny P.H.G. - 'The Theoretical Modelling of the Dynamics of Initially Non-Straight Barrels Using Finite Difference Techniques'; 5th US Army Symposium on Gun Dynamics, Rensselaerville, NY, September 1987.

[3] Unpublished MoD report.

Copyright (C) Controller, Her Majesty's Stationery Office,
London 1987.

TABLE 1:

<u>Barrel reference- NG 694</u>				
Dist. from muzzle (mm)	Barrel bend (mm)		Wall variation (mm)	
	Elevation	Azimuth	Elevation	Azimuth
305	0	0	0.178	0.025
914	0.318	0.036	0.152	0
1524	0.566	0.069	0.305	0.076
2134	0.706	0.132	0.152	0.229
2743	0.721	0.254	0.076	0.178
3353	0.622	0.325	-0.051	0.229
3962	0.399	0.262	-0.279	0.203
4572	0.155	0.127	-0.457	0.051
5182	0	0	-0.254	-0.051

Barrel data sign convention: Barrel bend data is positive downwards and to the right when viewed from the gun muzzle toward the breech. Wall thickness variation is positive when the upper measurement exceeds the lower or the right hand exceeds the left.

TABLE 2:

<u>Barrel reference- NG 987</u>				
Dist. from muzzle (mm)	Barrel bend (mm)		Wall variation (mm)	
	Elevation	Azimuth	Elevation	Azimuth
305	0	0	-0.152	-0.076
914	0.147	0.056	-0.152	-0.076
1524	0.330	0.097	-0.127	0.025
2134	0.541	0.036	0.381	-0.102
2743	0.688	-0.102	-0.076	-0.432
3353	0.658	-0.170	0.076	-0.279
3962	0.434	-0.150	-0.203	-0.356
4572	0.180	-0.074	-0.102	-0.102
5182	0	0	-0.254	-0.178

TABLE 3:

<u>Barrel reference- NG 6654</u>					
Dist. from muzzle (mm)	Barrel bend (mm)		Wall variation (mm)		
	Elevation	Azimuth	Elevation	Azimuth	
305	0	0	0.178	0.127	
914	0.196	0.043	0.737	0.127	
1524	0.513	0.127	1.499	0.660	
2134	0.859	0.236	1.448	0.838	
2743	0.848	0.264	1.219	1.067	
3353	0.671	0.274	0.914	0.940	
3962	0.411	0.180	0.559	0.813	
4572	0.152	0.094	0.229	0.711	
5182	0	0	0.076	0.305	

TABLE 4:

<u>Barrel reference- NG 12212</u>					
Dist. from muzzle (mm)	Barrel bend (mm)		Wall variation (mm)		
	Elevation	Azimuth	Elevation	Azimuth	
305	0	0	0.025	0.127	
914	-0.018	0.008	-0.229	0	
1524	-0.020	0.025	-0.051	-0.152	
2134	0.023	0.005	-0.102	-0.127	
2743	0.041	-0.013	-0.178	-0.152	
3353	0.041	-0.005	-0.152	-0.381	
3962	0.030	0.013	-0.381	-0.305	
4572	0.064	-0.008	-0.025	-0.279	
5182	0	0	0.025	-0.076	

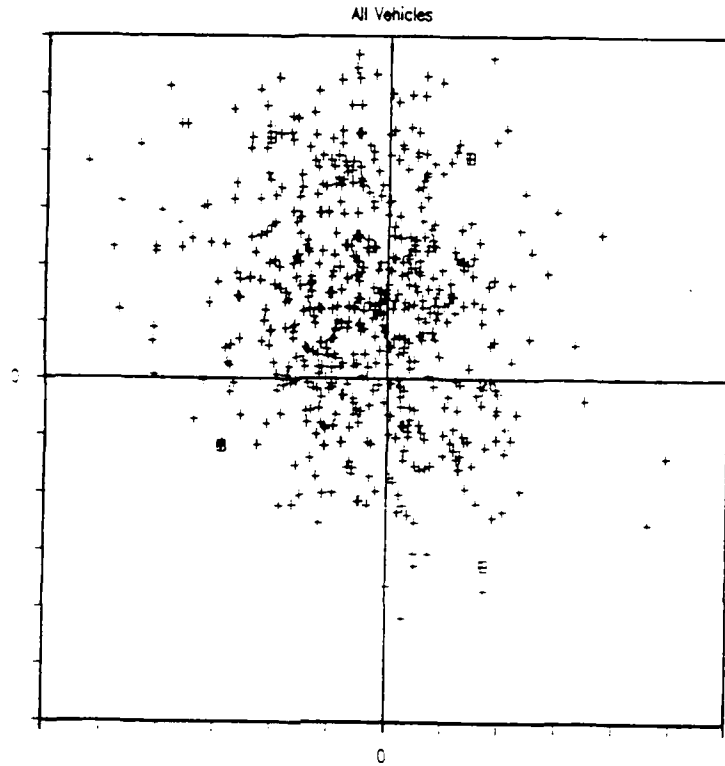


Figure 1: Commissioning Mean Points of Impact

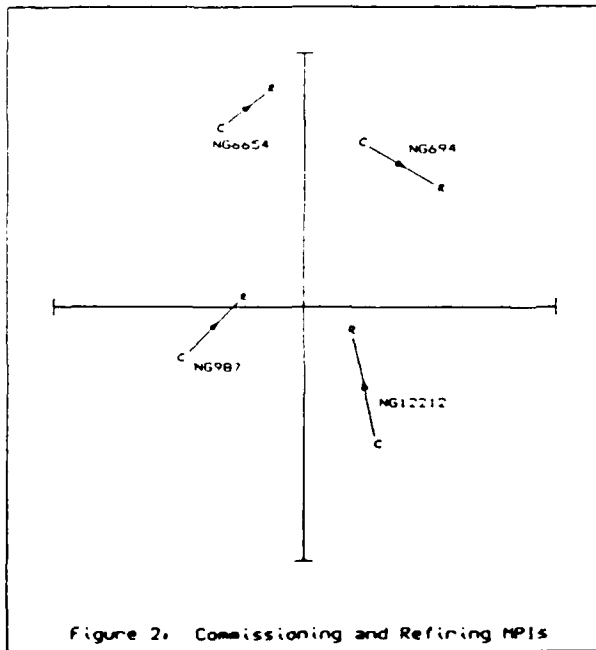


Figure 2: Commissioning and Refining NPIs

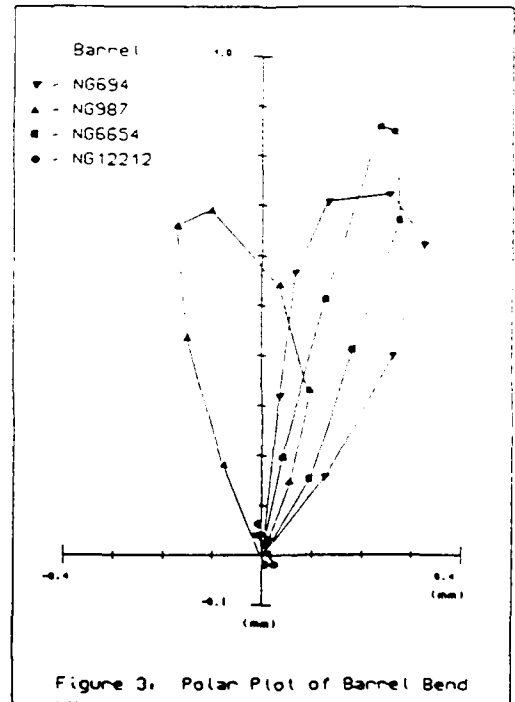
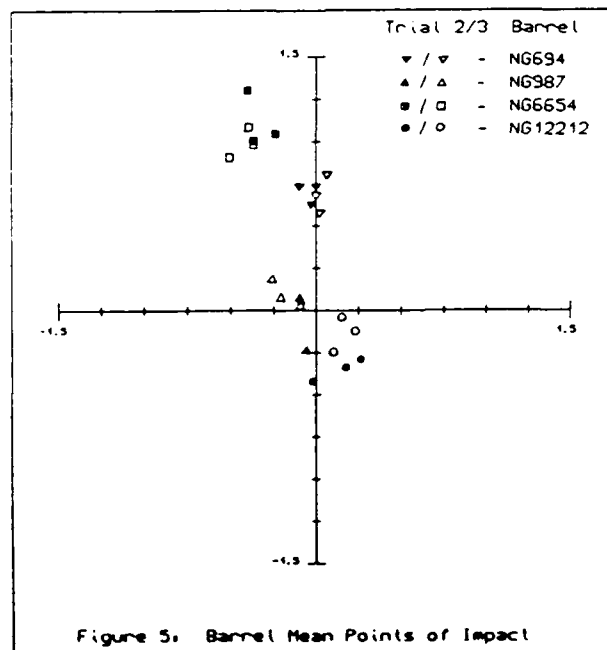
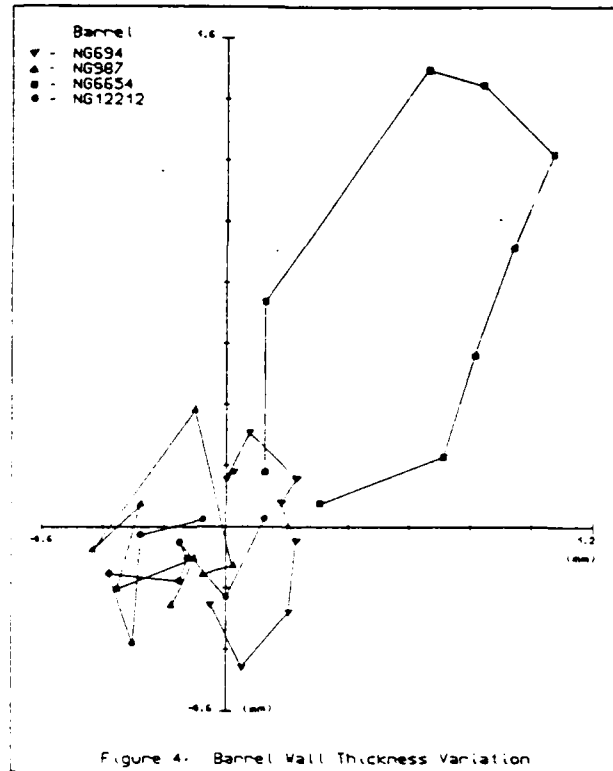


Figure 3: Polar Plot of Barrel Bend



AUTHOR INDEX

	<u>Page</u>
Andrade, C.A.	18, 41
Artus, B.	285
Bannister, K.A.	334
Baran, A.F.	136
Barker, G.	100, 114
Benson, R.C.	394
Benson, W.R.	394
Benzkofer, P.D.	298
Brosseau, T.L.	136
Bulman, D.N.	100, 251
Bundy, M.L.	149
Burton, L.	376
Carofano, G.C.	1
Chambers, A.E.	100, 114
Cox, P.A.	451
Cunningham, G.	285
Duffy, R.E.	18
Erline, T.F.	317
Exell, A.	115
Finlayson, D.F.	249, 285
Gabriele, A.	285
Gast, R.G.	230, 285
Haas, J.W.	41
Hasenbein, R.	285
Hopkins, D.A.	272
Hoyle, J.B.	116, 251
Kaste, R.P.	376
Kingsbury, H.	159
Kordich, M.M.	76
Kregel, M.D.	136, 317
Lyon, D.H.	412
Manners, N.D.	355
Nagamatsu, H.T.	18
Penny, P.H.G.	432, 472
Perry, J.A.	472
Pflegl, G.A.	252
Plostins, P.	412
Polcyn, M.A.	451
Powell, S.E.	432
Rabern, D.A.	334
Savick, D.S.	412
Schmidt, E.M.	412
Shick, D.V.	175
Simkins, T.E.	252
Sneck, H.J.	61
Sorenson, T.	394
Stilson, E.G.	252

	<u>Page</u>
Su, Y.-A.	199
Tadjbakhsh, I.G.	199
Tiersten, H.F.	175
Tsay, H.-S.	159
Witting, P.	61
Yagla, J.J.	76
Zepp, W.T.	98

TECHNICAL REPORT INTERNAL DISTRIBUTION LIST

	<u>NO. OF COPIES</u>
CHIEF, DEVELOPMENT ENGINEERING DIVISION	
ATTN: SMCAR-CCB-D	1
-DA	1
-DC	1
-DI	1
-DP	1
-DR	1
-DS (SYSTEMS)	1
CHIEF, ENGINEERING SUPPORT DIVISION	
ATTN: SMCAR-CCB-S	1
-SE	1
CHIEF, RESEARCH DIVISION	
ATTN: SMCAR-CCB-R	2
-RA	1
-RE	1
-RM	1
-RP	1
-RT	1
TECHNICAL LIBRARY	5
ATTN: SMCAR-CCB-TL	
TECHNICAL PUBLICATIONS & EDITING SECTION	3
ATTN: SMCAR-CCB-TL	
DIRECTOR, OPERATIONS DIRECTORATE	1
ATTN: SMCWV-OD	
DIRECTOR, PROCUREMENT DIRECTORATE	1
ATTN: SMCWV-PP	
DIRECTOR, PRODUCT ASSURANCE DIRECTORATE	1
ATTN: SMCWV-QA	

NOTE: PLEASE NOTIFY DIRECTOR, BENET LABORATORIES, ATTN: SMCAR-CCB-TL, OF ANY ADDRESS CHANGES.

TECHNICAL REPORT EXTERNAL DISTRIBUTION LIST

	<u>NO. OF COPIES</u>		<u>NO. OF COPIES</u>
ASST SEC OF THE ARMY RESEARCH AND DEVELOPMENT ATTN: DEPT FOR SCI AND TECH THE PENTAGON WASHINGTON, D.C. 20310-0103	1	COMMANDER ROCK ISLAND ARSENAL ATTN: SMCRI-ENM ROCK ISLAND, IL 61299-5000	1
ADMINISTRATOR DEFENSE TECHNICAL INFO CENTER ATTN: DTIC-FDAC CAMERON STATION ALEXANDRIA, VA 22304-6145	12	DIRECTOR US ARMY INDUSTRIAL BASE ENGR ACTV ATTN: AMXIB-P ROCK ISLAND, IL 61299-7260	1
COMMANDER US ARMY ARDEC ATTN: SMCAR-AEE	1	COMMANDER US ARMY TANK-AUTMV R&D COMMAND ATTN: AMSTA-DDL (TECH LIB) WARREN, MI 48397-5000	1
SMCAR-AES, BLDG. 321	1	COMMANDER US MILITARY ACADEMY ATTN: DEPARTMENT OF MECHANICS WEST POINT, NY 10996-1792	1
SMCAR-AET-0, BLDG. 351N	1		
SMCAR-CC	1		
SMCAR-CCP-A	1		
SMCAR-FSA	1		
SMCAR-FSM-E	1	US ARMY MISSILE COMMAND REDSTONE SCIENTIFIC INFO CTR ATTN: DOCUMENTS SECT, BLDG. 4484 REDSTONE ARSENAL, AL 35898-5241	2
SMCAR-FSS-D, BLDG. 94	1		
SMCAR-IMI-I (STINFO) BLDG. 59	2		
PICATINNY ARSENAL, NJ 07806-5000			
DIRECTOR US ARMY BALLISTIC RESEARCH LABORATORY ATTN: SLCBR-DD-T, BLDG. 305 ABERDEEN PROVING GROUND, MD 21005-5066	1	COMMANDER US ARMY FGN SCIENCE AND TECH CTR ATTN: DRXST-SD 220 7TH STREET, N.E. CHARLOTTESVILLE, VA 22901	1
DIRECTOR US ARMY MATERIEL SYSTEMS ANALYSIS ACTV ATTN: AMXSY-MP ABERDEEN PROVING GROUND, MD 21005-5071	1	COMMANDER US ARMY LABCOM MATERIALS TECHNOLOGY LAB ATTN: SLCMT-IML (TECH LIB) WATERTOWN, MA 02172-0001	2
COMMANDER HQ, AMCCOM ATTN: AMSMC-IMP-L ROCK ISLAND, IL 61299-6000	1		

NOTE: PLEASE NOTIFY COMMANDER, ARMAMENT RESEARCH, DEVELOPMENT, AND ENGINEERING CENTER, US ARMY AMCCOM, ATTN: BENET LABORATORIES, SMCAR-CCB-TL, WATERVLIET, NY 12189-4050, OF ANY ADDRESS CHANGES.

TECHNICAL REPORT EXTERNAL DISTRIBUTION LIST (CONT'D)

	<u>NO. OF COPIES</u>		<u>NO. OF COPIES</u>
COMMANDER US ARMY LABCOM, ISA ATTN: SLCIS-IM-TL 2800 POWDER MILL ROAD ADELPHI, MD 20783-1145	1	COMMANDER AIR FORCE ARMAMENT LABORATORY ATTN: AFATL/MN EGLIN AFB, FL 32542-5434	1
COMMANDER US ARMY RESEARCH OFFICE ATTN: CHIEF, IPO P.O. BOX 12211 RESEARCH TRIANGLE PARK, NC 27709-2211	1	COMMANDER AIR FORCE ARMAMENT LABORATORY ATTN: AFATL/MNF EGLIN AFB, FL 32542-5434	1
DIRECTOR US NAVAL RESEARCH LAB ATTN: MATERIALS SCI & TECH DIVISION CODE 26-27 (DOC LIB) WASHINGTON, D.C. 20375	1 1	METALS AND CERAMICS INFO CTR BATTELLE COLUMBUS DIVISION 505 KING AVENUE COLUMBUS, OH 43201-2693	1

NOTE: PLEASE NOTIFY COMMANDER, ARMAMENT RESEARCH, DEVELOPMENT, AND ENGINEERING CENTER, US ARMY AMCCOM, ATTN: BENET LABORATORIES, SMCAR-CCB-TL, WATERVLIET, NY 12189-4050, OF ANY ADDRESS CHANGES.